

Coordinated control of the Zero Inertia Powertrain

Citation for published version (APA):

Serrarens, A. F. A. (2001). *Coordinated control of the Zero Inertia Powertrain*. [Phd Thesis 1 (Research TU/e / Graduation TU/e), Mechanical Engineering]. Technische Universiteit Eindhoven.
<https://doi.org/10.6100/IR549998>

DOI:

[10.6100/IR549998](https://doi.org/10.6100/IR549998)

Document status and date:

Published: 01/01/2001

Document Version:

Publisher's PDF, also known as Version of Record (includes final page, issue and volume numbers)

Please check the document version of this publication:

- A submitted manuscript is the version of the article upon submission and before peer-review. There can be important differences between the submitted version and the official published version of record. People interested in the research are advised to contact the author for the final version of the publication, or visit the DOI to the publisher's website.
- The final author version and the galley proof are versions of the publication after peer review.
- The final published version features the final layout of the paper including the volume, issue and page numbers.

[Link to publication](#)

General rights

Copyright and moral rights for the publications made accessible in the public portal are retained by the authors and/or other copyright owners and it is a condition of accessing publications that users recognise and abide by the legal requirements associated with these rights.

- Users may download and print one copy of any publication from the public portal for the purpose of private study or research.
- You may not further distribute the material or use it for any profit-making activity or commercial gain
- You may freely distribute the URL identifying the publication in the public portal.

If the publication is distributed under the terms of Article 25fa of the Dutch Copyright Act, indicated by the "Taverne" license above, please follow below link for the End User Agreement:

www.tue.nl/taverne

Take down policy

If you believe that this document breaches copyright please contact us at:

openaccess@tue.nl

providing details and we will investigate your claim.

Coordinated Control of
The Zero Inertia Powertrain

CIP-DATA LIBRARY TECHNISCHE UNIVERSITEIT EINDHOVEN

Serrarens, Alexander F. A.

Coordinated control of the Zero Inertia Powertrain/by Alexander F. A.

Serrarens. – Eindhoven : Technische Universiteit Eindhoven, 2001.

Proefschrift. – ISBN 90-386-2583-9

NUGI 834

Subject headings: passenger car powertrain / vehicular transmission / continuously variable transmission / CVT / internal combustion engine / fuel saving / fuel economy / driveability/ powertrain ; flywheel / hybrid vehicles / zero inertia powertrain / stop-go powertrain / CVT powertrain modeling / powertrain ; parameter optimization / CVT powertrain ; jet-start behaviour / longitudinal ride comfort / engine-CVT control / coordinated powertrain control / driveline management / active driveability control / electronic throttle / drive-by-wire / DBW / non-minimum phase system / nonlinear model based control / control systems ; experimental

This thesis was prepared with the $\text{\LaTeX}2_{\epsilon}$ documentation system.

Printed by University Press Facilities, Eindhoven, The Netherlands.

Cover Design by Dirk Vroemen and Nanne Verbruggen, Rotterdam

Copyright ©2001 by A. F. A. Serrarens

All rights reserved. No parts of this publication may be reproduced or utilized in any form or by any means, electronic or mechanical, including photocopying, recording or by any information storage and retrieval system, without permission of the copyright holder.

This work forms a part of the EcoDrive project, subsidized by the Dutch government through EET (Economy, Ecology and Technology).

Coordinated Control of The Zero Inertia Powertrain

PROEFSCHRIFT

ter verkrijging van de graad van doctor
aan de Technische Universiteit Eindhoven
op gezag van de Rector Magnificus, prof.dr. R. A. van Santen,
voor een commissie aangewezen door het College voor Promoties
in het openbaar te verdedigen op
dinsdag 27 november 2001 om 17.00 uur

door

Alexander Franciscus Anita Serrarens

geboren op 6 september 1973 te Hulst

Dit proefschrift is goedgekeurd door de promotoren:

prof.dr.ir. M. Steinbuch
en
prof.dr.ir. P.P.J. van den Bosch

Copromotor:

dr.ir. F. E. Veldpaus

Contents

Summary	ix
I General Introduction	1
1 Introduction and Project Goals	3
1.1 Project chronology	5
1.2 Problem descriptions	6
1.3 Why coordinated powertrain control?	7
1.4 Main contributions and outline of this thesis	8
2 Fuel Saving Principles	11
2.1 Introduction	11
2.2 Improving component efficiency	12
2.2.1 Engine efficiency	12
2.2.2 Transmission efficiency	15
2.2.3 Power take-off	15
2.3 Reducing the external load	16
2.3.1 Vehicle mass	16
2.3.2 Rolling resistance	16
2.3.3 Air drag	17
2.4 Alternative powertrain operation	18
2.5 Non-vehicle technology	19
2.5.1 Driving behaviour	19
2.5.2 Infrastructure and traffic management	19
2.5.3 Law, policy and legislation	20
3 Normalized Innovation Values	21
3.1 Hybrid powertrains	21
3.2 Innovation values: fuel economy	23
3.2.1 Reference vehicle	24
3.2.2 Influence of driving cycles	25
3.2.3 Fuel economy	25
3.3 Innovation efforts	28
3.3.1 E-line tracking	29
3.3.2 Stop-Go operation	35
3.3.3 Start-Stop operation	36

3.3.4	Brake energy recovery	41
3.4	Innovation value versus effort	41
4	The Zero Inertia Powertrain	45
4.1	Zero Inertia principle	45
4.2	ZI Concept design	48
4.2.1	Resulting configuration	48
4.3	ZI Stop-Go	49
4.4	Further reading	50
II	Powertrain Control	51
5	Introduction to Part II	53
6	Powertrain Modeling	55
6.1	Introduction	55
6.2	Description of the CVT powertrain	56
6.2.1	Internal combustion engine	57
6.2.2	Hydraulically controlled variator	59
6.2.3	DNR set	61
6.2.4	Torque converter	62
6.2.5	Final drive, differential and drive shafts	65
6.2.6	Transmission efficiency	66
6.2.7	Tires, vehicle and external interactions	68
6.3	Description of the ZI powertrain	70
6.3.1	Key idea	71
6.3.2	Optimized functional design	72
6.4	Dissipative torsional compliance model	76
6.5	Comparison of the CVT and ZI powertrain	80
6.5.1	Linearized system analysis	80
6.5.2	Non-minimum phase behaviour	84
7	Coordinated Powertrain Control	89
7.1	Introduction	89
7.1.1	Contemporary CVT powertrain control	90
7.1.2	Gyristor term vs. control solutions	92
7.1.3	Organization of this chapter	93
7.2	Control objectives	93
7.2.1	Fuel economy: optimal operating line	93
7.2.2	Longitudinal driveability: course of output torque	98
7.3	Trade-off between the two objectives	104
7.4	Control design	106
7.4.1	Control model	107
7.4.2	Coordinated control for the CVT powertrain	108
7.4.3	Coordinated control for the ZI powertrain	114
7.5	Simulation results	118
7.5.1	CVT powertrain	118
7.5.2	ZI powertrain	121
7.6	Discussion	123

8	Experimental Results	125
8.1	Electronic powertrain control system	126
8.1.1	Sensors	127
8.1.2	Actuators	128
8.1.3	Real time implementation	129
8.2	Electronic throttle valve actuator	131
8.2.1	Throttle valve model	132
8.2.2	Feedback control	133
8.2.3	Feedforward control	134
8.2.4	Results	135
8.3	Experimental coordinated powertrain control	137
8.3.1	Control law for ϕ_d	138
8.3.2	Control law for $r_{cvt,d}$	138
8.3.3	Stability of the experimental control	139
8.3.4	Simulation with model (7.23)	140
8.4	Model validation: drive shaft resonance	140
8.5	Driveability	142
8.5.1	Semi kick-down	143
8.5.2	Pedal jogging	145
8.5.3	Kick-down	147
8.6	Fuel economy	148
8.6.1	Estimation of the OOL	149
8.6.2	Constant vehicle speeds	149
8.6.3	Drive cycles	151
8.6.4	Fuel consumption of ZI on the NEDC	151
8.7	Concluding remarks	153
8.7.1	Conclusions	154
8.7.2	Recommendations	154
III	Closure	157
9	Conclusions and Outlook	159
9.1	Overview	159
9.2	EcoDrive	160
9.3	Coordinated powertrain control	161
9.4	Outlook	163
9.4.1	Powertrain modeling and control	163
9.4.2	Powertrain design	164
	Bibliography	167
A	Nomenclature, Acronyms, Symbols	177
A.1	Abbreviations, Acronyms	177
A.2	Symbols	178
A.3	Subscripts	178

B Inertial Variable Shunt: Kinematics and Dynamics	181
B.1 Layout and definitions	181
B.2 Powersplit planetary gear set	181
B.3 Inertial variable shunt	184
B.4 Equivalent inertias: IVS becomes a CVT again	186
C Model Equations	189
C.1 Non-linear simulation model	189
C.2 Linearized model	192
C.3 Parameters	194
Samenvatting	195
Dankwoord	197
Curriculum Vitae	199

Summary

Powertrains for passenger cars have been receiving substantial improvements throughout the last few years. Successful efforts have been undertaken to improve the fuel economy by adapting the engine-, aerodynamical and tire design. Reduction of vehicle mass seems to have the highest potential but is hardly realizable in practice if at all. This is merely caused by the increased safety and comfort standards. The desire of society for a healthy and clean environment, preferably for a low price, encouraged car manufacturers to launch new and innovative solutions for better fuel economy and lower emissions. Mostly these innovations are forced though also financially supported by governments.

Since about ten years it is fully understood that improved fuel economy can also be realized by the transmission in the powertrain. Not only higher transmission efficiency but more importantly the way the engine and transmission jointly cooperate to increase the engine's combustion efficiency is the key to a substantial fuel economy improvement. The capabilities in this area can be intensified by utilizing a *continuously variable transmission* (CVT). A CVT can transmit the engine torque and change its speed continuously. Besides this advantage above other transmission (manuals, stepped automatic) it possesses a relatively high *overdrive* ratio with low penalties on volume.

For example, the CVT's overdrive can lower the engine speed to about 1500 rpm at 80 km/h, whereas standard transmissions manipulate at least 1900 to 2200 rpm at this vehicle speed. The former can be shown to gain about 10 to 15% fuel economy advantage. However, a disadvantage of the high overdrive is the lack of vehicle responsiveness (driveability) when pushing the accelerator pedal. Mostly because of safety reasons this kind of operation is socially unaccepted and solutions are mandatory to break the paradox between driveability and fuel economy.

In the framework of the *EcoDrive project* at the Technische Universiteit Eindhoven a technical innovation is elaborated that indeed banishes the mentioned paradox. Besides the work described in this thesis two other theses are written on this subject: 'Component Control for the Zero Inertia Powertrain' by Bas Vroemen en 'Transmission Design of the Zero Inertia Powertrain' by Roëll van Druuten.

The innovation originates from the idea to exploit the inertia of a flywheel beneficially for realizing an initial and persistent response at request. Connecting a planetary gear stage with the flywheel in parallel to the CVT, it is possible to decelerate the flywheel while accelerating the engine with the CVT (for example to facilitate a take-over manoeuvre). The torque stemming from the flywheel is directly transmitted to the wheels until the moment where the engine can deliver the requested power sustainably on its own. In this thesis an unique state of the powertrain is identified where the total torque stemming from the engine sided inertias are compensated exactly by that of the flywheel. This state is termed 'zero inertia' hence the denomination *Zero Inertia Powertrain*.

A proper coordination of engine torque and shift speed of the CVT ratio during and after the engine transitions is extremely important. By carefully choosing the setpoints for the engine's electronic air throttle and for the hydraulically controlled CVT, the driveability and fuel economy can be optimized at all times. This is termed *coordinated powertrain control* and together with demonstrating the improved fuel economy and driveability form the main subject of this thesis. Models are required to gain increased insights in the ZI powertrain. Moreover, for the coordinated control design and for validation dynamic models are mandatory. In part II of this thesis modeling, control and testing of the ZI and CVT powertrains are described.

In conjunction with Bas Vroemen and Roëll van Druten part I is written showing that improved fuel economy pays a price in terms of research capacity, resources, weight and volume. In Part I it is made plausible that the ZI powertrain forms a mediating solution amongst these actors.

Part I

General Introduction

Chapter 1

Introduction and Project Goals

The topic of this thesis is the technology assessment, modeling, control and testing of a new continuously variable transmission (CVT) based powertrain for passenger cars. This powertrain is termed *Zero Inertia (ZI) powertrain*; the origin of the naming will be elucidated further on. A more profound definition of ‘powertrain’ will be formulated in this thesis, but for now it is described by the compilation of engine, transmission, wheels and vehicle. This work is one out of three theses that describe different topics of the ZI powertrain. In [van Druten, 2001] the mechanical design and construction of the ZI transmission is focused on. In [Vroemen, 2001] modeling, control and testing of the CVT is the main topic. There, also a variant of the ZI powertrain is discussed, *i.e.*, the ZI powertrain with ‘Stop-Go’ facility and is actually introduced for additional fuel saving. The ZI and ZI Stop-Go are materializations of the goals set in the *EcoDrive project*. EcoDrive is a cooperation of Van Doorne’s Transmissie (VDT) in Tilburg, the Technische Universiteit Eindhoven (TU/e) and TNO Automotive in Delft. The project is initiated by VDT and funded by the Dutch governmental subsidization program EET (Economy, Ecology and Technology).

The ZI powertrain is born out of the assignment defined by EcoDrive to achieve considerable fuel saving with a CVT and an additional flywheel in a powertrain for passenger cars. The properties of a CVT can be exploited to save fuel actually by running the engine in operating points with better fuel economy. This should occur without deteriorating the vehicle’s longitudinal dynamic response, in other words, without compromising *driveability*. Compromising driveability disappears when utilizing the inertial properties of a flywheel as in the ZI powertrain.

The formulation of this assignment has a historical background at the Technische Universiteit Eindhoven. In the late 1970-ties a project was initiated concerned with the integration of a high speed flywheel in a powertrain that enabled the engine to operate intermittently as a constant speed aggregate in its most efficient operating point. This lead to the materialization of an optimized flywheel hybrid powertrain (FHD-III) and its fuel economy is demonstrated in [Kok, 1999]. The driveability was never assessed, nevertheless interest in this area began to increase.

EcoDrive

The main goal of the EcoDrive project is twofold. One part of the project concentrated merely on improving the efficiencies of the engine and the CVT, aiming at an increased total driveline

efficiency (System Integrated driveline, SI). The second part (HYbrid driveline, HY) was to design the hard- and software of a new powertrain with CVT and additional power source that saves 25% fuel on the New European Drive Cycle (NEDC) compared to a 5-speed manual transmission (5-MT) vehicle and that has a driveability level comparable to commercially available mid-sized passenger cars. The EcoDrive SI project was primarily a cooperation of VDT and TNO Automotive, whereas in the EcoDrive HY part VDT and TU/e worked together. The EcoDrive project started back in 1997 and is finalized at the end of 2001.

A year after kicking-off the EcoDrive HY project, it was reformulated into the 'EcoDrive ZI' project, for reasons that will be explained further on. Figure 1.1 elucidates the organization and the resulting concepts of the EcoDrive project.

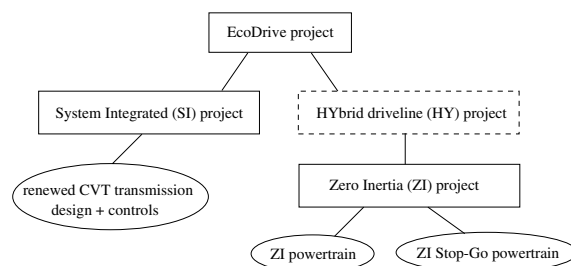


Figure 1.1: EcoDrive project organization

In this thesis and in [van Druten, 2001] and [Vroemen, 2001], the findings of the EcoDrive ZI project are described. Results of the renewed CVT transmission design and control achieved in EcoDrive SI can be found in [Veenhuizen and van Spijk, 2000].

Zero Inertia powertrain

The way to arrive at a materialization starting from a problem description depends for the larger part on the outcome of a preliminary investigation. In the case of EcoDrive HY, such a preliminary investigation lead to a simple configuration and operation principle of a hybrid powertrain with internal combustion engine, CVT, flywheel and a few clutches based on the findings of the FHD-III, [Serrarens and Veldpaus, 1998].

Along with the search for the 'ideal' flywheel hybrid powertrain, interest was put in the functional problems of basic CVT powertrains. A basic CVT powertrain is afflicted with the paradox that it can realize a high fuel economy and driveability, but hardly at the same time. Triggered by this phenomenon, the idea came up to try and find a way to break up this paradox with a flywheel inertia. This lead to the aforementioned Zero Inertia powertrain. ZI is based on the rationale that an unwanted inertial phenomenon of the powertrain can in principle be nullified by exchanging kinetic energy between an additional flywheel and the engine sided inertias. As such, high fuel economy forced by optimizing the engine operating points for fuel economy is no longer penalized by reduced driveability. It was decided to elaborate further on the ZI powertrain leading to a reformulation of the EcoDrive HY into the EcoDrive ZI project.

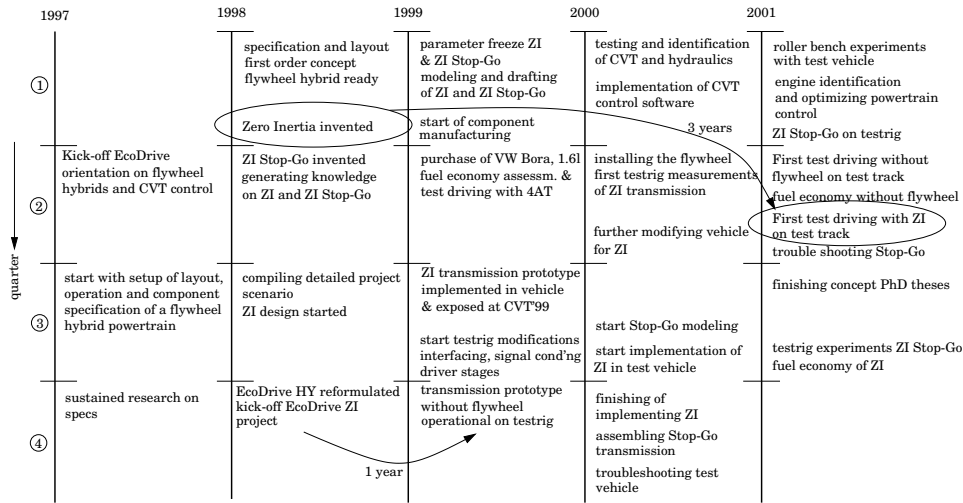


Figure 1.2: EcoDrive ZI project chronology

outline of this chapter

The remainder of this chapter is organized as follows. In Section 1.1, the chronology of the project is described. In Section 1.2 and 1.3 the problem descriptions underlying this thesis are described. Finally, in Section 1.4, the main contributions and outline of this thesis is described.

1.1 Project chronology

In Figure 1.2, the chronology of the EcoDrive ZI project is displayed. The decision to concentrate on the ZI and the ZI Stop-Go powertrains, required some organizational and financial re-formulations of the goals first set in EcoDrive HY. It was decided to design and built a prototype ZI transmission, develop control software and conduct fuel consumption and driveability tests. The ultimate project goal, *i.e.*, demonstrating 25% fuel consumption reduction on the NEDC, could not be reached by ZI alone. Therefore the Stop-Go extension upon the ZI powertrain was introduced. The feasibility of the original project goal was questioned and a new goal was set, being 25% reduction of fuel consumption of a 1.6 ℓ petrol engine with ZI Stop-Go compared to the same engine in conjunction with a 4-speed automatic transmission (4AT). Due to the limited time schedule and the desire to investigate systems step-by-step it was decided to implement ZI in a test vehicle and to test the feasibility of ZI Stop-Go on a test rig only. Regarding Figure 1.2, the main observation is that the time span between the invention of the ZI powertrain and first successful road testing covers just over three years. Conceiving and designing the ZI concept for a vehicle implementation took just over half a year. The materialization and mounting on the test rig of the first ZI transmission required around one year, whereas the testing of the transmission and its controls on a test rig and in a vehicle required an additional one and a half year. Reasons for the relatively short development time are given:

- the fact that the ZI idea itself hardly necessitates research on components, enabling the use of proven technology;
- the control system hardware requires no major adaptations compared to a standard CVT powertrain, instead new developments in software are achieved;
- prompt freezing of the mechanical layout through reasoning according to first principles;
- the use of simple kinematic, dynamic and energy models to gain quick insight in the mechanisms and to optimize the system parameters of the prototype ZI transmission;
- the use of an available CVT and other available transmission components to make the extension towards a ZI transmission;
- step-by-step testing of the ZI powertrain, by consecutively testing the available CVT transmission on a test rig, followed by the ZI transmission on the test rig and finally in the vehicle. This way, inevitable setbacks could be handled reasonably quickly;
- the use of flexible and state-of-the-art test rig facilities, which were developed within the EcoDrive project;
- the modest modifications required within the engine compartment in order to make the ZI powertrain fit into the test vehicle;
- coordinated teamwork, frequent team meetings and ticking off achieved milestones.

1.2 Problem descriptions

As explained, the main project goal for EcoDrive ZI is 25% fuel economy improvement on the NEDC cycle with respect to 4AT and CVT. In general there are different ways to achieve this. Four of them are mentioned:

- a) matching engine operating points with the highest combustion efficiency to the actual vehicle speed and power request;
- b) shutting down the engine at full vehicle stops to save the idle fuel consumption;
- c) matching the single engine operating point with highest efficiency to the average power request, and
- d) effective reuse of the vehicle's kinetic energy.

In EcoDrive HY all principles were chosen to be combined into one concept, whereas in EcoDrive ZI only the principles a) and b) are chosen. The above research questions are graphically illustrated for the EcoDrive ZI project in Figure 1.3. Targets on emissions and/or acceptance were not set by the project, but should in general be incorporated for pursuing additional relevance.

From Figure 1.3, three problem descriptions are identified. The first is how to motivate the choice for fuel saving principles a) and b). Both principles need a power assist system with corresponding power source in order to meet the driveability objective. The second problem then is how to motivate the choice for the power source, being a flywheel for both ZI and ZI Stop-Go. Thirdly, the question rises why or why not the main project target of 25% is met. In this thesis, the first and second research questions are answered in the remainder of this part, more specifically in Chapter 3. The third research question is answered in Chapter 9, Part III. Naturally, a number of open problems evolve when developing, examining and validating the new invention. These problems may be interesting or significant enough to formulate differentiating research projects. In this respect Part III also gives directions for future research.

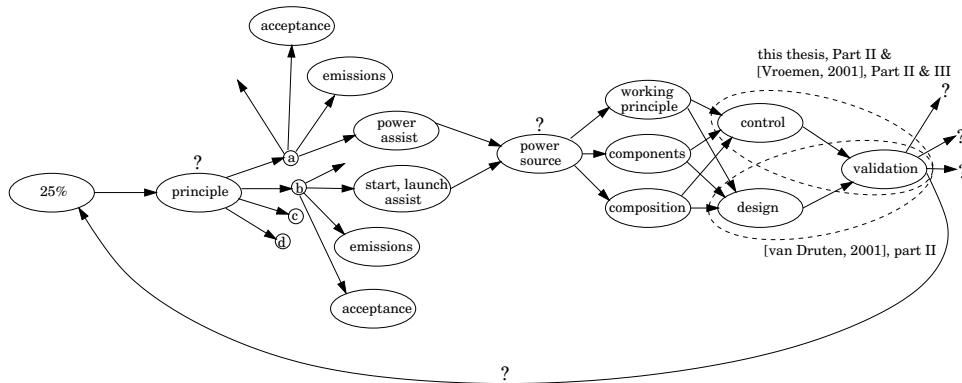


Figure 1.3: Research trajectory for EcoDrive ZI

1.3 Why coordinated powertrain control?

Besides the intrinsic mechanical and engine properties of any powertrain, coordinated powertrain control is a key factor in achieving the intended fuel savings. The engine and transmission need to function in concert in order to obtain the maximally possible fuel economy. In this thesis only fuel saving principle a) of Section 1.2 is pursued and the main control problem there is to schedule the engine operating points dynamically such that a desired response of the vehicle (driveability) and best fuel economy emerges. This research question is drawn up for both a conventional CVT powertrain as well as the ZI powertrain.

Scheduling the engine operating points is controlled with the air throttle and the transmission ratio and is termed *coordinated powertrain control* in this thesis. The idea of coordinated powertrain control is not new. Especially for CVT powertrains interesting control solutions are found in literature, see [Guzzella and Schmid, 1995], [Schmid *et al.*, 1995] and [Sackmann and Krebs, 1999]. An overview of methods applied in practice can be found in [Liu and Paden, 1997] and [Piffner, 1999]. Most methods focus both on fuel economy and driveability but control solutions for the latter are often exotic and strand into moderately tunable closed loop structures.

In this thesis it is attempted—at least for CVT based powertrains—to define the problem of driveability quantitatively, assign the variables that affect driveability and formulate controllers explicitly using this knowledge. In doing so it is pursued to end up with as less tuning parameters as possible. At the cost of flexibility this offers a rigorous and cheap way to calibrate and tune the controller in a practical environment.

In order to arrive at a suitable implementation of the coordinated powertrain control, a number of research stages have to be tackled, *viz.* :

- optimizing the functionality of the ZI powertrain by adequately choosing some mechanical design parameters;
- realizing a dynamic simulation model describing the majority of dynamic phenomena seen in the powertrains;
- finding a translation of the drive pedal deflection into a quantity representing the driveability of the vehicle;

- formulating control objectives related to fuel economy and driveability;
- designing a dynamic setpoint control for engine and CVT meeting these objectives;
- validating the control strategies by simulation;
- validating the control strategies by experiments and most importantly;
- validating the improvement of both fuel economy and driveability promised by the ZI powertrain with respect to an automatic transmission powertrain.

1.4 Main contributions and outline of this thesis

The main contributions of this thesis and the underlying research are listed below, at the same time indicating the outline of this thesis:

- a rather complete survey of fuel saving principles and associated efforts is provided, especially with respect to the powertrain (Chapters 2 and 3). Moreover, a *hybridization factor* is introduced, and a lower bound for the level of hybridization (see Chapter 3) is obtained, resulting in an upper bound for the associated fuel savings;
- a novel transmission concept, referred to as the Zero Inertia powertrain, is presented (Chapter 4). This transmission concept for automotive application combines a CVT and a low-speed flywheel, in a way that is unprecedented (see [van Druten *et al.*, 2000b;a]);
- the ZI extension of a basic CVT powertrain, *i.e.*, the flywheel unit, is given separate attention in Section 6.3. There also an optimization tool for function parameters of the flywheel unit based on normalized kinetic energy functions;
- a dynamic simulation model of the powertrain is indispensable to validate controller design and to perform detailed fuel economy simulations. The powertrain model is compiled out of the components seen in the powertrain. After introducing the respective components and models for them a *torsional compliance powertrain model* is introduced in Section 6.4;
- furthermore, in Chapter 6 a linearization of the simulation model is executed to facilitate a comfort analysis. Two eigenmodes were found, the first of which is relevant for comfort. This first eigenmode is termed 'drive shaft resonance'. It is shown that the flywheel provides additional damping of this resonance. Nevertheless, the real benefit for comfort in practice is disputed;
- finally in Chapter 6 the notion of non-minimum phase behaviour is quantified in terms of the single zero that applies for the CVT and ZI powertrain. This zero is positive real for every feasible ratio in the CVT powertrain, whereas the zero is negative real for more than half of the ratio range in the case of the ZI powertrain. A positive zero leads to non-minimum phase behaviour which essentially forms the driveability problem (jet start behaviour) recognized for CVT powertrains. In terms of control and system analysis the negative zero for the ZI powertrain provides appreciable dynamics rendering a rather straightforward coordinated control solution for this powertrain;
- solutions for the coordinated powertrain control problem are seen to be quite diverse in literature. This is mostly attributed to the control objectives that differ greatly among the solutions. Most of the solutions take optimal fuel economy as one of the control objectives but quantifying driveability as a control objective is often described in somewhat concealing ways or is not done at all. Compromises between fuel economy and driveability are therefore hard to tune with these control solutions. A literature overview is presented in Section 7.1;

- the fuel economy and driveability control objectives are quantified in Sections 7.2.1 and 7.2.2 respectively. The quantification of driveability exists in a translation of the drive pedal deflection set by the driver into a to-be-realized value for the torque applied to the front wheels;
- for validation of the driveability experiments in Chapter 8 a qualitative measure for driveability is also given in Section 7.2.2;
- in Section 7.3 the trade-off between fuel economy and driveability is described in a quantitative manner. Given step-wise (saturated) changes of the engine torque, upper bounds on the acceleration of the engine are derived such that the powertrain will not show non-minimum phase behaviour. Besides being incorporated in the control design, the trade-off results are used throughout this thesis to motivate explanations of the results obtained;
- in Section 7.4 the coordinated controllers for the CVT and ZI powertrain are derived. The CVT solutions uses the results of the trade-off described in Section 7.3. The control solution for the ZI powertrain also uses the results of the trade-off. For the ZI powertrain it was recognized that there is no limit on the (positive) accelerations of the engine within a large part of the CVT ratio control range. This is attributed to the negative zero (minimum phase) and is used beneficially in deriving an input for the CVT ratio shift speed;
- results of the controllers are presented and discussed in the final sections of Chapter 7;
- a test vehicle is equipped with the CVT and later on the ZI powertrain. Furthermore a coordinated control system is implemented comprising sensors, actuators, signal conditioning, driver stages, a digital signal processor, signal acquisition and software. This is covered in Section 8.1;
- a component controller for the electronic air throttle is designed establishing a high bandwidth closed loop being able to track requested excursions of the throttle opening with very small errors. The modeling, design and experimental results are shown in Section 8.2;
- an experimental controller is implemented essentially being a simplified version of the ZI controller derived in Chapter 7. Stability is proven and through simulations the performance of this controller applied to both powertrains is demonstrated. The experimental controller design and results are shown in Section 8.3; Although it was the intention to do so, the performance of the coordinated controller is not investigated in experiments.
- some model validation has been undertaken. In Section 8.4 the eigenfrequencies of the drive shaft resonance of the linearized powertrain model are compared to those seen in practice. The validation is performed with the CVT and ZI powertrains;
- driveability of the CVT and ZI powertrain is examined through three types of experiments: semi-kickdown, pedal jogging and a full kickdown. In the latter case also an experiment conducted with the 4AT powertrain is included. The ZI powertrain shows superior driveability with respect to the other powertrains;
- finally, the fuel economy of the ZI and ZI Stop-Go powertrains are examined in Section 8.6 in the following way. The fuel economy of the 4AT and CVT powertrain are measured in the test vehicle. The 4AT serves as the reference vehicle and the fuel consumption measurements of the CVT powertrain are used to validate the simulation model. With this model the reduction of fuel consumption of the ZI and ZI Stop-Go powertrains is estimated in the NEDC drive cycle.

Chapter 2

Fuel Saving Principles

2.1 Introduction

Modern passenger cars represent a technologically advanced form of flexible personal mobility. They are comfortable, high performing and relatively safe. Imagining global society without passenger cars is simply impossible. Despite all efforts, the passenger car is still a fairly inefficient means of individual transportation. Figure 2.1(a), from [Delsey, 1991], shows the distribution of fuel energy to the various heat producing processes involved with driving a passenger car. A more realistic graph might be the pie-chart of Figure 2.1(b), from [DOE and

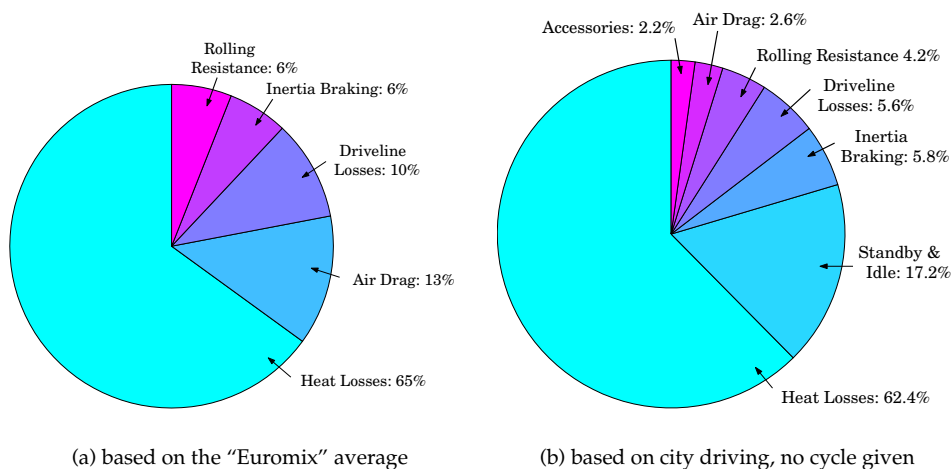


Figure 2.1: Typical energy distributions for a passenger car

EPA, 2001] (measured drive cycle is not given). From both figures it follows that only between 15% and 25% of the energy in the gasoline is actually used to propel the vehicle—that is to

overcome vehicle inertia, aerodynamic drag and rolling resistance—and to power accessory systems like air-conditioning. The rest of the energy is lost in the form of heat transfer to coolant and ambient air, friction within the engine and transmission, and pumping of air into and out of the cylinders (*e.g.*, during idling).

Regarding these figures, insight can be gained into how fuel economy might be improved. In general, methods for reducing the fuel consumption can be divided into four categories:

1. improving the efficiency of the individual powertrain components, *i.e.*, engine, transmission and power take-off;
2. reducing the external load of the powertrain, *i.e.*, vehicle mass, rolling resistance and air drag;
3. alternative powertrain operation, *i.e.*, E-line¹ tracking, Stop-Go¹, Start-Stop¹ and brake energy recovery (BER)¹;
4. non-vehicle technology, *i.e.*, driving behaviour, infrastructure and traffic management, law, policy and legislation.

In this chapter, all four categories are briefly discussed. The following chapter concentrates on alternative powertrain operation in more detail. Engine emissions are only briefly treated.

2.2 Improving component efficiency

A conventional passenger car driveline basically comprises an internal combustion engine, a launching device (friction plate clutch, torque converter, magnetic powder coupling, *etc.*), a torque amplifying transmission (any kind), differential and driveshafts, see Figure 2.2. The fuel tank, cooling system, battery, electric starter motor and various Power Take-Off (PTO) components, such as the alternator, fuel pump, water pump, power steering pump, and ignition, draw up the indispensable but fuel consuming periphery of the driveline. Part of the mechanical power generated by the engine is lost in the transmission and to the PTO. The net torque in the drive shafts propels the wheels. Ways for decreasing the driving resistance are discussed further on. First, various methods and potentials for fuel economy improvement by enhancing the efficiency of individual driveline components are discussed.

2.2.1 Engine efficiency

The engine efficiency has been strongly improved in the recent past, although it is still the least efficient component in the powertrain. Despite its disappointing efficiency, the modern combustion engine, the prime mover of road-going vehicles, is a more or less optimal combination of low manufacturing cost and -energy, power density, volume, efficiency, durability, maintainability, recyclability and controllability. A point of concern about this machinery is the load-dependent efficiency characteristic. Without employing more advanced powertrain concepts this dependency hampers the most fuel-optimal utilization of the combustion engine.

The fluctuating power requests needed for the vehicle's motion, demand the operating conditions of the engine to be changed accordingly. In this respect, there are two main reasons why fuel consumption may be larger than theoretically achievable, namely:

¹To be defined in Section 3.2.

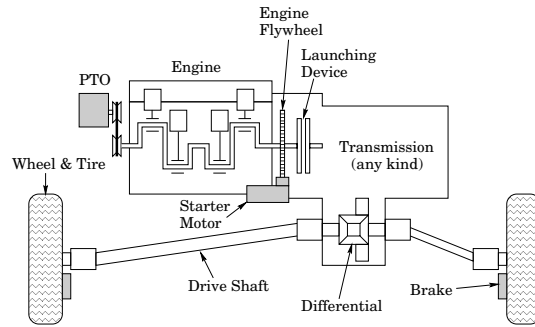


Figure 2.2: Basic (front wheel) powertrain

- the energy-specific fuel consumption [g/kWh], also known as “Brake Specific Fuel Consumption” BSFC, depends on the operating point, defined by the engine torque and speed, that fulfill the requested power;
- the BSFC varies with the power demand itself.

The BSFC is best viewed in a so called engine map. In this map various quantities may be visualized by iso-curves being a function of static engine speed and engine output torque. In the map of Figure 2.3 the BSFC curves of a 1.6 l, multi-point injection petrol engine are sketched. Also hyperbolas graphing constant engine power are drawn. The BSFC varies

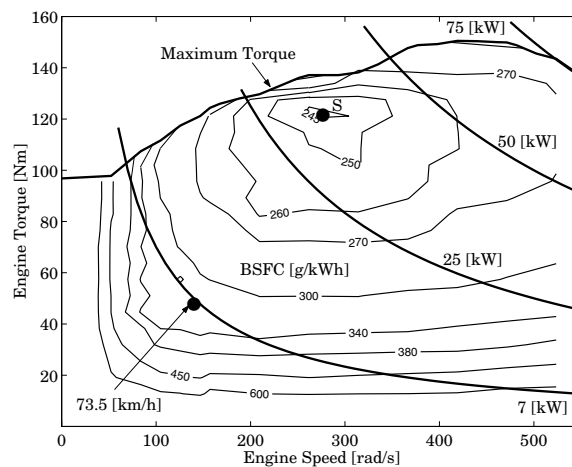


Figure 2.3: Brake specific fuel consumption (BSFC) in engine map

substantially along and between the power hyperbolas. The operating point with the lowest BSFC, indicated in Figure 2.3 by ‘S’, is termed the *sweet spot*.

The influence of the chosen operating point on the fuel economy is substantial. In an illustrative example a mid-sized passenger car runs at 73.5 [km/h], indicated by the dots in Figures 2.3, 2.4(a) and 2.4(b). Figure 2.4(a) displays the fuel consumption per traveled kilometer (DSFC) as a function of constant vehicle and engine speed. The fuel consumption per second (TSFC) as a function of engine output power is plotted in Figure 2.4(b).

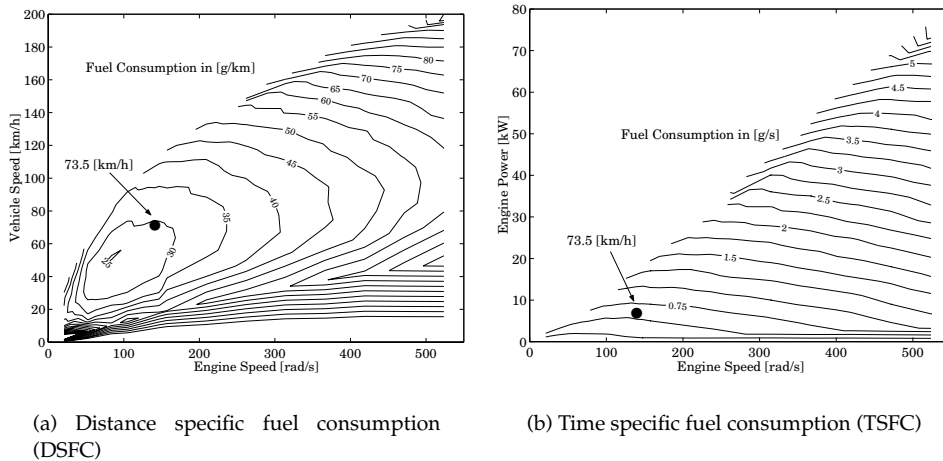


Figure 2.4: Alternative representations of the fuel consumption

Maintaining the constant vehicle speed at higher engine speeds substantially raises the fuel consumption per traveled kilometer, *cf.* Figure 2.4(a). For instance, up to twice as much fuel is consumed if the vehicle speed is kept at 73.5 [km/h] with an engine speed of 500 [rad/s]. Regarding Figure 2.4(b), a full acceleration (exploiting maximum engine power) from 73.5 [km/h] would consume about ten times more fuel!

engine improvements

Since decades many successful efforts to improve driveline component efficiency have been undertaken. The internal combustion engine has been given the most attention, leading to a multitude of solutions which improve the combustion efficiency, along with the emissions. Treating them all would go far beyond the scope of this thesis. However, the most important solutions for the petrol engine, being the engine type considered in the EcoDrive project, should receive some attention.

Variable valve timing has improved the efficiency, performance and emission quality. Advancing the intake valve timing for higher engine speeds improves the homogeneity of the air/fuel mixture and in general improves the combustion performance. This increases the engine torque or alternatively provides the same torque using less fuel. Furthermore, retarding the closing of the exhaust valve for higher engine speeds leaves part of the exhaust gases in the cylinder while the new air/fuel mixture is already entering the cylinder (overlapping of intake and exhaust period). Consequently, the mixture can be leaner resulting in further com-

bustion of unburned constituents and hence lower emissions. *Exhaust Gas Recirculation (EGR)* further exploits this technique by actively recirculating the exhaust gases through a by-pass channel controlled by a valve.

Through the combination of *variable spark timing* and metered *fuel-injection*, complete combustion (stoichiometric operation) is possible for varying engine speed, load and temperature, further reducing fuel consumption and emissions.

The fuel consumption, the emissions and the engine performance are often conflicting targets. Especially emission standards hinder the further improvement of the engine efficiency [Oppenheim *et al.*, 1994]. This is caused by the fact that engine operating conditions are often shifted to regions with less NO_x, HC and/or CO emissions, but increased specific fuel consumption (also leading to higher CO₂).

Techniques related to engine technology as described may result in a lower fuel consumption for *equal engine power* demands. On the other hand improving the efficiency of other driveline components such as the transmission and PTO will reduce the energy demand for *equal covered vehicle distance*.

2.2.2 Transmission efficiency

Only recently, improving the efficiency of stepped transmissions (MT and AT) has been given more attention, whereas that of the CVT has been a concern since *mature* versions of the push-belt CVT started to be commercially produced (early nineties). From [Kluger and Long, 1999] it is concluded manual transmissions have overall efficiency values of 96.2% and leave little room for improvement (up to 96.7% at most). Kluger and Long furthermore evaluate the overall efficiency of ATs at 85.3%, whereas the efficiency of the best current AT could be improved up to 86.3%. Finally, the overall efficiency of belt type CVTs is estimated at 84.6%, and may be improved towards 88.4% by reducing the pump losses. These hydraulic pump losses for the larger part determine the efficiency of CVTs and of ATs, and are relatively high at low transmission loads. Improved pump and hydraulic circuit design can substantially increase the efficiency of CVT and AT. The design of the pump, friction fluids and mechanical part of the CVT is subject of ongoing research. Alternatively, the actuation of the clutches and of the CVT may be (partly) electrical, thus replacing the hydraulic losses by potentially lower electrical losses. For instance, in [van Tilborg, 2001], it is shown that the pump losses in the CVT can be reduced by applying part of the pulley clamping force electro-mechanically.

Finally, the overall efficiency of toroidal or traction drive CVTs (*e.g.*, see [Machida, 1999]) is estimated by [Kluger and Long, 1999] at around 91%, and may be improved by 1.8% with the implementation of more advanced traction fluids. This type of transmission is well suited for high power applications, though production numbers are still limited.

2.2.3 Power take-off

The fuel consumption could be further reduced if also the power demand by the PTO is somehow lowered. For example, methods to improve the efficiency of the alternator are discussed in [Bürger *et al.*, 1994]. They projected a potential fuel saving of 1% when the alternator efficiency is improved by 5%. Enhancing the efficiency of all auxiliary systems is possible by increasing the on-board voltage level, giving rise to the recent development of a 42 Volt on-board grid. The alternator and starter can then be re-engineered into an integrated unit referred to as *starter-alternator (SA)*. A higher voltage leads to lower currents and reduced electric transmission losses. This is necessary for operating the increasing number of on-board electric systems, which in turn does not guarantee a lower fuel consumption altogether.

2.3 Reducing the external load

2.3.1 Vehicle mass

The increase of vehicle mass is mainly caused by higher safety and comfort standards. A better crash protection usually results in higher vehicle weight and thus fuel consumption. Vehicle weight is also increased due to the expanding amount of on-board auxiliary systems such as air-conditioning, power-assisted steering, electrically operated windows, sunroofs, mirrors, seats, door-locking, in-car entertainment, *etc.* Furthermore, these systems claim supplementary power to operate. Besides the growing demands for more safety and comfort, drivers also claim an unspoilt driving pleasure. For that reason, the enhanced engine efficiency may well be overshadowed by an increased power demand. This can also be seen in Figure 2.5 (sources

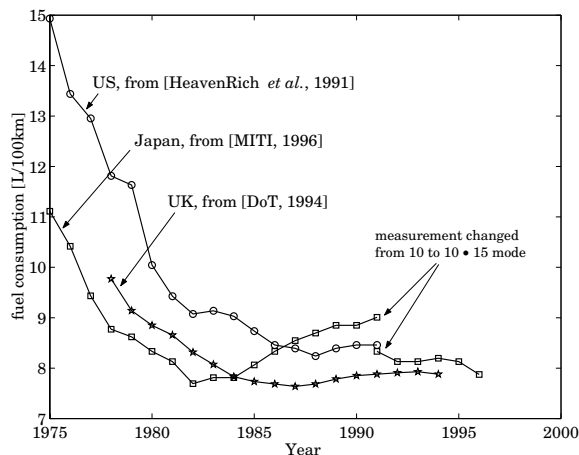


Figure 2.5: Average fuel consumption of new-sold passenger car fleet in UK, US and Japan from 1975 to 1996

from [Heavenrich *et al.*, 1991], [MITI, 1996], and [DoT, 1994]) where the fuel consumption of the average *new-sold passenger car* is shown between 1975 and 1996 for US, UK (assumed to be representative of Europe) and Japan. The absolute fuel consumption indicated by the curves can not be directly compared as such because they use different test driving cycles. The increase of fuel consumption after 1980 for Japan, which is not seen for the US and the UK, is explained by the increased use of rather inefficient vehicle electronics (for in-car convenience) and weight of the average Japanese car. The improvements in engine efficiency on the one hand, and especially the increase of auxiliary power demand on the other, start to even out in the US and the UK during the late 1980s, obviously flattening the average fuel consumption.

2.3.2 Rolling resistance

The rolling resistance of a vehicle is predominantly due to the tires, apart from negligibly small wheel bearing losses. The actual tire rolling resistance consists for a very small part of tire-road friction and for the larger part of tire deformation losses. The magnitude of these losses is determined by what might be termed 'internal' and 'external' factors. The internal factors such

as the tire material, the tire shape, and the tire size (width especially), substantially influence the rolling resistance. For example, two tire designs of the same overall size, but with different shapes and materials may differ in rolling resistance by a factor of two [Junio *et al.*, 1999]. External conditions influencing the tire rolling resistance are the tire pressure, tire load, road surface conditions, (internal and ambient) temperature, speed, dynamic conditions (wheel torque, cornering) and the wheel alignment (toe-in and camber). For instance, an additional 0.3 [bar] of tire pressure lowers the tire rolling resistance by about 7% [Junio *et al.*, 1999].

Reductions of tire rolling resistance may be accomplished by using better materials especially, and to a lesser extent by applying ‘smart’ tires (*e.g.*, monitoring and controlling the tire pressure) as well as active suspension (decreased dynamic tire load). The application of these technologies is limited by requirements for wet skid conditions, high speed driving, tire damping (noise and comfort) and cost. Nevertheless, a reduction of rolling resistance of 50% for 2006 (compared to 1999) is projected by Good Year [Junio *et al.*, 1999].

The rolling resistance is the dominant external load for vehicle speeds below circa 60 [km/h]; above that speed air drag becomes more important.

2.3.3 Air drag

The shape and size of the passenger vehicle body have changed during one hundred years of automotive technology. Frontal area and shape directly influence fuel consumption through friction with the ambient air. The car designers’ utmost challenge is to mediate between interior space and exterior aerodynamical shape and size. The air resistance is made up of the pressure drag including pressure induced turbulence drag, surface resistance and through-flow resistance. The longitudinal aerodynamical drag force on the vehicle is approximately proportional to the frontal area, the square of vehicle speed and a characteristic value c_d —better known as the air drag coefficient—depending on the body shape. Increasing comfort demands and occupants’ stature do not allow a significant further decrease of the average vehicle frontal area. For instance, the growing popularity of the Multi Purpose Vehicle (MPV), has even increased the average frontal area.

Nonetheless, continuous re-fashioning of the vehicle shape has reduced the c_d -coefficient tremendously, see Figure 2.6. The theoretical minimum of c_d lies somewhere around 0.15. The General Motors’ Precept concept vehicle, reaching $c_d = 0.163$, comes close to this minimum. For normal passenger cars, a number of important measures influence the aerodynamics. The most important measures are the decrease of the rear window angle with the horizontal axis, the smoothness and rounding of the rear window stile (C-stile) and a high but short trunk with a sharp transition down at the end. Taking such measures may lead to a higher vehicle mass because of the unfavourable ratio between surface and volume. This might be compensated by lighter materials or by improved constructional design.

The lower air resistance due to a smaller air drag coefficient leads to a higher maximum speed of the vehicle, hence requiring an increased speed ratio coverage of engine and/or transmission. The latter demands for a higher overdrive bringing the engine operating point towards lower engine speeds at virtually equal engine torque. Fuel economy can be improved by about 1% for 3% air drag reduction, [Seiffert and Walzer, 1989]. Naturally, this number depends on the combination of the specific vehicle and engine and should therefore be interpreted with care.

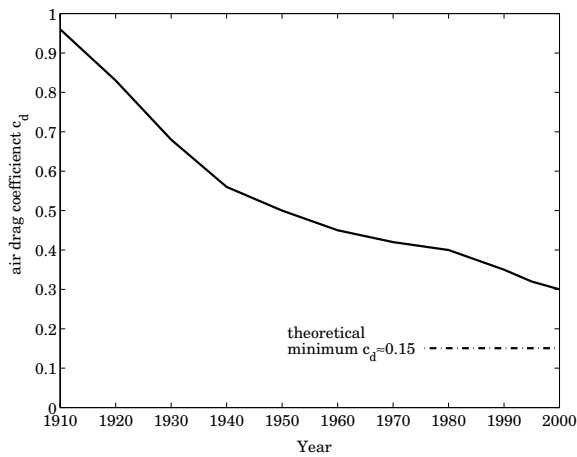


Figure 2.6: Historical trend of the average air drag coefficient

2.4 Alternative powertrain operation

Fuel economy can be improved by more optimal operation of the existing powertrain components or by extending the powertrain with more components to enhance its functionality. By such means operating regions with poor engine efficiency can be avoided. In this section, four principles which aim at more efficient engine operation, or at avoiding excessive fuel consumption otherwise, are briefly discussed. In Chapter 3, these fuel saving principles will be given more attention.

- *E-line tracking* amounts to controlling the engine in such a way that for each requested engine power the fuel consumption is minimal. For modest driving this comes down to restraining the engine speed to extremely low values.
- *Stop-Go (SG)* systems halt the engine during full vehicle stops and facilitate a new vehicle launch either by first restarting the engine and then launching the vehicle, first launching the vehicle and then restarting the engine, or launching and restarting at the same time. Clearly, the fuel otherwise consumed during engine idling can be saved.
- *Start-Stop (SS)* refers to delivering the required energy by intermittently operating the engine in the sweet spot (defined in Section 2.2.1). Because the engine power delivered in the sweet spot will generally be different (usually higher) than the demanded wheel power, some sort of energy buffer is needed, as well as a generator and motor to compensate for the momentary power surplus (while the engine is on) and power deficit (while the engine is off), respectively.
- *Brake Energy Recovery (BER)*. The mechanical energy stemming from the engine is partly accumulated in the vehicle's inertia. This energy can be recuperated whenever decelerations of the vehicle are requested by the driver. Reusing this energy for vehicle propulsion or to power auxiliary functions, in principle decreases the net fuel consumption.

In designing an alternative powertrain for the sake of a higher fuel economy, the drawbacks of such a redesign should have minor influence on the final vehicle concept, at least in proportion to the gained reduction of fuel consumption. A method for rating the fuel reduction against additional efforts and penalties is discussed in the next chapter. The following section lists some developments potentially leading to a better fuel economy, but not directly linked to vehicle technology.

2.5 Non-vehicle technology

There are a number of measures that are not directly related to powertrain or vehicle technology but are rather driven by external factors such as driving behaviour, legislation, policies, traffic management, infrastructure, *etc.* These factors are briefly illustrated in this section.

2.5.1 Driving behaviour

The behaviour of the driver and the traffic conditions strongly influence the fuel consumption. In [An and Ross, 1993] the fuel consumption as a function of *average* trip speed is measured, showing that minimal fuel consumption is reached between 65 and 80 [km/h]. On the other hand, if the fuel consumption is measured for *constant* vehicle speed this optimum lies around 50 [km/h], as will be shown in Chapter 8.

Average vehicle speed but also the number and intensity of accelerations and decelerations are highly related to the traffic conditions and the drivers' state-of-mind during a trip. Without increasing the travel time, a significant decrease of fuel consumption can be reached if the driver alters his or her driving behaviour. Theoretical studies by [Evans, 1979] and [Waters and Laker, 1980] showed that around 15% fuel reduction is possible. The evaluation of a driver-friendly fuel efficiency support tool as in [van der Voort *et al.*, 2001] showed that with a 5-speed manual transmission even 20% fuel can be saved in rural areas. Essentially, the support tool gives advice to the driver when to shift gears according to measurements of the vehicle conditions and of the actual accelerator pedal deflection.

2.5.2 Infrastructure and traffic management

Fuel consumption is closely related to the vehicle speed, which in turn is strongly influenced by the road infrastructure. In city driving the traffic flow is often hampered by frequent stop-and-go actions due to crossings, different speed of the traffic participants, *etc.*

Active control of traffic flow, also termed *traffic management* can decrease the congestion through leveling the traffic speed. Reducing the average speed by such means can also reduce the fuel consumption. Personal mobility is still the most favourable way of human transportation. On the other hand, when active control of traffic implies that traffic flow is homogenized, the distinction with public transportation becomes somewhat smaller. Traffic management therefore also requires a change in attitude of the traffic participants.

Recent investigations in intelligent vehicle guidance, platooning and automated highways look ahead in this direction. Through tight intercommunication between vehicles or indirectly through in-road sensors, active distance control between vehicles can minimize congestion and homogenize traffic density. Moreover, the safety can be increased but at the cost of individual vehicle control. Developments in this area are ongoing, mostly still encountering problems with robustness and safety.

Along with adapting traffic systems, vehicle technology itself should continuously reiterate to find a new optimum between fuel economy and the changing vehicle utilization. Governments can be effective in helping these actors to bring their influence in tune.

2.5.3 Law, policy and legislation

Speed limits set by law can manipulate the average speed in urban, rural and highway driving. On the other hand, a substantial decrease of speed limits is hardly accepted by society. Governmental legislation in the area of emissions and fuel consumption stimulate car manufacturers and research institutes in their search for new vehicle propulsion and fuel technologies. One can think of fuel taxes, emission standards and categorization of vehicles with respect to fuel consumption (using labels). Also subsidizing research initiatives in this area helps to find new ways for improving fuel economy and reducing emissions. Through educational programs, governments can make new generations more aware of the limited fossil fuel resources and the environmental impact of transportation. In this way the social basis for spending money and capacity of society into the improvement of fuel economy and reduction of emissions will get broader.

Chapter 3

Normalized Innovation Values

In practice, the most promising fuel saving principle is the one that achieves the highest ratio between fuel economy on the one hand and additional costs, size, weight, *etc.* on the other. The fuel economy obtained by exploiting an innovative idea may be termed *innovation value* whereas the mentioned penalties besides those related to development risks, complexity and driveability are termed *innovation efforts*. Hence, the most promising innovation is the one with the highest innovation values demanding the least innovation efforts. In this chapter, an attempt is made to judge the values over the efforts for the powertrain-related fuel saving principles mentioned in Section 2.4 or combinations thereof. This is defined as the *normalization* of the innovation values. Based on the normalization, the ZI powertrain proves to be the second best solution for saving fuel. The eventual decision to develop the ZI powertrain is supported by additional constraints overruling the outcome of the normalization. These constraints are set by the project target aiming at a fuel saving of 25% (the optimal solution can potentially save more) in combination with the limited project resources. The remainder of this chapter is organized as follows. Throughout this chapter, examples of so-called *hybrid* vehicles are presented. For completeness, first a number of definitions related to hybrid vehicles are given in Section 3.1. Next, in Section 3.2 the corresponding efforts, such as component efficiency, weight, driveability penalties and production costs, are discussed. In Section 3.3 the actual normalization of the innovation values is performed. Finally, in Section 3.4 conclusions are drawn with respect to the value of the ZI powertrain as a purely mechanical solution for saving fuel.

3.1 Hybrid powertrains

A *hybrid* powertrain uses different types of power sources to propel the vehicle. The power source which primarily determines the range of the vehicle, is called the *primary* source. Additional power sources are referred to as *secondary* sources.

Hybrid vehicles can be operated in four different *modes*. The *conventional* mode applies when the primary source is *mechanically* connected to the wheels and moreover is the only active power source. If besides the primary source, a secondary source is mechanically connected to the wheels and active, the *parallel* mode applies. The *series* mode refers to the situation where the primary source is *not* mechanically connected to the wheels, hence all wheel power is delivered by a secondary power source that acquires its energy non-mechanically

from the primary source. Finally, the parallel mode and the series mode can occur at the same time. That case is referred to as the *combined* mode.

It is chosen to indicate the different types of operation as *modes*, instead of reverting to the commonly used terms *series*, *parallel* and *combined hybrids*, since a hybrid vehicle can generally be operated in either of the four mentioned modes. In practice, the combined mode is mostly encountered in so-called *power-split* configurations, involving a planetary gear set.

Figure 3.1 schematically depicts a generic hybrid vehicle, capable of operating in all discussed modes. The component E represents the primary power source, whereas the wheel W on the right side of the figure represents the vehicle load. In between are a transmission T, a generator G, an accumulator A, and a motor M. The transmission T strictly has a variable transmission ratio, and possibly incorporates a planetary gear set. Fixed reductions are omitted for clarity, but may be present in any of the connections. All components may be separated by connecting interfaces, *e.g.*, mechanical (clutches) or electrical (actuation, wiring). The generator and motor can be separate devices but may also be combined into one component. In case of a flywheel as the secondary source, the motor, the generator and the accumulator are in fact all combined into a single device.

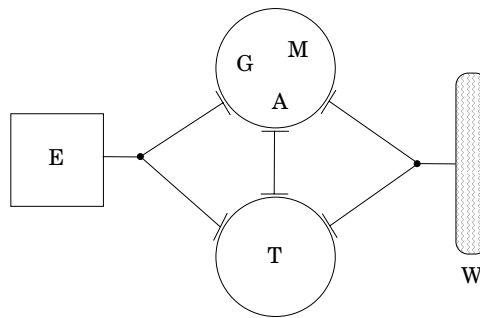


Figure 3.1: Generic hybrid powertrain configuration

As an example, the Toyota Prius powertrain is shown in Figure 3.2. Here the transmission T is a planetary gear set. The primary source E, a gasoline engine, is connected to the carrier of the planetary gear. The annulus gear is connected to the load W as well as to a secondary power source M1/G1, while the sun gear is connected to yet another secondary power source M2/G2. Both M1/G1 and M2/G2 can be operated as motor or as generator and are connected to the accumulator A. Because M1/G1 is directly connected to the wheels, it can be used as sole mover, hence the Prius is operated in series mode then. In all other cases, either the parallel or the combined mode applies. Charging the accumulator is possible using either parallel or combined mode. If the engine is delivering power, the secondary power source M2/G2 *must* always be active (motor or generator mode) to maintain a torque balance over the planetary gear set. Furthermore, the secondary source M1/G1 should always operate as a motor (either in series or combined mode) if the accumulator is fully charged.

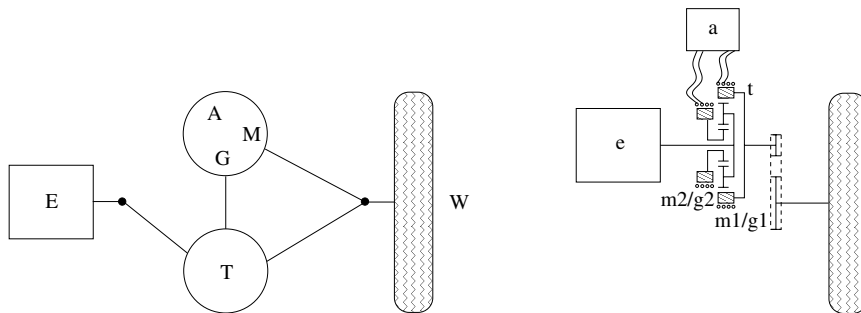


Figure 3.2: Toyota Prius powertrain (right) and its generic form (left)

3.2 Innovation values: fuel economy

First insights in fuel saving potentials are gained when mapping certain driving cycles directly onto the specific fuel consumption characteristics of the internal combustion engine. The innovation value (fuel economy) of each fuel saving principle is analyzed for the rural, city and highway driving cycle within the HYZEM (HYbrid technology approaching efficient Zero Emission Mobility) envelope and the NEDC. A driving cycle is a time representation of a requested vehicle speed trajectory, used for generating fuel consumption figures on a roller-bench with controllable brake facility (chassis dynamometer). In practice, a human driver has to follow the speed trajectory within a certain margin. Measuring the fuel consumption as such appears to be somewhat deceptive, depending on the type of powertrain. For powertrains with manual transmissions the gear changes are prescribed during the drive cycle. This is not true for (all kinds of) automatic transmissions, for which in principle the gear shift strategies—or equivalently the engine operating points—may be chosen freely.

In the calculations underlying this chapter, for simplicity the vehicle is assumed to track the reference speed exactly. Furthermore, the freedom of choosing the engine operating points is adopted here in order to fully exploit the fuel saving principles. These assumptions provide a clear understanding in the mechanisms of the four fuel saving principles.

The influence of the transmission and conversion efficiencies on the fuel saving principles is regarded separately. The efficiency is unknown a priori and maximizing it is seen as one of the developing efforts to be undertaken. The underlying computations of this section hence assume a transmission efficiency of 100%. This assumption implies that the computed fuel consumption over a particular drive cycle and according to a certain fuel saving principle will be a theoretical minimum. It is therefore interesting to investigate how close this minimum can be reached in practice. For the application under issue this is done in Chapter 8.

Using the outcome of this section, the innovation values will be corrected for efficiency and for increased weight and subsequently normalized in Section 3.4 using the efforts of various materializations presented in Section 3.3.

The fuel saving of the four principles, mentioned earlier in Section 2.4, is determined as follows:

- E-line tracking. The fuel saving of E-line tracking is determined with respect to operating lines roughly resembling operating lines seen in practice, see Section 3.2.1. Such lines are always a compromise between driveability and fuel economy.

- Stop-Go. The fuel saving due to Stop-Go operation is determined by subtracting the total amount of fuel otherwise consumed during engine idling at vehicle halt.
- Start-Stop. The fuel economy potential can be computed by assuming that the required energy is generated intermittently in the sweet spot if the momentary drive power is below or equal to the sweet spot power P_{ss} . Above P_{ss} , E-line tracking is performed.
- Brake energy recovery. The recovered energy can be used in a number of ways making it hard to determine the fuel saving potential unambiguously. In this section, the accumulated fuel required to deliver the energy needed for vehicle acceleration is assumed to be delivered in the sweet spot and is here assumed to be fully recovered.

3.2.1 Reference vehicle

The vehicle that will be used as a reference in all the comparisons throughout this chapter is a mid-size passenger car, that weighs 1360 [kg], has a rolling resistance of 55 [Nm] and a c_d value of 0.31. It is termed the *reference vehicle* and in fact constitutes the test vehicle with two occupants (see Chapter 8). The engine is a 1.6 l 4-cylinder petrol engine with a maximum power rating of 75 [kW] at 540 [rad/s], and is assumed to be operated on the *reference operating line*, that is defined further on. The engine used in this study is not that of the test vehicle though it is largely comparable. The E-line collects the engine operating points which are fuel-optimal for a given power level, and can be uniquely determined for any engine. Figure 3.3 depicts the E-line and operating lines $OL_{x\%}$ comprising operating points with $x\%$ higher fuel consumption compared to the E-line. Also depicted is the *Wide Open Throttle (WOT) line*, which represents the maximum engine torque as a function of the engine speed. The E-line

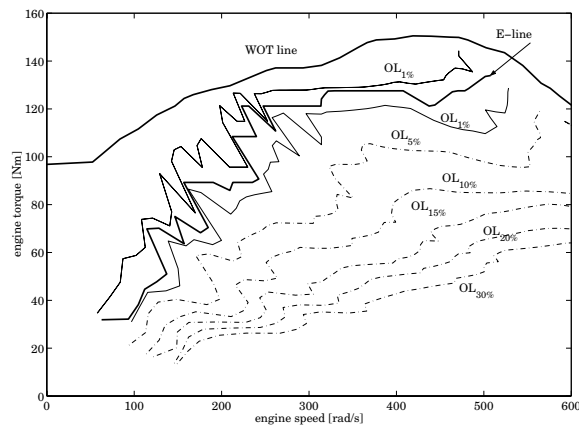


Figure 3.3: E-line and operating lines with $x\%$ more fuel consumption

is rather jagged because of the limited number of measurements combined with the small differences in fuel consumption around the E-line, as is shown by the two lines indicating a margin of 1% extra fuel consumption with respect to the E-line. In practical implementations, a smoothed version of the E-line is used.

In today's passenger cars, if equipped with either a CVT or AT, an operating line roughly between the $OL_{15\%}$ and $OL_{20\%}$ lines is applied for stationary situations. Using such an operating line results in an acceptable driveability but clearly penalizes the fuel economy, as compared to the E-line. Here, the $OL_{15\%}$ is chosen as the reference operating line for computing the fuel saving potentials. This operating line is highly similar to those used in 4-AT and CVT in 'performance mode'.

3.2.2 Influence of driving cycles

There exists a wide variety of certified driving cycles, showing large differences in power requests, dynamics, average speed, *etc.* From these cycles, the HYZEM and NEDC are chosen to determine the innovation values. The HYZEM cycle consists of three subcycles, namely the urban (city), rural and highway cycle. Since the HYZEM was obtained by averaging typical vehicle usage in Europe it is thought to be a good representation of everyday driving. The potentials of the four fuel saving principles depend highly on the considered cycle.

In Figure 3.4 power histograms of the HYZEM (urban, rural, highway) and NEDC cycles are shown. The required power is calculated using a model of the reference vehicle. The power histograms are obtained using steps of 1 [kW]. Especially for the NEDC and the urban drive cycle, the time fraction spent at zero power (vehicle halts) is remarkably large. Furthermore, power demands larger than half the maximum engine power are rare on the depicted driving cycles.

3.2.3 Fuel economy

In this section, the fuel savings with respect to the reference operating line $OL_{15\%}$ are evaluated, using the mentioned drive cycles, for each of the four fuel saving principles.

E-line tracking

The accumulated fuel consumption in [g] and the percentage of fuel consumption reduction for the four driving cycles are shown in Table 3.1. From this table it is apparent that the

CYCLE	$OL_{15\%}$ [g]	E-LINE [g]	E-LINE FUEL SAVING [%]	IDLE [g]	STOP-GO FUEL SAVING [%]
NEDC	556.7	493.5	11.4	64.4	11.6
rural	568.4	498.0	12.4	19.0	3.3
urban	205.1	183.5	10.5	30.5	14.9
highway	2460.3	2142.1	12.9	13.0	0.5

Table 3.1: Fuel savings using E-line tracking and Stop-Go

fuel consumption reduction for E-line tracking is between 10 and 13.0%, approximating the maximally achievable fuel saving ($(1 - 1/1.15) \times 100 = 13\%$) of E-line tracking with respect to the $OL_{15\%}$. The 13% fuel saving is reached when the contribution of engine idling converges to zero, which is almost the case on the highway subcycle, where a relatively short standstill time applies (5.5% of the total cycle time). Furthermore, the average power level on this cycle is high compared to the other cycles.

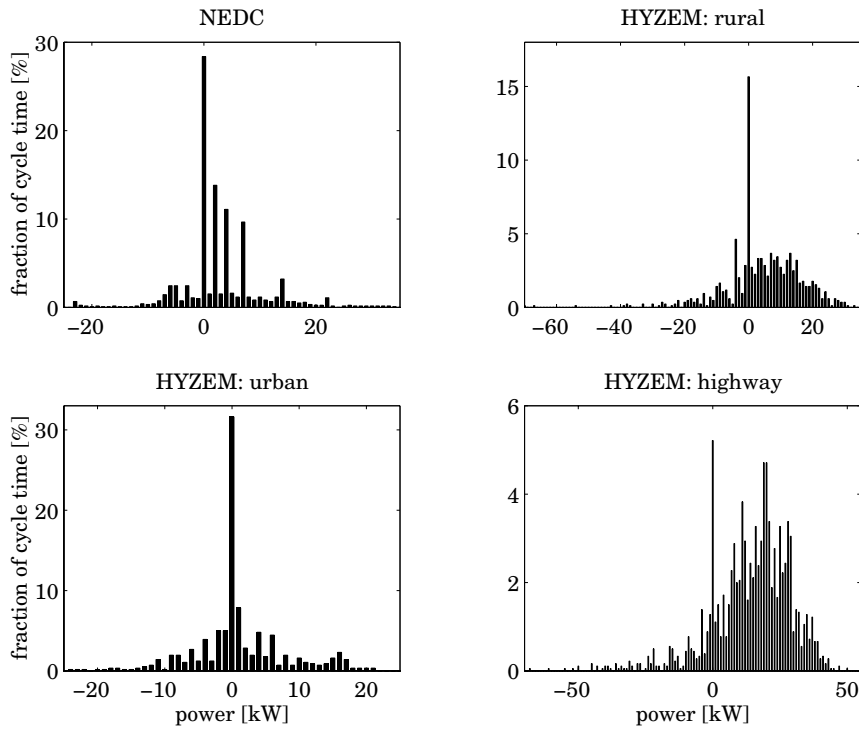


Figure 3.4: Time histograms of power distribution over the drive cycles

Stop-Go

The fuel savings when using Stop-Go (also see Table 3.1) can amount up to 15% on the urban subcycle, assuming that the restarts of the engine require no additional energy. Also, incomplete combustions during starting, leading to a slight increase in fuel consumption and emissions are not treated here. Hence it is assumed that the fuel saving exactly equals the accumulated idle fuel consumption (where the time-specific idle fuel consumption is taken to be 0.23 [g/s]). The impact of Stop-Go on the highway subcycle is obviously limited, again due to the limited contribution of engine idling.

Start-Stop

The Start-Stop principle can be best explained looking at the specific fuel consumption (BSFC) of the engine as a function of the output engine power. For the E-line and the $OL_{15\%}$ this BSFC characteristic is plotted in Figure 3.5. From this figure it can be concluded that around $P_{ss}=32$ [kW] there is a minimum, previously called the sweet spot. Consequently, fuel can be saved when for all requested powers below P_{ss} , the drive energy is delivered in the sweet spot operating point. Operating the engine in the sweet spot requires intermittent (duty-cycled) operation of the engine to match the generated energy to the required drive energy. Further-

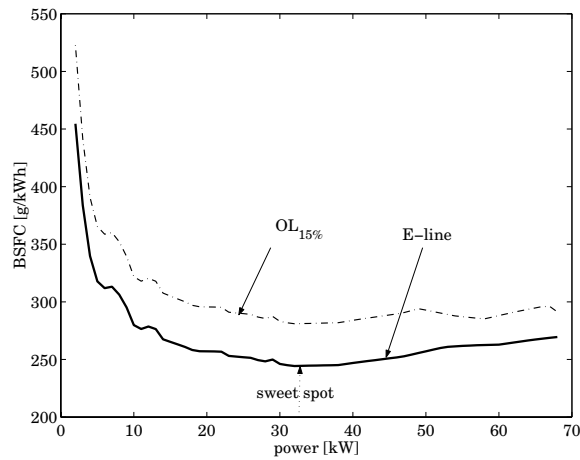


Figure 3.5: Brake specific fuel consumption for the $OL_{15\%}$ line and the E-line

more, an accumulator is required to store the generated energy. Apart from that, Start-Stop necessitates an extra motor and generator to compensate for the momentary power deficit and surplus, respectively. For power requests beyond P_{ss} the engine must be operated on a regular operating line. In this case, the E-line is chosen.

The maximum fuel saving potential for the Start-Stop principle with respect to $OL_{15\%}$ and with respect to E-line+Stop-Go, is shown in Table 3.2. The latter fuel savings (last column) are included to show the merit of Start-Stop for requested power levels larger than zero and smaller than P_{ss} . Note that Stop-Go and E-line tracking for power levels beyond P_{ss} were chosen to be an integral part of the Start-Stop principle.

CYCLE	$OL_{15\%}$ [g]	START-STOP [g]	FUEL SAVING [%]	FUEL SAVING W.R.T. E-LINE + STOP-GO [%]
NEDC	556.7	347.5	37.6	14.6
rural	568.4	419.4	26.2	10.5
urban	205.1	119.8	41.6	16.2
highway	2460.3	2018.4	18.0	4.6

Table 3.2: Fuel savings using Start-Stop

A number of observations are made. First, the saving potential is especially high for city driving (urban and NEDC). This can be explained by the poor engine efficiency at low output power levels even in case of E-line tracking, in combination with the large share of required power levels beneath P_{ss} for such cycles. Second, the improvement of fuel economy over E-line+Stop-Go is rather limited for the highway cycle. For such a cycle, the power histogram is largely concentrated around P_{ss} and beyond. Moreover, around the sweet spot the specific fuel consumption is already quite low and rather insensitive for the power level, *cf.* Figure 3.5. The resemblance between the fuel savings for urban and NEDC with respect to E-line+Stop-Go may become clear when observing the similarity between the power histograms of the two

(see Figure 3.4).

brake energy recovery

In principle, the kinetic energy of the vehicle that is normally dissipated at the wheel brakes can be recovered. In this section, a number of rigorous assumptions underlie the calculated fuel saving potentials of brake energy recovery:

- all vehicle braking is performed by a generator. This assumption implies radical demands on the maximum power of the generator and control periphery as well as its reliability and safety;
- the kinetic energy is completely re-used for propulsion of the vehicle;
- all transmission and conversions involved occur with 100% efficiency.

In Section 3.3, these assumptions are partly released. Table 3.3 lists the computed savings using these assumptions. The first (numerical) column repeats the fuel consumption figures for $OL_{15\%}$. The above assumptions imply that the required drive energy exactly equals the energy which is dissipated by the road load. The fuel needed for delivering this energy is calculated by operating the engine in the sweet spot, and hence is the minimal fuel consumption theoretically possible with the reference vehicle and the adopted engine. Delivering the road load energy using other strategies than sweet spot poses problems of ambiguity. The recovered brake energy can be reused for assisting the engine in a number of ways. The strict relationship between the requested drive power and specific fuel consumption may then disappear. This ambiguity does not occur when persistently delivering the cycle energy in the sweet spot. This implies that the computations assume that the Start-Stop principle is integrated in brake energy recovery.

Note that such operation is impossible during prolonged driving at power levels higher than P_{ss} . However, in the highway cycle, the power levels above P_{ss} (32 [kW]) are linked to short term vehicle accelerations, while the average power level on this cycle is still below P_{ss} . Also, in the computations it was implicitly assumed that the surplus of requested power beyond P_{ss} is delivered by the additional accumulator, in order to keep the engine in the sweet spot.

CYCLE	$OL_{15\%}$ [g]	ROAD LOAD IN SWEET SPOT [g]	FUEL SAVING [%]
NEDC	556.7	269.8	51.5
rural	568.4	284.8	49.9
urban	205.1	65.6	68.0
highway	2460.3	1823.2	25.9

Table 3.3: Fuel savings using brake energy recovery and Start-Stop

3.3 Innovation efforts

In this section a number of innovation efforts is defined and evaluated for the fuel saving principles. Somehow quantifying these efforts—often just using relative ranks such as ‘high’, ‘low’, ‘average’—provides ways to compare the saving principles. Efforts, when applicable, treated for each principle are:

- additional fuel economy penalties depending on the specific technology and configuration (transmission and conversion efficiencies, supplementary weight, *etc.*);
- driveability aspects such as instant power reserve, engine restarts, noise-vibration-harshness (NVH), comfort, predictability;
- impact on total vehicle design, for example packaging, vehicle dynamics, safety;
- additional costs of development, manufacturing, materials;
- complexity leading to penalties for robustness, durability, maintenance, control development;
- environmental aspects such as recyclability, emissions.

3.3.1 E-line tracking

transmission efficiency

The fuel economy for E-line tracking is influenced by the limited transmission efficiency η_T . Especially in the case of cycles showing insignificant idling phases, the influence of the transmission efficiency on the fuel economy is near to linear. For instance, increasing η_T from 80 to 100%, reduces the fuel consumption of the reference vehicle (at the OL_{15%}) on the urban cycle by 13.6%. For the highway cycle this fuel economy improvement is 18.6%, that is almost the transmission efficiency difference, 20%. Lowering the efficiencies of two identical vehicles, one controlled at the OL_{15%} and the other at the E-line, hardly influences the *relative* fuel saving (less than 0.5% when altering η_T from 80 to 100%).

driveability

Driveability is for the larger part determined by the instant availability of power when pressing the accelerator pedal. The so-called *power reserve* is the product of the actual engine speed and the *torque reserve*, where the torque reserve is defined as the difference between the actual and maximum (WOT) engine torque. As can be seen in the engine map (Figure 3.3), when for a given power level the engine is operated at a higher engine speed and a larger torque reserve, a much larger power reserve results at the expense of fuel economy. This observation is more exemplified in Figure 3.6, where the *power reserve* is plotted against the actually delivered engine power. The driveability is improved tremendously when leaving the E-line for an operating line below it. For instance, choosing OL_{15%} degrades fuel efficiency by 15% but increases the power reserve by a factor 4 to 7. The dashed line indicates the maximum power reserve possible, truncated by the engine speed that corresponds to maximum engine power. All operating lines coincide at this line, tending to zero power reserve when approaching the maximum engine power (75 [kW]).

In the previous reasoning it was assumed that the engine torque can be changed instantaneously and without penalty. Changing the engine speed could (eventually) increase the output power as well, though the dynamic response of the vehicle—and thus its driveability—is penalized greatly when the engine acceleration is too large.

The physical background for this can be found in the primary-sided or, for short, *primary inertia*, *i.e.*, the total inertia of the components directly connected to and including the engine. Although the primary inertia is relatively small compared to the vehicle inertia, for good driveability it is of great relevance that the engine can be swiftly accelerated by *shifting down*

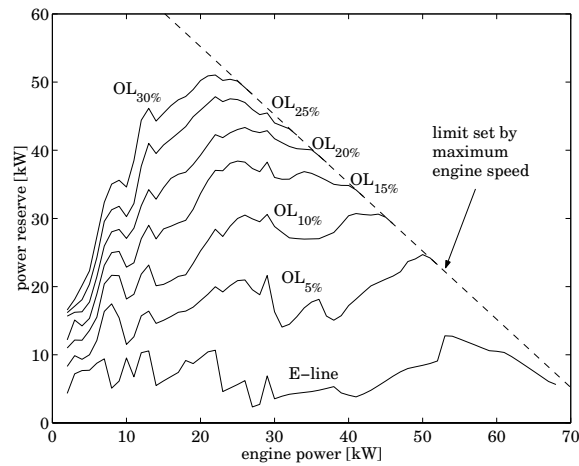


Figure 3.6: Power reserve as a function of stationary power for various operating lines

the transmission, *i.e.*, lowering the transmission ratio (defined as output speed divided by input speed). The engine power reaches its maximum at a fairly high engine speed. If the transient to this maximum power is required to be fast, the acceleration of the primary inertia (shortly) requires a power level similar to the power needed for the actual propulsion of the vehicle. When in such a case the engine was operating at low speed and high torque, *i.e.*, with a small power reserve, fulfilling an acceptable power transient is deemed impossible. Instead, to facilitate the acceleration of the primary inertia power flows from the vehicle to the engine, consequently shortly decelerating the vehicle instead of accelerating it.

When shifting down the transmission more slowly, the increase of wheel power might show a latency as the available power reserve is just enough to accelerate the primary inertia and cannot be used for a prompt increase of wheel power. This degrades the sensitivity of the accelerator pedal as the requested higher power is delivered after the primary inertia has accelerated. This phenomenon is referred to as ‘jet start’ (also known as shift-shock, rubber belt effect, torque hole, worn clutch effect). Jet start behaviour is known from aircraft propulsion, where initially all combustion power must be used to accelerate the turbines before the increased engine power can be used to propel the aircraft. For pedal back-out the phenomenon also occurs but then reversely, because the instant decrease of power is counteracted as the engine speed decreases.

Jet start can be minimized by persistently operating the engine at high speeds at the expense of fuel economy, for example using the line $OL_{15\%}$. Even then, the transmission ratio shift speed cannot be arbitrarily high, so an advanced control strategy is required to yield an acceptable compromise between fuel economy and driveability. The advantage of using controls (software) to counteract the driveability problem is that such a solution can be flexible and cheap, as opposed to rigid and generally more expensive hardware solutions. On the other hand, pure hardware solutions will be more robust and often inherently stable, whereas software solutions cannot extend physical system limitations. The additional costs for modified hardware (and to a lesser extent, software) largely depend on production numbers.

An example of a pure hardware solution is lowering the primary (engine) inertia while simultaneously increasing the number of cylinders in order to compensate for the lack in torsional damping, as suggested, *e.g.*, in [Guo *et al.*, 1988]. Such a solution is quite expensive and moreover rather ineffective, since the remaining inertia can still adversely influence driveability. If the primary inertia were zero, the engine output torque would be independent of the engine acceleration. The ‘Zero Inertia’ solution, to be elucidated in Chapter 4, will be shown to partly realize this.

If the compromise between fuel economy and driveability is considered unacceptable, E-line tracking demands an additional power source. The additional power source has to fill up the power gap between the actual power level and a (higher) requested power level. This should be done as long as the engine itself has not reached the requested power level yet, *i.e.*, during acceleration of the engine through altering the transmission gear ratio.

Figure 3.7 shows an illustrative example of this mechanism. In the example, it is assumed that the driveability level reached with the $OL_{15\%}$ is acceptable in practice. In other words, the additional power source should at least raise the power reserve of E-line tracking up to the power reserve reached when tracking the $OL_{15\%}$, see Figure 3.6. The left plot in Figure 3.7 depicts the engine combustion power $P_{\text{combustion}}$, the power from the primary inertia P_{inertia} , and their combined total $P_{\text{e,total}} = P_{\text{combustion}} + P_{\text{inertia}}$. The right plot shows the wheel power P_{desired} as it is assumed to be desired. To arrive at the desired power, an additional power, depicted in the middle as P_{assist} , is needed. In this example, a stepwise power transient from 20 [kW] (roughly corresponding to a stationary vehicle speed of 110 [km/h]) to 50 [kW] is desired. Operating on the $OL_{15\%}$, this step can be performed without increasing the engine speed, see Figure 3.6. When starting from the E-line, the engine power reserve is only 10 [kW], hence a power assist source of at least 20 [kW] is needed. However, for a prolonged increase of wheel power, the engine must be accelerated to arrive at a speed where it can maintain the desired power level of 50 [kW]. In this example the engine speeds up from 230 [rad/s] to 330 [rad/s] (corresponding to 20 and 50 [kW] on the E-line, respectively) in a time interval $\Delta t = 0.8$ [s]. Hence, an additional power P_{inertia} between 7 and 10 [kW] is required to perform the acceleration of the engine inertia. As a result, the necessary power level P_{assist} of the assist source amounts up to 27 [kW], such that $P_{\text{e,total}} + P_{\text{assist}} = P_{\text{desired}}$.

power assist sources

Examples of power assist solutions are:

- electric motor + battery
- electric motor + battery + ultracapacitor
- flywheel + transmission
- flywheel + electric motor

Table 3.4 lists some relevant weight-specific ($[\cdot/\text{kg}]$) quantities for a number of power source technologies and related components. In this table, PM refers to permanent magnet, EM means electric motor (synchronous and asynchronous), NiMH is Nickel Metal Hydride, Li-ion means Lithium-ion, FESS refers to Flywheel Energy Storage Systems and embodies high speed flywheels (carbon-glassfiber composites) in vacuum casing combined with a directly connected electric motor. The ZI flywheel refers to the low speed, steel flywheel that is used in the ZI powertrain, and is discussed in [van Druten, 2001]. Gearing and clutches are included to show the possibly needed efforts for extracting power mechanically. The specific values for

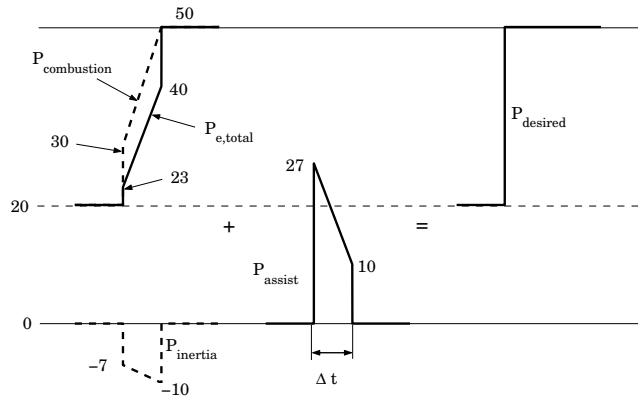


Figure 3.7: Realization of a power transient; power levels in [kW]

	P [kW/kg]	V [l/kg]	E [Wh/kg]	C [€/kg]	η [%]	L [cyc.]
PM synch. EM	1	0.3	–	?	87–92	
asynch. EM	0.4	0.7	–	15–80	85	
NiMH battery	0.18–0.9	0.6–1.3	17–100	10–50	65–85	$1-2 \cdot 10^3$
Li-ion battery	0.15–1.4	0.6–0.7	30–120	15–100	90	$> 10^3$
ultra-capacitor	1–5.5	0.8	1–50	> 10	85–98	$> 5 \cdot 10^5$
flywheels (FESS)	0.75–1.5	0.4–1.0	2–50	30	83–90	$> 10^7$
ZI flywheel	1.5–3.5	0.14	0.2–2	10	98–99	$> 10^8$
(planetary) gearing	1–3	0.3–0.8	–	10	96–99	$> 10^7$
clutch (slipping)	1.5–2	0.3	–	10	50	$< 10^5$

Table 3.4: Specific values: P=specific (peak) power, V=specific volume, E=specific (peak) energy, C=specific cost, η =conversion efficiency into mechanical or electrical power, L=lifespan.

clutches are valid for a slipping clutch, since those situations are limiting the power density, especially. Values are taken from [Dietrich, 2000], [Lehna, 1998], [Paefgen and Lehna, 1997], [Thoolen, 1993], [OTA, 1995] and [Kok, 1999] and include the corresponding power-electronics and cooling in case the energy domain is electrical. Some exceptions are not included in this table. For instance, [Dietrich, 2000] reports on *alu-elco* capacitors that reach specific power values of 10 [kW/kg] though always in combination with specific energies no higher than 0.01–0.1 [Wh/kg]. Furthermore, American Flywheel Systems, in conjunction with Honeywell claims energy densities which seem very high (over 130 [Wh/kg]) relative to other flywheels that have been built, though no official performance publications exist [OTA, 1995]. The lifespan of the ZI flywheel is deemed higher than FESS because the material stress is far below the maximum allowable value, and moreover, the bearing speeds are lower. Considering this table the following observations are made:

- the ultra-capacitor and the ZI flywheel have the highest specific power. The latter shows low energy density;

- batteries excel in energy density but are costly and lower in efficiency and lifespan;
- FESS possesses mediocre figures in every category; lifespan, however, is exceptional.

Some of the technologies are also graphically presented in a spider diagram, see Figure 3.8. Webs lying further outward indicate higher ranking, and thus lower efforts. For that purpose, specific cost and volume are inverted, whereas for the lifespan L , logarithmic values are used.

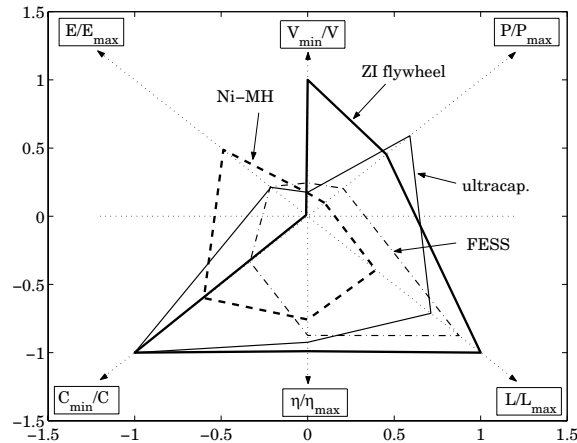


Figure 3.8: Spider diagram for comparison of innovation efforts related to various power sources, 'min' and 'max' respectively correspond to the minimum and maximum of the specific values in Table 3.4

An example power assist system is elaborated, for a power level of 27 [kW] and energy contents of 18 [Wh]. The power specification is based on the discussion in the above section, where a power assist level of 27 [kW] was concluded to be necessary for an acceleration from 110 [km/h], when operating the engine on the E-line. For lower vehicle speeds, the power requirements are smaller, mainly because the difference in engine power reserve between the E-line and the $OL_{15\%}$ decreases. On the other hand, the mentioned difference in engine power reserve increases with higher vehicle speed, in principle yielding higher power assist demands. However, the acceleration performance from vehicle speeds far beyond 110 [km/h] is considered to be less relevant in practice. The energy contents specification is obtained as the sum of the kinetic energy increase for the maximum speed transient (approximately from 100 [rad/s] to 550 [rad/s]) and the combustion energy that is lacked during the transient time interval Δt (Figure 3.7).

For these specifications, a mechanical system with ZI flywheel is compared with two electrical power assist systems, one with a NiMH battery and one with an ultra-capacitor, see Table 3.5. The ZI flywheel system clearly outperforms the other two. The NiMH system is least attractive, especially with respect to weight and total efficiency. Furthermore, both electrical systems are more expensive by an order of magnitude. On the other hand, the electrical systems can potentially be used for other functions in a more flexible way. As a commercially available example, the Honda Insight uses a 10 [kW] (peak) neodymium PM brushless DC

	mass [kg]	volume [l]	cost [€]	efficiency [%]
asynch. EM + NiMH	126	103	4970	41
asynch. EM + ultra-cap.	78	55	3330	60
ZI flywheel + gearing	34	16	340	91

Table 3.5: Comparison between three power assist systems for 27 [kW], 18 [Wh]

motor weighing approximately 50 [kg], a 0.94 [kWh] NiMH battery-pack weighing 20 [kg], and an ultra-capacitor of circa 6 [kg]. Besides, a high-density inverter is present which operates as a DC-DC converter as well as a motor cooler. In total, the additional weight of the secondary power source of the Honda Insight, which is designed for power assist and Stop-Go operation, is around 75 [kg]. The additional weight adversely affects fuel economy. The combined effects of efficiency and weight are evaluated in Section 3.3.

An interesting (not commercially available) example of a hybrid system for application in the upper-size vehicle class is the so-called *E-Automat* developed at the University of Chemnitz [Tenberge, 2001], which combines an existing 6-AT with a circa 10 [kW] electric motor.

miscellaneous efforts

Apart from the fact that an additional power source is needed to solve the driveability problem associated with E-line tracking, a CVT is required to exactly track the E-line. In case a stepped transmission is used, some penalty on the fuel consumption reduction is to be expected. On the other hand, the fact that the transmission efficiency of a CVT is generally lower than that of a stepped transmission (especially MT) will partly cancel out the obtained fuel reduction [Yamamoto and Aoki, 2000]. Moreover, for E-line tracking the transmission must be automatic (AT or CVT) or automated (Automated Manual Transmission, AMT). Furthermore, the ratio coverage of the transmission must generally be much larger than that of commercially available stepped transmissions and even CVTs. However, the penalty on fuel consumption reduction when using a 6-AT, 6-AMT or CVT (ratio coverage between 5 and 6) is comparatively small [Hofmann *et al.*, 1998]. Additionally, requiring the ratio coverage to be much higher necessitates significant modifications (*e.g.*, larger transmission size, '*i*²-transmissions' [Höhn, 1994; 2001]). Finally, an electronic throttle (drive-by-wire) is necessary, but is getting more common in modern passenger cars anyway and the additional cost is relatively small.

The remaining efforts are related to software development especially. Drive-by-wire poses additional safety and reliability issues. Furthermore, E-line tracking tends to decrease CO₂ emissions but increase NO_x, thus new engine management strategies dedicated to E-line tracking are mandatory. For a CVT or a wide-spread 6-AT, manufacturing costs and complexity are relatively high. The production numbers for AT are much higher than for CVT and the latter is still maturing with regard to durability, robustness and maintenance infrastructure. Operating the engine at very low speeds and high torques may introduce additional problems with respect to NVH. On the other hand, cruising at low engine speeds is generally associated with high comfort.

The additional power source may be used for other functions as well, *e.g.*, as a starter-alternator. Such a machine is well equipped to meet the increasing electric power demands (such as airconditioning, power steering and brake assist), which are debit to the increased research into a 42 Volt on-board electrical net. Furthermore, a starter-alternator but also a low speed flywheel may be used to implement a Stop-Go system, *i.e.*, engine shutdown at vehicle standstill. This is the topic of the following section.

3.3.2 Stop-Go operation

Stop-Go, like E-line tracking, requires an additional power source. Different technologies can be thought of to facilitate the frequent engine restarts, that is an electric motor, a flywheel, *etc.*

system requirements

The engine speed where combustion is resumed is a trade-off between starting-time and power demand on the one hand and emissions and noise on the other. Also, when the launching clutch is engaged after engine restart, the engine torque must be sufficient to propel the vehicle. When assuming the engine must be accelerated towards idle speed (around 800 [rpm]) within 0.15 [s], the power and energy requirements for Stop-Go are 12.6 [kW] and 0.26 [Wh], respectively. In case of an *impulse-start* (*i.e.*, using inertia force to start the engine, see [Vroemen, 2001]), the power requirements can be lower, but the starting-time may be longer if the inertia has to be accelerated first.

efficiency

The efficiency of the additional power source is important for the absolute amount of energy needed for an engine restart. The additional losses (*e.g.*, due to an increased mass) when not using the extra power source deteriorate fuel economy. Depending on the way the energy required for Stop-Go is subtracted from the powertrain, the fuel saving potentials may vary. For instance, when combining Stop-Go with brake energy recuperation, the fuel savings due to Stop-Go are as large as indicated in Table 3.1. On the other hand, when the energy is generated by the engine running in arbitrary operating points, the absolute fuel saving is as large as the fuel required for idling minus the fuel required for generating the accumulated restart energy. If the restart energy is generated in the sweet spot an unambiguous upper limit for the fuel saving can be obtained. Incorporating this as well as 50% efficiency (average) for the Stop-Go system itself (see Table 3.6), the *deterioration of the fuel saving* amounts up to just 0.3% for the urban and the NEDC cycle, whereas for the other two cycles the difference is even less significant.

In Stop-Go, the efficiency of the transmission between engine and wheels does not influence the *absolute* fuel-savings, but the *relative* savings instead. A decrease in fuel-consumption due to an improved transmission raises the relative fuel-savings for Stop-Go. For example, the fuel consumed on the urban cycle decreases by 13.6% when improving the transmission efficiency from 80 to 100%, while the potential relative fuel-savings from Stop-Go increase from 12.8 to 14.9%.

Table 3.6 compares the three systems from Table 3.5, but now for Stop-Go application. The two electrical systems are assumed to use *direct-start* (starter-alternator directly connected to the crank shaft), the flywheel system naturally uses impulse-start. An impulse-start system, whether purely mechanical or 'semi-electrical' (*i.e.*, the rotor of the starter-alternator is used as inertia) always requires an additional clutch. Again the mechanical solution offers advantages

	mass [kg]	volume [l]	cost [€]	efficiency [%]
asynch. EM + NiMH	56	46	2205	41
asynch. EM + ultra-cap.	35	25	1470	60
flywheel + gearing + clutch	20	9	200	49

Table 3.6: Comparison between three Stop-Go systems for 12 [kW], 0.26 [Wh]

over the two electrical systems, although the total efficiency is better for the ultra-capacitor variant.

driveability

In commercially available Stop-Go systems, the vehicle response to accelerator pedal motions is delayed, because none of them simultaneously start the engine *and* launch the vehicle. The combined time needed for engine restart followed by possible clutch-actuation delays, should not exceed approximately 0.2 [s]. Longer delays are known to cause annoyance and lack of confidence by the driver. The ZI Stop-Go solution, as treated in Part III, is able to immediately launch the vehicle and meanwhile restart the engine. The potential for acceptance is expected to be higher this way. For Stop-Go systems in general, the frequent engine restarts should be more refined and silent, for reasons of comfort.

miscellaneous efforts

The reliability of the engine start should be increased by an order of magnitude with respect to conventional starter systems, because of the more frequent engine restarts. Also, some dedicated type of (battery or flywheel) State-Of-Charge (SOC) management must anticipate for a possible energy deficit, and consequently decide not to shut down the engine.

The engine emissions can be lower than in a conventional engine start. They largely depend on the engine temperature and on the engine speed where combustion is resumed. More importantly, the temperature of the catalytic converter should not drop dramatically during engine shutdown. Straightforward solutions include heating and encapsulation of the catalyst, see [Kok, 1999]. The power take-off supply must be taken over by the secondary power source while the engine is shutdown.

A possible additional function of starter-alternators is active oscillation attenuation, for the driveline and for the engine especially, see [Zeyen and Pels, 1997]. Other than actively, the rotor of an electric machine will also attenuate oscillations in a passive way, mechanically and electrically. Because the additional power source can replace the conventional engine-flywheel, the impact on overall vehicle design may be relatively small, though larger than for E-line tracking due to the significant changes in vehicle operation.

3.3.3 Start-Stop operation

The efforts linked to duty cycled engine operation are related to the following three types of operation and the transitions between them:

- engine on: sweet spot operation
- engine off: driving on secondary power source
- conventional driving beyond sweet spot

Start-Stop at least requires the series mode. In terms of the definitions from Figure 3.1, the primary power source E then charges the accumulator A by the generator G while the motor M propels the wheels W. Depending on the accumulator's SOC, the primary source E is shut down intermittently. Start-Stop can also be realized using parallel mode, but then the series mode has to be incorporated as well. When E directly propels the wheels W, G diverts the surplus of power (delivered in the sweet spot) into A. When A is fully charged either M or E

should propel the vehicle. The former then equals the series mode, whereas the latter in fact is conventional driving.

component efforts

For sweet spot operation the surplus of power varying from zero to P_{ss} has to be stored in the accumulator. The transmission between the primary and secondary energy source has to be able to split P_{ss} into a varying power P_w to the wheels and a power $P_{ss} - P_w$ to the accumulator. Hence the generator, accumulator and motor have to be dimensioned such that powers maximally up to P_{ss} can be dealt with. The primary source must be shut down when either the SOC of the accumulator has reached its upper limit, or when the power request is below P_{ss} and the SOC has not reached its lower limit yet. The primary source must be restarted whenever the SOC drops below the lower limit or when the power request is higher than P_{ss} . This manner of engine operation requires sophisticated controls in order not to impair driveability under the constraint that fuel economy should be optimized. This is not always as straightforward as it seems. For instance, consider a stationary situation where the primary power source is shutdown and the secondary source is delivering a power slightly below P_{ss} . If the driver suddenly asks for a large increase in power, the primary power source must be restarted quickly. Clearly, the power reserve to restart the primary source is close to zero, and hence insufficient. In order not to withdraw this power from the vehicle, yet another secondary source is needed. The Nissan Tino [Matsuo *et al.*, 1999] operates as such. The situation is even worse in the Toyota Prius (recall Figure 3.2), where electric motor M2/G2 is responsible for restarting the engine E, and in doing so actually exerts a negative torque at the wheels through the planetary gear. Moreover, to enable the switching between the sources, clutches or some kind of infinitely variable transmissions are needed.

efficiency

The efficiencies of the conversion and transmission of energy greatly influence the fuel saving potential. Let E_{cyc}^+ be the energy needed at the wheels for driving a certain cycle, and E_{cyc}^- the potentially recoverable energy which is normally (*i.e.*, in a conventional vehicle) dissipated at the brakes or in the engine. The actually recovered energy E_{BER} will generally be smaller than E_{cyc}^- if the generator power is limited. The net energy that is minimally needed for all but the vehicle's kinetic energy is $E_{cyc} = E_{cyc}^+ - E_{cyc}^-$. If part of this energy is drained from the accumulator and not *replenished* before the end of the driving cycle, the type of operation is called *charge depleting* [Müller and Köhle, 2000]. If on the other hand no charging from outside the vehicle takes place during the driving cycle, the vehicle is said to be *charge sustaining*. If the vehicle is charge sustaining and, moreover, the accumulator's SOC at the start and at the end of the driving cycle are equal, all the required energy must be supplied by the primary power source. This situation is depicted in Figure 3.9, where η_T and η_{II} are the efficiencies of the transmission and of the 'secondary path', respectively. The latter efficiency at least comprises the efficiencies η_G , η_A and η_M of the generator, accumulator and motor, respectively, and also the mutual conversion efficiencies $\eta_{G \rightarrow A}$, $\eta_{A \rightarrow M}$, $\eta_{M \rightarrow W}$, and either $\eta_{E \rightarrow G}$ or $\eta_{W \rightarrow G}$, depending on the direction of the energy flow. If the secondary sources are directly connected to the primary source and the wheels, $\eta_{E \rightarrow G}$ and $\eta_{M \rightarrow W}$ are both equal to 1. The accumulator efficiency η_A is included to somehow reflect the effect of (time-dependent) self-discharge. For flywheels, η_A accounts for air drag induced self-discharge, while η_G and η_M are 1, since no energy conversion is required. For a hybrid vehicle like the Nissan Tino [Matsuo *et al.*, 1999], the power of both secondary power sources must pass through the transmission, hence the

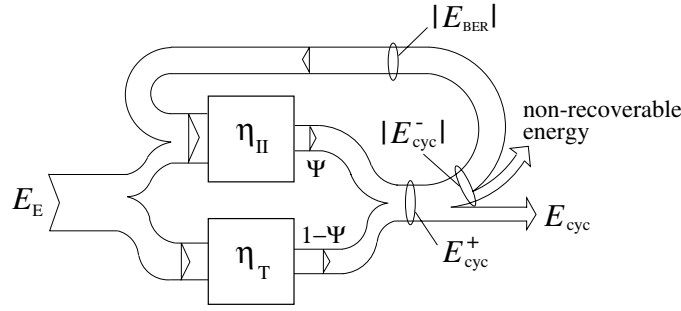


Figure 3.9: Energy flows

transmission efficiency η_T would appear twice in η_{II} . On the other hand, part of the secondary power may not always have to pass through the accumulator, thus increasing η_{II} . The total energy E_E that is to be delivered by the primary source, is given by

$$E_E = E_{cyc}^+ \left(\frac{1 - \Psi}{\eta_T} + \frac{\Psi}{\eta_{II}} \right) - E_{BER} \quad (3.1)$$

where the term E_{BER} is only present if brake energy can be recovered. Else, all energy E_{cyc}^- is non-recoverable.

The factors Ψ and $1 - \Psi$ represent the relative parts of E_{cyc}^+ that pass through η_{II} and η_T , respectively. Ψ depends on the duty-cycle strategy of the engine, as well as on the driving cycle, and is not known a priori for a given hybrid powertrain or arbitrary journey, except for a pure series hybrid, where $\Psi = 1$. If the engine is intermittently operated only in the sweet spot, Ψ must be larger than 0, in order to meet power demands below P_{ss} . In fact, Ψ can be viewed as a *hybridization factor*, although other definitions are encountered in literature. For instance, [Baumann *et al.*, 1998] defines the Degree Of Hybridization *DOH* for a hybrid vehicle operating in two different Energy Domains (ED), as

$$DOH = 1 - \frac{|P_{max,ED1} - P_{max,ED2}|}{P_{max,ED1} + P_{max,ED2}} \quad (3.2)$$

For $DOH = 1$ the hybridization is maximal, whereas $DOH = 0$ for a conventional vehicle and also for a purely electric vehicle. In [Müller and Köhle, 2000], hybrid vehicles are classified depending on the relative share of the battery in the total energy storage on the one hand, and of the electric motor in the total output power on the other.

In Figure 3.10 contour lines of the *relative fuel consumption* $\mathcal{F}(\Psi) = f / f_{OL_{15\%}}$ are drawn as a function of Ψ and η_{II} . Here, f represents the actual fuel consumption of the Start-Stop system with mechanical efficiency η_T , whereas $f_{OL_{15\%}}$ is the fuel consumption, when driving along the $OL_{15\%}$ operating line, with the same mechanical efficiency η_T . Realistic values $\eta_{II} = 0.44$ ($= \eta_G \cdot \eta_{G \rightarrow A} \cdot \eta_{A \rightarrow M} \cdot \eta_M = 0.88 \times 0.75 \times 0.88 \times 0.75$) for an *electrical* secondary power source and $\eta_T = 0.85$ for a CVT, are indicated in the figure by dashed lines. The increased weight of such a hybrid vehicle (around 120 [kg], see Section 3.4) is also taken into account. The bold line Ψ_{min} indicates the minimal hybridization factor that is required if it is assumed that the engine is running *only* for power demands *above* some threshold power level P_{th} , that is yet to be determined. Below P_{th} the secondary power source, that is the motor M, is

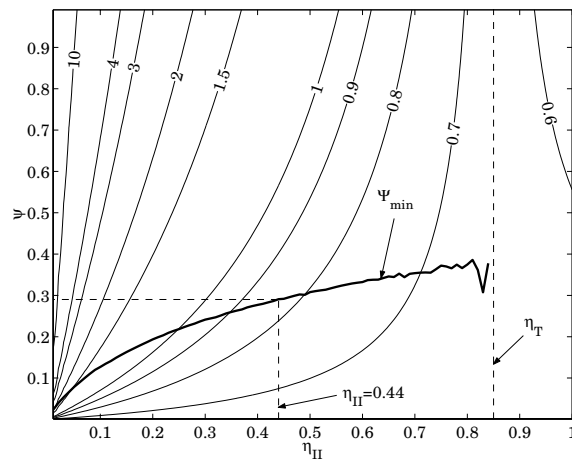


Figure 3.10: Hybridization factor Ψ and potential fuel savings as a function of total secondary source efficiency η_{II} for the urban drive cycle

activated for vehicle propulsion. Furthermore, for wheel power demands higher than P_{th} , but below $P_{ss}\eta_T$ (i.e., P_{ss} corrected with transmission efficiency), the engine E is running in sweet spot and the excessive energy is stored in the accumulator A by the generator G. Finally, for wheel power demands above $P_{ss}\eta_T$, the engine is assumed to operate as the sole mover (conventional mode) along the E-line. The activity of the engine E, the motor M and the generator G as a function of the wheel power is schematically displayed in Figure 3.11. For

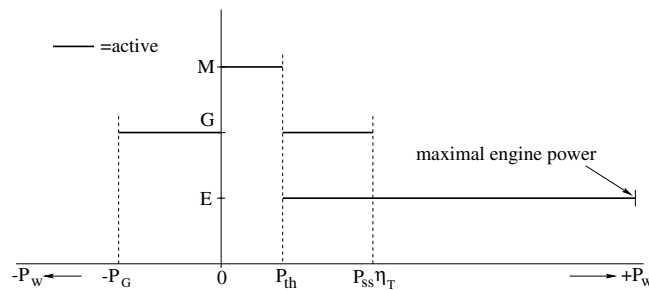


Figure 3.11: Activation of primary and secondary sources as a function of the (requested) wheel power P_w

negative wheel power the generator G could be used for regenerative braking up to a level equal to the maximal generator power P_G . This will be elaborated further in Section 3.3.4.

The threshold P_{th} is determined assuming that the total amount of energy accumulated in the intervals where $P_{th} < P_w < P_{ss}\eta_T$ should be just enough to supply the energy necessary for vehicle propulsion whenever $0 \leq P_w \leq P_{th}$. For an arbitrary journey, P_{th} can in principle not be

known beforehand. Instead, the standardized drive cycles are taken in order to obtain some practical indication for P_{th} . Thus $P_w = P_{cyc}$ and by solving the energy balance for P_{th} given the above assumption:

$$\int_{t_0}^{t_f} (P_{th} < P_{cyc}(t) < P_{ss}\eta_T) \cdot \left(P_{ss} - \frac{P_{cyc}(t)}{\eta_T} \right) dt = \int_{t_0}^{t_f} (0 \leq P_{cyc}(t) \leq P_{th}) \frac{P_{cyc}(t)}{\eta_{II}} dt \quad (3.3)$$

the threshold power can be determined. In Equation (3.3) t_0 and t_f are, respectively, the start and end time of the driving cycle. The Boolean expressions inside the integrands are included to set the appropriate interval of power levels which must actually be integrated. For the four cycles used here it appeared that the threshold power levels P_{th} do not differ that much, see Table 3.7. In practice P_{th} may be chosen at 10 [kW]. With P_{th} , Equation (3.1) can be solved for

CYCLE	P_{th} [kW]
NEDC	8.6
rural	11.0
urban	8.3
highway	12.2

Table 3.7: Drive cycle power threshold beyond which the engine is activated ($\eta_T = 0.85$ and $\eta_{II} = 0.44$)

Ψ . Proceeding as such for every η_{II} , the line Ψ_{min} emerges. For $\eta_{II} = 0.44$ the fuel saving of Start-Stop is highest for $\Psi = \Psi_{min}$ and then equals 16.8%, for the urban drive cycle.

The strategy of Start-Stop operation underlying the given analysis can not be pursued in all situations given a maximum and minimum SOC of the accumulator. For instance, when the accumulator is fully charged and the cycle power demand is still above P_{th} , either the secondary source must also be running to discharge the accumulator or the engine must supply the exact cycle power in the appropriate operating point below $P_{ss} \cdot \eta_T$. Note that for power demands larger than $P_{ss}\eta_T$, the engine is always running on its own to deliver the actual cycle power. Vice versa, if the SOC is down to its minimum, the engine must be running even though the demanded cycle power may be below P_{th} . These operational constraints are not considered here but are regarded as one of the main efforts in developing the energy management. Furthermore, the powertrain component controls must ensure the driveability, comfort and reliability. Also the cooling system of the engine (engine runs at $P_{ss} = 32$ [kW] when on) has to be reconsidered for low speed driving.

The size of the motor, accumulator and the generator partly determine the potential for fuel saving. The proposed strategy is not only favourable with respect to the combined efficiency of the primary and secondary path, but also reduces the power requirements for the generator G and the motor M to an absolute minimum. Consequently, in the case where $P_{ss} = 32$ [kW], $P_{th} = 10$ [kW] and $\eta_T = 100\%$ the necessary generator power is 22 [kW], whereas the required motor power is 10 [kW]. A lower transmission efficiency η_T will lower these demands even further. For instance, if $\eta_T = 0.85$, the engine can operate in the sweet spot already when $P_w = \eta_T \cdot 32 \approx 27$ [kW]. Hence, a generator size of 27-10=17 [kW] is sufficient. If the motor and generator are combined in one machine, the size of the generator determines the actual size of the secondary power source. Downsizing the secondary power source means that the engine operating point—which should ideally be in the sweet spot—moves towards a lower power level on the E-line. However, according to Figure 3.5, the penalty on specific fuel consumption is relatively low. For example, when shifting the intermittent engine operating

point to 20 [kW], the BSFC rises by a mere 5%. On the other hand, the power requirement for the generator drops from 22 to 10 [kW]. Table 3.8 compares the efforts for two systems with generator sizes of 10 and 22 [kW], respectively. The cost saving due to a smaller generator is

G [kW]	mass [kg]	volume [l]	cost [€]	fuel [%]
10	44	17	1740	105.2
22	96	36	3830	100

Table 3.8: Comparison of efforts for two Start-Stop generator (G) sizes

likely to outweigh the decreased fuel saving in practice. On the other hand, if Start-Stop is combined with brake energy recovery, the fuel saving penalty associated with downsizing the generator will be more significant.

3.3.4 Brake energy recovery

Brake energy recovery must always be combined with some strategy that re-uses the recovered energy. In the following example it is chosen to combine this fuel saving principle with a Start-Stop system that operates the engine at $P_{ss} = 32$ [kW] and uses a generator of 22 [kW]. The energy balance (3.3) is augmented with the recovered energy yielding

$$\int_{t_0}^{t_f} (P_{th} < P_{cyc}(t) < P_{ss}\eta_T) \cdot \left(P_{ss} - \frac{P_{cyc}(t)}{\eta_T} \right) dt =$$

$$\int_{t_0}^{t_f} (0 \leq P_{cyc}(t) \leq P_{th}) \cdot \frac{P_{cyc}(t)}{\eta_{II}} + \int_{t_0}^{t_f} (-P_G \leq P_{cyc}(t) < 0) \cdot P_{cyc}(t) dt \quad (3.4)$$

where it is seen that the energy demand from the engine (left hand side) lowers due to the (last) recovery term ($P_{cyc} < 0$). For brake energy recovery, a plot similar to Figure 3.10 can be made (not shown), where for a given η_{II} and Ψ , the potential fuel savings increase, but also the locus of minimal hybridization factors Ψ_{min} tilts towards higher values. Still, again for the urban drive cycle, the fuel saving at $\Psi = \Psi_{min}$ (for $\eta_T = 0.85$) increases significantly up to 36.6% for an electrical system and to 53.3% for a mechanical system, as will be summarized in Section 3.4. If it is decided not to increase the power level of the generator, the additional efforts for brake energy recovery are relatively small, and limited to a revision of the energy management system. Because this fuel saving principle in fact constitutes brake-by-wire, safety issues must be taken into account. Moreover, the brake feel and performance should not be different from a normal vehicle. Since the generator power is limited and dependent on battery state (SOC, temperature, age), conventional disc brakes are still indispensable.

3.4 Innovation value versus effort

In this section, the innovation values are weighed against the corresponding efforts, for all four fuel saving principles. These *normalized* innovation values are evaluated for a system with a mechanical secondary power source and compared to those of a system with an electrical secondary power source. To give an indication for city and highway driving, the comparison is performed for the urban and the highway cycle.

The normalized innovation values are obtained simply as the quotient of the percentage of fuel saving and the effort (be it cost, weight or volume), always with respect to the reference vehicle. The additional weight, volume and cost are determined for the mechanical and electrical system, based on output power demands taken from the sections corresponding to the various fuel saving principles.

Additionally, the power demand for the accumulator using Start-Stop was set at 26 [kW] ($\approx 22/\eta_G$). For the electrical system, these *power* requirements are normative, but not for the mechanical system, where the *energy* demand is normative and is set at 200 [Wh], taken from [van Druten, 2001]. The additional weights are then obtained using Table 3.4, where the specific values for the electrical system are taken from the asynchronous EM combined with an ultracapacitor. For the mechanical system, values between those of the ZI flywheel and FESS are taken. In practice, the electrical system may additionally require a battery.

The fuel savings presented in this section are obtained taking all the relevant efficiencies as well as the increased weights into account. Figures 3.12 and 3.13 depict the normalized innovation values for the mechanical and the electrical system, being the fuel saving relative to the additional cost [% per €], the fuel saving relative to the increased weight [% per kg] and the fuel saving relative to the additional volume [% per dm³].

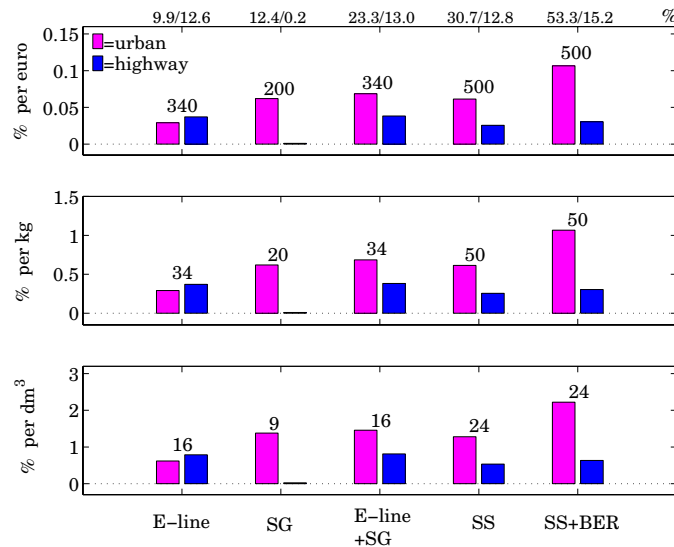


Figure 3.12: Normalized innovation values for a *mechanical* secondary source. At the abscissa are the four saving principles (E-line, SG=Stop-Go; SS=Start-Stop; BER=Brake Energy Recovery) and combinations thereof. On top of the bars in the upper plot is the corresponding increase of cost [€], in the middle plot the increase of weight [kg] and in the lower plot the increase of volume [dm³]. Above the figure are the fuel saving percentages, corresponding to the two driving cycles.

At the abscissa are the four saving principles (where 'SG' means Stop-Go, 'SS' is Start-Stop and 'BER' stands for Brake Energy Recovery) and combinations thereof. For each saving principle, the left (grey) bar indicates the weighted fuel saving for the urban cycle and the right

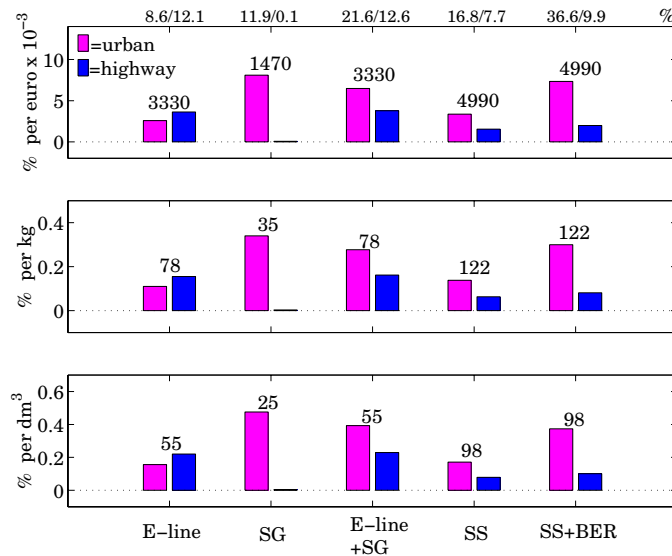


Figure 3.13: Normalized innovation values for a *electrical* secondary source. At the abscissa are the four saving principles (E-line, SG=Stop-Go; SS=Start-Stop; BER=Brake Energy Recovery) and combinations thereof. On top of the bars in the upper plot is the corresponding increase of cost [€], in the middle plot the increase of weight [kg] and in the lower plot the increase of volume [dm³]. Above the figure are the fuel saving percentages, corresponding to the two driving cycles.

(black) bar that for the highway cycle. Written on top of the bars is the corresponding increase of cost [€], weight [kg] and volume [dm³], respectively. Above the figure, the fuel saving percentages are listed, corresponding to the two driving cycles and the different fuel saving principles. The bars for 'E-line+SG' and 'SS+BER' are included because these are obvious combinations. Besides that, BER cannot exist on its own.

From Figure 3.12 it is seen that the mechanical system performs well on the urban cycle for all fuel saving principles, though to a lesser extent for E-line. SS+BER scores highest, with the large fuel saving of 53.3%.

The situation is somewhat different on the highway cycle, where the use of SG becomes close to nil. E-line (and the combination E-line+SG) achieves the best value for this cycle. The same trends are seen for the electrical system (see Figure 3.13), but in no category can such a system perform nearly as well as its mechanical counterpart (note the different orders of magnitude of the ordinate values in both figures). At least for the urban cycle, the electrical system shows a preference for SG. Because the mechanical system is much cheaper than the electrical alternative (by a factor of ten), the difference between the two with respect to the normalized values is striking. However, the electrical system can be expected to be more flexible and easier to conceive.

The fact that the achievable fuel savings are systematically higher for the mechanical system, is due to higher efficiencies of the secondary path (in case of SS and SS+BER), and a smaller increase of weight as compared to the electrical system (E-line and SG, in particular).

The penalty on fuel consumption due to additional weight proved to be between 0.13 and 0.38% per % mass increase, or on average 1% fuel for every 4% additional weight. Notably, the fuel savings obtained by SS and SS+BER on the highway cycle drop towards the values for E-line in case of the mechanical system, and even below that for the electrical system. The latter is explained by the fact that on the highway cycle, the required powers below P_{ss} are still concentrated close to the sweet spot (unlike a ‘proper’ city cycle) where the best strategy is to use E-line and not SS. Also, the substantially increased weight (+122 [kg]) ruins part of the fuel saving. Averaging the results of the two driving cycles reveals that both the electrical and the mechanical system score well on the combination of E-line and SG, at least on their own scale, see Table 3.9. The mechanical variant scores even somewhat higher for SS+BER than for E-line+SG. As mentioned before, the electrical systems show about ten times lower

System	E-line	SG	E-line+SG	SS	SS+BER
mechanical	33	32	53	44	69
electrical	3.1	4.1	5.1	2.5	4.7

Table 3.9: Normalized innovation value (cost-specific fuel saving [%/k€]), averaged over the urban and highway cycle, for the mechanical and electrical system

normalized innovation values than the mechanical counterpart. On the other hand (less quantitative) aspects such as driveability, safety and developing efforts level out the two principles somewhat. For instance, realizing a mechanical system for SS+BER requires a CVT with an exceptionally large ratio coverage (more than 20), and a high energy flywheel with mechanical components like clutches and gear stages, see [van Druten, 2001]. This yields additional issues of driveability and safety. The severity of these issues is much smaller for E-line+SG than for SS+BER, because of lower energy contents of the flywheel. Electrical systems, on the other hand, require few mechanical adaptations, and are flexible with regard to the controls. An electrical E-line+SG hybrid may additionally be utilized to supply electrical power for several purposes (*e.g.*, 42 Volt net). The robustness and predictability of batteries is still troublesome.

ZI powertrain: mechanical mild hybrid

The combination of E-line and SG may be termed *mild hybrid* as opposed to *full hybrid* in case of SS+BER [van Druten *et al.*, 2001]. From this section, it is concluded that a mechanical hybrid is preferable above an electrical hybrid, with respect to cost especially. Furthermore, the mechanical full hybrid scores higher than the mechanical mild hybrid. Therefore, a mechanical full hybrid seems favourable for reducing fuel consumption in a passenger car. However, the development effort (engine and catalyst adaptations, control of intermittent engine operation, *etc.*) for a full hybrid, relative to its potential is large compared to that for a mild hybrid. In the EcoDrive project it was decided to develop a mechanical mild hybrid, using two new concepts, called ZI and ZI Stop-Go. Choosing for ZI and ZI Stop-Go, the project goal can largely be met using the available development time, research and engineering capacity. Furthermore, the two concepts can be designed, realized and tested separately enabling a step-by-step implementation and hence reducing development risks.

The fuel saving of E-line+SG, (here embodied as ZI Stop-Go) is estimated by computations similar to those conducted in Section 3.2.3. The estimated fuel saving of ZI Stop-Go on the NEDC with respect to $OL_{15\%}$ is around 21%.

Chapter 4

The Zero Inertia Powertrain

This chapter presents the conceptual design of the Zero Inertia powertrain in a nutshell. Section 4.1 translates the findings from the previous chapter that are related to E-line tracking into a problem description. After that, the ZI solution is derived in Section 4.2. A brief description of the ZI Stop-Go transmission is given in Section 4.3.

4.1 Zero Inertia principle

In the previous chapter it was concluded that the use of E-line tracking as a fuel saving principle necessitates an additional power assist system. Electric power assist systems are able to supply the power needed to compensate for primary inertia effects in slow transient situations, and, when physical limits are not reached, even overcompensate. However, arbitrarily fast speed changes generally cannot be compensated for, due to power and torque limitations of the electric machine. A counteracting inertia, capable of supplying the power needed to overcome inertial effects would therefore be very interesting. This mechanical power assisting device, *i.e.*, a *flywheel*, should speed down when the primary inertia speeds up and vice versa, at a rate dictated by, among others, the ratio of flywheel inertia and primary inertia. To link the speed of the flywheel to that of the primary side of the powertrain, a component with a continuously variable transmission ratio is needed. Possible components to realize this are:

1. Continuously Variable Transmissions (CVTs)
2. Couplings
3. Torque converters
4. Planetary gears

continuously variable transmissions

Automotive CVTs can be mechanical, hydraulic, or electrical. Hydraulic CVTs are used especially in heavy vehicles (construction vehicles, trains, agricultural machinery), but have moderate efficiencies. So called electrical CVTs require an electric motor and an electric generator both of which are capable of handling the maximum power of the primary source of propulsion. Compared to an internal combustion engine with the same maximum power,

electric machines and their overhead (battery, inverter) are bulky and rather expensive, as well as rather inefficient, as was seen in the previous chapter. Modern mechanical CVTs are capable of transmitting the required power for almost every size of passenger car at efficiencies not much lower than that of conventional stepped transmissions (MT and AT). Commercially available CVTs are the Van Doorne metal V-belt CVT (*e.g.*, in the Nissan Primera), the Audi Multitronic chain belt CVT (*e.g.*, in the Audi A6), the Bando dry hybrid belt CVT (*e.g.*, in the Daihatsu Mira) and the dual cavity toroidal CVT (*e.g.*, in the Nissan Cedric).

couplings

Couplings can transmit torque between two bodies with a continuously variable speed ratio. The torque ratio is always equal to 1. A coupling that transmits the torque hydraulically is known as a *fluid coupling* (or *fluid flywheel*), otherwise the term *clutch* is more common. The torque transmitted by a fluid coupling can be influenced by varying the amount of oil. In a clutch that transmits torque mechanically, the torque can be manipulated by changing the clutch engaging pressure, either hydraulically, mechanically or electro-magnetically. 'Intermediate' solutions such as electro-magnetic and electro-rheological clutches use electro-magnetic fields to change the viscosity of the torque transmitting medium. The latter still somewhat exotic clutch is in some ways comparable to the fluid coupling because of the viscous torque transmission. Current applications of this technology are found primarily in active engine mounts. The electro-magnetic powder clutch on the other hand, has been applied successfully, *e.g.*, in the Subaru CVT.

torque converters

A torque converter basically is a fluid flywheel combined with a stator (or reactor) which is connected to the transmission casing by a one-way clutch. When the torque on the stator is such that the one-way clutch locks, this third torque transmitting member enables the amplification of input torque whenever the input speed exceeds the output speed. In effect, the torque converter acts as a hydrodynamical CVT with a quite moderate efficiency. Some torque converters have a (mechanical) lock-up clutch to enlarge the efficiency by eliminating the slip when the torque ratio approximates 1. The continuous variability is then obviously lost.

planetary gears

Planetary gears are widely used, for instance in stepped automatic transmissions. A *basic* planetary gear has three main rotating members and three submembers, see Figure 4.1. The inner member is termed the *sun*, the outer member is the *annulus* or *ring*. The intermediate member carries the three *planets* (submembers) and is therefore called *carrier*. More complex epicyclic configurations can have several sun, annulus and carrier wheels or double planets with different teeth numbers connected to the same axis, for instance see Figure 4.2. Also, planets can run on opposing planets, instead of on an opposing sun or annulus. An example of this can be found in the DNR (Drive-Neutral-Reverse) set, see Figure 4.3. Epicyclic sets as seen in practice (*e.g.*, Simpson, Ravigneaux, see, *e.g.*, [Lechner and Naunheimer, 1999]), are composed of several basic planetary gears, possibly combined with alternative planet configurations. In most automotive applications, the planetary gear is used as a concentric reduction gear, where any rotating member can be connected to ground (*i.e.*, the transmission housing). Given the speed of one member, varying the speed of a second member in turn varies the speed of a third member. This creates two speed ratios which are both continuously variable.

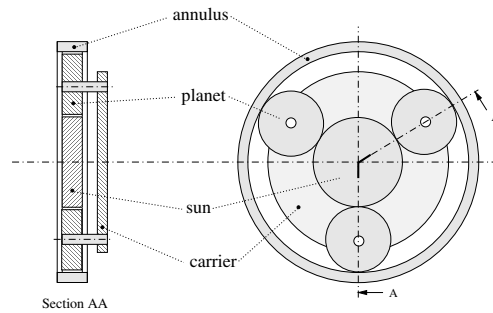


Figure 4.1: Basic planetary gear

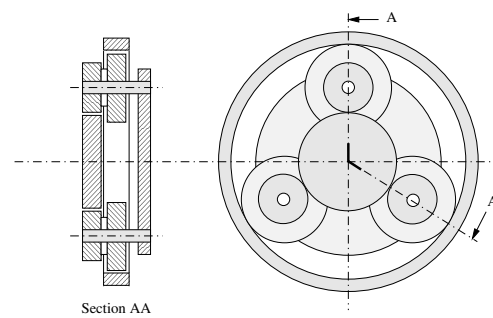


Figure 4.2: Planetary gear with stepped planet

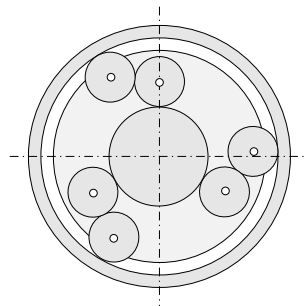


Figure 4.3: DNR (Drive Neutral Reverse) reversal stage

In this example, the speed of the second member must somehow be controllable. This is possible by active control of the torque applied to one of the members. For example, in the hybrid powertrain of the Toyota Prius [Riezenman, 1998], the speed of the members is controlled by an electric motor/generator connected to the sun. The engine is connected to the carrier and

the wheels to the annulus.

Summarizing, a number of components exist which in principle can transmit power between two rotating bodies at variable transmission ratios. In the following, further constraints will decide what solution is favourable for the intended application.

4.2 ZI Concept design

The drive train of the vehicle must be able to combine a given range of vehicle speeds with appropriate engine speeds and flywheel speeds. In general, the flywheel speeds should be high for low engine speeds and vice versa. Strictly speaking, this calls for two CVTs or similar power transmitting components. Obviously, the application of two CVTs, be it mechanical, electrical, or hydraulic, is unacceptably expensive and bulky. Furthermore, the required ratio coverage, needed to link all practical speed combinations, using a flywheel with an inertia comparable to the primary inertia, is by far larger (typically 30) than the ratio coverage of standard mechanical CVTs (typically 6). Hydraulic CVTs are not an option due to their moderate efficiencies, whereas an electrical layout would offer possibilities, although preferably not in a series hybrid configuration.

The use of a planetary gear arrangement as in the Toyota Prius is reasonably cost-effective, although the Prius uses two electric motors which renders this solution still rather expensive. An alternative solution, incorporating a planetary gear, does not control the speed of one rotational member electrically, but mechanically instead, through the use of a mechanical CVT. Such a solution would again be overexpensive, if the CVT could be used only for regulating the flywheel speed. However, if the CVT can also be used to control the engine speed, such a solution becomes increasingly interesting.

4.2.1 Resulting configuration

The easiest way to realize the suggested solution is to have a fictitious line connecting the engine and flywheel speed that rotates around a pivot in between, as illustrated in Figure 4.4. A sensible choice is to make the median speed the vehicle speed, hence the secondary speed

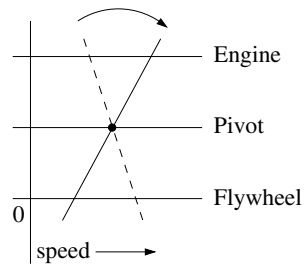


Figure 4.4: Pivot mechanism

of the CVT. By downshifting the CVT, it is seen that while the engine increases speed with respect to the vehicle speed, the flywheel speeds down, and vice versa. This is exactly the mechanism needed to create the energy exchange between engine and flywheel. In terms of a basic planetary gear, the sketched mechanism can be realized by connecting the secondary

speed to the carrier, whereas the engine and flywheel are connected to the annulus and sun, respectively, or possibly, the other way around. The outlined topology (see Figure 4.5), which

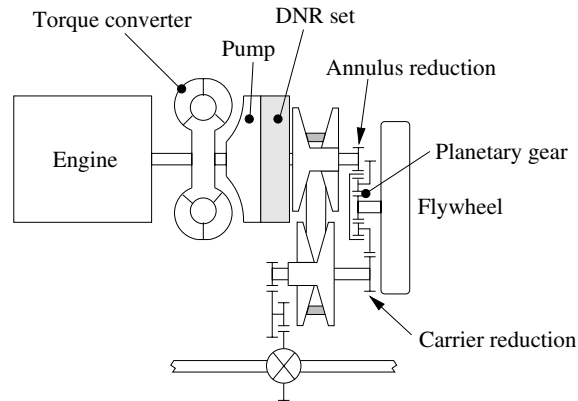


Figure 4.5: ZI powertrain concept layout

is just one possibility out of many, will serve as the layout to be used throughout this thesis, and will in fact prove to be a good starting point, see [van Druten, 2001].

4.3 ZI Stop-Go

The Stop-Go functionality (proposed in Section 2.4 to increase the fuel efficiency and evaluated as an interesting technology in Section 3.3) is investigated in combination with the Zero Inertia powertrain. Naturally, before vehicle launch, the energy contents of the flywheel must be sufficiently high. For this purpose, at least one additional clutch is needed in order to enable disengagement of the flywheel from the drive train at a flywheel speed high enough to facilitate a new vehicle launch. The flywheel preferably should be able to launch the vehicle and start the engine *at the same time*. Such a specification is certainly not trivial, since most commercially available Stop-Go systems *first* start the engine, *after* which the engine can start to propel the vehicle. As was mentioned in Section 3.3.2, cranking up the engine is conceivable as a *direct-start* or an *impulse-start*, for instance see [Reik, 1999]. The first strategy has one clutch only, positioned between the starter and the primary side of the transmission, as in a conventional driveline. The impulse-start strategy uses the inertia of the starting device, which can be disengaged from the engine by an additional clutch, see [Seiffert and Walzer, 1989]. Depending on the starter-clutch(es) configuration, and on the size of the electric starter motor, the combined time needed for restarting the engine and engaging the launching clutch may be more than the driver is willing to accept. This is the case in the former Volkswagen Eco-Golf/Ecomatic [Adcock, 1998, Greve and Liesner, 1993] and supposedly also in the current Volkswagen Lupo 3L [Healey, 1999]. In the Honda Insight with Integrated Motor Assist (IMA), the electric motor power is much larger, thus enabling a pleasant vehicle launch.

To enable the flywheel system to simultaneously speed up the engine and the vehicle, one additional clutch is needed to decouple the CVT from the driveline. To see this, it is crucial to understand that, while the flywheel contributes torque to the wheels (secondary

side of the CVT) it drains (some) torque from the primary side of the CVT and hence the engine. Therefore, while launching the vehicle, the flywheel tends to speed up the engine in the wrong direction. To avoid this, the CVT has to be decoupled from the secondary shaft and the DNR set must be set in reverse. In Figure 4.6 the ZI Stop-Go layout is depicted showing the two additional clutches (C_f and C_s) as well as the existing clutches (C_l , C_d and C_r) that will be operated differently. In [Vroemen, 2001] the physical background, as well as the supervisory

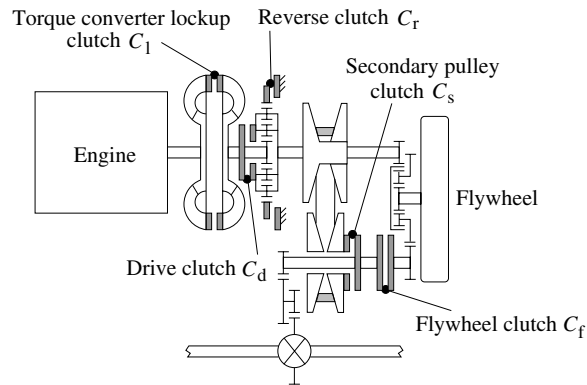


Figure 4.6: ZI Stop-Go powertrain concept layout

and clutch control strategies needed to operate the Stop-Go facility is elucidated.

4.4 Further reading

Given the concepts of the ZI and ZI Stop-Go powertrain, an extensive though achievable list of development (or innovation) efforts has to be tackled. These efforts are reported in this thesis, in [van Druten, 2001] and in [Vroemen, 2001], also see Figure 1.3.

In [van Druten, 2001] the designs of the ZI and ZI Stop-Go concepts are illustrated as well as general ideas about flywheel usage in passenger cars. In [Vroemen, 2001] component controller and models for the CVT are developed. Furthermore, a second part concerns the operation, modeling and control of the ZI Stop-Go transmission. The control problem of generating appropriate setpoints for engine and CVT along with developing dynamic models for and testing of the ZI powertrain is the subject of this thesis.

Part II

Powertrain Control

Chapter 5

Introduction to Part II

In Part I it was motivated that the ZI and ZI Stop-Go possess a promising innovation value. This is especially true compared to purely electrical power assist systems. Further developing the powertrains is given green light despite the anticipated violation of the project goal by a mere 4%.

Proceeding with the ZI and ZI Stop-Go powertrains, a number of research and engineering goals have to be tackled. More specifically, the powertrains have to be designed and manufactured, component controllers for the CVT, engine throttle and clutches have to be designed, as well as a coordinated controller translating the fuel economy and driveability targets into appropriate setpoints for the CVT and the engine.

The latter is applied for both the CVT and ZI powertrains and is the subject of the remainder of this part. Elaborating on a new coordinated control within the wide variety of already existing strategies for basic CVT powertrains may offer clues for sustained research in this area. Moreover, focusing on a common description and treatment of the control problem for both powertrains provides a better understanding of the ZI powertrain.

Coordinated control issues for the ZI Stop-Go powertrain are treated in part III of [Vroemen, 2001]. The design and materialization of the ZI and ZI Stop-Go powertrains are described in [van Druten, 2001]. The ultimate goal of part II is to arrive at a test platform with which fuel economy and driveability tests can be conducted conforming the project goals. This test platform actually comprises of a passenger car with 1.6 l petrol engine adapted for installation of the ZI transmission. As said, to show the fuel economy and driveability benefits of the ZI powertrain, a coordinated control strategy has to be designed. This itself demands for dynamic models of the powertrain. Such models, having different complexity, are used for design and validation of the coordinated control and to predict intrinsic dynamic behaviour of the powertrains.

In order to arrive at the final validation of the ZI powertrain, the following approach is adopted. In Chapter 6, modeling of the ZI powertrain is the main focus. In that chapter, three different levels of modeling are suggested. First, properties of components in the powertrain are investigated. Also the tires and vehicle are modeled up to a level relevant for this research. The additional components embodying the ZI principle, that are a planetary gearset, additional gearing and the flywheel, together termed 'flywheel unit', are given separate attention. A simple kinetic energy model of the powertrain is introduced to find optimal design values for the flywheel unit with. This is an alternative approach of what is suggested in [van Druten, 2001] for optimizing the flywheel unit. The second model approach is much more in

depth and describes a dynamic simulation model including internal losses, inertias, engine dynamics, CVT dynamics, stiffnesses, clutches and tire-road slip. Moreover, directions for a hybrid model approach are given in order to incorporate discrete events such as locking clutches. This model is termed 'torsional compliance powertrain model'. Apart from being instrumental in dynamic simulations also longitudinal comfort aspects are analyzed with this model. The third model describes the non-minimum phase behaviour introduced by connecting inertias through a time dependent kinematic variable, *i.e.*, the CVT ratio. The parametric structure of the model is such that one can easily switch from a basic CVT powertrain towards the ZI powertrain.

In Chapter 7, the last mentioned model is also used in the control synthesis for both powertrains. Before arriving at this synthesis, a literature overview of powertrain control with CVT based powertrains in particular is given. Then, ideas on optimal fuel economy and driveability are conveyed. These ideas are translated into control objectives and are explicitly adopted in deriving the coordinated powertrain controllers. Two suggestions for such controllers are given, *i.e.*, one for the CVT powertrain and one for the ZI powertrain. The two differ in that the CVT powertrain controller introduces an additional dynamic variable leading to dynamic state feedback, whereas for the ZI powertrain controller a static state feedback is suggested. The controllers are validated using closed loop simulations with the (non-linear) control model and the torsional compliant model of Chapter 6. Considering the simulation results, conclusions are drawn and suggestions for future research are given with respect to the designed controllers.

In Chapter 8 a survey of experimental results obtained with a test vehicle is given. The instrumentation of the test vehicle with sensors, actuators, signal processing and a μ processor is discussed. Also implementation aspects of the software are given some attention. A component controller fitted for the engine's electronic air throttle is also elaborated. Most importantly, the driveability improvement of the ZI powertrain is demonstrated through three types of experiments: semi kick-down, pedal jogging and a full kick-down. Also the fuel economy of the ZI powertrain is assessed through simulations and compared with fuel consumption measurements conducted with 4 geared automatic gearbox (4AT) and with a CVT powertrain. Chapter 8 is concluded with a discussion.

The total of this thesis is concluded in Part III which consists of Chapter 9 only. There, conclusions, recommendations and a future outlook are presented given the results of the Parts I and II and of course the EcoDrive project target defined in Chapter 1.

Chapter 6

Powertrain Modeling

6.1 Introduction

Modeling of the CVT and ZI powertrain is the main subject of this chapter. The impact of the flywheel inertia on the dynamics of the powertrain is substantial and needs to be analyzed prior to the actual implementation in a test vehicle. In this chapter the impact on vehicle comfort is of interest. Furthermore the implications for the driveability and for the control design is questioned.

In order to arrive at this analysis, dynamic powertrain models have to be available. In the next sections models of the CVT and ZI powertrain are derived. First, descriptions of all relevant components and their main properties are presented. Basically, the ZI powertrain is a standard CVT powertrain augmented by a planetary gearset and the intentional flywheel. It appears that the CVT and ZI powertrain models can be described with identical parameter structures. This enables switching between the models by altering the values for the flywheel inertia only.

The model principles used are for the larger part in agreement with those presented in [Cho and Hedrick, 1989]. There a model is derived for a powertrain equipped with an automatic transmission. They present a more physical description of the engine model than proposed here, although the number of states is equal. Lockup of the torque converter was not separately modeled there, contrary to this chapter where it receives special attention.

In deriving the equations of motion strict sign conventions for torque and speed are used, see Figure 6.1. In this figure 'n' denotes a mass-less node at which transmitted torques of interest may be monitored.

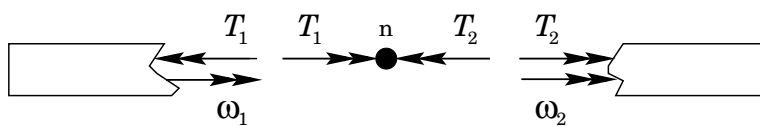


Figure 6.1: Sign conventions for torques and speed

As noted in [Jacobson, 1993] the behaviour of the powertrain is determined by *physical components* all of them having *mechanical properties* and some of them also showing *engineering*

phenomena either autonomously (*e.g.*, non-linear damping) or by external interactions (*e.g.*, air drag). The model used for simulation and evaluation purposes is subdivided in blocks, not necessarily representing physical components. Some model blocks are represented by algebraic equations such as the geometric ratio between gear wheel radii. The physical component representing this gear ratio generally also has mechanical properties such as inertia and stiffness. The dynamic impact of these properties is represented by differential equations. Other model blocks embody engineering phenomena mostly described by experimentally determined data in the form of diagrams or tables.

There are three most common ways to arrive at the model equations, that is to say using Newton's laws of motion, using variational methods as in the Lagrange method or using the bondgraph formalism. The first method is considered most favourable here and will be used throughout in the sequel.

The remainder of this chapter is organized as follows. Section 6.2 describes the CVT powertrain, treating the purposes and properties of all relevant components. Section 6.3 describes the additional components of the ZI powertrain. In Section 6.4 the physical properties and phenomena are linked together into what is called a *torsional compliance powertrain model*. This model constitutes first order non-linear differential equations, and discrete states. The discrete states are obviously present due to discrete events that occur in the powertrain, *e.g.*, engaging of a clutch. The combination of continuous and discrete states forms a so called hybrid dynamic system. This hybrid model is used for simulation and validation only. Further on it is simplified into various purely continuous models, their complexity varying with the context of the analysis. In Section 6.5 for instance, the model is reduced to seven first order differential equations by leaving out all engine dynamics and reducing the order of the CVT dynamics. Furthermore, the discrete states are chosen such that the simplified model represents a very common driving situation. Consequently, the differences in the dynamic properties of the CVT and ZI powertrain can unambiguously be demonstrated.

In Section 6.5.2 the model order is reduced even more to demonstrate the minimum phase and non-minimum phase behaviour of the ZI and CVT powertrains respectively. Two non-linear first order differential equations are thought to be sufficient for this analysis. In Section 6.3 a functional optimization method is discussed starting from an expression for the kinetic energy in the powertrain. This reduces the model description to a purely algebraic form.

6.2 Description of the CVT powertrain

In general, the term *powertrain* refers to the entire system necessary to propel the *vehicle*. It arguably extends from the prime energy source, *e.g.*, fuel tank, to the element interfacing with the road, *i.e.*, the tires. The powertrain may be divided into: the fuel tank, petrol engine as the converter from chemical to mechanical energy (including injection, spark, air intake and exhaust system, the cooling system and accessories), the continuously variable transmission (comprising the hydraulic pump and circuit, torque converter, the Drive/Neutral/Reverse (DNR), the variator, the final reduction gear and the differential gear), the drive shafts connected to the wheels, the brakes, and the tires which form the actual interface with the road. The vehicle body itself is generally left out of the definition of the powertrain.

The vehicle body interacts with the ambient air and the to be propelled vehicle mass also influences the tire rolling resistance. These phenomena determine the vehicle speed, wheel speed, and ultimately the speed of the secondary mounted inertias, that is all inertias from and including the secondary pulley to and including the differential cage. Thus, the interaction between the powertrain dynamics and those of the vehicle can be considered strong.

Although it is regularly not included in the definition of the *powertrain* the vehicle is seen here as a part of the *powertrain model*. For simplicity, the considered powertrain is drawn *without* the vehicle body in Figure 6.2.

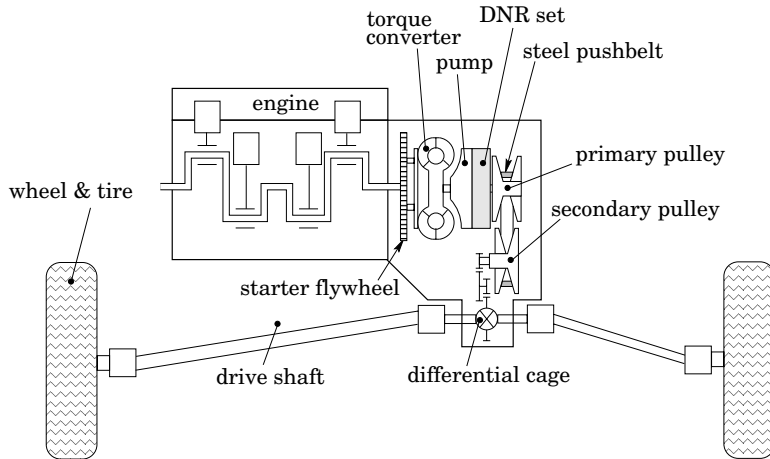


Figure 6.2: CVT based powertrain

The braking system is omitted intentionally. The braking dynamics in essence heavily overrule the influence of the powertrain as a drive system, and may therefore be considered separately though its details remain outside the tenor of this thesis. Instead an instrumental description of the brake system is given. The cooling, air intake, fuel injection, spark ignition and exhaust system are left out of the engine model. Dynamics governing individual combustions are not included, but their influence is characterized as a disturbance signal with well known frequency content.

6.2.1 Internal combustion engine

The applied internal combustion engine is a naturally aspirated, multi point direct injection (MPI), spark-ignition (SI), petrol fueled aggregate with a 1.6 l displacement divided over 4 cylinders running in 4 stroke manner and breathed by one intake valve as well as one exhaust valve each. The fuel injection and the ignition timing are controlled by an Electronic Control Unit (ECU). Electronic engine control, or engine management, of this kind requires extended sensory information. The main variables are the engine speed, crankshaft position and intake air mass flow.

The motive for using an engine management system is to provide the essential accuracy and adaptability in order to minimize exhaust emissions (CO, CO₂, NO_x), minimize evaporative emissions (HC) and fuel consumption (CO₂ is directly linked to this), provide optimal driveability for all operating conditions, and provide system diagnosis when malfunctions occur, [Hirschlieb *et al.*, 1999]. In order to comply with legal emission limits, car manufacturers are very keen on controlling engine exhaust emissions whereas fuel consumption is often somewhat penalized. Driveability is generally less penalized through specific control scenarios for ignition and injection primarily during instationary situations of engine speed, throttle

and temperature. A brief overview of the engine management applicable for the engine under investigation is presented next. In this thesis no adaptation of the engine management is suggested. Instead, it was decided to control the air intake throttle electronically and adopt the torque response of the engine and its management as is.

engine model

The operation of the engine as a transformer of chemical to mechanical energy is extremely complex and depends on many variables such as temperature, engine speed, geometries, fuel quality, *etc.* It would lead too far afield to investigate all phenomena involved with internal combustion of fuel. However, the dynamic impact of the fluctuating engine torque due to the individual combustions is of interest for several reasons. Especially when investigating the periodic responses of the powertrain, the frequency content of the engine torque is very relevant. When considering the engine torque as a control input, the periodic character of the engine torque is less relevant and only the mean value is of interest, [Karlsson and Fredriksson, 1999]. After a sudden throttle angle change the mean engine torque needs some time to reach a new value. This is mainly caused by the time intervals between the individual combustion, [Serrarens and Veldpaus, 2000]. For a four cylinder four stroke engine it takes at least two crank shaft revolutions before a new mean torque value has established. In the model presented next, this idea is adopted. Thereto, a non-linear second order model is proposed where the engine speed ω_e is used as a variable parameter.

Taking both the dynamics of the mean value torque T_e and the periodic part ΔT_e of the total torque into account, a simple model for the total engine torque $T_{e,\Delta}$ is given by:

$$\ddot{T}_e = -c_1 (T_e - \bar{T}_e(\phi, \omega_e)) \omega_e^2 - c_2 \omega_e \dot{T}_e \quad (6.1)$$

$$T_{e,\Delta} = T_e + \Delta T_e \quad (6.2)$$

$$\Delta T_e(t) = \Delta T_e \left(t + \frac{\pi}{\omega_e} \right), \quad \overline{\Delta T_e(t)} = 0, \quad (6.3)$$

where ϕ is the throttle angle, ω_e is the angular engine speed and \bar{T}_e is a stationary torque stemming from a speed-throttle-torque map. Furthermore in these equations the parameters c_1 and c_2 are determined in the following way. The rise time is defined as the time interval required before the system output crosses a step-wise reference value for the first time. For a second order underdamped system this rise time t_{rs} is inversely proportional with the (damped) natural frequency, here $\sqrt{c_1} \omega_e$. The numerical values of $c_1 = 0.24$ and $c_2 = 0.882$ ensure that the rise time always matches two crank shaft revolutions, thus $t_{rs} = 4\pi/\omega_e$ and has a slight overshoot of 0.15% at step-wise inputs \bar{T}_e .

The map $\bar{T}_e(\phi, \omega_e)$ in fact contains a grid of stationary mean value engine output torques obtained utilizing a speed controllable load (dynamometer) and operating the engine for constant throttle angles and constant engine speeds, see also Figure 6.3. Some authors, *e.g.*, [Dorisen and Höver, 1995], [Hendricks and Sorensen, 1990] and [Vanvuchelen, 1997] propose first order models for the mean value torque T_e . The second order description (6.1), however, is capable of describing the response transient up to the actually requested torque \bar{T}_e within a preset time t_{rs} , whereas the first order description reaches this torque only asymptotically for $t \rightarrow \infty$. In [Cho and Hedrick, 1989] also a second order model for the indicated engine torque is presented. This model is based on dynamics of the intake air, fueling and time delays in indicated torque production. It relies therefore very much on the physical data of the engine, which are not available for the engine used in this chapter and Chapter 7. Even less information is available for the engine used in the experiments described in Chapter 8.

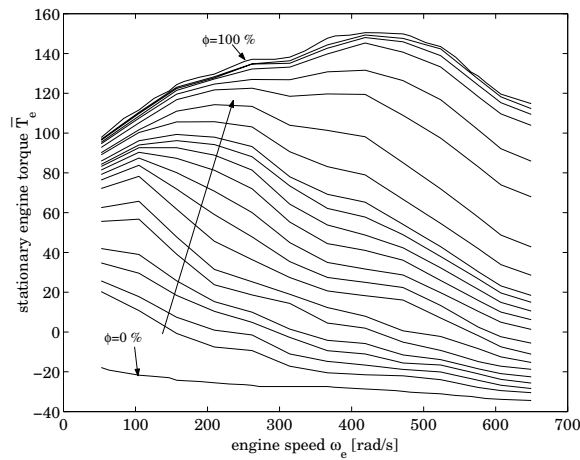


Figure 6.3: Stationary engine torque \bar{T}_e as a function of stationary throttle ϕ and speed ω_e

6.2.2 Hydraulically controlled variator

The hydraulically controlled metal pushbelt variator, see Figure 6.4, applied in the underlying project, has an extremely rich miscellanea of components, phenomena and interactions both hydraulically and mechanically. Research on the hydraulics has resulted in a variety of hydraulic circuit models [James and Vaughan, 1996], [Vroemen and Veldpaus, 1998]. The mechanical phenomena within and interactions between the metal belt and pulleys (together also termed *the variator*) are far from fully understood. Extensive, sometimes unsound, research has been undertaken in this area. Static mechanical descriptions of the variator are found in [Becker, 1987] and [van Rooij and Schaerlaeckens, 1993]. The modeling of all mechanical properties of the variator, especially in dynamic situations, is far too complicated for the analysis undertaken here, and is therefore left out of this thesis. More contributions in this field can be found in [Vroemen, 2001]. Even in the extensive simulation model no information on mechanical or hydraulic phenomena between belt and pulleys is taken into account. Instead, the behaviour of the hydraulically actuated variator is described using a switched black box model for the transfer from a desired variator ratio $r_{cvt,d}(t)$ towards a realized ratio $r_{cvt}(t)$. The underlying hard- and software for this control task is discussed extensively in [Vroemen, 2001].

The CVT ratio is defined as

$$r_{cvt} := \frac{\omega_s}{\omega_p}, \quad r_{ud} \leq r_{cvt} \leq r_{od}. \quad (6.4)$$

in which ω_p and ω_s are the primary and secondary pulley speed respectively. The possible range of the ratio is limited by the underdrive ratio $r_{ud} = 0.416$ and the overdrive ratio $r_{od} = 2.15$. The quotient of the two defines the ratio coverage RC:

$$RC := \frac{r_{od}}{r_{ud}} = \frac{2.15}{0.416} = 5.17, \quad (6.5)$$



Figure 6.4: Picture of a variator by Van Doorne's Transmissie

and in fact gives the spread in primary speeds that can be achieved at a given secondary speed and vice versa.

The dynamic CVT ratio model has a switched model structure, one second order model for a demanded upshift, *i.e.*, $\dot{r}_{\text{cvt,d}} > 0$, and a first order model for downshifting, *i.e.*, $\dot{r}_{\text{cvt,d}} < 0$. The logarithmic CVT ratio ν is defined:

$$\nu = \ln(r_{\text{cvt}}), \quad (6.6)$$

and the desired logarithmic ratio ν_d is defined equivalently. The CVT model with ν_d as the input and ν as the output is given by:

$$\text{upshifting } (\dot{\nu}_d > 0) : \dot{\nu} = -c_3(\dot{\nu} - \dot{\nu}_d) - c_4(\nu - \nu_d) \quad (6.7)$$

$$\text{downshifting } (\dot{\nu}_d < 0) : \dot{\nu} = -c_5(\nu - \nu_d).$$

The switched model structure is chosen because it is frequently seen that downshifting has more of a first order nature, whereas upshifting often occurs with overshoots demanding for at least a (underdamped) second order model. The choice for using the logarithmic CVT ratio is not arbitrary but it rather transforms the variator ratios, which are apparently not symmetric (see equation (6.5)) around $r_{\text{cvt}} = 1$ (medium), into a symmetric form. The parameters $c = [c_3 \ c_4 \ c_5]^T$ have to be determined from the results of experiments with the controlled CVT. Here, a least squares approach is chosen to obtain the parameters using experiments. Let $\nu_d(t)$ be the known input for $t \in [t_1, t_n]$ and let $m_i (i = 1, 2, \dots, n)$ be the measured value for the output at time t_i . Furthermore, let $\nu_i(\hat{c})$ be the output at time t_i as determined with the black

box model, using the known input ν_d and any choice \hat{c} for the parameters. The parameters c then follow from

$$c = \arg \left(\min_{\hat{c}} \sum_{i=1}^n (m_i - \nu_i(t_i, \hat{c}))^2 \right). \quad (6.8)$$

Figure 6.5 displays the results, using a fragment of a large experiment ($n=14300$). The minimization is performed with a Nelder-Mead simplex method (`fminsearch.m` in MATLAB 5.3) with initial guess $[1 \ 1 \ 1]^T$ for the estimated parameters \hat{c} . The output, according to the model, is determined using an Euler integration scheme with a time step of 10^{-2} sec.

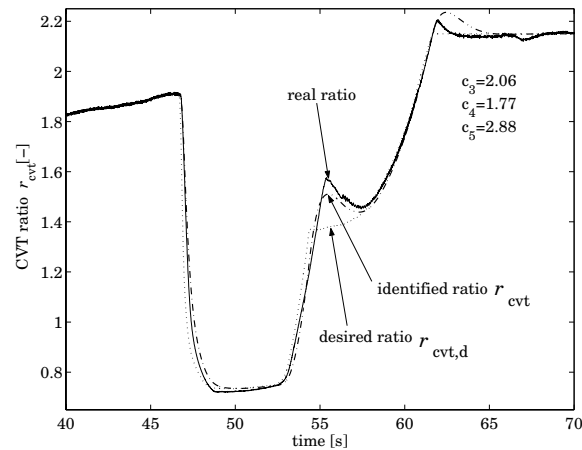


Figure 6.5: Identification of CVT model (6.7), estimated model parameter values are upper right

6.2.3 DNR set

The standard CVT powertrain contains a Drive/Neutral/Reverse set. This DNR set consists of an arrangement of two multiplate wet clutch packs together with a planetary gear set, see Figure 6.6. The three pairs of planet gear wheels are borne on a carrier frame. The input shaft is connected to the turbine of the torque converter, whereas the output shaft is connected to the primary pulley of the CVT. From Figure 6.6 it is clear that the sun and the carrier frame are directly connected if the drive clutch is engaged. The speeds of the input and output shaft are equal then. This constitutes the 'D' for forward driving. When only the reverse clutch is engaged, that is when the ring gear is connected to the transmission casing, the rotation direction of the input shaft is opposite to that of the output shaft. The gear ratio then depends on the sizes of the planet wheels (in pairs serving as reversal stage) and their spatial arrangements. The latter is in fact imposed by the radius of the ring gear. For the DNR set at hand this gear ratio is -1.1. This constitutes the 'R' for reverse driving. When both 'D' and 'R' are disengaged the Neutral ('N') function is enabled, and clearly no torque can be transmitted from the engine to the transmission.

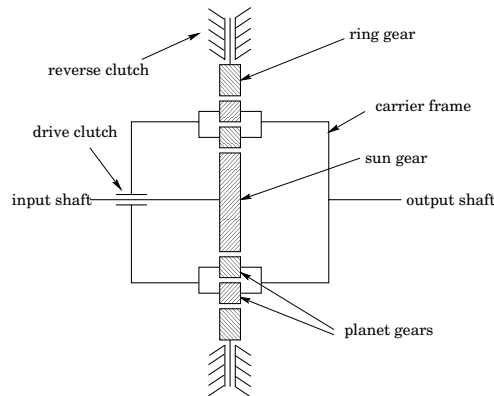


Figure 6.6: DNR set

The DNR set also may serve as an internal transmission brake if either the reverse or the drive clutch is engaged while the other is transmitting torque at a slip unequal to zero. The transmission casing then provides the reaction torque. This principle is used in the ZI Stop-Go transmission discussed in [Vroemen, 2001].

6.2.4 Torque converter

The torque converter, see Figure 6.7, essentially is a fluid coupling. Its purpose is to transmit and amplify the torque stemming from the engine during vehicle launches, *i.e.*, start propelling from zero powertrain speeds. Inside the fluid filled housing are three members, being the impeller, *i.e.*, a vaned rotor directly bolted on the engine starter flywheel, the turbine, *i.e.*, a vaned rotor connected to the transmission input shaft, and a stator, *i.e.*, a vaned body connected to the transmission housing.

The rotating impeller blades increase the velocity of the present fluid. The fluid is then thrown into the turbine blades, resulting in a change of impulse that drives the turbine. The discharge from the turbine is opposite to the impeller rotation, caused by the curvature of the turbine blades. This is corrected by the stator, which has a series of blades curved in the reverse direction of the turbine. This causes the fluid to pass through the impeller and to push on the turbine vanes again. The subsequent torque multiplication at the turbine is particularly manifest when the rotational speed of the impeller is substantially higher than that of the turbine.

During a vehicle launch, the impeller speed (equal to the engine speed ω_e), is higher than the turbine speed ω_t . This difference in speed (slip) essentially makes it possible for the torque converter to transmit the engine torque but it also results in a power loss in the torque converter. Therefore, most torque converters have a so-called lockup clutch that can mechanically connect the impeller to the turbine to prevent slippage. Under certain conditions, this clutch is engaged improving the efficiency of the total transmission. The lockup clutch is attached to the back of the turbine rotor and when it is closed it connects the impeller to the turbine. Isolator springs (total stiffness k_l) are embodied in the lockup clutch to level off torque peaks that might occur during lockup engagement. Hence, an internal degree of freedom still exists

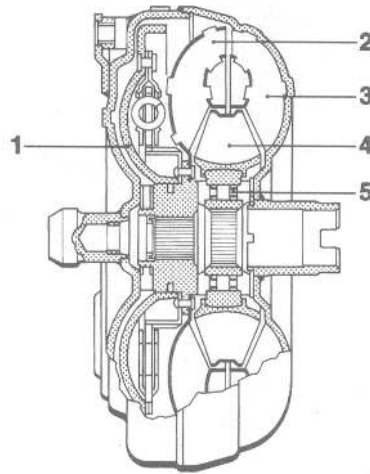


Figure 6.7: Cross section of a torque converter. 1 lockup clutch, 2 turbine, 3 impeller, 4 stator, 5 one-way clutch

in the locked up mode, influencing on the dynamic properties of the powertrain. This will be analyzed further in Section 6.5.1.

The speed ratio r_{tc} between the engine shaft and turbine shaft is defined as

$$r_{tc} := \frac{\omega_t}{\omega_e}. \quad (6.9)$$

Clearly, $r_{tc} = 1$ when the lockup clutch is engaged. The slip ratio together with the impeller speed determines the reaction torque T_i at the impeller according to:

$$T_i = b_{tc}(r_{tc})\omega_e^2, \quad (6.10)$$

where $b_{tc}(r_{tc})$ is the torque converter capacity factor. Furthermore, the torque amplification also depends on the torque converter slip and causes the hydraulic torque acting on the turbine:

$$T_t = \alpha_{tc}(r_{tc})T_i. \quad (6.11)$$

For the torque converter under investigation, both b_{tc} and α_{tc} are plotted as a function of r_{tc} in Figure 6.8.

The torque amplification of the unlocked torque converter is especially valued during vehicle launches. In stepped automatic transmission powertrains the unlock mode is frequently altered to quickly speed up the engine after a moderate drive pedal deflection. In many such cases, no gear shift is necessary then since the temporarily requested increase of power is met through the shifted engine operating point. The lockup is engaged again if the driver keeps his pedal steady. On the other hand, in practice the strategy to unlock and shift gears is a matter of extensive tuning and in fact the corporate differences in these strategies determine the particular driveability feel that sharply contrasts one car brand from the other. In the

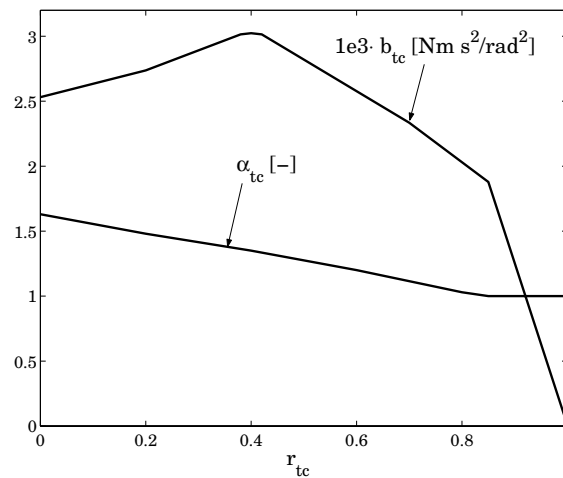


Figure 6.8: Torque capacity b_{tc} and torque amplification α_{tc} characteristics of the torque converter as a function of torque converter slip r_{tc}

case of a CVT powertrain this lockup strategy is not applied, as the CVT itself is capable of continuously shifting the engine speed to a slightly higher value. Unlocking of the torque converter can also be applied to dampen oscillations induced at the drive shafts. They may occur particularly at low gear ratios, in case of disturbances induced by the engine or gear shifting itself.

The torque amplification is quite remarkable as can be seen in Figure 6.8. There, at a speed ratio of zero, the amplification almost amounts up to 170 %. This speed ratio occurs at the very first instant of a vehicle launch, since ω_t in definition (6.9) is zero then. With increasing turbine speed ω_t the torque amplification drops to lower values. In Figure 6.9 the torque amplification as a function of vehicle speed is illustrated. In this figure the torque at the wheels is plotted for Wide Open Throttle (WOT) engine torque at different transmission gear ratios with and without the torque amplification. During vehicle launches, the CVT is in underdrive. Clearly, in underdrive the torque amplification by the converter stops at a relatively low vehicle speed. In practice this short term amplification is judged as pleasant.

The highest possible torque at the wheels, here almost 2500 [Nm], in practice is only reached in an extreme case of launching. In that case, the powertrain is put in a so called stalled state: the engine throttle is put in WOT position while the brakes keep the vehicle in standstill. The engine then reaches a stationary speed that can be solved from relation (6.10) by equating T_i to $T_{WOT}(\omega_e)$ and using $r_{tc} = 0$. For the present case this *stall engine speed* equals 230 [rad/s]. This speed and the corresponding WOT torque define an operating point at which all generated power can be dissipated in the torque converter. The subsequent launch after brake release is then the highest possible (at least if the traction at the tires is sufficient). In practice however, this kind of launching is rare: the driver rather releases his brake pedal and starts pushing the drive pedal more or less. In that case, even when WOT is reached, the maximum wheel torque is far less than the torque during stall. During such a launch all powertrain inertias as well as the oil in the torque converter need to be accelerated. This takes a substantial

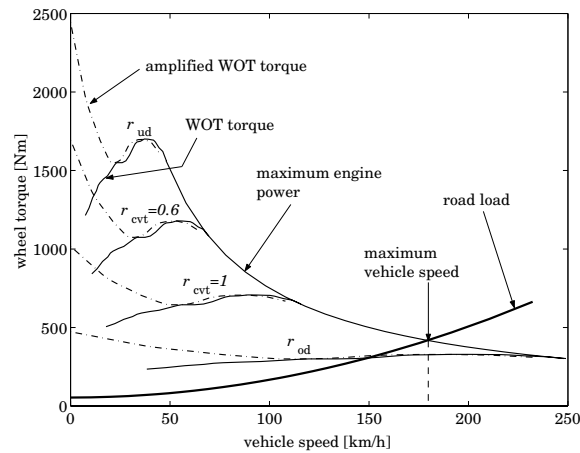


Figure 6.9: Torque amplification by the torque converter

amount of engine torque, lowering the torque at the wheels. Engine speeds approaching the stall speed then occur at a moment where the slip already has deviated substantially from zero, diminishing the torque amplification even further. In [Vroemen, 2001] an experiment showing the torque at the wheels emerging from a kickdown from standstill is compared to a simulation result of a kickdown with the ZI Stop-Go transmission.

6.2.5 Final drive, differential and drive shafts

The final drive, differential and drive shafts transmit the torque stemming from the secondary pulley to the wheels. In the model the inertias of these elements are projected onto the secondary pulley inertia.

The final drive essentially consists of two stages of gear sets that decrease the speed of the secondary pulley ω_s to the wheel speed ω_w by the overall final drive ratio $r_d = 0.2127$, i.e.,

$$r_d = \frac{\omega_w}{\omega_s}. \quad (6.12)$$

The differential allows the laterally opposed shafts and wheels in a front driven vehicle to rotate at different speeds rates during cornering while providing uniform distribution of the propelling torque stemming from the final drive. The present research, however, only investigates straight driving without cornering.

Finally, the drive shafts transmit the drive torque T_d from the differential to the wheels. The drive shafts are relatively flexible and the stiffness k_d can therefore not be neglected when performing comfort analysis, as is Section 6.5.1. The speed difference over the drive shaft is governed by the amount of torque transmitted and complies to the first order differential equation

$$\dot{T}_d = k_d(r_d\omega_s - \omega_w). \quad (6.13)$$

In the model $k_d = 6100$ [Nm/rad] and is obtained experimentally by a test bench suited for torsional shaft stiffness calibration.

6.2.6 Transmission efficiency

The CVT transmission, comprising the pump, torque converter, DNR set, variator and the final drive gearset performs with limited efficiency. Two sources for power losses can be distinguished: power losses for driving the hydraulic pump and mechanical losses caused by friction within the aforementioned components of the transmission. These losses are modeled next, and an explanation of the equivalence between *efficiency* and *torque loss* is given.

hydraulic torque loss

The torque T_{pump} needed to drive the hydraulic pump is relevant for the powertrain model, for instance for the computation of the fuel consumption in driving a prescribed velocity cycle. This pump torque depends on the operating point of the pump, *i.e.*, the pressure difference over the pump and the angular velocity of the pump shaft, and, to a lesser extent, on the oil temperature. To circumvent intricate analysis of the fluid dynamics in the pump it was decided to use a black box pump model, based on measurements in a number of operating points. The measurements are conducted by putting the DNR set in neutral position, lockup

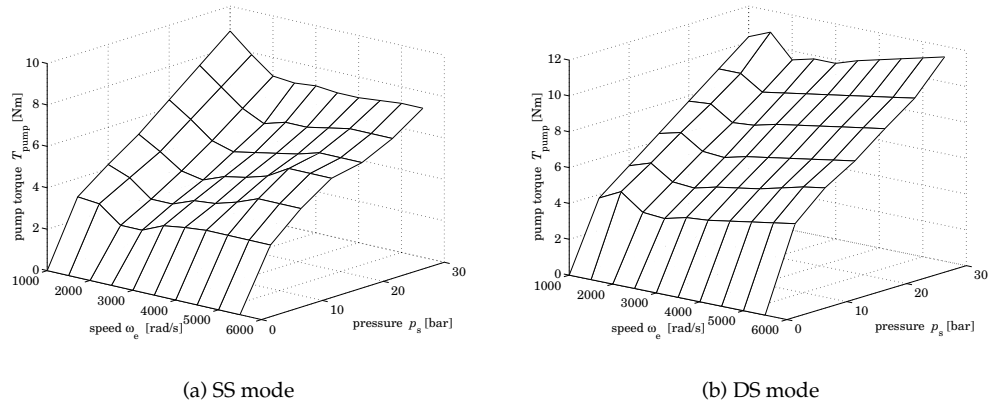


Figure 6.10: Pump loss torques T_{pump} as a function of speed and line pressure

the torque converter and drive the pump for various operating points at 80° C. In fact, also the mechanical losses in the bearings as well as the drag losses in the wet-plate DNR clutch are undeliberately incorporated then. It is assumed that this has minor contribution to the pump torque. The results of these measurements are shown in Figure 6.10, for two modes of the binary displacement type roller vane pump, *i.e.*, the single sided (SS) and double sided (DS) mode, the latter producing about two times more oil flow than the SS mode.

mechanical torque loss

Another source of power loss in a CVT is caused by friction and (micro) slip between belt and pulleys, bearing and sealing losses and friction losses within the gear wheel sets of the final

reduction and differential cage. For the CVT system under investigation it is hard to measure, let alone model, the power loss of every isolated element and therefore rather the total loss is reconstructed from measurements for a number of operating points. In these measurements the CVT was put under load at the drive shaft. Reconstructing the mechanical torque losses, the total torque loss is reduced with the pump torque. The results for the measured torque losses T_{mech} projected at the primary pulley are plotted in Figure 6.11, for input torques between 0 and 150 [Nm], and CVT ratios between 0.465 and 2.15.

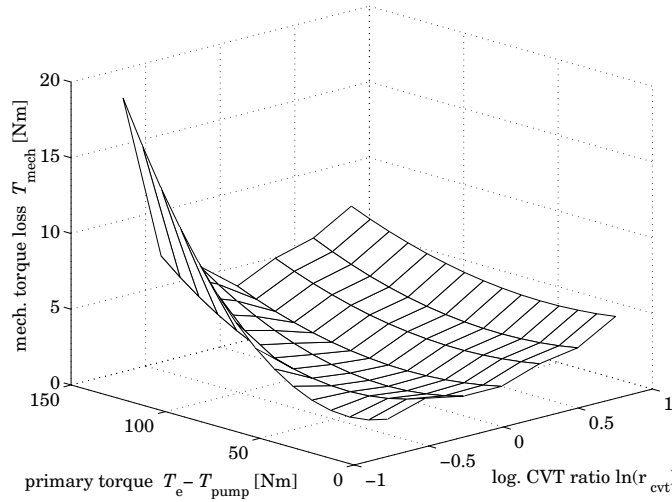


Figure 6.11: Mechanical CVT torque losses T_{mech} in CVT as a function of ratio r_{cvt} and primary torque $T_e - T_{\text{pump}}$

efficiency vs. torque loss

In general the efficiency of the transmission or a power transmitting component thereof is described as the quotient of stationary output power over the stationary input power. For the CVT transmission as a whole, the input power is the engine power $P_e = T_e \omega_e$ and the output power is the power $T_d \omega_w$ transmitted through the drive shaft. The efficiency η_{cvt} of the CVT transmission is then described as:

$$\eta_{\text{cvt}} = \frac{T_d \omega_w}{P_e} \quad (6.14)$$

For the CVT $\eta_{\text{cvt}} < 1$, caused by the pump loss torque T_{pump} and a mechanical torque loss T_{mech} . On the other hand, the torque losses are equivalent with the efficiency description (6.14) if $\eta_{\text{cvt}} < 1$ is caused by torque losses only. In other words without a gross difference between the input and output speed (ω_e and ω_w) other than caused by the kinematic transmission ratio.

In the case of the variator as a part of the total CVT, reduced efficiency is also caused by slip especially between the bands and segments of the belt. For the variator it is therefore hard to describe the difference between the *geometric* (torque transmitting) ratio α_{tc} and the *kinematic* (speed) ratio r_{cvt} .

For the moment assuming that the description in torque loss is correct the power at the wheels is described by:

$$T_d \omega_w = (T_e - T_{\text{pump}} - T_{\text{mech}}) \omega_e. \quad (6.15)$$

In describing the *mechanical efficiency* of the CVT the torque ratio α_{cvt} and speed ratio r_{cvt} can be used:

$$\eta_{\text{mech}} = \left(\frac{T_d}{T_i} \right) \left(\frac{\omega_w}{\omega_e} \right) = \left(\frac{\alpha_{\text{cvt}}}{r_d} \right) (r_d r_{\text{cvt}}), \quad (6.16)$$

where $T_i = T_e - T_{\text{pump}}$. From equation (6.16) it is obvious that a reduced efficiency emerges if

$$\alpha_{\text{cvt}} r_{\text{cvt}} < 1. \quad (6.17)$$

It also shows that the origin of the reduced efficiency (either torque loss or internal slip) does not have to be clear in order to *quantify* the efficiency. For computational purposes, the losses may therefore be described solely as a (fictitious) torque loss. Rewriting equation (6.16) then indeed yields equation (6.15):

$$T_d \omega_w = T_i \eta_{\text{mech}} \omega_e = (T_e - T_{\text{pump}} - \overbrace{(1 - \eta_{\text{mech}}) T_i}^{T_{\text{mech}}}) \omega_e. \quad (6.18)$$

In the case of an open torque converter lockup the equivalence between efficiency and torque loss can not be derived straightforwardly because gross slip between the input speed ω_e and output speed ω_p occurs. Furthermore, the impeller and turbine torque depend on this slip making it hard to write the torque loss explicitly. The efficiency of the CVT including the open torque converter can be written as:

$$\eta_{\text{cvt}} = \underbrace{\frac{T_i}{T_e}}_{\text{hydraulic efficiency}} \cdot \underbrace{\frac{T_t - T_{\text{mech}}}{T_t}}_{\text{mechanical efficiency}} \cdot \underbrace{\frac{T_t \omega_p}{T_i \omega_e}}_{\text{torque converter efficiency}} = \frac{T_i (r_{\text{tc}}) - T_{\text{mech}}}{T_e} r_{\text{tc}}, \quad (6.19)$$

which obviously depends on the torque converter slip r_{tc} .

6.2.7 Tires, vehicle and external interactions

Slip (skid) between tires and road is instrumental in generating the traction force for vehicle propulsion. The external load on the powertrain is determined by the (two-) wheel inertia J_w , vehicle mass m_v , tire deformation (roll resistance), hill grade θ and friction with the outside air. The forces, torques and parameters relevant for describing the vehicle and wheel dynamics are illustrated in Figure 6.12.

wheels

The front wheel dynamics are the result of the tractive force F_w between tire and road, the drive shaft torque T_d , the rolling resistance torque T_{rr} of the front tires (discussed later on) and the brake torque T_{brake} :

$$\dot{\omega}_w = \frac{T_d - F_w R_w - T_{\text{rr}} - T_{\text{brake}}}{J_w}, \quad (6.20)$$

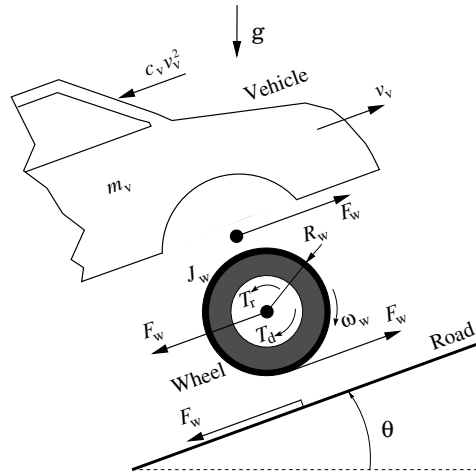


Figure 6.12: Road-wheel-vehicle interaction

where J_w represents the total moment of inertia of the combined front wheels. In this equation it is assumed that the brake torque T_{brake} is entirely applied at the front wheels. In practice, all four wheels have disc brakes and generally the brake torques are distributed over the front and rear wheels. In this thesis braking performance is not seen as one of the subjects of interest and vehicle braking is therefore only adopted instrumentally to facilitate fuel economy simulations. Such simulations could be compared to those measured in practice on a chassis dynamometer. As only the driving wheels (front in this case) are placed on the dynamometer rollers the brake torque can only be applied to the front tires. A first approximation of the brake torque is assumed to have a linear relation with the brake pedal force β :

$$T_{\text{brake}} = c_{\text{brake}} \beta. \quad (6.21)$$

In this equation β is a normalized braking force $\beta \in [0..1]$ and $c_{\text{brake}} = 1500$ [Nm] was seen to give satisfactory results in simulations¹.

In equation (6.20), the tire tractive force F_w essentially is generated through the road surface adhesion coefficient μ and the normal force acting on the front wheels:

$$F_w = \mu(\psi) m_{v,f} g \cos \theta. \quad (6.22)$$

where $m_{v,f} = 800$ [kg] (for the test vehicle, Chapter 8) represents the part of the total vehicle mass supported by the front wheels and g is the gravity. The coefficient μ depends on the relative slip ψ between tire and road. The slip ψ is defined differently when the wheels transmit a *driving* torque from the drive shaft and when they experience a *driven* torque from the road,

¹In simulations a virtual driver presses the brake pedal with force β according to a prescribed velocity pattern that needs to be tracked.

i.e., during braking and coasting.

$$\psi = \begin{cases} \left(1 - \frac{\omega_w R_w}{v_v}\right), & \omega_w R_w \leq v_v, \text{ driven} \\ \left(1 - \frac{v_v}{\omega_w R_w}\right), & \omega_w R_w > v_v, \text{ driving.} \end{cases} \quad (6.23)$$

At least for slip rates smaller than 0.15 the shape of the function $\mu(\psi)$ can be approximated by a linear function [Cho and Hedrick, 1989], *i.e.*,

$$\mu(\psi) = b_w \psi \text{sign}(\omega_w R_w - v_v), \quad (6.24)$$

where b_w is approximately 8.8 [-].

Due to the non-symmetric deformation of the tire at the contact interface with the road, the normal force from the road on the tire acts at a small lever $x_r \approx 0.004$ [m] (for asphalt) away from the wheel center. This causes the so-called roll resistance torque T_r for all tires together. The rolling resistance torques for the (combined) front T_{rf} and rear T_{rr} wheels differs if the vehicle mass distribution is inhomogeneous, which is the case here. The rolling resistance torques then become:

$$T_r = T_{rf} + T_{rr} \quad (6.25)$$

$$T_{rf} = x_r m_{v,f} g \cos \theta \quad (6.26)$$

$$T_{rr} = x_r (m_v - m_{v,f}) g \cos \theta \quad (6.27)$$

vehicle

The vehicle acceleration is established by the resulting torque of the tire tractive force, air drag and the rolling resistance of the rear wheels (which do not contribute to the traction), *i.e.*,

$$\dot{v}_v = \frac{F_w - T_{rr}/R_w - c_v v_v^2 - m_v g \sin \theta}{m_v + J_w/R_w^2}, \quad (6.28)$$

in which c_v^2 is the air drag coefficient. The term $m_v g \sin \theta$ represents the hill climbing resistance for $\theta > 0$ or downgrade force when $\theta < 0$.

6.3 Description of the ZI powertrain

The ZI powertrain, as developed in the underlying project, is basically a standard CVT powertrain where a planetary gear stage is connected in parallel to the primary and secondary pulley. The key mechanism of the ZI powertrain was briefly discussed in Chapter 4. Here, it will be repeated in order to facilitate some definitions relevant for the adaptation of the CVT powertrain model into the ZI powertrain model. Surprisingly, it appears that the ZI model structurally equals the CVT powertrain, though additional parametric non-linearities modify the dynamics of the original CVT powertrain significantly.

Before the ZI powertrain was actually built a number of optimisations on different conceptual levels were undertaken. One of them will be briefly discussed in the next section. Others can be found in [van Druten, 2001].

²The air drag coefficient c_d in Section 2.3.3 and c_v in this section relate as $c_v = \frac{1}{2} \rho A c_d$, where ρ is the ambient air density and A the frontal vehicle surface.

6.3.1 Key idea

The key idea behind the zero inertia powertrain started with the engineering question “is it somehow possible to cancel the detrimental effect of the primary inertias (engine, pump, DNR, torque converter, primary pulley) exploiting another inertia, *i.e.*, an additional flywheel?” [Mussaesus and Veenhuizen, 1998]. This appeared to be possible by connecting a planetary gear set in parallel with the CVT and connecting the flywheel to one of the planetary gear set members, [van Druten *et al.*, 2000a]. The design concepts of this parallel unit are described in [van Druten, 2001]. There, also the motivations behind choosing the particular order of connecting the members to respectively the primary pulley, secondary pulley and flywheel are given. This resulted in a configuration where the annulus is connected to the primary pulley, the carrier is connected to the secondary pulley and the sun is integrated with the flywheel, *viz.* Figure 6.13.

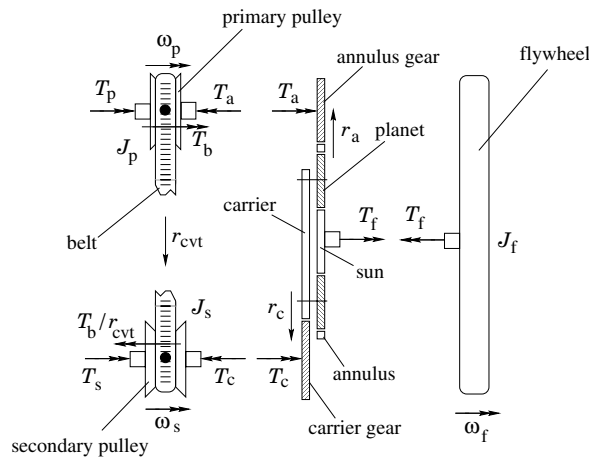


Figure 6.13: Key configuration of ZI: CVT with planetary set and flywheel in parallel

main characteristics of the ZI configuration

Consult for the following analysis also Appendix B. The flywheel speed is determined by the primary and secondary pulley speed, *i.e.*,

$$\omega_f = -\frac{z+1}{r_c} \omega_s + \frac{z}{r_a} \omega_p. \quad (6.29)$$

Using the definitions:

$$\alpha_s := \frac{z+1}{r_c}; \quad \alpha_p := \frac{z}{r_a}; \quad r_{gn} := \frac{\alpha_p}{\alpha_s}, \quad (6.30)$$

and (6.4) it follows that the flywheel speed is given by³

$$\omega_f = -\alpha_s \left(1 - \frac{r_{gn}}{r_{cvt}} \right) \omega_s. \quad (6.31)$$

³Note that for $r_{cvt} > r_{gn}$ the flywheel speed is negative.

Obviously, the flywheel speed becomes zero whenever $r_{\text{cvt}} = r_{\text{gn}}$. Therefore, r_{gn} is called the geared neutral ratio.

The torque $T_f = J_f \dot{\omega}_f$, stemming from the accelerating or decelerating flywheel, is split by the planetary gear set into a torque T_a at the annulus gear and a torque T_c at the carrier gear, such that (see Appendix B):

$$T_a = -\alpha_s r_{\text{gn}} J_f \dot{\omega}_f; \quad T_c = \alpha_s J_f \dot{\omega}_f. \quad (6.32)$$

Hence, T_a and T_c are related by

$$T_a = -r_{\text{gn}} T_c. \quad (6.33)$$

From this last equation the operation of the flywheel unit can be readily explained as follows. If $\dot{\omega}_f$ becomes positive (flywheel decelerates) then the annulus gear *demand*s a reaction torque T_a from the primary pulley given in (6.32) through which the carrier gear can *deliver* a torque T_c to the secondary pulley. This torque T_c is an amplification of T_a if $r_{\text{gn}} < 1$. The inverse reasoning holds for an accelerating flywheel. The net torque stemming from the flywheel at the secondary pulley is given by

$$T_n = T_c + \frac{T_a}{r_{\text{cvt}}} = \alpha_s \left(1 - \frac{r_{\text{gn}}}{r_{\text{cvt}}} \right) J_f \dot{\omega}_f, \quad (6.34)$$

which is obviously positive for $(r_{\text{cvt}} - r_{\text{gn}})\dot{\omega}_f > 0$. Taking into account that $\dot{\omega}_s$ is typically an order of magnitude smaller than $\dot{\omega}_f$, it can be seen from equation (6.31) that the flywheel decelerates as the CVT ratio r_{cvt} decreases, and vice versa. Decreasing the CVT ratio increases the primary speed and thus also the engine speed, resulting in the primary pulley, torque converter and engine inertias J_p , J_t and J_e absorbing part of the torque. Provided the flywheel inertia J_f is chosen large enough and the CVT speed ratio is manipulated appropriately, then the engine torque T_e may take the acceleration of J_e , J_p and J_t on its account, while the flywheel unit delivers the desired net torque T_n as in (6.34) to the secondary pulley. This is exactly the behaviour necessary to overcome the reluctance in vehicle response whenever large pedal deflections are accompanied by large leaps in engine speed. An optimal design of the geared neutral ratio r_{gn} and J_f is required to let the sizing of the flywheel unit be in concert with its function.

The net assisting torque T_n in equation (6.34) basically only depends on inertial forces and kinematics that are controllable by the CVT ratio. The parametric description of the dynamics is similar to the description for the CVT powertrain and is derived in Appendix B.

6.3.2 Optimized functional design

In the previous section a number of parameters of the ZI system was identified. The flywheel unit is added to the powertrain of a commercially available car without any further essential modification of that powertrain. Hence, only the parameters J_f , z , r_a and r_c of the flywheel unit have to be optimized for the chosen car. The value of these parameters determines the effectiveness of the flywheel. This effectiveness is large if the stored flywheel energy can be exploited as much as possible during a CVT downshift. This has to do with the location of the geared neutral ratio r_{gn} within the ratio coverage of the variator. In practice, a downshift often occurs from the overdrive ratio down to around medium. If r_{gn} is chosen at medium, then the flywheel energy is maximally used at least for this situation. On the other hand, the CVT ratio is also frequently controlled below medium, *e.g.*, during launching of the vehicle. The flywheel rotates in the opposite direction for $r_{\text{cvt}} < r_{\text{gn}}$, and basically increases (in absolute

sense) for further decrease of r_{cvt} . A vehicle launch then results in an (unwanted) acceleration of the flywheel. This acceleration is higher if r_{gn} is closer to r_{od} . Hence, the effectiveness of the flywheel as a power-boost unit is penalized by the situation during launch. Clearly, an optimization strategy is required to maximize the boost effectiveness while minimizing the launch penalty. Both aspects therefore need to be quantified in some sense in order to use them in a to-be-minimized objective function.

energy functions

Regarding the kinetic energy within the powertrain the optimization criteria can easily be quantified. The purpose of the system is to cancel the influence of the primary inertias, using a counteracting flywheel inertia. In terms of energy this means that the total kinetic energy should preferably decrease for decreasing CVT ratio and vice versa. The kinetic energy of the primary inertias (assuming a locked torque converter) is given by

$$E_p = \frac{1}{2}(J_e + J_p + J_t)\omega_p^2 = \frac{1}{2}(J_e + J_p + J_t)\frac{\omega_s^2}{r_{\text{cvt}}^2} \quad (6.35)$$

and for the flywheel by

$$E_f = \frac{1}{2}J_f\omega_f^2 = \frac{1}{2}J_f\alpha_s^2 r_{\text{gn}}^2 \left(\frac{1}{r_{\text{cvt}}} - \frac{1}{r_{\text{gn}}}\right)^2 \omega_s^2. \quad (6.36)$$

The kinetic energy of all secondary sided inertias including the vehicle is given by

$$E_s = \frac{1}{2}(J_s + r_d^2 J_v)\omega_s^2, \quad (6.37)$$

where

$$J_v = m_v R_w^2 + 2J_w \quad (6.38)$$

The relative energies of the primary inertias and the flywheel with respect to the secondary inertias follow from

$$e_p = \gamma \frac{1}{r_{\text{cvt}}^2}; \quad e_f = \gamma \gamma_f \left(\frac{1}{r_{\text{cvt}}} - \frac{1}{r_{\text{gn}}}\right)^2, \quad (6.39)$$

where γ and γ_f are defined by

$$\gamma = \frac{J_e + J_p + J_t}{J_s + r_d^2 J_v}; \quad \gamma_f = \alpha_s^2 r_{\text{gn}}^2 \frac{J_f}{J_e + J_p + J_t}. \quad (6.40)$$

The constant γ is completely determined by parameters of the unmodified CVT powertrain whereas γ_f depends on the design parameters of the flywheel unit.

Obviously, for a given design of the flywheel unit, the relative energies e_p and e_f and also their sum $e = e_p + e_f$ only depend on the CVT ratio r_{cvt} . For an arbitrary but realistic design these functions are plotted in Figure 6.14. The minimum of e occurs for $r_{\text{cvt}} = r_{\text{zi}}$, where the so-called zero inertia ratio r_{zi} is given by:

$$r_{\text{zi}} = \left(1 + \frac{1}{\gamma_f}\right) r_{\text{gn}}. \quad (6.41)$$

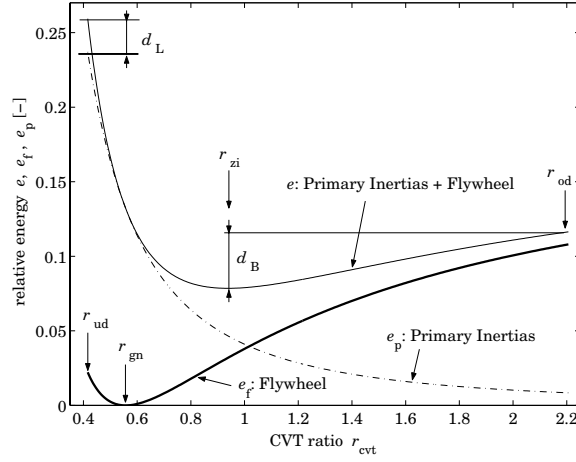


Figure 6.14: Kinetic Energy Functions

This ratio has to do with the ‘zero inertia’ situation: when shifting the CVT through this ratio the equivalent inertia felt at the primary side is equal to zero. This remark is in agreement with the observation that the total relative energy does not change when shifting the CVT through this ratio.

In terms of energy, the boost effect of the flywheel can be explained by the decreasing total relative energy for decreasing CVT ratios r_{cvt} as long as $r_{cvt} > r_{zi}$. For the unmodified powertrain the primary inertias J_e , J_p and J_t always require increasing energy for decreasing CVT ratio. Stated otherwise, the released flywheel energy for decreasing CVT ratios will boost the vehicle as long as $r_{cvt} > r_{zi}$. Therefore, the first variable for the (yet to be defined) objective function Γ_{LB} is the so-called boost energy d_B , defined as the difference between the total relative energy for $r_{cvt} = r_{od}$ and this energy for $r_{cvt} = r_{zi}$. Using the definition of the zero inertia ratio it is readily seen that

$$d_B = \frac{\gamma}{1 + \gamma_f} \left(\frac{1 + \gamma_f}{r_{od}} - \frac{\gamma_f}{r_{gn}} \right)^2. \quad (6.42)$$

For decreasing CVT ratios r_{cvt} with r_{cvt} between r_{ud} and r_{gn} the increase of the total relative energy e for the powertrain with the flywheel unit is larger than the increase of the relative energy e_p for the unmodified powertrain. Obviously, the largest difference between e and e_p needs to be minimized. This difference, denoted by d_L , occurs for $r_{cvt} = r_{ud}$, so

$$d_L = \gamma \gamma_f \left(\frac{1}{r_{ud}} - \frac{1}{r_{gn}} \right)^2. \quad (6.43)$$

This quantity serves as the second variable in the objective function Γ_{LB} .

For decreasing CVT ratios r_{cvt} with $r_{gn} < r_{cvt} < r_{zi}$ the total relative energy for the powertrain with the flywheel unit also increases but less fast than for the unmodified powertrain. Therefore, this part of the curves in Figure 6.14 is not taken into account in the objective function Γ_{LB} .

Summarizing, it can be stated that the boost effectiveness of the flywheel unit is large whenever d_B is large, whereas the penalty on the vehicle launch is small whenever d_L is small.

optimization

The adopted objective function Γ_{LB} to optimize the design parameters of the flywheel unit is given by

$$\Gamma_{LB} = d_L + \frac{W_B}{d_B}, \quad (6.44)$$

where the positive number W_B weighs the relative importance of the launch penalty d_L over the boost effectiveness d_B . Substitution of the earlier given relations for d_B and d_L yields

$$\Gamma_{LB} = \gamma \gamma_f \left(\frac{1}{r_{ud}} - \frac{1}{r_{gn}} \right)^2 + \frac{W_B}{\gamma} (1 + \gamma_f) \left(\frac{1 + \gamma_f}{r_{od}} - \frac{\gamma_f}{r_{gn}} \right)^{-2}. \quad (6.45)$$

There are several constraints on the design parameters. From Figure 6.14 it is clear that r_{gn} must be greater than r_{ud} and that r_{zi} must be smaller than r_{od} . Since $r_{gn} < r_{zi}$ (see equation (6.41)) this also implies $r_{gn} < r_{od}$. With the definition of the zero inertia ratio r_{zi} in equation (6.41) and using the fact that $\gamma_f > 0$, these constraints can be rewritten as

$$r_{gn} > r_{ud}; \quad \gamma_f(r_{od} - r_{gn}) > r_{gn}. \quad (6.46)$$

Other constraints have to do with the available space in the engine compartment and with the strong desire to minimize the weight of the flywheel unit and the power losses in this unit. The main source of these losses is the air drag between the rotating flywheel and the flywheel casing. A further elaboration, combined with the endeavor to make the flywheel as compact as possible, resulted in maximal allowable values $J_{f,max}$ and $\omega_{f,max}$ for, respectively, the moment of inertia and the stationary speed of the flywheel. The values $J_{f,max} = 0.4$ [kgm²] and $\omega_{f,max} = 750$ [rad/s] turned out to be quite reasonable, *cf.* [van Druten and Kok, 1998].

To investigate the consequences of the requirement with respect to the maximal stationary flywheel speed it is assumed that the vehicle moves with a known, constant velocity on an horizontal road, experiencing a known load due to air drag and rolling resistance. Then the secondary speed ω_s and the power P_v to drive the vehicle are known. It is assumed that this power P_v is delivered by the engine in an engine operating point on the E-line. In operating points on the E-line the engine speed (and, since the torque converter is assumed to be locked, also the primary speed ω_p) is a function of the delivered power. Hence, in stationary situations there is a fixed relation between the secondary and the primary speed, *i.e.*, $\omega_p = \omega_{E-line}(\omega_s)$. This relation holds for the unmodified powertrain as well as for the ZI powertrain. Substitution in equation (6.31) gives the stationary flywheel speed ω_f as a function of ω_s . The requirement $\omega_f \leq \omega_{f,max}$ then boils down to

$$\alpha_s(\omega_s - r_{gn} \omega_{E-line}(\omega_s)) \leq \omega_{f,max} \quad (6.47)$$

or, formulated in terms of the parameter α_s , to $\alpha_s \leq \alpha_{s,max}$ with

$$\alpha_{s,max} = \frac{\omega_{f,max}}{\max_{\omega_s}(\omega_s - r_{gn} \omega_{E-line}(\omega_s))} \quad (6.48)$$

Combined with the demand $J_f \leq J_{f,max}$ this results in a constraint for the parameter γ_f :

$$\gamma_f \leq \alpha_{s,max}^2 r_{gn}^2 \frac{J_{f,max}}{J_e + J_p + J_t} \quad (6.49)$$

#	$J_{f,\max}$	W_B	d_B	d_L	Γ_{LB}	r_{gn}	r_{zi}
1	0.20	0.020	0.032	0.246	0.866	0.901	1.153
2	0.20	0.004	0.021	0.098	0.287	0.766	1.152
3	0.40	0.020	0.056	0.112	0.448	0.698	0.940
4	0.40	0.004	0.040	0.036	0.136	0.595	0.948
5	0.40	–	0.039	0.029	–	0.577	0.944

Table 6.1: Functional optimization results

Summarizing, the relevant constraints for the minimization of the objective function Γ_{LB} are given by

$$r_{gn} > r_{ud} \quad (6.50)$$

$$\gamma_f > 0; \quad \gamma_f(r_{od} - r_{gn}) - r_{gn} > 0 \quad (6.51)$$

$$\gamma_f(J_e + J_p + J_t) - \alpha_{s,\max}^2 r_{gn}^2 J_{f,\max} \leq 0 \quad (6.52)$$

The constrained minimization problem is solved for r_{gn} and γ_f , using the optimization toolbox in MATLAB. Some results for different values of the weight W_B and the maximal allowable flywheel inertia $J_{f,\max}$ are presented in Table 6.1.

Solution # 5 in this table stems from an optimization performed through an extensive amount of simulations with alternating $J_{f,\max}$ and r_{gn} . In this optimization also the gear sizing and the absolute speeds (minimal bearing losses) of the gear wheels in the planetary gearset played an important role, see [van Druten, 2001]. This solution was the starting point for the design of the prototype flywheel unit that is actually realized and tested. The parameters of this design resemble the results of solution # 4 fairly close.

It is inferred from the table that the launch penalty d_L is high whenever the boost effectiveness d_B is high. A larger value for the allowable moment of inertia $J_{f,\max}$ of the flywheel would result in a lower minimum for Γ_{LB} but this is not desirable in terms of additional vehicle weight. Applying a lower weight W_B suppresses the boost effectiveness and consequently also the launch penalty. This illustrates that W_B can effectively be used to manipulate the trade-off between d_B and d_L .

It can easily be shown that unconstrained minimization of the objective function Γ_{LB} does not yield a feasible solution for r_{gn} and γ_f : the requirement that the derivative of Γ_{LB} with respect to r_{gn} is equal to 0 results in a contradiction. Hence, at least one constraint will be active in the constrained minimization of Γ_{LB} . For the current minimizations this turns out to be the constraint (6.52). This implies that for the solution of the constrained problem not $J_{f,\max}$ and $\omega_{f,\max}$ itself but only the combination $J_{f,\max} \omega_{f,\max}^2$ is relevant. Much higher maximal speeds than 750 [rad/s] are not desirable as air drag losses within the flywheel housing would increase substantially then. Moreover, the first rotor-dynamical eigenmode of the flywheel will start manifesting (1100 rad/s, [van Druten *et al.*, 2000c]).

6.4 Dissipative torsional compliance model

The previous sections provide all ingredients to compile the total powertrain model. Implicitly, some inertias were introduced but their origin was not explained in detail for all cases. This is redeemed here when imaginatively bolting all components to one another arriving at

a *dissipative torsional compliance powertrain model*. This model is drawn in Figure 6.15. The indicated dots represent nodes where transmitted torques can be monitored according to the definition in Figure 6.1. The characters near the dots refer to the index of the respective torque. The rod shaped elements refer to inertias, the half circular pairs to dissipative pro-

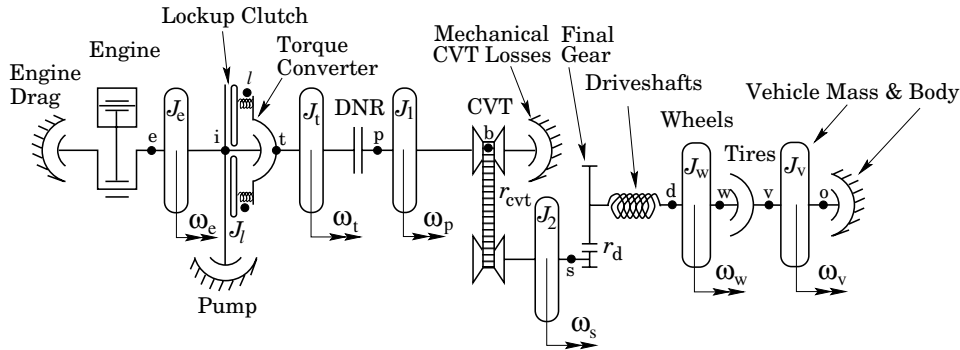


Figure 6.15: Dissipative torsional compliance powertrain model

cesses (*e.g.*, damping), two parallel vertical lines to clutches and the spring shapes to compliances. Transmission ratios being that of the CVT and the final reduction gear are symbolized separately. The definition of the respective inertias is somewhat tricky as the naming generally covers less than the actual inertia represents. The ‘engine inertia’ J_e for instance includes not only the crankshaft, pistons, camshaft, cylinders and starter flywheel, but also the impeller inertia as well as the pump as they are directly connected to the engine starter flywheel. The ‘turbine inertia’ J_t includes both the turbine as well as the sun gear of the DNR set. The ‘primary equivalent inertia’ J_1 includes the carrier with planets and annulus of the DNR set and of course the equivalent primary pulley inertia. The ‘secondary equivalent inertia’ J_2 comprises the secondary equivalent pulley inertia, the projected final drive inertia and the differential cage inertia. The ‘wheels inertia’ J_w represent the inertia of the two front wheels, and finally the ‘vehicle inertia’ J_v represents the rotational equivalent of the vehicle mass raised with the combined inertia of the two rear wheels.

Although the real powertrain system may arguably be considered as *continuous*, modeling it within the area of interest urge the introduction of *discrete transitions*. Often, a system (either real or a model) is termed a ‘hybrid dynamic system’ if it is of mixed continuous and discrete nature, [van der Schaft and Schumacher, 1999]. In Appendix C, the hybrid equations for the powertrain model of Figure 6.15 are given. There, also a descriptive, though not formal, list of discrete modes q is given. For analyzing certain properties of the powertrain model, often the jump from one continuous state mode to another (event) is of less interest. For instance, in the mutual comparison of the CVT and ZI powertrain one continuous state mode is considered.

On the other hand, for simulating the possible operations of the powertrain, it is important to incorporate all relevant discrete state events. In the case of the switched CVT model (6.7), the engagement of the ‘D’ clutch and lockup of the torque converter constitute discrete events in that the number of state variables reduces or increases. In the next paragraph, however, a method is presented to *maintain* the number of state variables at the cost of slightly more computational effort. Other events occur when input or state saturations are reached. For instance, the engine torque can not become larger than the WOT torque, and the CVT

ratio is limited between r_{ud} and r_{od} . Special measures have to be undertaken to cope with these boundaries. In simulations, the handling of discrete events within the continuous model structure is basically established through carefully controlling the resetting of the time integrators involved. Two examples are elaborated to illustrate this. The first example illustrates the lockup of the torque converter. The second example illustrates the switching between the up- and down shifting models for the CVT ratio.

discrete event: lockup of torque converter

Schematically, the torque converter (see also Figure 6.15) is modeled as in Figure 6.16. The

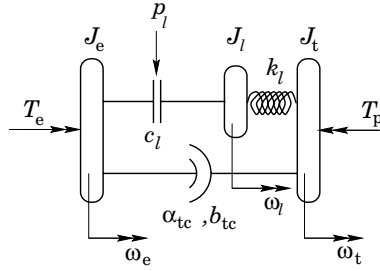


Figure 6.16: Schematic representation of the torque converter with lockup

control pressure p_l aims at engaging the two clutch plates of the lockup arrangement, after a lockup control signal is given ($p_l = 0$ for open torque converter). Whenever the plates are not completely engaged the governing equations of motion are given by:

$$J_e \dot{\omega}_e = T_e - b_{tc} \omega_e^2 - c_l p_l \text{sign}(\omega_e - \omega_l) \quad (6.53)$$

$$J_l \dot{\omega}_l = c_l p_l \text{sign}(\omega_e - \omega_l) - T_l \quad (6.54)$$

$$\dot{T}_l = k_l (\omega_l - \omega_t) \quad (6.55)$$

$$J_t \dot{\omega}_t = \alpha_{tc} b_{tc} \omega_e^2 + T_l - T_p, \quad (6.56)$$

which obviously represents a fourth order system. If the clutch is completely engaged the number of equations, and thus also the system order, is reduced by one, *i.e.*,

$$(J_e + J_l) \dot{\omega}_e = T_e - T_l \quad (6.57)$$

$$\dot{T}_l = k_l (\omega_e - \omega_t) \quad (6.58)$$

$$J_t \dot{\omega}_t = T_l - T_p. \quad (6.59)$$

To compute the torque T_x at the so-called cutting edge, *i.e.*, the torque in between the inertias J_e and J_l , the original 4-state model can also be used when the lockup clutch is completely engaged, see [Karnopp, 1985]. For simulation purpose this is assumed to be true if $|\omega_e - \omega_l| < \varepsilon$, with a positive threshold ε . For an engaged lockup the equations are rewritten as:

$$J_e \dot{\omega}_e = T_e - T_x \quad (6.60)$$

$$J_l \dot{\omega}_l = T_x - T_l \quad (6.61)$$

$$\dot{T}_l = k_l (\omega_l - \omega_t) \quad (6.62)$$

$$J_t \dot{\omega}_t = T_l - T_p, \quad (6.63)$$

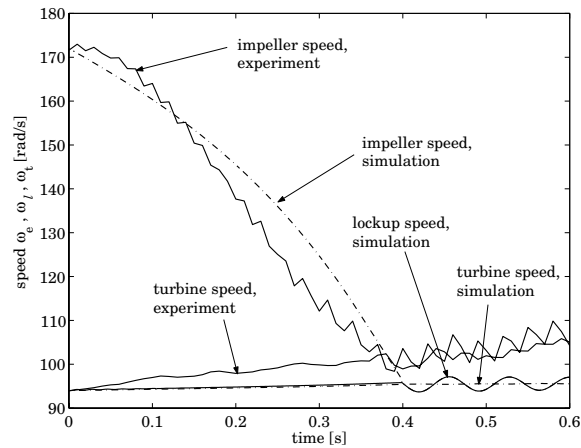


Figure 6.17: Simulation and experiment of lockup transition

with cutting edge torque

$$T_x = \frac{J_e T_i + J_i T_e}{J_e + J_i}.$$

This expression is found by equating $\omega_e = \omega_i$ and reworking the equations (6.60) and (6.61). If the engagement is detected, the integrator for $\dot{\omega}_i$ is reset at $\omega_i = \omega_e$, essentially increasing the actual ω_i by at most ε . The first two equations result in exactly the same speeds as long as the lockup is closed. Using these equations has the advantage that the model structure does not have to be changed. A disadvantage might be the slightly more computational load, but the current state-of-the-art in computing does not put any restrictions on these additional efforts. Furthermore, the value ε should not be too large, because resetting the integration of $\dot{\omega}_i$ introduces a stepwise change in the kinetic energy. On the other hand the inertia J_i is extremely small ($1e-5$ [kgm²]) compared to the other inertias in the powertrain, see Appendix C. The same holds for the value ε chosen at 1 [rad/s] and is comparatively small with respect to the absolute values seen for ω_i and ω_e .

In Figure 6.17 the solution for the equations (6.60) until (6.63) is shown. For comparison also a field experiment with the lockup clutch is included. The simulation resembles the experiment fairly well. The turbine speed slightly grows in the experiment due to the CVT which, contrary to the simulation, moderately shifts down.

discrete event: switching CVT ratio models

The second example shows how the CVT ratio model (6.7) is implemented such that the ratio can track a continuous course in time. The current time instant is t_q , being the instant where mode q (either up or downshifting) has become active. The choice for either of the two

switched models is detected by Boolean operators:

```

if  $\dot{\nu}_d(t_q) < 0 \wedge \dot{\nu}_d(t_q^-) \geq 0$ ,
     $\dot{\nu} = -c_5(\nu - \nu_d)$ , for  $t_q \leq t < t_{q+1}$ ;  $\nu(t_q) = \nu(t_q^-)$ 
elseif  $\dot{\nu}_d(t_q) > 0 \wedge \dot{\nu}_d(t_q^-) \leq 0$ ,
     $\ddot{\nu} = -c_3(\dot{\nu} - \dot{\nu}_d) - c_4(\nu - \nu_d)$ , for  $t_q \leq t < t_{q+1}$ ;  $\dot{\nu}(t_q) = \dot{\nu}(t_q^-)$ ;  $\nu(t_q) = \nu(t_q^-)$ 
end

```

Here, again, the logarithmic CVT ratio $\nu = \ln(r_{\text{cvt}})$ is used. The first statement checks if the mode has to be shifted from up to downshifting, whereas the second statement checks for the reverse jump. The integration of either model continues until a new mode shift $q + 1$ needs to be initialized. The initial conditions of the integrations in fact put the initial state of the new mode to coincide with the last state of the previous mode. Results of this method were already shown in Figure 6.5.

6.5 Comparison of the CVT and ZI powertrain

6.5.1 Linearized system analysis

The simulation model described in the previous section is far too complex for an analysis in closed form. Therefore a simplified model is proposed, essentially picking out one of the many discrete model modes and leaving out both pump and mechanical losses. The chosen model mode refers to forward driving with driving wheels on a flat road. The engine and CVT dynamics, in fact *actuator* dynamics, from setpoint to realized output are left out. Rather the response of these actuators is seen as an external input to the powertrain system. The system is described by a set of 7 nonlinear first order differential equations:

$$\dot{x}(t) = f(x(t)) + g(x(t))u(t). \quad (6.64)$$

The chosen state $x = [\omega_e \ T_t \ \omega_p \ r_{\text{cvt}} \ \omega_w \ T_d \ v_v]^T$ describes the engine dynamics, torque converter dynamics, variable shunt dynamics (Appendix B), CVT input dynamics, tire-road dynamics, drive shaft dynamics and longitudinal vehicle dynamics. The external input vector u stores the engine torque and the CVT ratio shift rate, *i.e.*, $u = [T_e \ \dot{r}_{\text{cvt}}]^T$. The expressions for $f(x)$ and $g(x)$ are given in Appendix C.2. There, also the linearization of (6.64) around a stationary point (x_0, u_0) is described. The perturbations δx and δu around a stationary state x_0 with input u_0 are assumed to be small enough to remain in close proximity of the equilibrium state x_0 . Therefore the dynamics of these perturbations may be described as the first order approximation

$$\delta \dot{x} = \left(\left. \frac{\partial f(x)}{\partial x} \right|_{x_0} + u_0 \left. \frac{\partial g(x)}{\partial x} \right|_{x_0} \right) \delta x + g(x_0) \delta u, \quad (6.65)$$

or, using \tilde{x} and \tilde{u} instead of δx and δu , in standard linear state space formulation:

$$\dot{\tilde{x}} = A \tilde{x} + B \tilde{u}. \quad (6.66)$$

magnitude frequency responses: drive comfort

The linearized powertrain model appears to be appropriate for predicting the level of comfort. In literature, frequently also linear models are used to investigate the influence of for example clutch judder in manual transmission powertrains, [Rabeih and Crolla, 1996] or total vibration analysis, [Wang *et al.*, 2000]. The former puts focus on internal gearbox stiffnesses more than on the damping capabilities of the tires. Due to slip between tires and road these capabilities are instrumental in that they predominantly determine the damping of the powertrain-vehicle vibration system, see also [Mitschke, 1997].

In Figure 6.18(a) the 7th order linear system (6.66) shows a variety of magnitude frequency responses (MFR) from perturbations of the engine torque $\tilde{T}_e = \tilde{u}_1$ to the vehicle acceleration \tilde{v}_v , whereas in Figure 6.18(b) the MRF is shown from the CVT ratio shift speed $\tilde{r}_{cvt} = \tilde{u}_2$ to \tilde{v}_v . The vehicle acceleration is chosen as the output as this quantity is a direct measure for passenger comfort (see also Chapter 7).

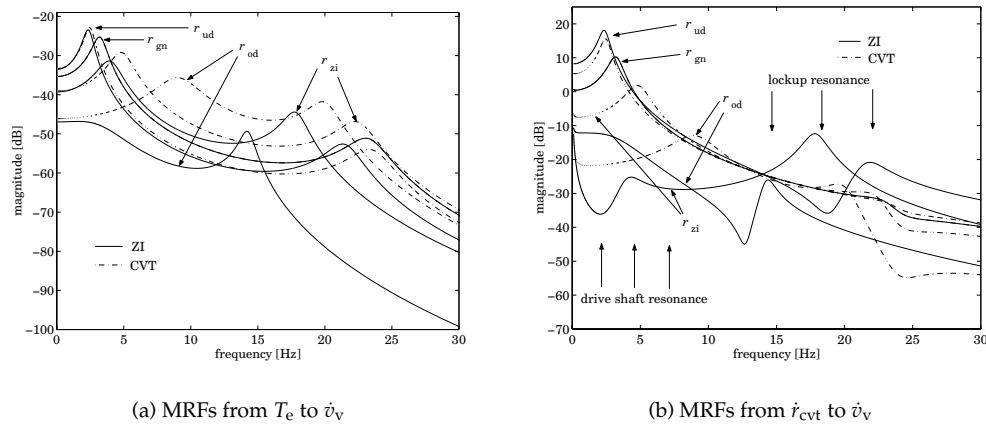


Figure 6.18: MRFs from the input vector to the vehicle acceleration for $r_{cvt} = r_{ud}, r_{gn}, r_{zi}, r_{od}$ and $\omega_{e0} = 150$ [rad/s]

The MRFs show two eigenfrequencies. Inspection of the stiffness parameters of the lockup spring and the drive shafts and of the surrounding inertias learns that the first eigenfrequency (2-9 Hz) is most related to the drive shaft, whereas the second eigenfrequency can be linked to the torque converter spring. In the following analysis, the first eigenmode is therefore referred to as *drive shaft resonance* and the second as *lockup resonance*. From the figures it becomes clear that the ZI flywheel affects the vibration dynamics considerably. The drive shaft resonance shows lower eigenfrequencies in case of ZI, except at $r_{cvt} = r_{gn}$ where the eigenfrequencies are exactly equal. The amplitudes for the drive shaft resonance are considerably lower for the ZI system, at least for $r_{gn} < r_{cvt} < r_{od}$. The flywheel pushes the frequency of the lockup resonance to lower values, though the amplitudes show a less straightforward character. The amplitudes of the lockup resonance of the MRF from T_e to v_v for ZI are higher for ratios smaller than approximately r_{zi} . On the other hand, the amplitude of the lockup resonance for ZI is considerably lower when $r_{cvt} = r_{od}$. From the MRFs also the influence of the periodical

part ΔT_e of the engine torque as in equation (6.2) can be identified. For constant engine speed ω_{e0} , the individual combustions (each cylinder chamber combusts once every two crankshaft revolutions) lead to a periodical torque fluctuation with a prominent power content at $\frac{\omega_e}{\pi}$ [Hz]. In practice the minimum engine speed with locked torque converter is about $\omega_e = 100$ [rad/s], hence the dominant frequency is at least 32 [Hz]. It can be seen from Figures 6.18(a) that the magnitude of the MRFs are already decayed substantially at 30 [Hz]. This is especially so for the ZI powertrain, in particular the MRF for r_{od} has decayed enormously. For moderate driving—where usually comfort is of great importance—the ratio $r_{cvt} = r_{od}$ occurs frequently, and obviously in the case of the ZI powertrain torque fluctuations from the engine are completely suppressed then. The MRF from \dot{r}_{cvt} to \dot{v}_v of the ZI shows a relatively high maximum at 18 [Hz] for r_{zi} .

It may be concluded that the flywheel provides additional virtual damping to the drive shaft resonance while shifting its eigenfrequencies to lower values. Also for the torque converter resonance, frequencies are shifted to lower values, but the amplitudes are influenced adversely. In terms of passenger comfort the additional damping may be judged positively, however, the shift of eigenfrequencies to lower values may penalize the comfort level. Humans are generally more sensitive for disturbances at lower frequencies. However, they become completely insensitive for frequencies approximating zero. To gain more insight in the comfort level of the powertrains the ISO 2631-1 (see [ISO, 1997]) human sensitivity filter for longitudinal vibrations is used. The human sensitivity filter decays for frequencies above

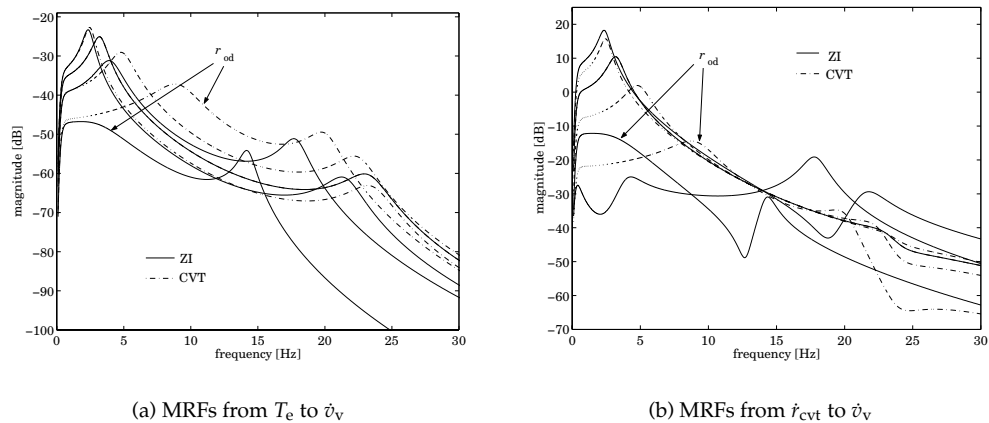


Figure 6.19: MRFs corrected with the ISO 2631-1 longitudinal human sensitivity filter

2 [Hz] with approximately 3 dB per decade, and the MRFs including this filter are shown in Figure 6.19. Comparing the amplitudes around the drive shaft resonance in Figure 6.18 with those in Figure 6.19 shows that not much has changed for this frequency range. Note the sharp decay in magnitude for the frequency approaching to zero. Finally, the lockup resonance has become even less important in terms of comfort due to the decay of the filter at this resonance (approximately -3 [dB]). In other words the conclusion that the flywheel unit in the ZI powertrain increases the (longitudinal) comfort still holds.

rootloci

For the linear system (6.66) an algebraic eigenvalue problem is solved for both the CVT and ZI powertrain models around four stationary engine speeds ω_{e0} and for a dense set of stationary CVT ratios r_{cvt0} between r_{ud} to r_{od} . This leads to 7 eigenvalues and eigenmodes for each (ω_{e0}, r_{cvt0}) pair. For both systems one eigenvalue is always zero, two are strictly negative real and finally there are two sets of conjugate complex eigenvalues, or poles, in the open left half plane, see Table 6.2.

POLE	FORM	PHYSICAL INTERPRETATION
s_1	0	CVT shift rate
s_2	$-\rho_1$	wheel speed
s_3	$-\rho_2$	vehicle speed
s_4	$-\zeta_1 + j\Omega_1$	lockup resonance
s_5	$-\zeta_1 - j\Omega_1$	lockup resonance
s_6	$-\zeta_2 + j\Omega_2$	drive shaft resonance
s_7	$-\zeta_2 - j\Omega_2$	drive shaft resonance

Table 6.2: Poles of the linearized 7th order powertrain model

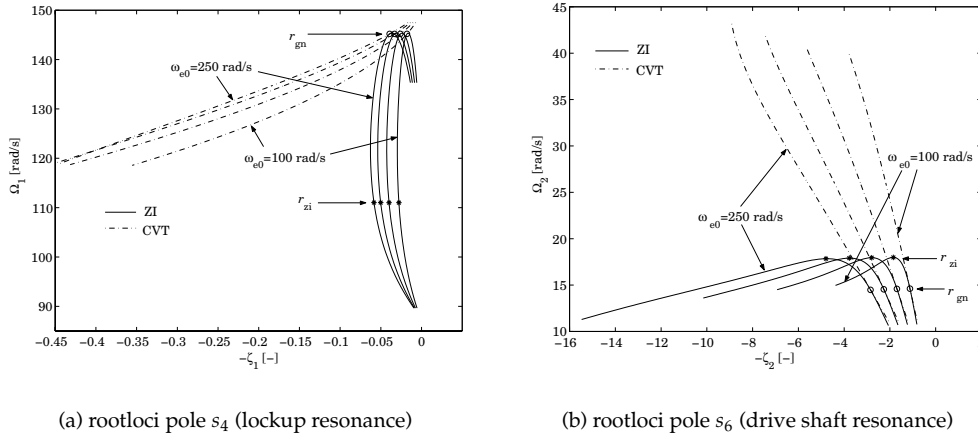


Figure 6.20: Comparison of CVT and ZI rootloci stemming from *lockup resonance* and *drive shaft resonance* for engine speeds of 100, 150, 200 and 250 [rad/s]

For four different stationary engine speeds, the rootloci of the poles s_4 and s_6 (see Table 6.2) are determined as a function of r_{cvt} . The results are plotted in Figure 6.20. From Figure 6.20(a) it becomes clear again that the lockup resonance is more pregnant for the ZI powertrain, *i.e.*, the damping ζ_1 for ZI is much lower than for CVT. The damping for the drive shaft resonance is comparable for both powertrains, but the eigenfrequencies for ZI are lower, making its relative damping higher. This is in agreement with the MRFs discussed in the previous

section.

Interestingly, at the ratio r_{gn} the poles as well as the tangent of the rootloci for the CVT and for ZI coincide. As explained in the previous section, the ZI and CVT system are exactly the same in r_{gn} because the flywheel is at a complete standstill. The eigenfrequency Ω_2 is maximal for the ratio r_{zi} . The equivalent inertia seen at the driveshaft is minimal then, obviously maximizing the eigenfrequency.

6.5.2 Non-minimum phase behaviour

Perhaps the most interesting plot to rate some performance aspects of both CVT and ZI powertrain is the locus of the single zero. The zero z_1 exposes some interesting changes in the dynamics of the ZI and the CVT powertrain, and in the next chapter, this knowledge is incorporated in the control design.

There exists one strictly real zero z_1 for both powertrains in the transfer from the input $\dot{r}_{cvt} = u_2$ to the vehicle acceleration. The locus of the zero as a function of r_{cvt} is numerically computed for both systems at $\omega_{eq} = 150$ [rad/s], see Figure 6.21. Clearly, for the CVT the zero

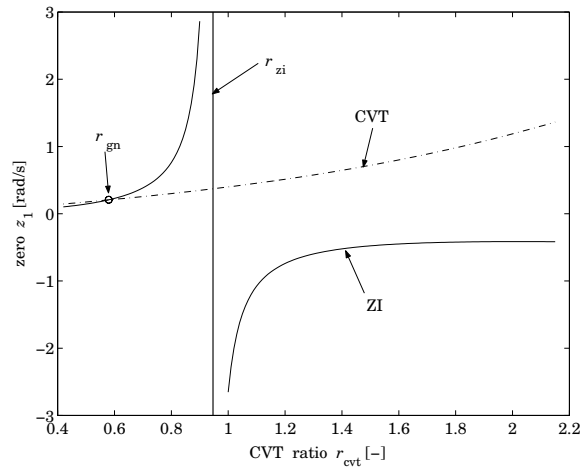


Figure 6.21: Comparison of the zero for CVT and ZI stemming from the ratio shift speed \dot{r}_{cvt}

locus lies in the open right half plane (RHP) for the entire CVT ratio range, whereas for the ZI powertrain this is true only for $r_{ud} \leq r_{cvt} < r_{zi}$. A zero located in the open right half plane—also known as non-minimum phase (NMP) zero—implies loss of performance as it generally leads to initially inverse responses. This is indeed seen for the CVT powertrain in practice and was earlier denoted as *jet start behaviour*. This behaviour becomes worse whenever the magnitude of the positive zero becomes smaller, *i.e.*, here for ratios approaching r_{ud} .

The negative zero for ZI and $r_{cvt} > r_{zi}$ is very beneficial because then the phase between the actuation \dot{r}_{cvt} and the vehicle acceleration response is minimal, leading to an instant vehicle response in the same direction as the actuation. For ratios approaching r_{zi} the effect of the zero is diminished as the magnitude tends to infinity. In fact, the vehicle acceleration becomes insensitive for \dot{r}_{cvt} (not for r_{cvt}) when passing through r_{zi} .

For ratios smaller than r_{zi} the zero z_1 is positive real even for ZI. Between $r_{gn} < r_{cvt} < r_{zi}$ the inverse response behaviour is faster than for the CVT powertrain as it lies further in the open right half plane. For ratios below r_{gn} the behaviour of the ZI powertrain becomes worse, though in a very limited sense, *i.e.*, the magnitude of the zero for ZI is not that much smaller than for the CVT powertrain. In fact, the optimization procedure of Section 6.3.2 minimizes the impairing influence of r_{gn} , when located somewhere between r_{ud} and r_{od} . The result of this is obviously also reflected in the z_1 locus.

closed form expression for z_1

For the 7th order linearized system, it is very hard to derive a closed form expression for the zero z_1 . Therefore the original 7th order system is reduced into a 2nd order system, basically collapsing all projected primary and secondary inertias into two inertias, setting the lockup and drive shaft flexibilities to zero and neglecting the tire and lockup dampers. An approximation \ddot{v}_v^* for the vehicle acceleration then becomes:

$$\ddot{v}_v^* = \frac{r_d R_w}{J_v^* r_{cvt}^2 r_d^2} \left(r_{cvt} T_e - r_d r_{cvt}^2 T_{rv} + \frac{J_1^* v_v^*}{r_{cvt} R_w r_d} \dot{r}_{cvt} \right), \quad (6.67)$$

$$\dot{r}_{cvt} = u_2 \quad (6.68)$$

where

$$J_1^*(r_{cvt}) = J_e + J_p + J_t + \alpha_p (\alpha_p - \alpha_s r_{cvt}) J_f \quad (6.69)$$

$$J_v^*(r_{cvt}) = \left(\frac{\alpha_p}{r_{cvt}} - \alpha_s \right)^2 \frac{J_f}{r_d^2} + \frac{J_e + J_p + J_t}{r_{cvt}^2 r_d^2} + \frac{J_s}{r_d^2} + (m_v R_w^2 + 2J_w) \quad (6.70)$$

$$T_{rv} = T_r + c_v R_w v_v^{*2} \quad (6.71)$$

Similar as in model (6.64) the inputs $T_e = u_1$ and $\dot{r}_{cvt} = u_2$ are taken. A stationary state $v_v^* = v_{v_0}^*$, $r_{cvt} = r_{cvt_0}$ is considered. This leads to $u_{1_0} = r_d r_{cvt_0} T_{rv_0}$ and $u_{2_0} = 0$. Perturbations \tilde{u}_1 and \tilde{u}_2 around $(v_{v_0}^*, r_{cvt_0})$ yields for the perturbed state (indicated by $\tilde{\cdot}$) in the Laplace domain:

$$\begin{bmatrix} \mathcal{L}\{\tilde{v}_v^*\} \\ \mathcal{L}\{\tilde{r}_{cvt}\} \end{bmatrix} = \frac{1}{s \left(J_{v_0}^* s + 2c_v R_w^2 v_{v_0}^{*2} \right)} \begin{bmatrix} \frac{R_w}{r_d r_{cvt_0}} s & \frac{J_{1_0}^* v_{v_0}^*}{r_d^2 r_{cvt_0}^3} s - \frac{R_w T_{rv_0}}{r_{cvt_0}} \\ 0 & J_{v_0}^* s + 2c_v R_w^2 v_{v_0}^{*2} \end{bmatrix} \begin{bmatrix} \mathcal{L}\{\tilde{u}_1\} \\ \mathcal{L}\{\tilde{u}_2\} \end{bmatrix} \quad (6.72)$$

For the transfer between $\mathcal{L}\{\tilde{u}_2\}$ and $\mathcal{L}\{\tilde{v}_v^*\}$ a single zero z_1 exists and is given by:

$$J_{1_0}^* v_{v_0}^* z_1 = r_{cvt_0}^2 r_d^2 R_w T_{rv_0} = r_{cvt_0}^2 r_d^2 \left(R_w T_r + c_v R_w^2 v_{v_0}^{*2} \right), \quad (6.73)$$

and was also found in [Guzzella and Schmid, 1994] and [Liu *et al.*, 2000]. In Figure 6.21 this zero was already plotted for the original 7th order model. It can be shown that the expression of the zero for the 7th order model is equal to (6.73).

gyrator element

The control variable \dot{r}_{cvt} together with T_e drives the (simplified) system (6.67). The input \dot{r}_{cvt} deserves separate attention. The CVT ratio links one coordinate (primary pulley rotation) in the powertrain to an other (secondary pulley rotation), so only one of these coordinates

can be seen as a generalized coordinate. When expressing the equation of motion for the inertia associated with this generalized coordinate, an additional term occurs due to the time dependence of r_{cvt} . For equation (6.67) this term T_G appears to be

$$T_G = \frac{J_1^* v_v^*}{r_{\text{cvt}} R_w r_d} \dot{r}_{\text{cvt}}. \quad (6.74)$$

This term is known as a *gyristor element* in bondgraph literature, [Allen, 1979]. The term

$$G = \frac{J_1^*(r_{\text{cvt}}) \dot{r}_{\text{cvt}}}{r_{\text{cvt}} R_w r_d}, \quad (6.75)$$

called the *gyrator modulus*, typically adds torque affine with the absolute speed, *i.e.*,

$$T_G = G(r_{\text{cvt}}, \dot{r}_{\text{cvt}}) v_v^* \quad (6.76)$$

The contour plot of G as a function of its arguments is drawn in Figure 6.22 for both the CVT ($J_f = 0$) and ZI powertrains.

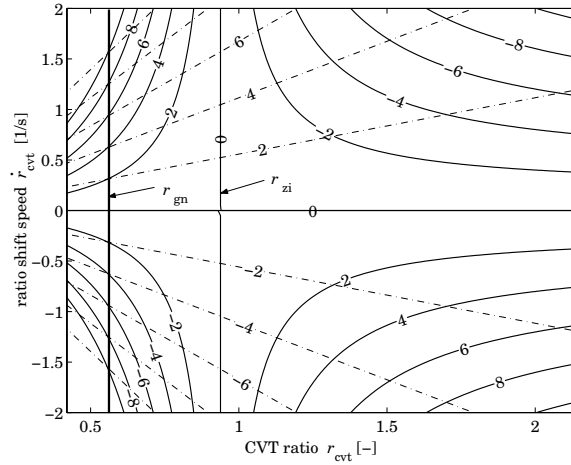


Figure 6.22: Contour plots of the gyrator modulus as a function of \dot{r}_{cvt} and r_{cvt} for ZI and CVT powertrains, CVT ($J_f = 0$) is dash-dotted.

From these contour plots it is readily seen that the ZI flywheel with planetary gearset changes the sign of G at least for $r_{\text{cvt}} > r_{\text{zi}}$. Furthermore, at least in the vicinity of r_{zi} the value of G for the ZI powertrain is much lower than for the CVT powertrain. Again these are observations of the intrinsic properties of the powertrain. The properties can be altered by changing some physical measures such as gear ratios, or inertias. For example, the gyrator term for a CVT powertrain is used beneficially in [Spijker, 1994] and [Shafai and Geering, 1996], where an intentionally installed large primary inertia (flywheel) provides positive power to the wheels at induced ratio *upshifts* ($\dot{r}_{\text{cvt}} > 0$). Actually, the gyrator is used there as the power source to drive the vehicle (at least in the lower vehicle speed regime). When its energy is depleted the engine moves the vehicle by running in sweet spot and passing the surplus of power to recharge the flywheel ⁴.

⁴See also Chapter 3 where this kind of operation was termed Start-Stop.

More can be said about G , for example that it can be defined as a new control variable rather than \dot{r}_{cvt} itself. The benefit of this approach is that the torque T_G can be controlled imposing a predefined vehicle acceleration. For the ZI powertrain this is rather straightforward, at least for $r_{\text{cvt}} > r_{\text{zi}}$. For the CVT powertrain, however, the control variable $u_1 = T_e$ needs to be chosen such that (at least part of) the gyristor term is compensated whenever $\dot{r}_{\text{cvt}} \neq 0$. Both ideas are adopted in the next chapter, where the design of control laws for T_e and \dot{r}_{cvt} is the main subject.

Chapter 7

Coordinated Powertrain Control

7.1 Introduction

Electronic powertrain control has become very attractive ever since the dramatic reduction of costs and the increase of capabilities of automotive sensors, real time digital controllers and actuators. Back around 1990 it was—contrary to Japan—not widely spread in Europe and the USA, [Schwab, 1990]. Since then this situation has changed dramatically, and not only for powertrain control, [Harms, 2001]. Control engineers, researchers and scientists have been eager in formulating sophisticated control strategies for various purposes related to the operation of the existing large diversity of powertrains, *e.g.*, with manual transmission, automated manual transmission, automatic transmission, continuously variable transmission, and hybrid propulsion. Most of the proposed strategies focus either on minimization of fuel consumption, maximizing performance, optimizing comfort, driveability and safety or combinations thereof (see [Narumi *et al.*, 1990]), and commercially available passenger cars in fact constitute a compromise amongst all of them.

Concerning electronic powertrain control, a foursome of definitions is made for clarity and is used throughout this thesis:

- *The electronic powertrain control system* is defined as both the control system hardware (sensors, digital controllers, actuators) and the control strategies captured in the software;
- The software constituting control and/or steering strategies for engine and transmission is termed *coordinated powertrain control*;
- The software constituting control of local components, *e.g.*, actuators, is referred to as *powertrain component control*

Coordinated powertrain control for common vehicle propulsion systems refers to deriving setpoints for engine and transmission. In literature this terminology is also used, see [Kolmanovsky *et al.*, 1999]. A term seen more frequently is '*integrated powertrain control*', [Deacon and Brace, 1996], [Sakaguchi *et al.*, 1999], [Vahabzadeh and Linzell, 1991], [Yasuoka *et al.*, 1999] or simply '*drivetrain, driveline or powertrain control*', [Dorey *et al.*, 1995], [Ha *et al.*, 1989], [Ohyama *et al.*, 1991], [Spijker, 1994], [Vanvuchelen, 1997], [Vaughan *et al.*, 1994], [Wright *et al.*, 1992]. References [Fukuba and Morita, 1992], [Kim and Kim, 1999] and [Takiyama and

Morita, 1999] use the term ‘consolidated powertrain control’. Furthermore, the terms ‘drive-or powertrain management’, [Mussaesus *et al.*, 1998], [Spijker, 1994] and ‘engine–transmission management’ are also seen. Finally, the term ‘hierarchical powertrain control’ is in vogue, [Schlüter and Wälterman, 1995], [Streib and Leonhard, 1992], [Vroemen *et al.*, 2000].

For CVT based powertrains in particular the naming is often somewhat confusing. Many authors refer to the generation of setpoints for the CVT ratio as ‘CVT control’, [Ironsides and Stubbs, 1980], [Liu and Paden, 1997], [Sackmann and Krebs, 1999], [Vroemen *et al.*, 2000]. In this thesis this is avoided in order to predestinate this denomination to the control problem of actually realizing the CVT ratio, [Vroemen, 2001]. Coordinated CVT powertrain control is usually very keen on optimizing the operating points of the engine for obtaining high fuel economy. Therefore the underlying powertrain control strategies are also often referred to as ‘optimization of operating points’, [Fukuba and Morita, 1992], [Guo *et al.*, 1988], [Jamzadeh and Frank, 1982], [Mayer and Schröder, 1995], [Mussaesus *et al.*, 1998] and [Piffner, 2001].

Another special case in the field is the operation of hybrid powertrains. They heavily rely on an electronic powertrain control system, carefully tailored for the specific, often somewhat deviant hardware involved, [Hochgraf *et al.*, 1996], [Jo *et al.*, 2000], [Mayer and Schröder, 1996], [Paganelli *et al.*, 2000], [Schlüter and Wälterman, 1995], [Schmid *et al.*, 1995], and [Wallentowitz and Ludes, 1994].

This chapter discusses two strategies to realize a desired longitudinal vehicle behaviour by coordinated control of the engine and the continuously variable transmission. The first strategy is tailored for a basic CVT powertrain whereas the second is designed for the ZI powertrain. First, in the next section a literature overview of coordinated powertrain control especially for CVT based powertrains is given.

7.1.1 Contemporary CVT powertrain control

Ever since its introduction in the automotive world, the CVT was asserted to gain superior fuel economy benefits over common transmissions (automatic, manual). This claim was enforced by the ability of the CVT to run the engine in extremely fuel economic operating points. The downside, however, is the somewhat disappointing efficiency of the CVT, resulting in a better fuel economy only with respect to 4 or 5 geared automatic transmissions. On the other hand, the driveability potential of the CVT surpasses that of conventional transmissions by far. Even performance of the vehicle is claimed to be improved, since the CVT is able to let the engine continuously operate in the point of maximal engine power, regardless of the actual vehicle speed (at least if not restricted by the underdrive ratio). Again, because of lacking CVT efficiency this performance improvement is sometimes quite moderate if at all true.

Solutions for coordinated CVT powertrain control exist in a wide variety, diversified between very practical and fairly academical. [Liu and Paden, 1997] and [Piffner, 1999] present extensive overviews of actually applied coordinated control strategies. They present three types of widespread strategies: ‘Single Track’, ‘Speed Envelope’ and ‘Off the Beaten Track’. The former two are applicable without an electronically controlled engine throttle (drive by wire, DBW) although DBW may enlarge their potentials for performance. The first strategy exactly tracks the E-line without concerning driveability. The second method is applied most in practice and chooses desired engine speeds as interpolated values between calibrated speed curves (speed envelopes) as a function of vehicle speed and drive pedal position. The calibration of the speed envelopes is performed heuristically for the larger part and in general stresses driveability more than fuel economy. Different calibrations may be chosen depending on the drive style, *e.g.*, ‘performance mode’ or ‘economy mode’, [Vahabzadeh and Linzell, 1991]. The ‘off the beaten track’ method actually controls the engine torque using a DBW system. This

method uses the single track strategy except for the engine torque, taking deviating trajectories during transients in order to enhance the driveability. In practice a stationary operating line can be chosen that is more or less a compromise between fuel economy and performance. The same holds for the trajectories during transients.

In this chapter strategies, similar to single track (for ZI) and to off the beaten track (for the CVT powertrain) are proposed. The contribution of the control strategies derived in this thesis to those seen in literature lies in the fact that explicit solutions for quantified fuel economy and driveability objectives are given. The former is most related to the CVT ratio r_{cvt} and engine torque T_e whereas for the latter the ratio shift speed \dot{r}_{cvt} is of great importance. The adopted strategies use the actual wheel speed ω_w and drive pedal position δ as the main inputs, see Figure 7.1. The result of the strategies is the emission of a desired engine throttle position ϕ_d and the CVT ratio $r_{\text{cvt,d}}$ or CVT shift speed $\dot{r}_{\text{cvt,d}}$. In fact these are reference inputs for the powertrain component controllers, *i.e.*, 'Hydraulic Control' and 'Throttle Control' in Figure 7.1. In

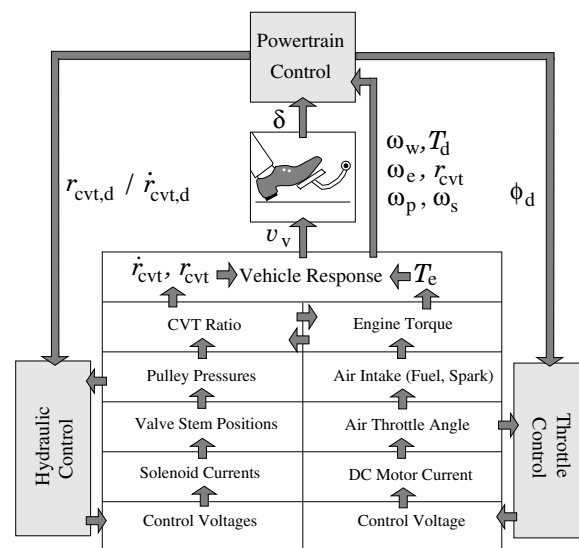


Figure 7.1: Hierarchy in electronic powertrain control

deriving the coordinated powertrain control further on in this chapter, the dynamics of actually realizing the engine torque, CVT ratio and CVT shift speed are left out. Basically the engine torque T_e and the CVT ratio shift speed \dot{r}_{cvt} are designated as control variables. Furthermore, it is assumed that these control variables can be realized instantly, but the physical bounds on T_e and r_{cvt} are taken into account explicitly. Several measured or reconstructed quantities may be used in the control laws for T_e and \dot{r}_{cvt} . In Figure 7.1, the wheel speed and torque, engine speed, CVT ratio and primary and secondary pulley speed are chosen as the most applicable candidates.

REF.	CONTROL	y	u	OBJECTIVE
[Guzzella and Schmid, 1995]	I/S Lin.	ω_w, r_{cvt}	\dot{r}_{cvt}	time opt. lin. sys.
[Kolmanovsky <i>et al.</i> , 1999]	I/O Lin.	T_d	T_e, r_{cvt}	dis. att., stab.
[Mayer and Schröder, 1998]	SMC	T_d, T_e	T_e, \dot{r}_{cvt}	T_d (freq.) shaping
[Mussaesus, 1998]	dyn. state fb.	$T_d \omega_w$	T_e, \dot{r}_{cvt}	$T_{d,d} \omega_w$ preshaping
[Sackmann and Krebs, 1999]	pole assign.	ω_w, r_{cvt}	\dot{r}_{cvt}	asym. hyp. stab.
[Schmid <i>et al.</i> , 1995]-1	P control	T_d	\dot{r}_{cvt}	static $T_d \rightarrow T_{d,d}$
[Schmid <i>et al.</i> , 1995]-2	I/O Lin.	T_d	\dot{r}_{cvt}	$T_{d,d}$ tracking
[Schmid <i>et al.</i> , 1995]-3	dyn. state fb.	T_d	\dot{r}_{cvt}	$\omega_{w,d}, r_{cvt,d}$ tracking
[Shafai and Geering, 1996]	I/O Lin.+P	T_d	\dot{r}_{cvt}	$T_{d,d}$ tracking
[Spijker, 1994]	I/O Lin.+PID	T_d	\dot{r}_{cvt}	T_d (freq.) shaping
[Vahabzadeh and Linzell, 1991]	sched. PID	T_d	T_e, \dot{r}_{cvt}	T_d shaping
This thesis (CVT)	dyn. state fb.	T_d	T_e, \dot{r}_{cvt}	T_d shaping
This thesis (ZI)	stat. state fb.	T_d	\dot{r}_{cvt}	$T_{d,d}$ tracking

Table 7.1: Literature overview of non-linear CVT powertrain control. Legend: I/S=input-state, I/O=input-output, Lin.=linearization, SMC=sliding mode control, fb.=feedback, sched.=scheduled, dyn.=dynamic, stat.=static, opt.=optimality, dis. att.=disturbance attenuation, stab.=stabilization, asym.=asymptotic, hyp.=hyper

7.1.2 Gyristor term vs. control solutions

Especially when fuel economic operating points (for example the E-line introduced in Chapter 3) are chosen, fastly modifying the engine output power must frequently be accompanied with leaps in engine speeds, [Chan *et al.*, 1984]. When controlling the CVT for changing the engine output power a trade-off between the time-optimality and the inverse vehicle response caused by transients in r_{cvt} should be considered. Both the CVT ratio r_{cvt} and its derivative \dot{r}_{cvt} can be used as the control variable. Here, the latter is chosen as such. Mostly for technical reasons, quite some authors also propose \dot{r}_{cvt} as a control variable. Table 7.1 in the first column shows an (incomplete) list of references on coordinated control strategies for powertrains (some of them are hybrid powertrains) equipped with a CVT. The second column lists the type of control strategy, the third shows the to-be-controlled system output y , the fourth holds the chosen control variables u , and finally the last column briefly describes the control objectives. As mentioned, the control model (discussed in more detail in Section 7.4.1) neglects the limited bandwidth of the local actuators for CVT and throttle and assumes that desired inputs for engine and CVT are realized instantly. The authors in Table 7.1 also assume this in order to simplify the model based controllers. The control strategies discussed in this chapter are evaluated using the simplified model (6.67), (6.68). For brevity the powertrain model is written in a affine non-linear state space formalism with input u and output y :

$$\dot{x}(t) = f(x(t)) + g(x(t))u(t) \quad (7.1)$$

$$y(t) = h(x(t)) + m(x(t))u(t) \quad (7.2)$$

Almost all references in the table use a similar dynamic model. The to-be-controlled output y differs but some sort of tracking of the E-line is considered in all the publications, and is therefore not mentioned separately in the table.

None of the authors considers the dynamic impact of \dot{r}_{cvt} via the gyristor term *explicitly*, except for [Mussaesus, 1998]. There, specific preshaping of the desired *wheel power* $T_{d,d} \omega_w$ is introduced to mediate between time optimality and driveability. In [Mayer and Schröder, 1998], tracking of a desired (not preshaped) path of the wheel torque $T_{d,d}$ is the control objective.

The gyristor term is very important then and through realizing a desired bandwidth with a sliding mode controller its influence is minimized in some unclear sense. In [Vahabzadeh and Linzell, 1991] specific scheduling of the PID parameters in order to shape the transients of drive torque T_d is considered, although not quantitative. The work in all other references focuses more on finding stabilizing controllers, or enforcing some closed loop performance for the feedback linearized systems derived there. As a consequence, some of these control strategies constitute fairly indirect methods to manipulate the impact of \dot{r}_{cvt} on T_d .

Before it is embraced by the end user, extensive tuning—often state dependent—of the controller parameters is required, in effect not different from common practice. This may lead to a well accepted implementation but at the cost of interchangeability because other vehicle-CVT combinations will often demand for renewed parameter tuning. A contribution to the coordinated powertrain control might exist in formulating a strategy with only a few tuning parameters. Of course this should rely on powertrain knowledge, *i.e.*, a model similar to (7.1), (7.2), as much as possible. Availability of physical parameters such as inertias is mandatory. An attempt in this direction is made hereafter for both the CVT and the ZI powertrain. Getting ahead of the results, the control solutions both end up with one tuning parameter only. Above publications take some optimality in fuel economy and often also driveability as the main control objectives. In deriving the coordinated powertrain control strategies here both objectives are considered to be equally important.

7.1.3 Organization of this chapter

First, in Section 7.2, background and definitions for the two control objectives will be presented. In Section 7.3 the trade-off between the two objectives is explained quantitatively. Then, in Section 7.4, the controller design for both CVT and ZI powertrains is explained. Performance and other closed loop properties will be elaborated on in Section 7.5. Finally in Section 7.6, the chapter is concluded with a discussion.

7.2 Control objectives

In controlling a CVT powertrain two objectives are pursued, taking into account physical restrictions such as minimal and maximal engine speed, CVT ratio and engine torque. These objectives, *i.e.*, high fuel economy and good driveability, need to be quantified somehow in order to be reflected in the control laws for engine torque and CVT ratio shift speed. Choosing two objectives controlled by two input variables makes the system functionally controllable. Throughout the remainder of this thesis three powertrain state conditions are distinguished. First, a *stationary* condition refers to the powertrain being in complete steady-state. Second, *quasi-stationary* conditions are established whenever the engine speed changes very slowly or not at all, whereas the vehicle is in transient, *i.e.*, accelerating or decelerating. Third, in *transient* conditions the state of both the engine and the vehicle are non-(quasi)stationary.

7.2.1 Fuel economy: optimal operating line

The area Ξ_e of possible operating points (ω_e, T_e) of an internal combustion engine is bounded by the minimum engine speed $\omega_{e,\text{min}}$, the maximum engine speed $\omega_{e,\text{max}}$, the line T_{WOT} for the torque at wide open throttle and the line $T_{\phi=0}$ for the (negative) torque at closed throttle. The dotted lines in the engine map of Figure 7.2 represent lines of constant brake specific fuel consumption b_e (BSFC, *i.e.*, fuel flow rate per unit engine power in stationary situations).

Although the results in Figure 7.2 are based on measurements in stationary situations it is assumed that these results may also be used in transient situations.

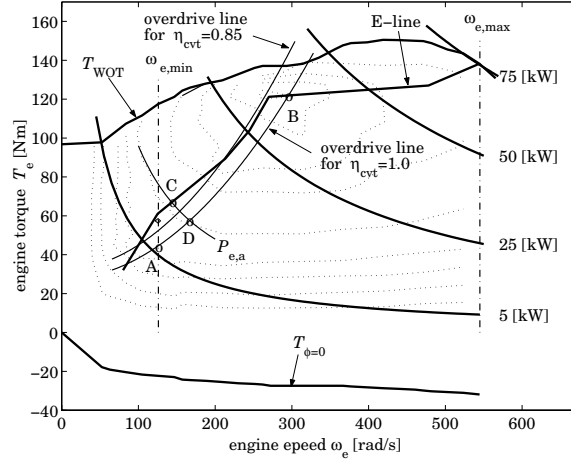


Figure 7.2: E-line in engine map

From the engine map two extreme engine output powers can be distinguished; the minimal power $P_{e,\min} = \omega_{e,\max} T_{\phi=0}(\omega_{e,\max}) < 0$ and the maximal $P_{e,\max} = T_{WOT}(\omega_{e,\max})\omega_{e,\max}$. For every positive valued engine output power $P_e \in [0, P_{e,\max}]$ there is one operating point in which the power P_e is delivered with minimal fuel consumption. The collection of these operating points for all such P_e is called the *E-line*. The speed and torque in an operating point on the E-line, denoted by respectively $\omega_{E\text{-line}}$ and $T_{E\text{-line}}$, depend on the delivered power P_e in that point. Quite formally,

$$(\omega_{E\text{-line}}(P_e), T_{E\text{-line}}(P_e)) = \arg \left(\min_{(\omega_e, T_e) \in \Xi_e} (b_e(\omega_e, T_e)) \right) \quad (7.3)$$

under the constraint

$$\omega_e T_e = P_e. \quad (7.4)$$

The E-line as determined from the measured b_e is fairly erratic. In Figure 7.3 this so-called measured E-line is drawn together with the curves of operating points in which the BSFC is equal to the minimal BSFC+1%. For control purposes the measured E-line is replaced by a much smoother line, *i.e.*, the smoothed E-line in Figure 7.3. The error in minimal BSFC, caused by this simplification, will be less than 1%.

closed torque converter lockup

The required engine power P_e to maintain a realizable stationary vehicle operating point (ω_w, T_d) depends on the wheel speed ω_w , the wheel torque T_d and the transmission efficiency

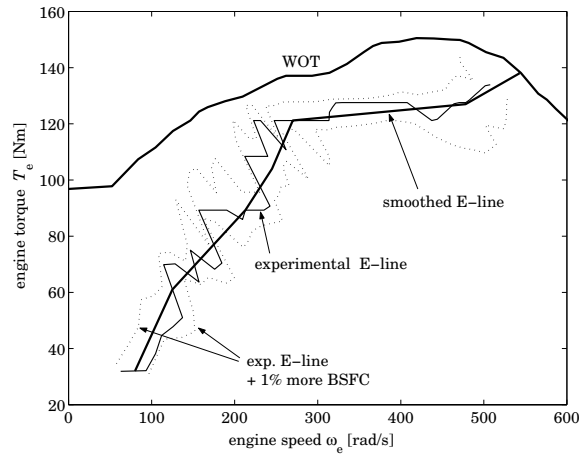


Figure 7.3: Smoothed E-line used for control

$\eta_{\text{cvt}} = T_d \omega_w / P_e$. For the moment it is assumed that the torque converter lockup is closed, so $\omega_w = r_d r_{\text{cvt}} \omega_e$. From $\eta_{\text{cvt}} P_e = \omega_w T_d$ it follows that r_{cvt} should satisfy

$$T_{\text{E-line}} \left(\frac{\omega_w T_d}{\eta_{\text{cvt}}} \right) = \frac{r_d r_{\text{cvt}}}{\eta_{\text{cvt}}} T_d. \quad (7.5)$$

Especially for small stationary wheel torques T_d (for instance in driving downhill) and a substantial part of the practical wheel speed operating range ω_w this can result in a desired CVT ratio larger than the maximally possible one, *i.e.*, the overdrive ratio r_{od} . Due to this so-called overdrive limitation it is impossible then to have the engine operating points on the E-line in every situation. The alternative operating point approaching the E-line as close as possible then becomes

$$(\omega_e, T_e) = \left(\frac{\omega_w}{r_d r_{\text{od}}}, \frac{T_d r_d r_{\text{od}}}{\eta_{\text{cvt}}} \right). \quad (7.6)$$

A realistic model for the wheel torque in stationary situations and on a flat road is given by $T_d = T_r + c_v R_w^3 \omega_w^2$ with T_r the rolling resistance torque and c_v the air drag coefficient. For a constant efficiency η_{cvt} it is possible to plot the engine operating points (ω_e, T_e) according to (7.6) for different values of ω_e . Two curves for, respectively, $\eta_{\text{cvt}} = 1.0$ and $\eta_{\text{cvt}} = 0.85$ are plotted in Figure 7.2. Let $P_{e,a}$ be the required engine power to maintain a given stationary vehicle operating point. Then, due to the overdrive limitation, the engine operating point cannot be chosen in point C on the smoothed E-line (see Figure 7.2). The best possible choice then is point D if $\eta_{\text{cvt}} = 1$ or a point between C and D (with a lower BSFC than in D!) if $\eta_{\text{cvt}} < 1$. This is a somewhat surprising result: if the overdrive limitation is encountered then the engine efficiency improves whenever the CVT efficiency deteriorates.

The CVT efficiency η_{cvt} is not constant, even not if the torque converter is locked. Then, in general, η_{cvt} depends on the wheel speed ω_w , on the wheel torque T_d and on the CVT ratio r_{cvt} . For this reason the engine operating points (ω_e, T_e) that minimize the fuel flow rate \dot{m}_f

for a certain realized wheel power $T_d \omega_w$ are not necessarily equal to those minimizing BSFC. Next, it is investigated up to what extent such differences occur.

Minimizing \dot{m}_f for a given stationary vehicle operating point (ω_w, T_d) within the envelope Ξ_w of realizable vehicle operating points leads to the problem of finding the engine operating point $(\omega_e, T_e) \in \Xi_e$ according to

$$(\omega_e, T_e) = \arg \left(\min_{(\omega_e, T_e) \in \Xi_e} \dot{m}_f(\omega_e, T_e) \right) \quad (7.7)$$

$$\dot{m}_f = b_e(\omega_e, T_e) \omega_e T_e \quad (7.8)$$

under the constraint

$$T_d \omega_w = (T_e - T_{\text{pump}} - T_{\text{mech}}) \omega_e. \quad (7.9)$$

Figure 7.4 shows some results of the optimization (7.7) for wheel speeds ω_w ranging between 20 [rad/s] or 22 [km/h] and 120 [rad/s] or 133 [km/h] and desired wheel torques between T_d between 250 [Nm] and 500 [Nm]. Here, the experimentally obtained and not the smoothed E-line is used. For $T_d = 250$ [Nm] the minimal engine speed constraint $\omega_e = \omega_{e,\text{min}}$ is active. From this figure it can be concluded that engine operating points minimizing \dot{m}_f (instead of b_e) also lie on the E-line.

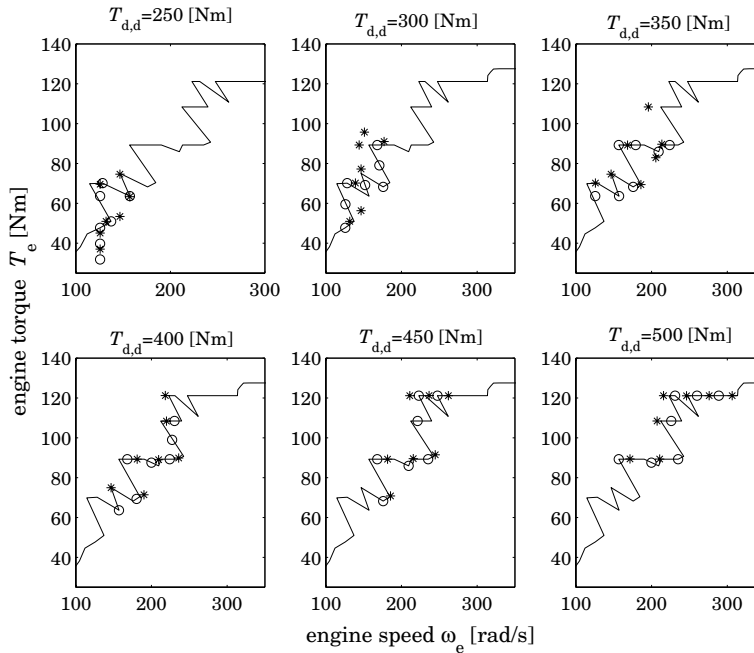


Figure 7.4: Quasi-stationary engine operating points optimized for minimal fuel consumption, 'o'=points on E-line with $T_{\text{mech}} = T_{\text{pump}} = 0$ [Nm], '*'=points optimized for $T_{\text{mech}} \neq 0$, $T_{\text{pump}} \neq 0$, the successive points indicate wheel speeds ranging between 20 and 120 [rad/s]

open torque converter lockup

The determination of the optimal engine operating point is more difficult if the torque converter lockup is not closed. Using relation (6.11) and $T_i = T_e - T_{\text{pump}}$ the constraint (7.9) of the optimization problem (7.7) is adapted into:

$$T_d \omega_w = (\alpha_{tc}(T_e - T_{\text{pump}}) - T_{\text{mech}}) \omega_p. \quad (7.10)$$

In this constraint, α_{tc} depends on the torque converter slip $r_{tc} = \omega_p / \omega_e$ (see also Figure 6.8). Furthermore, only the primary pulley speed ω_p can be directly manipulated by r_{cvt} rather than the engine speed ω_e . For an open torque converter lockup the latter also depends on the engine torque T_e according to equation (6.10) and $T_i = T_e - T_{\text{pump}}$. Hence, determining the engine operating points (ω_e, T_e) that minimizes m_f and meet the constraint (7.10) is an iterative process between r_{cvt} , the engine torque T_e and the constraint (7.10). For a closed lockup this process takes place between ω_e, T_e and the constraint (7.9).

Obviously, the optimal engine speed and torque can be calculated off-line for a large number of realizable vehicle operating points (ω_w, T_d) and stored in lookup tables. Alternatively, the optimal engine torque and optimal CVT ratio can be determined and stored in lookup tables. In theory this strategy would yield a fuel saving on the NEDC drive cycle of 4 to 5%, see [Mussaey *et al.*, 1998]. Nonetheless, in the experimental implementation discussed in the next chapter such tables for an open lockup are not adopted. The reason for this is the rather poor controllability of the CVT ratio at low vehicle speeds, *i.e.*, the operating range where the lockup is kept open. Instead, a fuel optimizing strategy exists in closing the lockup at vehicle speeds as low as possible, obviously diminishing efficiency loss due to torque converter slip. After the lockup has closed, tracking of the E-line is the preferred strategy as motivated above.

optimal engine operating points: control objective 1

The fuel optimal engine operating points (ω_{OL}, T_{OL}) meeting the overdrive limitation and the minimal engine speed constraint are

$$\omega_{OL}(P_e) = \max \left(\omega_{E\text{-line}}(P_e), \frac{\omega_w}{r_d r_{od}}, \omega_{e,\min} \right) \quad (7.11)$$

$$T_{OL}(P_e) = \min \left(T_{E\text{-line}}(P_e), \frac{T_d r_d r_{od}}{\eta_{cvt}}, \frac{T_d \omega_w}{\eta_{cvt} \omega_{e,\min}} \right) \quad (7.12)$$

These engine operating points form the optimal operating line (OOL), to distinguish it from the E-line, which does not account for the constraints. Resuming, the following remarks can be made with respect to the fuel economy objective:

- the smoothed rather than the experimental E-line presented in Figure 7.3 is used;
- boundaries set by the minimal engine speed overrule the E-line operating points;
- OOL or any other fuel optimizing strategy is dropped if the torque converter lockup is open, *i.e.*, during launch;
- the overdrive limitation is accounted for explicitly;
- the demand for OOL tracking is restricted to quasi-stationary conditions.

7.2.2 Longitudinal driveability: course of output torque

Most propulsion principles compromise between driveability and fuel economy for reasons discussed throughout this thesis and in Section 3.3.1. Minimal fuel consumption is often less stressed than acceptable driveability. However, driveability is rather subjective and is rated through panels of test drivers carrying out driving test manoeuvres and elucidating their experiences via forms and/or interviews. Therefore endorsing an acceptable driveability is a costly and time-consuming undertaking, which is often not reproducible (see [List *et al.*, 1998]). This renders a complete reiteration for every released powertrain variant inevitable. If, on the other hand, driveability could be measured and rated more objectively, incorporating it somehow in the design of powertrain components and control strategies could take place much earlier and more decisively, leading to apparent benefits.

terminology of longitudinal driveability

A unique description of vehicle driveability does not exist and grasping it into a single definition would be a nuisance. First of all there is a large difference between lateral and longitudinal driver-vehicle interaction. In literature this is often differentiated in the terms ‘handling’ and ‘driveability’ respectively. However, according to the definition given in [Bergman, 1973] *handling* refers to a more general context, *viz.*

“An interaction between driver, vehicle and environment, which takes place during transportation of people or goods from place to place.”

This definition may also include the longitudinal behaviour of the vehicle. Subjective assessment of the longitudinal behaviour is more often linked to *driveability*. Definitions of driveability are also encountered in literature:

“Driveability describes how dependably and smoothly a car’s powertrain operates under all kinds of weather and operating conditions. Driveability does not include ride and handling quality, braking performance, or abnormal combustion phenomena such as knock”, [Everett, 1971].

and

*“Good vehicle driveability is characterized by the driver having ease of control of the vehicle and confidence in both predictable and desirable system responses to the driver’s demands. It is very much dominated by the performance of the powertrain and vehicle in transient conditions,” [Brace *et al.*, 1999].*

In the first definition of driveability ‘handling’ is explicitly excluded, basically violating the definition of [Bergman, 1973]. This definition seems to stress comfort more than the ease of vehicle manipulation. The second definition, on the other hand, focuses more on the *interaction* between driver and vehicle and is considered more tailored to the application discussed in this thesis. Driveability has emphatically nothing to do with *performance* of the vehicle which is related to the elapsed time for normed vehicle speed changes, *e.g.*, 0 to 100 km/h or 80 to 120 km/h, [van Druten *et al.*, 2001]. On the other hand, a shorter elapsed time implies higher installed power (relative to the vehicle mass), which generally has the potential to improve driveability as well.

characterizing longitudinal driveability

Up to now, no standardized ways are found to characterize driveability objectively. The subjective driveability assessments—which experienced some standardization [CEC, 1983]—rate driveability aspects through judging the vehicle acceleration ‘feel’ or (dis)comfort. Hence, vehicle acceleration or wheel torque may be chosen as variables that reflect the level of driveability, [Pesgens, 2001]. According to the definition by [Brace *et al.*, 1999] driveability is determined predominantly by the behaviour of the powertrain in *transient* situations. As driveability is a matter of human-vehicle interaction, vehicle acceleration in general (thus also stemming from powertrain oscillations) might be the most suited variable to objectively quantify longitudinal driveability. Is it, however, also the best variable for use in a powertrain control strategy? Strongly related to the vehicle acceleration, the drive torque at the wheels is another employable candidate for driveability characterization as well as for control purposes.

The key problem is to infer a desired value for either of the two candidate variables from the information that is given by the driver pressing the drive pedal. However, the control problem is more tricky than this as for standard powertrains with moderate engines the *desired* and *realizable* trajectories are closely intertwined. Clearly, the driveability problem, formerly denoted as the jet start phenomenon, is the result of the engine not being able to fulfill desired output power requests in all transient circumstances. Especially for smaller engines this problem is intensified. Driveability, expressed in either of the two variables, could be impaired if the control of the engine transients is not examined carefully. However, it is generally harder to formulate what behaviour the driver still accepts than actually realizing it. Using definitions of behaviour that is *not* accepted or is judged badly, it is attempted next to qualitatively formulate acceptable driveability.

qualitative driveability objective

Accepting the exclusion of specific engine running problems, driveability will be formulated using the following terms, [Everett, 1971], [Graham *et al.*, 1988]:

- Hesitation: a temporary lack (time delay) of initial response in the acceleration;
- Sag: a short, sharp reduction in the acceleration, a loss of power;
- Stumble: same as sag but the acceleration is actually negative for a short time;
- Shuffle: fore- and aft longitudinal oscillations in vehicle acceleration;
- Stretchiness: lack of acceleration performance during light to moderate accelerations.

Shuffle is most related to *comfort*, which can be seen as a subset of driveability. All the mentioned aspects relate to situations where changes in the drive pedal position are imposed by the driver. In Figure 7.5 measurements conducted with the CVT test vehicle (discussed in the next chapter) show four of these driveability phenomena. Shuffle is caused by (induced) drive shaft oscillations in transients, discussed earlier in paragraph 6.5.1. Hesitation, stumble, sag and stretchiness originate from the gyristor term in equation (6.74) dominating the wheel torque transient.

Driveability is judged poor when the above aspects are manifest for the driver through accelerations forced upon him or her via the seat- back and surface. Hence, driveability could be judged ‘good’ if the human body accelerations are:

- 1 imposed directly after altering the pedal position, both for pedal tip-in and for back-out. The response time should typically be within the 0.2 [sec] time delay humans take to consciously percept and judge actions, and

2 persistent, low frequent or described by functions showing one extremum as in Figure 7.6.

For stepped transmissions this kind of acceleration patterns is absolutely infeasible when the vehicle acceleration is accompanied with gear shifts, see Figure 7.7. Even for powertrains with a CVT the conditions posed above can not be met without compromising *time optimality*. If the pedal deflection is quite moderate, the ideal acceleration might be induced by raising the engine torque only, basically common practice when driving a vehicle with manual transmission. On the other hand, driveability is often judged less important if the driver demands for performance, for instance imposed by a complete pedal kick down (demand for instant avail-

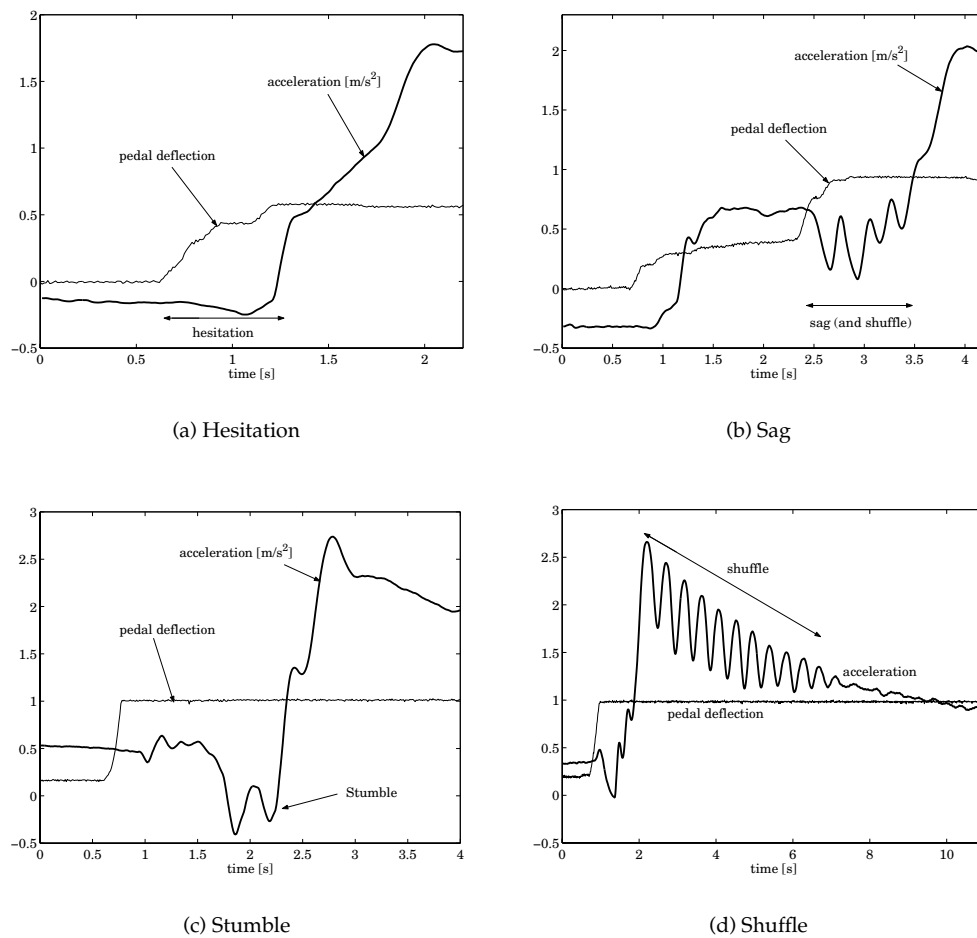


Figure 7.5: Measurements of driveability phenomena induced with the CVT test vehicle

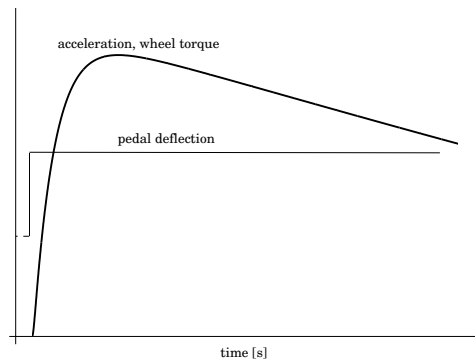


Figure 7.6: Possible course of desired vehicle acceleration after a positive drive pedal deflection. Acceleration and wheel torque descend again due to limited requested or installed power at an increasing vehicle speed, thus road load.

ability of maximum engine power). Hence, the driveability definition might be tightened to all vehicle instationary situations excluding kick downs. In practice also distinguished attention is given to kick downs, in fact focusing on performance mostly. In this thesis, it is assumed that driveability is important up to step-wise changes in pedal deflections $\Delta\delta$ —in succession to the actual deflection δ —which arguably are at most 50% of the total deflection range. Above that, performance becomes important implying that in such cases smooth ac-

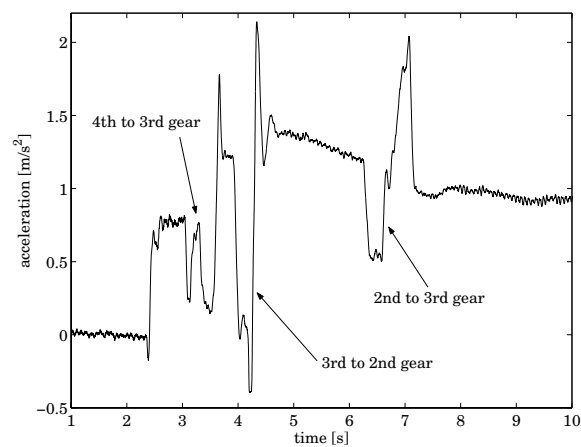


Figure 7.7: Vehicle acceleration response after an imposed kick down from 80 km/h in the case of a powertrain with a 4 gear automatic transmission (4AT)

celeration patterns such as in Figure 7.6 may be dropped as a control objective. Note, that driveability still is assumed to be important when pressing the pedal from 49% to 99% of the

total pedal travel, almost a kick down.

In Chapter 8, the qualitative driveability objective defined in this section is used to judge the driveability of the 4AT, CVT and ZI powertrains.

quantitative driveability: control objective 2

To actively control the driveability, the pedal deflection δ needs to be translated somehow into a quantity related to driveability. In the previous paragraph, vehicle acceleration or wheel torque were mentioned as variables related to driveability. In fact, this translation sets a reference input for the powertrain control that attempts to make the closed loop system track this reference input.

For several reasons, the vehicle acceleration a_v might not be the ideal choice for the translation. This acceleration is the result of the drive torque T_d and the actual road load, *i.e.*,

$$a_v = \frac{T_d - T_{rv}}{R_w m_v} \quad (7.13)$$

Hence, translating the pedal deflection into a desired vehicle acceleration always requires the road load torque T_{rv} to be known (measured or reconstructed). The main problem, however, is that δ needs to be associated with stationary vehicle speeds as well, since in many situations a change in δ means that the driver wants to drive at a higher velocity rather than prescribe the acceleration itself. Furthermore, the driver generally does not expect the powertrain to compensate for changing road loads. Clearly, if a certain change in pedal deflection at the actual velocity would correspond to a desired vehicle acceleration, then the controller would try to achieve this acceleration (within the physical boundaries of the powertrain of course) regardless of—possibly rapid—changes in the road load. On the other hand, drivers are often aware of sudden changes in road load, for example at the foot of a hill. If in such cases the driver pushes his pedal to *maintain speed*, the vehicle will start *accelerating* instead, which may lead to unexpected behaviour.

A normal driver is well able to control a desired vehicle acceleration through changing T_d and to compensate reasonably automatically for changes in T_{rv} . This argues for a translation of δ in terms of the wheel torque T_d . Doing so, the driver can easily manipulate the relative position, speed and acceleration of the vehicle with respect to other vehicles in traffic, which gives him or her a feeling of safety and reliability. Furthermore, if the response of the vehicle to pedal deflections is direct (without, or with a very short time delay) the driver's workload expressed in terms of the pedal deflections is low, possibly accompanied with a low level of annoyance. Some aspects of the above reasoning are also seen in [Schmid *et al.*, 1995].

In the foregoing it was assumed that the wheels have enough traction to move the vehicle with the exerted wheel torque. This will not always be true. Especially at wet and slippery surfaces wheel skid frequently occurs. The driver then loses the interaction between drive pedal deflections and response of the vehicle. Trimming of the control inputs T_e and \dot{r}_{cvt} is essential in order to limit or nullify wheel skid. This area of powertrain control, referred to as 'traction control', [Park and Kim, 1999], lies outside the tenor of this work. Nevertheless it is noted that, if the wheel torque is carefully manipulated, traction control has a large potential to be seamlessly integrated in the coordinated powertrain control.

The pedal deflection δ is translated in terms of the desired wheel torque $T_{d,d}$. This torque is a function of δ and of the actual wheel speed ω_w , see Figure 7.8(a). In the translation, the transmission efficiency $\eta_{cvt} = 1$ is assumed. It is assumed that the driver itself is very well able to compensate for transmission losses. The translation as in Figure 7.8(a) is not trivial, but two

boundaries are fairly straightforward. First, at maximum pedal deflection, $\delta = 1$, the desired wheel torque $T_{d,d}$ should resemble the maximal possible torque $T_{d,d}^{\max}$, i.e.,

$$T_{d,d}^{\max}(\omega_w) = \begin{cases} \frac{T_{\text{WOT}} \left(\frac{\omega_w}{r_d r_{ud}} \right)}{r_d r_{ud}} & \text{for } \omega_w < r_{ud} r_d \omega_{e,\max} \\ \frac{P_{e,\max}}{\omega_w} & \text{for } \omega_w \geq r_{ud} r_d \omega_{e,\max} \end{cases} \quad (7.14)$$

Clearly, this maximum wheel torque is governed by a full throttle opening and maximum engine power $P_{e,\max}$. The latter applies whenever the engine speed is not kinematically restricted by the underdrive ratio r_{ud} anymore. Second, at complete pedal back-out, the throttle valve should be closed completely. In general the driver then wants to (moderately) brake the vehicle using the engine drag torque $T_{\phi=0}$. Assume that before the pedal back-out occurs, the wheel speed ω_w is constant. Then the torque at the wheels cannot be less than $T_{d,d}^{\min}$, where

$$T_{d,d}^{\min} = \frac{T_{\phi=0}(\omega_{OL}(P_{rv})) \omega_{OL}(P_{rv})}{\omega_w} \quad (7.15)$$

$$P_{rv} = \omega_w (T_r + c_v R_w^3 \omega_w^2), \quad (7.16)$$

with rolling resistance T_r and air drag coefficient c_v . Now, using the maximum and minimum for $T_{d,d}$, the translation of pedal deflection δ into desired wheel torque is chosen as

$$T_{d,d}(\omega_w, \delta) = \begin{cases} \sigma(\delta) T_{d,d}^{\max}(\omega_w) & \text{for } \delta > \varepsilon \\ T_{d,d}^{\min}(\omega_w) & \text{for } \delta \leq \varepsilon \end{cases} \quad (7.17)$$

The S-shaped function $\sigma(\delta)$ is shown in Figure 7.8(b). The threshold value ε to detect pedal back-out or tip-in, is generally very small and is set by practical constraints at $\varepsilon = 0.02$. In practice, the pedal interpretation is dropped when the torque converter lockup is open (only for launching up to a fairly low wheel speed, e.g., 20 [rad/s]). Up to that speed the pedal deflection δ is directly linked to a throttle opening ϕ , hence $\phi = \pi \delta / 2$ (still 'by-wire' though). An alternative strategy is proposed in [Vroemen, 2001], where the pedal interpretation is extremely important for smoothly controlling vehicle launch with the Stop-Go extension upon the ZI powertrain.

conclusion

Resuming, the following remarks can be made with respect to the driveability objective:

- the wheel torque T_d is chosen as the to-be-controlled variable;
- the desired wheel torque $T_{d,d}$ is obtained from the pedal deflection δ and the actual wheel speed ω_w as in Figure 7.8;
- driveability is defined and evaluated only for steps in the pedal deflections (on top of the actual position) no more than 50% of the total pedal travel;
- the realized wheel torque should react significantly within 0.2 [sec].
- the course of the wheel torque should show one maximum after a step-wise change of the pedal deflection, in fact similar to what is depicted in Figure 7.6.

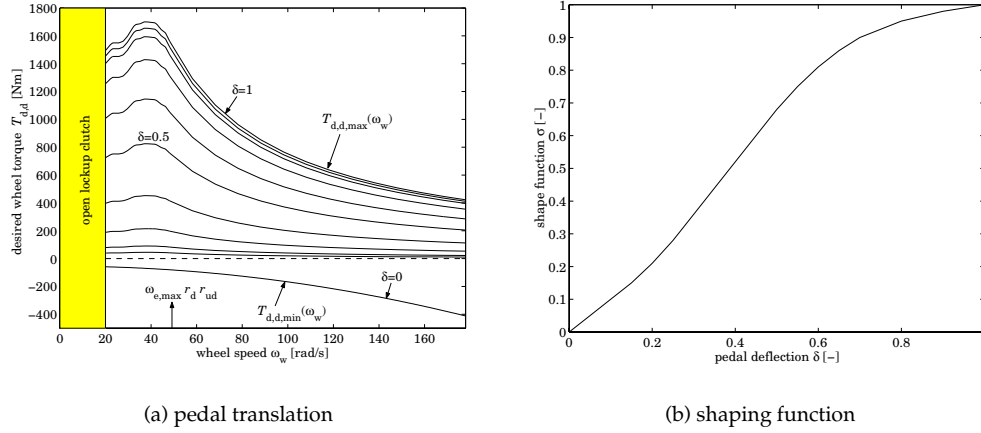


Figure 7.8: Drive pedal translation: desired wheel torque $T_{d,d}$ as a function of pedal position δ and actual wheel speed ω_w

7.3 Trade-off between the two objectives

For basic CVT powertrains, higher fuel economy generally leads to a lower rating of driveability. Decreasing the overdrive ratio degrades the fuel economy but improves the potential for driveability. Obviously, the stationary operating lines in between the points A and B in Figure 7.2 will lie at higher engine speeds and lower torque then, implying a lower fuel economy. Other ways to investigate the trade-off between fuel economy and driveability may apply. One of them was graphically shown in Figure 3.6, where operating lines of lower fuel economy are traded for higher power reserve. The following reasoning explains how a lower CVT ratio leads to a higher allowable acceleration of the primary inertias and amplification of the torque reserve. Both may lead to a higher potential in driveability. Here, the implications of the limited torque reserve are further elaborated in terms of the maximal allowable CVT shift speed \dot{r}_{cvt} . It is assumed that for $t < 0$ the state of the vehicle and of the engine is stationary, with wheel speed ω_{w_0} , engine speed ω_{e_0} and engine torque T_{e_0} . Furthermore, it is assumed that the torque converter lockup is closed and that power losses in the powertrain may be neglected. At $t = 0$ a large, sudden increase of the pedal deflection occurs, meaning that a large, fast increase of the engine power is requested. However, at $t = 0$ it is only possible to increase of the engine power very fast from the value $\omega_{e_0} T_{e_0}$ to the value $\omega_{e_0} T_{WOT}(\omega_{e_0})$ by opening the throttle as fast as possible. If the requested power is larger than this, the engine has to be speeded up by shifting down the CVT. For large negative shifting speeds \dot{r}_{cvt} , the engine acceleration $\dot{\omega}_e$ will be large positive, eventually at the cost of an unacceptable deceleration \dot{v}_v of the vehicle. From equation (6.67) and (6.74) it is seen that the vehicle will not decelerate (*i.e.*, $\dot{v}_v \geq 0$) if

$$J_1^* \dot{r}_{cvt} \geq -\frac{r_d R_w}{v_v^*} (T_e - r_d r_{cvt} T_{rv}) r_{cvt}^2 \quad (7.18)$$

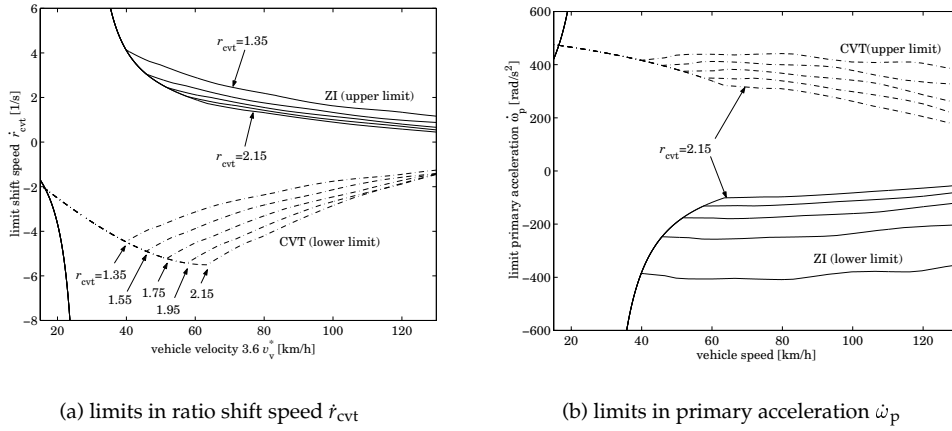


Figure 7.9: Limits for CVT ratio shift speed and primary acceleration

If sudden changes of the road load T_{rv} are left out of consideration it may be assumed without any restriction that in the case at issue (increasing pedal deflection) the torque $T_e - r_d r_{cvt} T_{rv} > 0$. For basic CVT powertrains the inertia $J_1^*(r_{cvt})$ is positive for all $r_{cvt} \in [r_{ud}, r_{od}]$, meaning that the acceptable downshifting speed of the CVT is limited. This is not the case for the ZI powertrain if $r_{cvt} > r_{zi}$ because then $J_1^*(r_{cvt})$ is negative, meaning that \dot{r}_{cvt} is only restricted by a positive value. Hence, for the ZI powertrain any downshift speed is acceptable in the considered case as long as $r_{cvt} > r_{zi}$. In Figure 7.9(a) the limits of the inequality (7.18) are drawn for CVT and ZI as a function of stationary vehicle speeds (with engine operating points on the OOL) for some values of r_{cvt} between 1.35 and 2.15.

Perhaps quite surprisingly, the CVT shift speed may be initially more negative for larger r_{cvt} . On the other hand, expressing the limits of the shift speed in terms of \dot{r}_{cvt} is somewhat misleading since equal changes in CVT ratio lead to higher changes in $\dot{\omega}_p$ if r_{cvt} is smaller or v_{v0}^* is higher¹.

For clarity it is therefore more clear to express the shift speed limit in terms of $\dot{\omega}_p$. Using $\dot{\omega}_p = (\dot{v}_v^*/r_d R_w - \omega_p \dot{r}_{cvt})/r_{cvt}$, the limit for the primary acceleration is set by:

$$J_1^* \dot{\omega}_p \leq T_e - r_d r_{cvt} T_{rv}. \quad (7.19)$$

The limits are drawn in Figure 7.9(b), for the same five CVT ratios between 1.35 and 2.15 used in Figure 7.9(a). In Figure 7.9(b) it can be seen that for the CVT powertrain the limits for $\dot{\omega}_p$ are—contrary to the limits for \dot{r}_{cvt} —more stringent for a higher r_{cvt} . This agrees with the expectation that the torque reserve is amplified more at lower CVT ratios r_{cvt} , obviously overruling the effect of increasing equivalent primary inertias projected at the wheels, *i.e.*, $J_1^*/(r_d r_{cvt})^2$.

¹This paradox disappears if the CVT ratio is defined as $r_{cvt} = \frac{\omega_p}{\omega_s}$ instead of $r_{cvt} = \frac{\omega_s}{\omega_p}$ as in eqn. (6.4).

7.4 Control design

In the previous section two objectives for controlling the CVT and the ZI powertrains are suggested. Fuel economy basically boils down to quasi-stationary tracking of the OOL, whereas driveability is translated in attempting to realize a desired wheel torque transient with one extremum and a prompt reaction after a pedal deflection. Figure 7.10 presents the basic blocks of the closed loop in which the role of the pedal translation becomes apparent. In the figure,

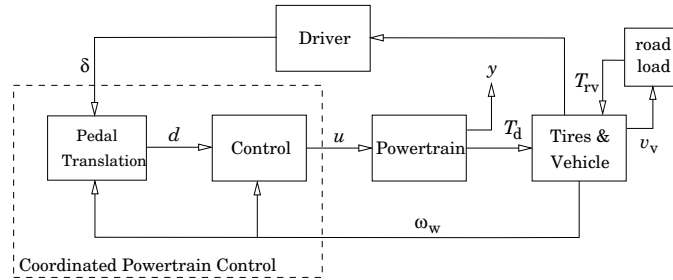


Figure 7.10: Block scheme of powertrain control

the driver moves the pedal to express his wishes with respect to the behaviour of the powertrain. In the block ‘Pedal Translation’ the pedal deflection δ is translated into a desired wheel torque $T_{d,d}$ according to equation (7.17) and a desired speed ω_{OL} (or torque T_{OL}) for the engine according to equation (7.11) (and (7.12)). This translation requires a measurement of the actual wheel speed ω_w . Both reference values ω_{OL} and $T_{d,d}$ are stored in the vector d . With the reference d control inputs u for the CVT and engine are computed by the ‘Control’ block, which also uses the measurement of the wheel speed ω_w . In the vector y the to-be-controlled engine speed ω_e and the wheel torque T_d are stored and are in fact the realizations of the desired values in d . These variables are not fed back into the controller, although the closed loop should somehow make the difference between d and y as small as possible. Instead, it is decided to use a non-linear powertrain model such that the control input u can be computed given the reference input d and the measurement of ω_w .

The engine and CVT are actuators within the ‘Powertrain’. It is assumed that these actuators can realize the system input u perfectly. The powertrain exerts a torque T_d to the vehicle. The latter experiences an external load torque T_{rv} . The resulting vehicle acceleration, speed and in traffic situations also the distance to other vehicles, are sensed by the driver, closing the loop by deflecting the pedal to a value δ .

In this section the design of the input u is the main topic. Investigation of the behaviour of the driver is left for future research. Instead trajectories for the pedal signal δ are assumed to be given.

A problem in realizing the driveability objective is the presence of the positive real zeros for the entire control range $[r_{ud}, r_{od}]$ in the case of the CVT powertrain and for a part of the control range $[r_{ud}, r_{zi}]$ in the case of the ZI powertrain (see paragraph 6.5.2).

For linear systems having a positive zero the emerging system behaviour is referred to as non-minimum phase (NMP) behaviour, the system itself may be termed a NMP system. For the considered non-linear system the NMP-like response was termed *jet start behaviour* in Chapter 3.

For such systems, no control laws achieve perfect or asymptotic convergent tracking errors for all desired trajectories. Especially an inverse system model controller immediately shows the limitation as the controller itself will become unstable. Rather should be sought for controllers *minimizing* the tracking errors as much as possible, [Slotine and Li, 1991]. Needless to say, the best way to obviate jet start behaviour is to alter the physical design of the system, ZI being a tentative example thereof. However, there are some other approaches known in literature. The simplest form is to design a controller for an approximate system in which the NMP zero is removed by pole/zero cancellation and apply this controller to the real system. In [Chockalingam and Singh, 2000] this idea is successfully elaborated for an undersea vehicle. Another method is, if allowed, to preshape the desired trajectories in order to take the dynamic capabilities of the system into account. In the case of a basic CVT powertrain this approach is adopted in [Mussaesus, 1998]. There, the gradient and offset of desired linear wheel power trajectories are determined every time instant assuming that inflicted drive pedal deflections are kept steady for at least the time interval set by the desired power trajectory. In Table 7.1 this was termed dynamic state feedback, which it basically is, though more specifically it could be viewed as a form of model predictive control (MPC).

Somehow modifying the system or model seems to be a feasible possibility to handle the jet start problem in a control environment. Especially for the CVT powertrain a sophisticated control strategy must be defined. A shifting law for the CVT ratio is proposed that circumvents the jet start behaviour. For the ZI powertrain jet start behaviour is obviated through the flywheel and there precautions have to be taken only for ratios equal and below r_{zi} . This is captured in the control strategy tailored for ZI which is designed next. Prior to formulating the strategies a control model is proposed.

7.4.1 Control model

In this section a model for the design of the non-linear feedback control for both powertrains is presented. In the descriptions the independent time variable t is omitted for brevity. The model presents the state equations and output equations in a form similar to (7.1) and (7.2). In both models the state x , input u , reference d , and output y are given by:

$$x = \begin{bmatrix} \omega_w \\ r_{cvt} \end{bmatrix}; \quad u = \begin{bmatrix} T_e \\ \dot{r}_{cvt} \end{bmatrix}; \quad d = \begin{bmatrix} \omega_{OL} \\ T_{d,d} \end{bmatrix}; \quad y = \begin{bmatrix} \omega_e \\ T_d \end{bmatrix}. \quad (7.20)$$

The desired values (setpoints) d were previously given in equation (7.11) for ω_{OL} and equation (7.17) for $T_{d,d}$. The output y is a set of variables that are related to the two control objectives.

The model given by (6.67) and (6.68) is used as the control model, but here the vehicle acceleration v_v^* is replaced by $\omega_w R_w$. Furthermore, in this model it is assumed that $T_{mech} = T_{pump} = 0$ [Nm], that the slip between the tires and the road is negligible and that the drive shaft and torque converter stiffnesses k_d and k_t are infinite. Moreover the torque converter is assumed to be locked. Among others, these assumptions imply that $\omega_e = \omega_w / (r_d r_{cvt})$, and $\omega_p = \omega_e$. In the following, ω_e and ω_p are used interchangeably without notice! As the drive shaft stiffness k_d is assumed infinite, the secondary inertia J_2 and the combined wheel and vehicle inertia J_v are in fact lumped, see Figure 6.15. Therefore, the torque T_d is described as the cutting edge torque between the secondary inertia J_2 and the combined wheel and vehicle inertia J_v . Choosing for this cutting edge torque T_d is seen earlier in [Shafai and Geering, 1996]. Similar as in there, the torque T_d becomes:

$$T_d = \frac{\left(\frac{T_e}{r_{cvt} r_d} + \frac{J_1^* \omega_w \dot{r}_{cvt}}{r_{cvt}^3 r_d^2} \right) J_v + T_{rv} J_d}{J_v^*}, \quad (7.21)$$

where J_v is defined as in equation (6.38), J_1^* as in (6.69), J_v^* as in (6.70) and

$$J_d = J_v^* - J_v. \quad (7.22)$$

The non-linear state space model with input u and output y is described as:

$$\dot{x} = \underbrace{\begin{bmatrix} \frac{-T_{rv}(x_1)}{J_v^*(x_2)} \\ 0 \end{bmatrix}}_{f(x)} + \underbrace{\begin{bmatrix} \frac{1}{J_v^*(x_2)x_2 r_d} & \frac{J_1^*(x_2)x_1}{J_v^*(x_2)x_2^3 r_d^2} \\ 0 & 1 \end{bmatrix}}_{g(x)} u \quad (7.23)$$

$$y = \underbrace{\begin{bmatrix} \frac{x_1}{r_d x_2} \\ \frac{J_d(x_2) T_{rv}(x_1)}{J_v^*(x_2)} \end{bmatrix}}_{h(x)} + \underbrace{\begin{bmatrix} 0 & 0 \\ \frac{J_v}{J_v^*(x_2)x_2 r_d} & \frac{J_v J_1^*(x_2)x_1}{J_v^* x_2^3 r_d^2} \end{bmatrix}}_{m(x)} u \quad (7.24)$$

When linearizing model (7.23), (7.24) about $x = x_0$ it can be shown that a similar locus of a (single) zero emerges as in Figure 6.21. This zero exists for the $u_2 \rightarrow y_2$ input/output path. Resuming, this zero is positive real for the entire control range $r_{cvt} \in [r_{ud}; r_{od}]$ in the case of the CVT powertrain. For the ZI powertrain, the zero is negative real in the range $r_{zi} < r_{cvt} \leq r_{od}$. Furthermore it does not exist for $r_{cvt} = r_{zi}$, and is positive real for $r_{cvt} < r_{zi}$. Most importantly, it is observed that—similar to what can be seen by equation (6.73)—the zero is always negative real if $J_1^* < 0$ (and $v_{v0}^* > 0$). This notion is used in deriving a controller for the ZI powertrain. For the CVT powertrain the above condition never holds which prompts complications in the control design. By inequality (7.18) the lower constraint is given for the shift speed input \dot{r}_{cvt} such that guaranteed positive vehicle accelerations take place after positive pedal deflection from a stationary state. By equation (7.19) an equivalent limit was defined by computing the upper limit for the primary acceleration $\dot{\omega}_p$. This notion is used in deriving the controller for the CVT powertrain.

7.4.2 Coordinated control for the CVT powertrain

For the CVT powertrain, precautions with respect to the CVT shift speed \dot{r}_{cvt} have to be taken in order to obtain an increasing vehicle acceleration when the drive pedal is pressed, see Section 7.3. Similarly, the vehicle acceleration should decrease if the pedal is released. This implies that accelerations/decelerations of the primary inertias should not occur with arbitrarily high rate.

Suppose that the pedal is pressed stepwise from some value to a higher value, than it is the driver's wish to increase the power (or torque) at the wheels stepwise. For power demands that cannot be established by an engine torque increase only, an engine speed transition is required as well. This is shown schematically in Figure 7.11, where a transition of engine power is demanded from level $P_{e,0}$ to $P_{e,1}$. Clearly restricted by the maximal engine torque T_{WOT} , the desired power $P_{e,1}$ cannot instantly be delivered by increasing the engine torque, *i.e.*, scenario 'a'. Instead, a conceivable alternative is to instantly increase the engine torque towards T_{WOT} and increase the engine speed until $P_{e,1}$ is reached, *i.e.*, scenario 'b'. Then, a transition towards the OOL can be made so as to deliver $P_{e,1}$ in the most fuel economic operating point for that power level, *i.e.*, the point marked by '1'. The engine torque step towards T_{WOT} can

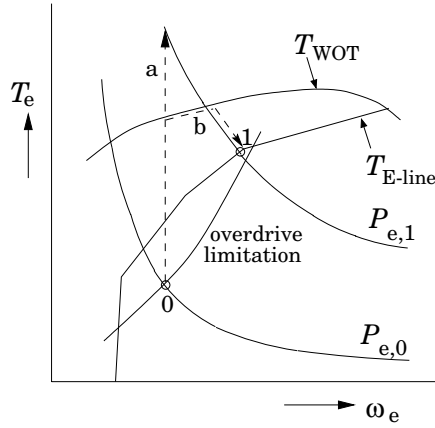


Figure 7.11: Transients in the engine map for power increase from $P_{e,0}$ to $P_{e,1}$

be made instantly (apart from restricting engine dynamics) contrary to the engine speed leap from point '0' to '1'. In the following, first a strategy for transitions of the engine speed is suggested and then the strategy for the engine torque is given.

control law for \dot{r}_{cvt}

First of all, in the model (7.23) it is assumed that T_{mech} and T_{pump} are zero, *i.e.*, that $\eta_{cvt} = 1$. This assumption is also adopted for the optimal operating points ω_{OL} and T_{OL} in equations (7.11) and (7.12). Assume that at the actual wheel speed $\omega_w(t_0)$ at time instant $t = t_0$ a certain pedal deflection (pedal tip-in) δ is exerted. Then, the desired wheel torque $T_{d,d}$ is given by (7.17). According to the OOL, and $\eta_{cvt} = 1$ the desired engine operating point equals $(\omega_{OL}(T_{d,d}\omega_w), T_{OL}(T_{d,d}\omega_w))$. Furthermore assume that, similar to the schematic in Figure 7.11, an engine speed leap has to be made from the actual engine speed $\omega_p = \omega_w/(r_d r_{cvt})$ towards ω_{OL} . As motivated earlier, this speed leap has to take place with some graduality, hence somehow restrictions have to be put on $\dot{\omega}_p$. An attempt in doing so suggests a first order (non-linear) stable filter:

$$\dot{\omega}_{p,d} = \kappa_p \frac{\arctan(\kappa(\omega_{OL} - \omega_{p,d}))}{\frac{1}{2}\pi}, \quad \omega_{p,d}(t_0) = \omega_p(t_0) \quad (7.25)$$

with a filter gain κ_p , yet to be determined, and an additional constant gain κ . Here, $\omega_{p,d}$ is used in order to distinguish it from the actual primary speed ω_p . For the model under consideration this is not crucial because it is assumed that desired trajectories of ω_p can be perfectly realized by $u_2 = \dot{r}_{cvt}$. On the other hand, in practice this is not true because of the limited dynamics of the (hydraulically controlled) variator. In other words, $\omega_{p,d}$ and ω_p will not be equal then. For the suggested filter (7.25) holds

$$\left| \frac{\arctan(\kappa(\omega_{OL} - \omega_{p,d}))}{\frac{1}{2}\pi} \right| < 1 \quad \forall (\omega_{OL} - \omega_{p,d}). \quad (7.26)$$

Since (7.26) holds, a particular choice can be attributed to the filter gain κ_p in order to manipulate the restrictions that have to be put on $\dot{\omega}_{p,d}$. For a guaranteed positive acceleration of the vehicle the upper bound in inequality (7.19) has to be satisfied. Assume for the moment that the aforementioned step-wise change in pedal position δ occurred at a stationary power-train state, hence $u_1(t_0) = r_d x_2(t_0) T_{rv}(x_1(t_0))$. At $t = t_0^+$ the engine torque u_1 is assumed to be increased towards $T_{WOT}(\omega_p(t_0))$. Thus according to inequality (7.19) the upper bound for the primary acceleration is determined as

$$\dot{\omega}_{p,d} \leq \frac{T_{WOT}(\omega_p(t_0)) - u_1(t_0)}{J_1^*} \quad (7.27)$$

The following definition applies:

$$T_{WOT}(\omega_p(t_0)) - u_1(t_0) := T_{res}(t_0), \quad (7.28)$$

and $T_{res}(t_0)$ is called the 'torque reserve' at $t = t_0$. Having the condition (7.26), the transient of $\omega_{p,d}$ computed through (7.25) is guaranteed to induce a positive wheel acceleration if κ_p satisfies:

$$\kappa_p = \rho \frac{T_{res}(t_0)}{J_1^*}, \quad (7.29)$$

where $\rho \leq 1$. The filter gain κ_p is viewed as a driveability gain and ρ as the single tuning parameter for that. $\kappa = 0.075$ is chosen such that the torque responses T_d in simulations give near-linear trajectories. However, any positive value larger than zero may be chosen for κ . The difficulty in determining $T_{res}(t_0)$ is that it is only defined for transients from stationary situations. Without loss of generality this is relaxed to quasi-stationary situations. Then still some detection mechanism is required to determine whether or not a certain engine state has become (quasi-)stationary. In other words, a new initial time t_1 has to be determined with which the initial condition of the filter (7.25) can be reset towards $\omega_{p,d}(t_1) = \omega_p(t_1)$. Until that time the filter has to sustain integration with the initial condition $\omega_{p,d}(t_0)$ and with $T_{res}(t_0)$ also when in the meanwhile the pedal is deflected even more. In that case, nothing more can be done than keeping the engine torque on T_{WOT} and sustain acceleration of the engine towards the engine operating point on the OOL corresponding to that new pedal deflection. Since by the specific choice of the filter (7.25) the engine will become stationary only when $t \rightarrow \infty$ some threshold value ε is introduced to detect t_1 , *i.e.*,

$$t_1 = \arg \min_t (|\omega_{OL}(t) - \omega_{p,d}(t)| \leq \varepsilon) \quad (7.30)$$

Note that this mechanism also assumes that t_1 is detected even when $\omega_{OL}(t)$ itself is not stationary. In practice, the condition $|\omega_{OL}(t) - \omega_{p,d}(t)| \leq \varepsilon$ can only be met in quasi-stationary situations at least if ε is small enough. The detection mechanism also implies that t_1 equals the continuous time t until the moment when $|\omega_{OL}(t) - \omega_{p,d}(t)| > \varepsilon$, *i.e.*, when a pedal deflection is induced which is large enough to diverge ω_{OL} substantially from $\omega_{p,d}$.

The filter (7.25) with update mechanism (7.30) also applies for negative pedal deflections (pedal back-out). Then, however, the reserve torque is given by:

$$T_{res}(t_0) = u_1(t_0) - T_{\phi=0}(\omega_p(t_0)), \quad (7.31)$$

i.e., it is the difference between the actual torque $u_1(t_0)$ and the negative engine torque at total closing of the throttle. For pedal back-out from some state condition, the optimal engine

operating point ω_{OL} is lower than the actual one $\omega_{p,d}(t_0) = \omega_p(t_0)$ and thus with (7.31) the primary acceleration becomes negative.

In the foregoing it was tacitly assumed that the desired primary acceleration $\dot{\omega}_{p,d}$ is realized by enforcing an appropriate CVT shift speed u_2 . Using $x_1 = r_d x_2 \omega_p$, $\dot{x}_2 = u_2$, $\dot{x}_1 = f_1(x) + g_{11}(x) u_1 + g_{12}(x) u_2$ and reworking yields for u_2 :

$$u_2 = \frac{x_2}{x_1} (\dot{x}_1 - r_d x_2 \dot{\omega}_{p,d}) = \frac{x_2(f_1(x) + g_{11}(x) u_1 - r_d \dot{\omega}_{p,d} x_2)}{x_1 - x_2 g_{12}(x)}. \quad (7.32)$$

In this expression, $\dot{\omega}_p$ is replaced by $\dot{\omega}_{p,d}$. Having the control input u_2 for the shift speed, next the control input for the engine torque u_1 is derived.

control law for T_e

The control law for u_1 accounts for constraints put by the OOL, the wide open throttle limit T_{WOT} and the minimal engine torque $T_{\phi=0}$. Furthermore, it is a switched control law to differentiate between pedal tip-in ($\delta > 0$) and back-out ($\delta < 0$). The control law for u_1 is given as:

$$u_1 = \begin{cases} \min \left(\underbrace{T_{WOT} \left(\frac{x_1}{r_d x_2} \right)}_{B \rightarrow C,D}, \max \left(\underbrace{T_{d,d} r_d x_2 + J_1^* \dot{\omega}_{p,d}}_{C \rightarrow E}, \underbrace{T_{OL}(T_{d,d} x_1)}_{E,A} \right) \right)_{D \rightarrow E}, & \delta \geq 0 \\ \max \left(T_{\phi=0} \left(\frac{x_1}{r_d x_2} \right), \min \left(\underbrace{T_{d,d} r_d x_2 + J_1^* \dot{\omega}_{p,d}}_{F \rightarrow H}, \underbrace{T_{OL}(T_{d,d} x_1)}_{E,H} \right) \right)_{G \rightarrow H}, & \delta < 0 \end{cases} \quad (7.33)$$

This control law will choose T_{WOT} as the best realizable if $T_{d,d} r_d x_2 + J_1^* \dot{\omega}_{p,d} > T_{WOT}$. Equivalently, the torque at completely closed throttle $T_{\phi=0}$ is chosen if $\delta = 0$. According to Figure 7.8, for $\delta = 0$ the desired wheel torque then becomes negative and is associated with 'engine braking'. The deceleration of J_1^* for $\delta < 0$ according to (7.33) can not be compensated for in such cases. The engine braking then is somewhat disappointing. It can be alleviated considerably by relaxing the shifting law (7.32), more specifically by lowering the driveability gain ρ in equation 7.25. In all other cases where $\delta < 0$, the deceleration of J_1^* can be compensated for, all the more since shifting law (7.32) explicitly reckons with the available torque reserve down to $T_{\phi=0}$.

simulation with model (7.23)

Next, the mechanisms of the control laws (7.25) \rightarrow (7.32) and (7.33) are discussed in more detail by considering the responses from a sequence of two step-wise changes of the drive pedal. In the engine map of Figure 7.12 the paths of the engine operating points during

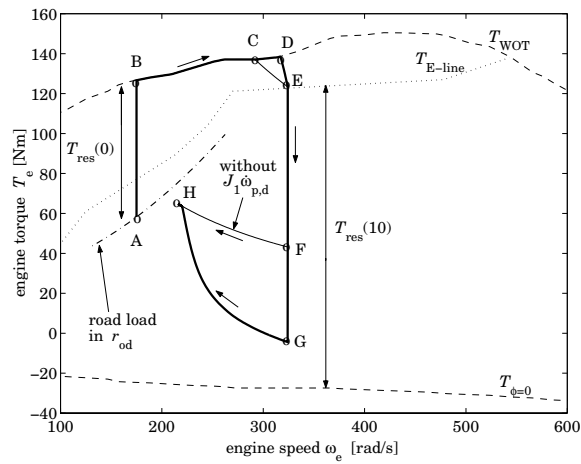


Figure 7.12: Transient in the engine map for the control laws (7.25)→(7.32) and (7.33). The thick line indicates the transient with control law (7.33) including $J_1^* \dot{\omega}_{p,d}$, whereas the thin line indicates the same but without the term $J_1^* \dot{\omega}_{p,d}$

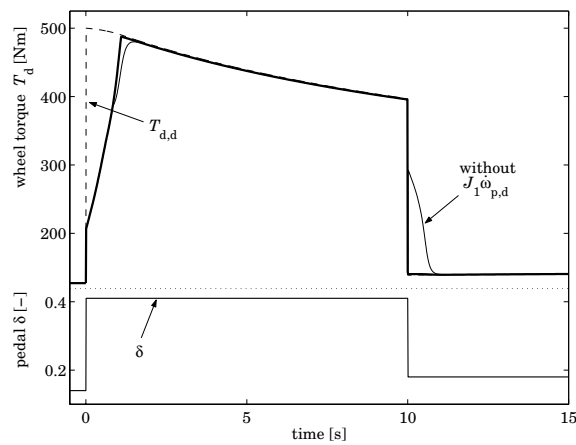


Figure 7.13: Transient in wheel torque T_d responding to the step-wise changes in the drive pedal position δ

these transients are drawn. The symbols 'A' to 'H' in the figure can be matched with those indicated in equation (7.33). In this map also the response is given if the term $J_1^* \dot{\omega}_{p,d}$ would not be included in (7.33). Figure 7.13 shows the excursions of the wheel torque T_d as well as the step-wise changes in the pedal deflection δ .

pedal tip-in

The transient starts in point A where a stationary wheel speed $x_1 = 80$ [rad/s] is controlled on the overdrive line. At $t = 0$ [sec] the pedal is pressed from 0.15 to 0.41 ($\delta > 0$) in fact demanding the *wheel power* to increase from 10.6 to 40 [kW] (see also Figure 7.8). Immediately, the engine torque jumps to T_{WOT} in point B and the desired final engine speed is set to ω_{OL} (40[kW]). If $J_1^* \dot{\omega}_{p,d}$ is omitted, tracking of T_{WOT} goes on until point C where the condition $T_{d,d} r_d x_2 = T_{WOT}$ is met. According to equation (7.33) the line $T_{d,d} r_d x_2$ is tracked until point E is reached. There, the increase of the engine speed according to law (7.25) has nearly come to halt naturally, as the difference $(\omega_{OL} - \omega_{p,d})$ is tending towards zero. In E a point on the E-line would be reached for $t \rightarrow \infty$, hence $u_1 = T_{OL}$ there. A slightly different scenario is followed when including the term $J_1^* \dot{\omega}_{p,d}$. Then, T_{WOT} is tracked until $T_{d,d} r_d x_2 + J_1^* \dot{\omega}_{p,d} \leq T_{WOT}$, where the equality applies in point D. Beyond point D an engine torque $u_1 = T_{d,d} r_d x_2 + J_1^* \dot{\omega}_{p,d}$ applies until $u_1 = T_{OL}$, which occurs in point E. Point E is a global asymptotic stable point on the OOL (here coinciding with the E-line). This stability is proved later on.

pedal back-out

The point E is kept steady (thanks to its stability) as the pedal does not change until $t = 10$ [sec]. Then, a pedal back-out occurs towards $\delta = 0.18$. *Excluding* the term $J_1^* \dot{\omega}_{p,d}$, the engine torque drops to point F where $u_1 = T_{d,d}(10) r_d x_2(10)$. *Including* the term $J_1^* \dot{\omega}_{p,d}$, the control law (7.33) decreases the engine torque to point G where $u_1 = T_{d,d}(10) r_d x_2(10) + J_1^* \dot{\omega}_{p,d}(10)$. Clearly, the torque reserve T_{res} is such that the acceleration law (7.32) has a relatively large gain. The initial deceleration $\dot{\omega}_{p,d}$ at $t = 10$ [sec] therefore is quite high. Unlike the pedal tip-in case, now $J_1^* \dot{\omega}_{p,d}$ can be exactly compensated for during the speed transition towards point H. Point H is a quasi-stationary point of the OOL, where $x_2 = r_{od}$ applies. H becomes stationary and coincides with the line indicated by 'road load in r_{od}' if $\dot{x}_1 = 0$ is established.

stability

Define the difference $\xi = \omega_{OL} - \omega_{p,d}$ and the Lyapunov function V :

$$V = \xi^2. \quad (7.34)$$

Furthermore assume that ω_{OL} is constant and using equation (7.25) the time derivative of V yields

$$\dot{V} = 2\xi \dot{\xi} = -4\xi \kappa_p \frac{\arctan(\kappa \xi)}{\pi}. \quad (7.35)$$

Thus $\dot{V} < 0$ as long as $\xi \neq 0$, so that $\xi = 0$, *i.e.*, $\omega_{p,d} = \omega_{OL}$, is a globally asymptotically stable equilibrium point. Furthermore, with $x_1 = r_d x_2 \omega_{p,d}$ the equilibrium $\omega_{p,d} = \omega_{OL}$ leads to

$$T_{d,d} r_d x_2 + J_1^* \dot{\omega}_{p,d} = \frac{T_{d,d} x_1}{\omega_{OL}} = T_{OL}(T_{d,d} x_1). \quad (7.36)$$

Hence the arguments of $\max(T_{d,d} r_d x_2 + J_1^* \dot{\omega}_{p,d}, T_{OL}(T_{d,d} x_1))$ in the control law (7.33) coincide when operating points become quasi-stationary, *i.e.*, when they asymptotically reach the OOL.

discussion

For pedal back-out the deceleration $\dot{\omega}_{p,d}$ is relatively high because the torque reserve $T_{res}(10)$ used in the filter gain κ_p as in (7.29) is high. Clearly this is caused by the large difference between the engine torque in the OOL point E and the drag torque $T_{\phi=0}$. For pedal tip-in, this torque reserve $T_{res}(0)$ is much smaller, obviously lowering the filter gain κ_p . From this it can be concluded that when the shifting law 7.25 (or equivalently (7.32)) is used compensation of the torque $J_1^* \dot{\omega}_{p,d}$ is more important for pedal back-out than for pedal tip-in. From Figure 7.13 it can indeed be concluded that the penalty for not including $J_1^* \dot{\omega}_{p,d}$ is higher for pedal back-out than for pedal tip-in. Such observations are also made in the experiments discussed in the next chapter.

7.4.3 Coordinated control for the ZI powertrain

Control for the ZI powertrain will appear to be considerably more straightforward. This is at least true for the range $r_{zi} < x_2 \leq r_{od}$ which will be considered first. Then the control design is extended for the entire ratio range $r_{ud} \leq r_{cvt} \leq r_{od}$.

control laws for \dot{r}_{cvt} and T_e when $r_{cvt} > r_{zi}$

The control laws (7.33) and (7.32) for the CVT powertrain did not incorporate anything about the secondary inertia J_2 as defined in appendix B, equation (B.22). This inertia happens to be very small for $J_f = 0$, *i.e.*, the CVT powertrain. For the ZI powertrain, however, J_2 should not be ignored. See for instance Figure B.5, where it can be seen that J_2 deviates considerably from J_s (*i.e.*, from J_2 for $J_f = 0$). Incorporating the compensation for the torque required to accelerate J_2 in the control law for the engine torque yields:

$$u_1 = T_{OL} + \frac{J_2(x_2) \dot{x}_1 x_2}{r_d} = \frac{r_d T_{OL} + (f_1(x) + g_{12}(x) u_2) x_2 J_2(x_2)}{r_d - J_2(x_2) g_{11}(x_2) x_2} \quad (7.37)$$

with T_{OL} as in equation (7.12). Furthermore, for $x_2 \neq r_{zi}$ ($J_1^*(r_{zi}) = 0$) the control input u_2 that realizes $T_d = T_{d,d}$ can be computed in closed form when equating $y_2 = T_{d,d}$ in (7.24):

$$u_2 = - \underbrace{\frac{x_2^3 r_d}{J_v J_1^*(x_2) x_1} (J_d r_d T_{rv}(x_1) - J_v^*(x_2) T_{d,d} r_d)}_{a(x)} - \underbrace{\frac{x_2^2 r_d}{J_1^*(x_2) x_1}}_{b(x)} u_1. \quad (7.38)$$

Substitution of this law in equation (7.37) yields:

$$u_1 = \frac{r_d T_{OL} + (f_1(x) - g_{12}(x) a(x)) x_2 J_2}{r_d - (g_{11}(x_2) - g_{12}(x) b(x)) x_2 J_2} \quad (7.39)$$

Control law (7.38) was proposed earlier in a slightly different form in [Serrarens *et al.*, 2001]. The right hand side expressions for u_1 and u_2 lead to OOL tracking only in *stationary* situations, *i.e.*, when besides the engine also the wheel speed has become stationary ($\dot{x}_1 = 0$). This can be seen from equation (7.37) and (7.38) respectively yielding $u_1 = T_{OL}$ and $u_2 = 0$ if $\dot{x}_1 = 0$.

For quasi-stationary situations tracking of the OOL is less penalized if the compensation of J_2 is discarded in u_1 , thus

$$u_1 = T_{OL}. \quad (7.40)$$

Including or excluding the influence of J_2 in the control law for u_1 is impartial for the drivability objective as long as $r_{\text{cvt}} > r_{\text{zi}}$. Clearly, the shifting law (7.38) compensates for u_1 in order to realize $T_d = T_{d,d}$. The consequences for the engine operating points using (7.37) or (7.40) is illustrated in the simulation results discussed next.

simulation with model (7.23)

Simulations of the closed loop behaviour are performed using control laws (7.38), (7.39) and (7.40). The same pedal excursions are made as for the simulations in Figures 7.12 and 7.13. The CVT ratio remains well above r_{zi} ($J_1^* = 0$), hence adaptation of the control law (7.38) can be omitted in this example. The results are shown in Figures 7.14, 7.15 and 7.16. For comparison, the simulation result for the closed loop response of CVT powertrain is shown again. A

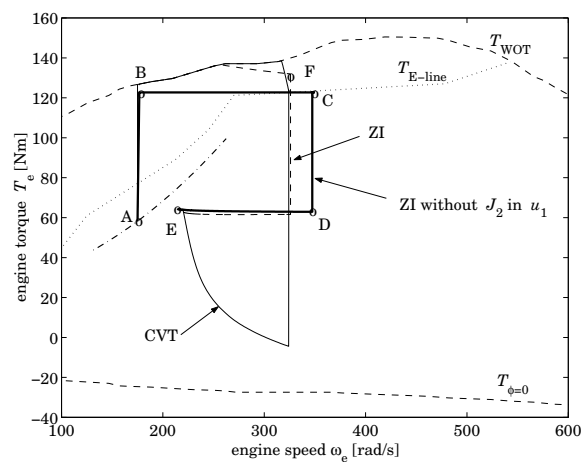


Figure 7.14: Transient in the engine map for ZI powertrain using engine torque control laws (7.39) indicated by 'ZI', and (7.40) indicated by 'ZI without J_2 in u_1 '. For the CVT ratio shift speed (7.38) is applied. The CVT response using control laws (7.33) and (7.32) is included for comparison.

multitude of observations is made from these figures:

- During a transient, deviations from the OOL are smaller for ZI than for CVT, especially when using control law (7.40) for u_1 .
- During quasi-stationary operation the engine power is higher for ZI than for CVT because for ZI compensation of J_2 demands additional power. When using control law (7.40), this additional power is lower (power in point C is lower than that in point F) since the value of J_2 is lower in that case (see also Figure B.5 in Appendix B, where decreasing ratios—though above r_{gn} —decrease J_2).
- For $x_2 > r_{\text{zi}}$, which is the case here, the closed loop ZI powertrain can perfectly realize the desired wheel torque $T_{d,d}$ ($T_{d,d}$ and T_d are indistinguishable) in either of the two control strategies.
- Downshifting for ZI and CVT is almost identical (see Figure 7.16(c) and (d)).

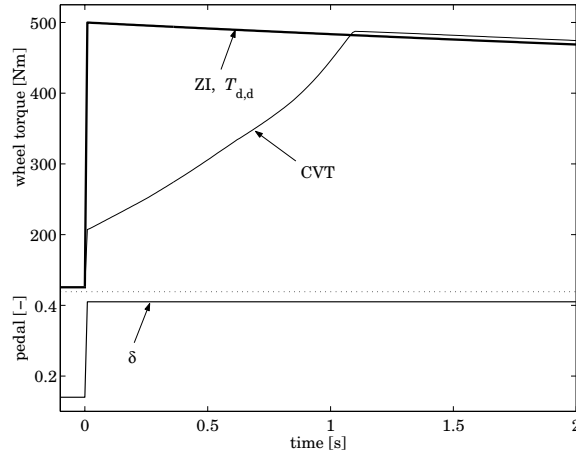


Figure 7.15: Transients in wheel torque T_d responding to the step-wise tip-in and back-out changes in the drive pedal position δ

- Upshifting at pedal back-out (see Figure 7.16(c) and (d)) is restricted more for the ZI powertrain in order not to undershoot the desired wheel torque $T_{d,d}$ (see also Figure 7.9).

discussion

The latter two observations imply that in the case of the ZI powertrain the constraints put on \dot{r}_{cvt} (to be realized by the hydraulic CVT actuation) are not more stringent than for the normal CVT powertrain. In [Vroemen, 2001], on the other hand, it is argued that the bandwidth of the variator in the CVT is slightly penalized as the torque transmitted by the belt *while shifting* is substantially different for the ZI powertrain.

The control scenarios (7.39), (7.40) and (7.38) can track the OOL only in stationary situations. Tracking of the OOL also in quasi-stationary situations is possible including the compensation of J_2 in the desired wheel torque $T_{d,d}$, *i.e.*,

$$T_{d,d} + \frac{J_2}{r_d^2} \dot{x}_1 \quad (7.41)$$

The engine torque is determined from $u_1 = T_{\text{OL}}((T_{d,d} + \frac{J_2}{r_d^2} \dot{x}_1)x_1)$. One could substitute the equation for \dot{x}_1 as in (7.23) in the argument of T_{OL} in order to express u_1 in terms of the state x . On the other hand, the input u_1 is also present in the equation for \dot{x}_1 . Hence, writing the expression for u_1 explicitly requires an invertible functional between T_{OL} and u_1 . However, the function T_{OL} —which for the larger part consists of a data vector (E-line)—is non-smooth and not invertible in closed form. Similar manipulations as were done to obtain equation (7.39) can thus not be performed here. Smooth and invertible approximations of T_{OL} could be beneficial though.

For now, the best results for both control objectives in the range $r_{\text{zi}} < r_{\text{cvt}} \leq r_{\text{od}}$ are obtained with the control laws (7.40) for u_1 and (7.38) for u_2 . The global stability of this control law

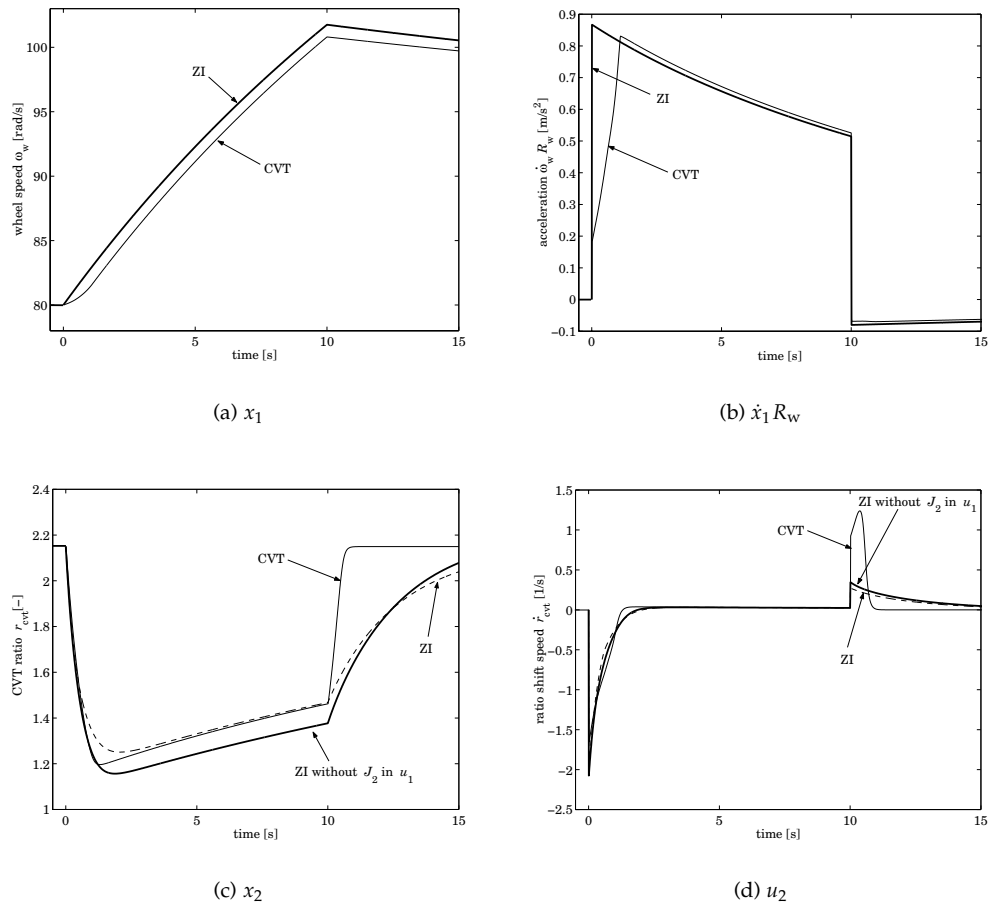


Figure 7.16: Wheel speed, vehicle acceleration, CVT ratio and -shift speed for pedal tip-in and back-out

is not yet investigated. On the other hand instability is not observed in simulations. For implementation this might be unsatisfactory though and therefore, but also for other reasons, a simpler control law for u_2 is decided to be implemented. This is covered in Chapter 8, where also the stability of the simpler control law is derived.

control law for \dot{r}_{cvt} within entire ratio range

The same control problem as for the CVT powertrain arises for $r_{ud} \leq r_{cvt} < r_{zi}$, *i.e.*, the locus of the zero is positive real. Equivalently, the primary inertia J_1^* is positive in this control range. If $r_{cvt} = r_{zi}$, the input \dot{r}_{cvt} has no impact on the output dynamics (7.24). Therefore, the output

y should be differentiated once more in order to make \dot{r}_{cvt} appear again in the output dynamics. Apparently, the relative degree changes from zero to one for $r_{\text{cvt}} = r_{\text{zi}}$. Systems with alternating relative degree are said to have a *not-well defined relative degree*. In literature, control solutions have been proposed that handle such systems. In [Hauser *et al.*, 1992], for example, three approximations for the well-known ball and beam system are proposed. Controllers that exactly input-output linearize these approximate systems are derived. One of the approximations simply discards the term associated with the changing relative degree. In the case of the ZI powertrain this, of course, would be the gyristor term ($m_{22}(x)$ in equation (7.24)). Doing so, however, changes the lowest possible relative degree of the original system to a higher relative degree in the case of the approximate system. Provided a system (or model) with a low relative degree increases the potential for performance in a control environment. It is therefore desirable to formulate an approximate system model that possesses a well defined relative degree which is *not higher* than that of the *lowest relative degree* appearing in the original system. The adopted approximate system is essentially the same as (7.23), (7.24), but J_1^* is replaced by an approximate term $J_{1,a}^*$ having the following properties:

$$J_{1,a}^*(x_2) = \min(a, J_1^*(x_2)), \quad (7.42)$$

where $a < 0$ represents the approximation of $J_1^*(x_2)$ for $J_1^*(x_2) > a$. Hence, with $J_{1,a}^*$ instead of J_1^* the relative degree is well defined and minimal for the entire control range. Furthermore, the locus of the single zero then turns out to remain negative for the entire control range. The parameter a may be seen as a driveability tuning parameter similar to ρ in equation (7.29).

discussion

The approximation (7.42) may appear to be a quite rigorous way to modify the model description. On the other hand, control design, analysis and tuning turns out to be extremely simple. Other modifications of the output equation might be to replace the gyristor term with a slow pole or pure time delay. Especially the latter may show the same reluctance in the time response as emerges from the NMP zero although the inverse response is obviously not present. Designing a controller based on the approximate system leads to a satisfactory performance for the original system. This is merely caused by the trajectories of r_{cvt} in practice not having to pass r_{zi} fastly (high u_2) to meet the driveability objective. For vehicle *performance*, passing r_{zi} is generally not without penalties and rudiments of the jet start phenomenon are sometimes seen for the ZI powertrain.

7.5 Simulation results

In this section results conducted with the simulation model discussed in Chapter 6 (and Appendix C) are shown. The driver-vehicle closed loop is excluded and instead pedal deflections are induced on the closed loop powertrain.

7.5.1 CVT powertrain

In Figure 7.17 and 7.18 simulation results of the closed loop CVT powertrain are shown for a sequence of step-wise pedal deflections that could be typically seen in practice. The driveability tuning gain ρ in equation (7.29) was set to 0.5 for pedal tip-in and 0.15 for pedal back-out. As can be seen in Figure 7.18, the vehicle initially moves steadily at 80 [km/h] ($\delta = 0.12$). At $t = 1$ [sec] the pedal is depressed to $\delta = 0.4$, the vehicle is for instance initiating a merge into

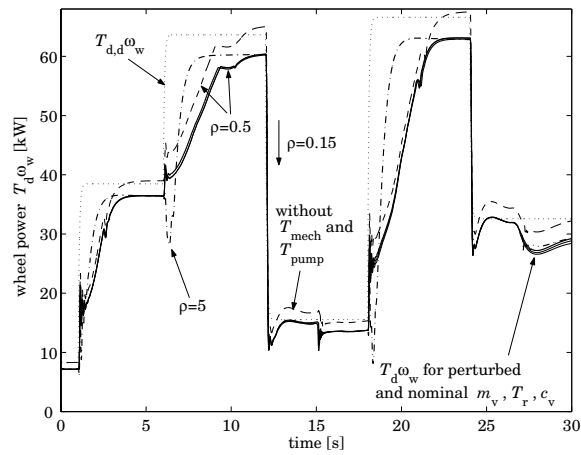


Figure 7.17: Wheel power $T_d \omega_w$ for sequence of step-wise changes in drive pedal deflection δ

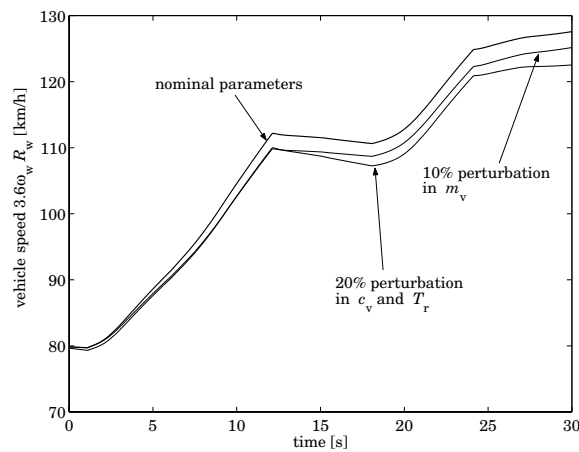


Figure 7.18: Vehicle speed $3.6 \omega_w R_w$ for parameter perturbations and sequence of step-wise changes in drive pedal deflection δ

highway traffic from an acceleration lane. The vehicle gradually accelerates and at $t = 6$ [sec] the pedal is depressed further to $\delta = 0.65$. Then at $t = 12$ [sec] the pedal is released back to $\delta = 0.2$, where it is kept for 6 seconds for instance to let another vehicle pass before the merge actually takes place. At $t = 18$ [sec] the pedal is raised towards $\delta = 0.7$ upon which the vehicle accelerates more severely; the merge is actually taking place and the driver accelerates steadily to adapt his or her speed to the other vehicles' speed. Finally, the vehicle speed is passing a

value typical for highway driving when a pedal back-out is induced towards $\delta = 0.35$ at $t = 24$ [sec]. After that the vehicle speed approximates a constant value.

In Figure 7.17 the performance of the powertrain is shown in terms of wheel power $T_d \omega_w$. This variable is chosen because the desired wheel power $T_{d,d} \omega_w = \sigma(\delta) P_{e,\max}$ is in fact independent of the wheel speed for $\omega_w > r_{ud} r_d \omega_{e,\max}$ (see equation (7.14)), which is the case in these simulations. The figure shows five trajectories, three of which can be hardly distinguished. These three simulations indicate the wheel power results for perturbed and unperturbed system parameters. The parameter perturbations are +10% for m_v and +20% for the road-load parameters c_v and T_r . The results of the vehicle speeds with the nominal (unperturbed) system and the perturbed system can be seen in Figure 7.18. The dashed line in Figure 7.17 indicates the fictive response in case the mechanical and hydraulic losses are reduced to zero. Finally, the dash-dotted line shows the result for $\rho = 5$ in the case of $\delta \geq 0$.

parameter perturbations

As the powertrain control does not cope with feedback of the realized wheel torque (and thus power) or feedforward on T_{mech} and T_{pump} , a difference between the realized and desired wheel power exists. The closed loop excluding these torque losses (dashed line) shows some overshoot. For the intervals between 12 and 18 [sec] and around 30 [sec] it can be seen that the realized wheel power tends to the desired level, as expected for zero torque loss.

The influence of parameter variations in the system is extremely limited. Variations up to 20% in road load do not affect the realized power significantly. The explanation for this is rather simple. Since the actual wheel speed is measured and used in the pedal translations and the control laws, the result of an increased road load or vehicle mass is indirectly measured through this wheel speed. This will consequently not affect the realized *wheel power*. The courses of the *wheel speed* of the perturbed systems with respect to the nominal system show significant differences as can be seen in Figure 7.18. If a driver wants to track the speed course of the nominal system, it should simply press the pedal more or less. This is an agreement with Section 7.2.2 where it was argued that the driver should compensate for changes in road load and mass.

time optimality vs. driveability gain

It can be seen that the overall response time for power increases of the closed loop CVT powertrain is rather disappointing. The positive steps in the desired wheel power (discarding the bias due to T_{mech} and T_{pump}) are realized not earlier than after 3 to 4 seconds. This response time can be improved at the cost of driveability. Therefore the gain tuning term ρ in equation (7.29) has to be increased (at least for pedal tip-in) towards higher values, possibly even larger than 1. In the figure also a simulation result is shown using $\rho = 5$ (dash-dotted line) which forces an (undesirable) jet start transient, though the stationary power level will be reached much faster.

discussion

Initially, the power transients show oscillations. The drive shaft resonance discussed in Section 6.5.1 is responsible for this oscillation being triggered by the sudden increase in the engine torque at the edges of the pedal steps. At $t \approx 2, 15$ and 22 [sec], awkward dips in the power response are seen. This is caused by the limited bandwidth of the hydraulically controlled CVT

(see also model (6.7)) putting limitations on the tracking accuracy of the desired ratio and ratio shift speed. Hence, the realized primary acceleration $\dot{\omega}_p$ does not resemble the desired one $\dot{\omega}_{p,d}$ as used in the control law (7.33) for u_1 . Disturbances of these kind are not assumed to degrade the driveability or comfort significantly. Nevertheless, altering the filter design (7.25) taking the dynamic properties of the hydraulically controlled CVT into account, might phase out these disturbances.

7.5.2 ZI powertrain

The simulations underlying the results discussed in this paragraph use $J_{1,a}^*$ chosen as:

$$J_{1,a}^*(x_2) = \min(-0.1, J_1^*(x_2)). \quad (7.43)$$

which implies $a = -0.1$ in (7.42). The same sequence of step-wise pedal changes are used as in for the CVT in the previous paragraph. In Figure 7.19 the several wheel power responses are shown.

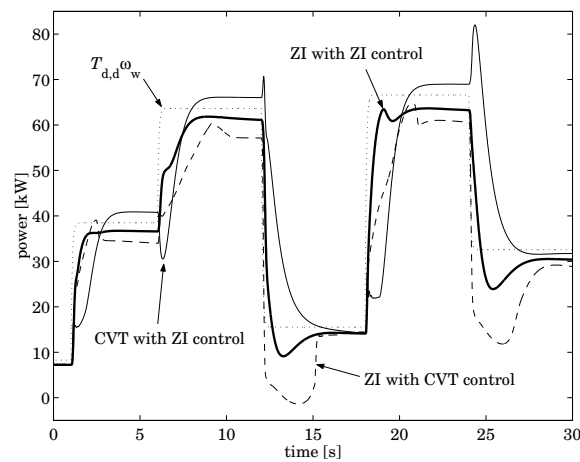


Figure 7.19: Wheel power $T_{d,d}\omega_w$ for sequence of step-wise changes in drive pedal deflection δ

The bold line indicates the response for the closed loop ZI powertrain using controls (7.40) and (7.38). Furthermore, the dashed line indicates the response of the ZI powertrain in closed loop with control laws (7.33) and (7.32). Finally, the thin solid line indicates the CVT powertrain controlled by the laws (7.40) and (7.38).

ZI with ZI control

As expected, the response of the ZI powertrain performs satisfactory for pedal tip-in. Torque responses are prompt and persistent. Again, the offsets occur due to the mechanical and hydraulic losses in the transmission. For pedal back-out, however, relatively large undershoots occur. This can be attributed again to the limited shifting dynamics of the CVT causing errors in the deceleration of the primary inertias. Especially whenever the CVT ratio approaches

r_{od} —thus upshifting of the CVT—the sensitivity to errors in shift speed is quite high. This is caused by the gyristor term being larger (in absolute sense) for high ratios, see also Figure 6.22.

ZI with CVT control

This effect is magnified when applying the CVT control strategy on the ZI powertrain. Due to the specific control strategy for the engine torque (equation (7.33) for $\delta < 0$) of the CVT powertrain, upshifting may be executed relatively fast. On the other hand, for the ZI powertrain this implies a violation of the shifting limits as indicated in Figure 7.9.

CVT with ZI control

Applying the ZI control laws to the CVT powertrain generally also does not reveal satisfactory results because shift speed is too large for pedal tip-in and the engine torque is not decreased enough for pedal back-out. Both situations then lead to jet-start behaviour in fact violating the driveability objective substantially.

speed and headway distance

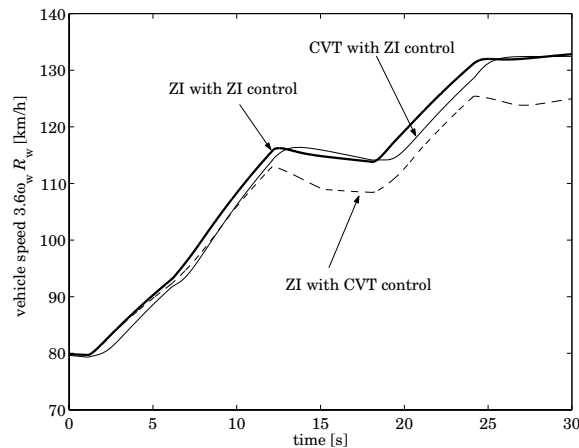


Figure 7.20: Vehicle speed $3.6\omega_w R_w$ for sequence of step-wise changes in drive pedal deflection δ

In Figures 7.20 and 7.21 the vehicle speeds and the headway distance of the ZI vehicle and ditto control with respect to the other vehicles are shown respectively. In the latter plot, contrary to the others, the corresponding results for the CVT vehicle with ditto control law are also plotted. From these figures it can be concluded that the ZI vehicle with CVT control laws shows the worst performance. The CVT equipped with ZI control behaves best with respect to the ZI vehicle in terms of speed and distance. From Figure 7.19, however, it was concluded that the driveability of this configuration would probably be rated worst, because of the jet-start behaviour.

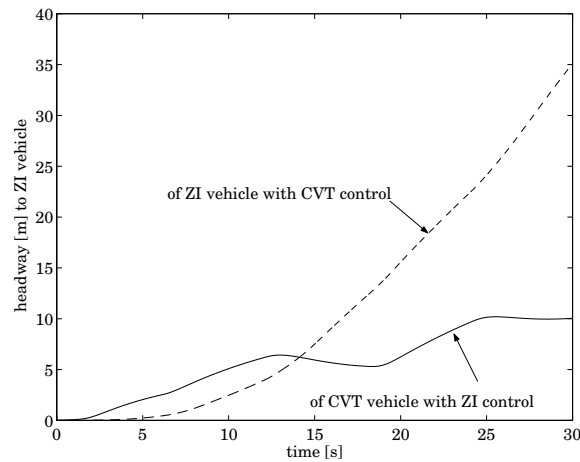


Figure 7.21: Headway to ZI vehicle for sequence of step-wise changes in drive pedal deflection δ

7.6 Discussion

In this chapter several aspects of coordinated powertrain control in general and for CVT based powertrains in particular are shown. Notions on controlling fuel economy, quantifying driveability and translation of the drive pedal signal have been shown. Two objectives were defined; one for fuel economy and the second for driveability. These were used in the control laws for the CVT and the ZI powertrain. For the CVT powertrain the driveability objective could not be used explicitly in the control laws. Instead, quantitative notions on the trade-off between the objectives are applied. For the ZI powertrain, however, the driveability objective could be applied successfully in the control range $r_{zi} < x_2 \leq r_{od}$. Exact realization of the desired wheel torque $T_{d,d}$ was possible within that control range. Of course, this is mainly attributed to the specific dynamics of the ZI powertrain. Applying the control laws for ZI, the fuel economy objective could only be met in stationary situations. The results in quasi-stationary situations are still satisfactory though.

The responses of the CVT powertrain are disappointing when compared to those of the ZI powertrain. They can be improved by moving the OOL to lower engine torques. In that case more reserve torque T_{res} becomes available for acceleration of the primary inertia and the vehicle, however at the cost of fuel economy.

In this chapter nothing is said about the influence of the driver in the control loop. The demands of the driver depend heavily on the traffic situation he or she is in. The closed loop behaviour of the powertrain in principle strongly affects the actions of the driver when demanding specific manoeuvres of the vehicle. It is left for future research up to what extent the ZI powertrain contributes in a safer and more accurate driving behaviour.

The validation of the ZI controller excluded closed loop stability analysis. In numerous simulations instability never occurred. Although this is far from being a proof for stability it is however promising. Demonstrating the stability in a closed form is left for further research.

The powertrain controllers suggested in this chapter may not be optimal in every sense.

The controller for the CVT powertrain, for instance, may be fitted with alternative filters for the primary acceleration. Furthermore, nothing is undertaken to phase out the oscillations seen in the simulations. Sophisticated adaptation of the control laws might alleviate or circumvent these oscillations. Similar oscillations do not occur for the ZI powertrain because of the beneficial damping features of the additional flywheel (see Chapter 6). The controller for the ZI powertrain is designed with a straightforward approximation of the original system for CVT ratios $r_{\text{cvt}} \leq r_{\text{zi}}$. Other approximations might be exploiting the capabilities of the ZI powertrain more.

Chapter 8

Experimental Results

Through experiments, the *qualitative driveability* (defined in Section 7.2.2) and *fuel economy* of the CVT and ZI powertrain are investigated. Moreover, the dynamics of the linearized model proposed from Section 6.4 are validated through experiments with both powertrains. The simulation model schematically displayed in Figure 6.15 is validated by comparison with fuel economy measurements.



Figure 8.1: Test vehicle

For the experiments, a test vehicle is equipped with a basic CVT transmission (Van Doorne's P920 transmission) extended with a planetary gearstage. Later on the flywheel is installed to obtain the ZI powertrain. The test vehicle is a Volkswagen Bora ('Jetta' in The Americas) with a 1.6 ℓ gasoline engine and originally equipped with a 4-gear automatic transmission (4AT). Modifications within the engine compartment were required to install the developed *prototype*

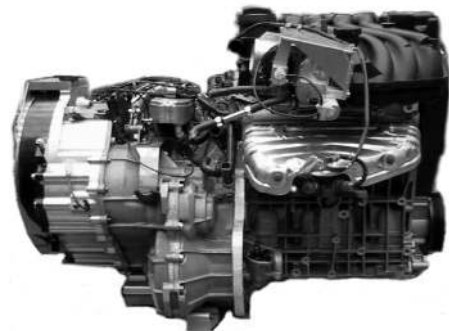
ZI transmission, which is about 70 mm longer than a *commercially* available CVT transmission. More details about the mechanical design of this prototype are given in [van Druten, 2001].

Software is developed for the control of the hydraulic actuation of the CVT (see [Vroemen, 2001]), for the control of the air throttle and to generate setpoints for the CVT and the throttle valve. These setpoints constitute the realization of the fuel economy and driveability objective as derived in Chapter 7.

Prior to surveying the experimental results, the *electronic powertrain control system* implemented in the test vehicle is discussed in Section 8.1. In Section 8.2 the design of a component controller for the electronic throttle valve is given. In Section 8.3, the implementation of the coordinated powertrain control is explained. The Section 8.4, the frequency analysis of the drive shaft resonance defined in Section 6.5.1 is performed. In Section 8.5 and 8.6 respectively measurements with respect to the fuel economy and driveability objectives are discussed. The chapter concludes with a summary of the obtained results in Section 8.7.

8.1 Electronic powertrain control system

In Figure 8.2 the ZI powertrain and its electronic control system hardware are pictured. At the left of Figure 8.2(a) the housing of the flywheel (black) can be seen. In Figure 8.2(b) a dSPACE AutoBox, an electronic unit (signal conditioning and driver stages) and a signal amplifier (black) for a torque transducer can be seen. These devices are placed in the trunk of the test vehicle.



(a) ZI powertrain: engine and transmission seen from the back



(b) Block scheme of electronic powertrain control system

Figure 8.2: ZI Powertrain and electronic control system

In Figure 8.3 an inventory of hardware units is shown¹ drawing up the entire electronic powertrain control system. Apart from a hierarchical overview it provides guidance in the discussions throughout this Chapter. It is in fact the same overview as in Figure 7.1 but here

¹without intentionally disrespecting the ‘driver’ as a ‘hardware unit’

the hardware units are stressed more than the signals. Most of the blocks are self-explanatory

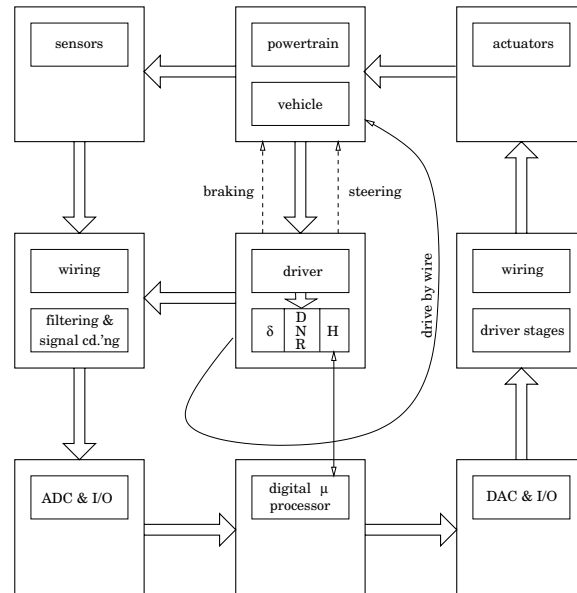


Figure 8.3: Electronic powertrain control system

though a few of them need some explanation. The 'driver stages' comprise the power electronics to operate the actuators. The 'H' symbol in the driver block represents a host PC to monitor and to store variables real-time from the μ processor on the host's block device (*e.g.*, a hard disk). Moreover, the two-way connection between H and the μ processor allows the driver (or the co-driver) to change control parameters on-line. Some of the blocks in the figure are discussed here in more detail.

8.1.1 Sensors

For coordinated powertrain control not all sensors of the test platform are relevant. For instance, the pressure transducers used in the hydraulic CVT control do not have any significance in the powertrain control setup. Furthermore not all sensors are 'in the loop' because some of them are used only for diagnosis and validation afterwards. The most important validation sensor is the telemetric torque transducer at one of the drive shafts.

In Table 8.1 an overview of the sensors and their purpose for coordinated powertrain control is given. The engine speed is used to determine a setpoint for the throttle controller. Furthermore the measured engine speed, primary speed and secondary speed are used in the control of the torque converter lockup. These speeds determine the torque converter slip ratio r_{tc} and the CVT ratio r_{cvt} which are also used in the lockup control logic.

VARIABLE	SENSOR	PRINCIPLE	PURPOSE
engine speed, ω_e	magnetoresistive sens	anisotr. magn. res.	throttle setpoint, lockup
primary speed, ω_p	magnetoresistive sens	"	reset, lockup
secondary speed, ω_s	magnetoresistive sens	"	diagnosis, lockup
(rear) wheel speed, ω_w	magnetoresistive sens	"	in the loop
half shaft torque, $T_d/2$	strain gauge bridge	telemetric (FM)	diagnosis
pedal deflection, δ	potentiometer	proportional res.	in the loop

Table 8.1: Inventory of sensors used for diagnosis and in the coordinated powertrain control

8.1.2 Actuators

The actuators for the coordinated powertrain control are the actuators for CVT, the electronic air throttle, the DNR arrangement and the torque converter lockup clutch, see Table 8.2. The

VARIABLE	ACTUATOR	PRINCIPLE
engine torque, T_e	throttle body	dc motor
engine speed, ω_e	belt variator	hydraulic pulley clamping
converter slip, r_{tc}	lockup clutch	hydraulic pressurizing
turbine slip (D), $\omega_t - \omega_p$	multiplate clutch	hydraulic pressurizing
turbine slip (R), $\omega_t - \omega_p$	multiplate clutch	hydraulic pressurizing

Table 8.2: Inventory of actuators used in the coordinated powertrain control

lockup clutch is controlled using an on/off solenoid, whereas the throttle, the CVT ratio and the drive clutch are controlled proportionally. The reverse clutch is operated manually by the driver when putting the selector lever in 'R'. The lever is mechanically connected to a hydraulic circuit which pressurizes the reverse clutch. At the same instant, a safety valve is operated by an on/off solenoid to assure that the CVT will not shift up during reverse driving.

The hydraulic CVT pressures and the drive pressure are controlled by hydraulic valves, the stem positions of which are manipulated through proportional solenoids. The hydraulic circuits around the reverse and lockup clutch possess enough damping in order to operate these devices with the appropriate graduality even though their control valves are operated step wise.

CVT actuator

In Chapter 6 it is argued that the CVT is seen as a black box actuator that responds to a given setpoint for the CVT ratio $r_{cvt,d}$ and shift speed $\dot{r}_{cvt,d}$. The purpose of the CVT ratio actuator essentially is to force the actual CVT ratio $r_{cvt}(t)$ to follow the desired trajectory $r_{cvt,d}(t)$ while transmitting the torque from the primary to the secondary shaft. Currently, the implemented CVT component controller is such that r_{cvt} tracks $r_{cvt,d}$. Hence $\dot{r}_{cvt,d}$ is not taken as the reference input. The interested reader is referred to [Vroemen, 2001] for a profound survey on the hydraulic control of the CVT

Throttle actuator

The throttle valve is actuated electronically by a dc motor. The valve angle ϕ has to track a desired valve angle ϕ_d as accurate as possible. The values for ϕ_d stems from the coordinated powertrain control and represents the desired engine torque at the actual engine speed. In Section 8.2 a model of the throttle with dc motor is derived. The model is used to design a component controller existing of a feedback and feedforward term.

8.1.3 Real time implementation

The component and coordinated controllers (Figure 7.1) are implemented in the SIMULINK graphical programming language, see Figure 8.4. A C-code generator translates the SIMULINK model into real-time C-code. This code is compiled into an object file that can be loaded and run on a Texas Instruments C40 DSP processor. The processor is embedded in a dSPACE platform including digital I/O boards, an ADC board and a DAC board.

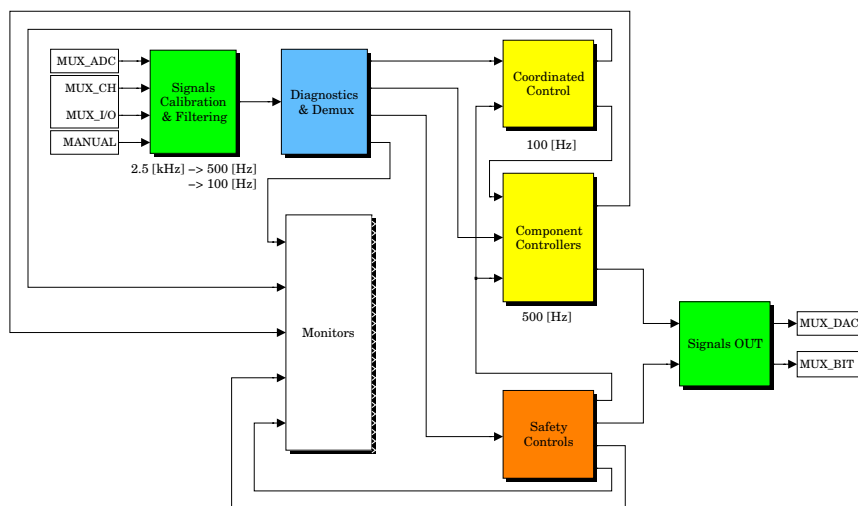


Figure 8.4: Top shield of SIMULINK real-time implementation

Variables of interest can be monitored and stored on-line on the host PC via an ethernet link between the processor's communication bus and the host PC. Moreover, control variables used in the object file running at the C40 DSP can be changed at the PC. Storage of variables is controlled by the TRACE program, whereas monitoring and adaptation of variables is done through the COCKPIT program, see Figure 8.5. Both programs run on the host PC.

digital filtering

To limit the prefilter hardware it is decided to acquire sensor signals digitally at $f_s = 2.5$ [kHz] and to implement digital filtering within the real-time code. This does not circumvent the aliasing of the (analogue) signals at frequencies larger than f_s . On the other hand, none of the

computation frequency

Running the entire process at 2.5 [kHz] is impossible due to computational overload of the C40 DSP, hence a lower computation frequency has to be chosen for the various hierarchical control layers. For the coordinated control 100 [Hz] is chosen which is conveniently above the drive pedal deflection frequencies being not higher than about 5 [Hz]. This is obviously limited by physiological capabilities of human drivers. For the component controllers, 500 [Hz] is more than sufficient as the response frequencies of the pulley pressures and the throttle valve opening are predominantly limited by actuator saturation. The phase margin of the open loop throttle control is equal to 32 degrees at a frequency of 12 [Hz]. A sampling rate of 500 [Hz] then degrades the phase margin by a mere 4 degrees³ which is considered small enough not to run into stability problems. This is especially so with a feedforward term in the throttle control basically diminishing the majority of uncertainties and disturbances. Control of the throttle valve is discussed in the next section.

8.2 Electronic throttle valve actuator

In Figure 8.6 the throttle body is shown. By turning the butterfly valve within the throttle body a venturi can be opened between 0 and 90 degrees (wide open throttle, WOT). Besides an

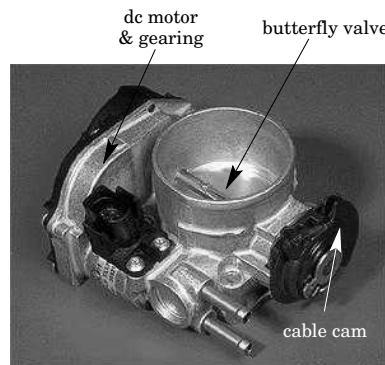


Figure 8.6: Throttle body

actuation by a throttle cable the valve can also be turned by a dc motor with torque amplifying gearing. The dc motor can be operated one-sided only, that is, it can not produce negative torques to close the throttle. For that reason, but mostly for safety, a pre-stressed torsional spring is installed to push the valve back. The combination of the spring and dc motor can veer out the valve for partial closing.

The original throttle body in the vehicle is already equipped with a dc motor to facilitate the installed cruise control system and possibly to enable an additional airflow on top of the by-pass air flow in case of high idle load. It can, in principle, also be used for the present drive-by-wire setup. However, the engine controller (ECU) does not 'allow' electronic interference with this device, hence a second dc motor is installed to replace the conventional actuation by

³Due to the ZOH effect computational delays are assumed to be less.

foot through cable and cam, see Figure 8.6. Mechanically, the standard dc motor and the new dc motor do not interfere because they both apply torque on the valve by a one-sided contact and they can exert positive torques only. In effect, the dc motors apply mutual *superpositions* of valve angles, basically not different from the original situation (foot and dc motor).

With a given engine torque setpoint u_1 and using the measurement of the actual engine speed ω_e a corresponding *stationary* desired valve opening ϕ_d is determined from the throttle map, see Figure 6.3. The dc motor has to be operated such that the actual valve opening ϕ tracks ϕ_d . The developed valve controller will be discussed next.

8.2.1 Throttle valve model

The schematic representation of the electronic throttle actuator is given in Figure 8.7. This

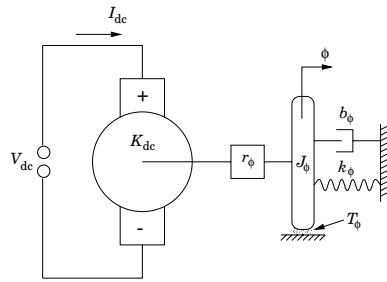


Figure 8.7: Schematic of the throttle valve with dc motor

system consists of an electro-mechanical part described by:

$$V_{dc}(t) = L_{dc} \dot{I}_{dc}(t) + R_{dc} I_{dc}(t) + \frac{K_{dc} \dot{\phi}(t)}{r_{\phi}}, \quad (8.1)$$

in connection with a mechanical subsystem described by:

$$J_{\phi} \ddot{\phi}(t) + b_{\phi} \dot{\phi}(t) + k_{\phi}(\phi(t) + \phi_0) = \frac{K_{dc} I_{dc}(t)}{r_{\phi}} - T_{\phi}(\phi, \dot{\phi}). \quad (8.2)$$

In these equations, V_{dc} is the control voltage, I_{dc} is the current through the dc motor, ϕ is the valve angle (in radians), and T_{ϕ} is a friction torque. L_{dc} , R_{dc} and K_{dc} are the inductance, resistance and torque constant of the dc motor. Furthermore, J_{ϕ} , k_{ϕ} , ϕ_0 and b_{dc} respectively are the lumped moment of inertia projected at the valve, the lumped stiffness of the torsional springs, the pre-stress angle, and a damping constant. Finally, $r_{\phi} = \frac{81}{4544}$ is the overall ratio of the two-stage gearing from dc motor to valve.

In the throttle's driver stage, the current I_{dc} through the dc motor is controlled using an OP-AMP with current feedback loop. Moreover, the driver stage also includes a current saturation (1.5 [A]) to protect the dc motor from thermal overloads. The driver stage is able to control positive currents with a bandwidth above 1000 [Hz], which is far beyond the desired bandwidth (≈ 10 [Hz]) of the mechanical subsystems. Therefore the current I_{dc} in equation (8.2) can be seen as a direct control variable to be used for valve angle control if $I_{dc} > 0$, *i.e.*, one-sided control.

Positive currents can also be generated by the dc motor itself. For instance when the control voltage V_{dc} is set to zero and the valve is fastly closed by the spring ($\dot{\phi} \ll 0$ in equation (8.1)). The generated electric power can not be dissipated by the driver stage, consequently the closing of the throttle often shows interaction of the electro-mechanical and mechanical subsystem. This will be exemplified by an experiment later on.

The model parameters J_ϕ and k_ϕ of equation (8.2) are estimated from experimental results, using the physical components. These estimates served as an initial guess for the identification of model (8.2). For one nominal position of the throttle ($\phi \approx \pi/4$ [rad]) a frequency bounded (between 0.1 and 10 [Hz]) noisy voltage signal—representing a desired I_{dc} —is injected into the driver stage. The response is measured and correlated with the noise input. The emerging frequency response estimate is approximated by the second order model (8.2). The model and estimated transfer function were in good agreement for $J_\phi = 5.2 \cdot 10^{-3}$ [kgm²], $b_\phi = 0.234$ [Nms/rad], $k_\phi = 0.25$ [Nm/rad] and $K_{dc} = 1.62 \cdot 10^{-2}$ [Nm/A], see Figure 8.8. In the Laplace

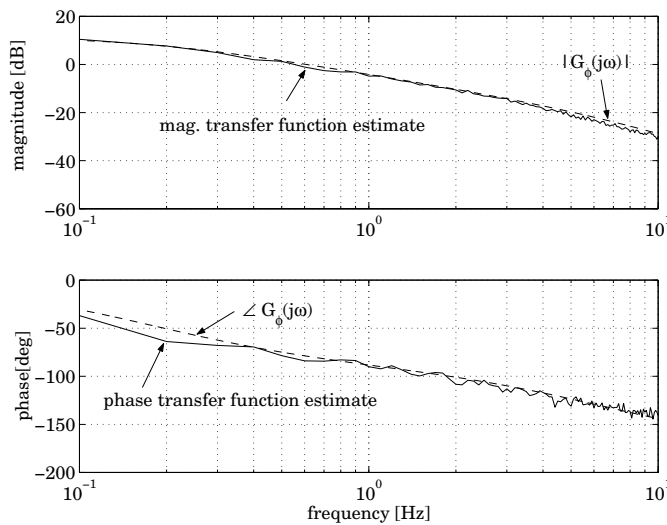


Figure 8.8: Identification of the throttle valve dynamics

domain the transfer function $G_\phi(s)$ from current I_{dc} to valve opening ϕ becomes:

$$G_\phi(s) = \frac{175}{s^2 + 45s + 48}. \quad (8.3)$$

8.2.2 Feedback control

A PID control structure $C_\phi(s)$ is proposed to force the actual valve position $\phi(t)$ to track the desired one $\phi_d(t)$, resulting in the closed loop transfer function $H_\phi(s)$:

$$H_\phi(s) = \frac{G_\phi(s) C_\phi(s)}{1 + G_\phi(s) C_\phi(s)}. \quad (8.4)$$

The PID controller $C_\phi(s)$ has to take care that the closed loop $H_\phi(s)$ has a:

- rise time of about 0.2 sec;
- bandwidth of at least 10 [Hz];
- phase margin of at least 60 degrees;
- limited overshoot for the system with input (current) saturation.

There is no explicit constraint put on the speed of convergence towards a steady state value. Fast steady-state convergence demands for a relatively high integral term, which often degrades the accuracy in transient situations. The closed loop performance of steady-state behaviour is investigated a posteriori. Loop shaping resulted in the controller $C_\phi(s)$:

$$C_\phi(s) = \frac{36s^2 + 374s + 54}{s^2 + 10s}. \quad (8.5)$$

Frequency and time domain results are shown in Figure 8.9. Except for the phase margin, it can be seen from the Bode plot and the step response that all design constraints are met. The phase margin of 32 [deg] appears to be violated by 28 degrees, which is quite a lot. The computing frequency must therefore be chosen high enough to circumvent stability problems. This is taken into account in Section 8.1.5.

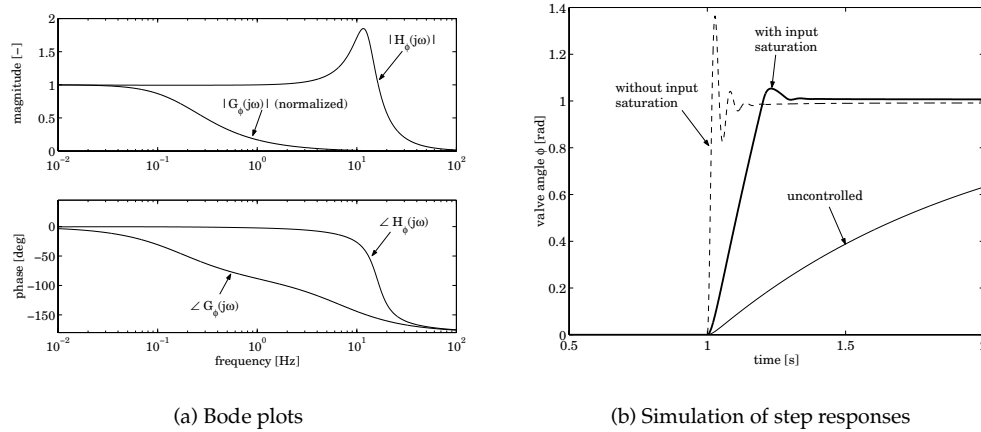


Figure 8.9: Frequency and time domain results of $H_\phi(s)$

The controller $C_\phi(s)$ is designed using the approximation $G_\phi(s)$ of the throttle system around a nominal valve position ($\phi \approx \pi/4$ [rad]). The gearing, bearings, valve and encasement of the torsional springs cause substantial non-linear friction phenomena. This can not be taken into account using only a fixed value for the damping parameter b_ϕ for the entire throttle's operating envelope. Therefore, the friction torque T_ϕ needs to be considered in more detail.

8.2.3 Feedforward control

More knowledge of the friction torque offers the possibility to improve the throttle performance by incorporating it in a feedforward control law. If all parameters in the model 8.2

are well known the desired current $I_{dc}(t)$ can be computed from a given $\phi_d(t)$ trajectory. The feedback controller $C_\phi(s)$ is kept to nullify the remaining tracking errors introduced by disturbances and model discrepancies. The design of the feedforward control is discussed next.

It is assumed that T_ϕ does not depend on the actual valve position ϕ , but only on the speed $\dot{\phi}$. Furthermore, it is assumed that the friction torque is caused by Coulomb friction and viscous damping. The mechanical model (8.2) then can be written as:

$$J_\phi \ddot{\phi}(t) + b_\phi \dot{\phi}(t) + k_\phi(\phi(t) + \phi_0) + T_{\text{coulomb}} \text{sign}(\dot{\phi}(t)) = \frac{K_{dc} I_{dc}(t)}{r_\phi} - \tilde{T}_\phi \quad (8.6)$$

The term \tilde{T}_ϕ represents the remainder of all unmodeled (friction) phenomena. The goal is to formulate a feedforward control input $I_{dc,ff}$ that compensates as far as possible the left hand side of equation (8.6) for a given desired trajectory $\phi_d(t)$. The parameters k_ϕ , J_ϕ and K_{dc} are assumed to be estimated well enough by the identification around the nominal operating point. Furthermore, the unknown disturbance \tilde{T}_ϕ is put to zero in the model. Taking these assumptions into account the to be identified parameters are b_ϕ and T_{coulomb} , see Figure 8.10. In

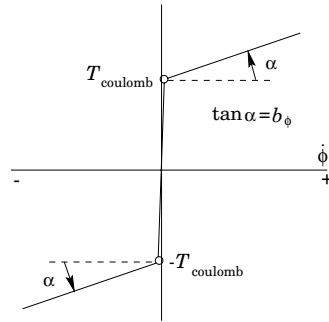


Figure 8.10: Viscous and coulomb friction as a function of valve angle speed $\dot{\phi}$

principle it possible to identify b_ϕ and T_{coulomb} by forcing the valve to track a linearly increasing and decreasing (sawtooth) desired speed pattern $\dot{\phi}_d$. This can be executed by the control law:

$$I_{dc}(t) = \frac{r_\phi}{K_{dc}} (J_\phi \ddot{\phi}_d(t) + k_\phi(\phi_d(t) + \phi_0)) + \mathcal{L}^{-1} \{C_\phi(s)(\Phi_d(s) - \Phi(s))\}(t), \quad (8.7)$$

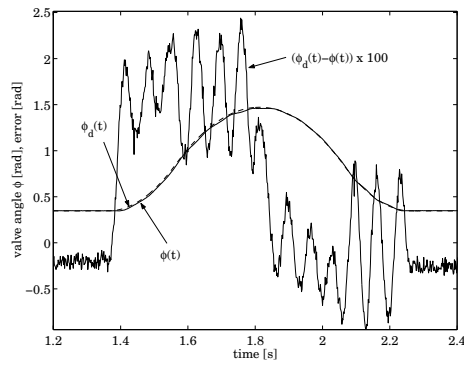
which is a combination of feedforward of the acceleration and stiffness term and feedback using controller $C_\phi(s)$. Through a posteriori inspection of the feedback term the friction parameters can be estimated from the test sequence. This is done in [Hitzert, 2001], and the parameters turned out to be $b_\phi = 4.0 \cdot 10^{-2}$ [Nms/rad] and $T_{\text{coulomb}} = 0.21$ [Nm], see Figure 8.11(a), (b) and (c).

8.2.4 Results

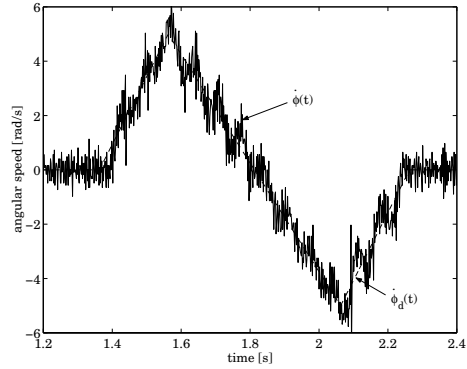
Having all parameters for feedforward control and the feedback controller, the total throttle valve control law becomes:

$$I_{dc}(t) = I_{dc,ff}(t) + \mathcal{L}^{-1} \{C_\phi(s)(\Phi_d(s) - \Phi(s))\}(t) \quad (8.8)$$

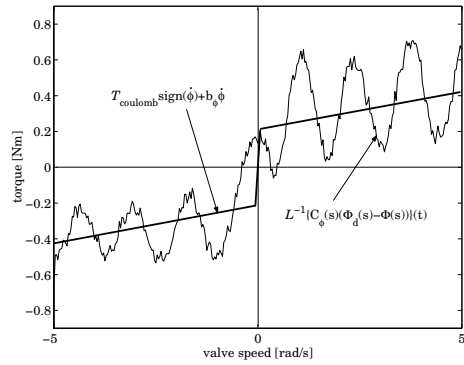
$$I_{dc,ff}(t) = \frac{r_\phi}{K_{dc}} \{J_\phi \ddot{\phi}_d(t) + b_\phi \dot{\phi}_d(t) + k_\phi(\phi_d(t) + \phi_0) + T_{\text{coulomb}} \text{sign}(\dot{\phi}_d(t))\} \quad (8.9)$$



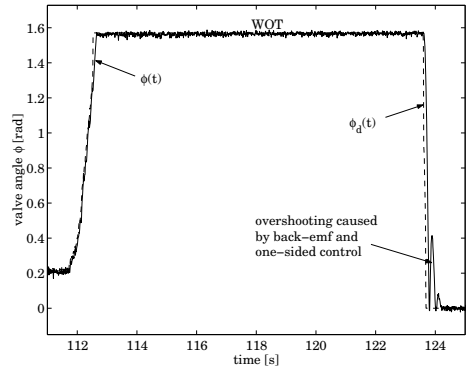
(a) Valve angle



(b) Valve speed



(c) Control torque



(d) Closed loop experiment

Figure 8.11: Experiments for identification of viscous $b_\phi \dot{\phi}$ and Coulomb $T_{\text{coulomb}} \text{sign}(\dot{\phi}_d)$ friction torques. In plot(d) a closed loop performance test is shown

Since the term $|J_\phi \ddot{\phi}_d|$ is very small compared to the other terms in equation (8.9) this term is excluded from the feedforward law. This apparently yields some implementation benefits as the desired acceleration $\ddot{\phi}_d$ does not have to be available.

The closed loop experiment in Figure 8.11(d) shows satisfactory results for a wide open throttle (WOT) manoeuvre. Abrupt closing of the throttle valve shows the effect of the one-sided current control. For such an abrupt closing ($\dot{\phi}(t) \ll 0$), the control voltage V_{dc} (see equation (8.1)) is set to 0 [V] and hence the valve is closed mainly by the torsional spring with stiffness k_ϕ . From equation (8.1) it can be seen that the term $L_{dc} \dot{I}_{dc} + R_{dc} I_{dc}$, driven by the back-electromotive voltage $K_{dc} \dot{\phi} / r_{\phi_r}$, becomes positive. If the valve reaches its mechanical

stop (at completely closed position) obviously the generated positive current I_{dc} reopens the throttle shortly. This initiates a short term oscillation of the two interacting systems (8.1) and (8.2) until all electric power is dissipated by the friction in the throttle body and by the dc motor resistance R_{dc} .

In Figure 8.12 another experiment is shown. It comprises a 16 [sec] logging of $\phi_d(t)$ and $\Phi(t)$ taken from an arbitrary field experiment with the test vehicle. In a high transient at 9.5 [sec] the error increases to about 0.13 [rad]. Because the error occurs on a very short time scale this is not considered harmful. Within the entire time interval it can be seen that the average error decreases to zero slowly. This is also seen in the simulation in Figure 8.9, at least for the input saturated ($\max(I_{dc}) = 1.5$ [A]) closed loop. The error is small though and does not introduce limitations in practice.

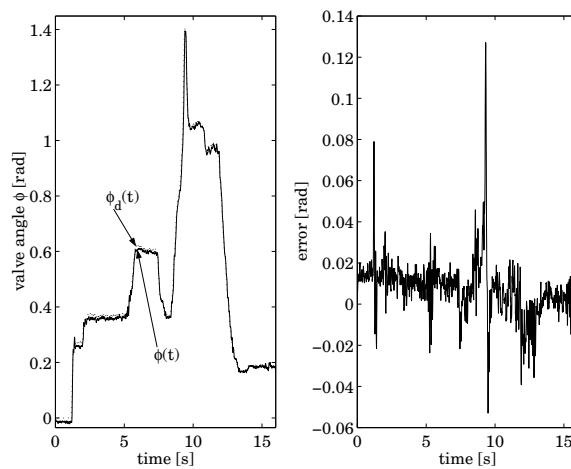


Figure 8.12: Throttle valve trajectory taken from an arbitrary field experiment

8.3 Experimental coordinated powertrain control

In this section, the coordinated powertrain control laws as they are implemented in the vehicle are discussed. In the sequel, this control will be termed 'experimental control'. Through altering the throttle valve angle ϕ the intended engine torque generated by the coordinated powertrain control has to be controlled. The intended engine torque has to be translated into a desired value ϕ_d for ϕ .

In Section 8.1.3 it is argued that a *desired CVT ratio* $r_{cvt,d}$ is the required reference input for the CVT component controller discussed in [Vroemen, 2001]. At the level of coordinated powertrain control the generation of $r_{cvt,d}$ instead of $\dot{r}_{cvt,d}$ is equivalent whenever an initial condition for the ratio is given. In this section the input $u_2 = \dot{r}_{cvt}$ is replaced by $r_{cvt,d}$, hence dropping the term ' u_2 '.

8.3.1 Control law for ϕ_d

For both powertrains, control law (7.40) is adopted to derive the setpoint for the engine. This setpoint u_1 and the measured engine speed ω_e are substituted into the inverse of the throttle map $\bar{T}_e(\phi, \omega_e)$ introduced in equation (6.1). This leads to the setpoint ϕ_d for the throttle valve:

$$\phi_d = \bar{T}_e^{-1}(u_1, \omega_e), \quad 0 \leq \phi_d \leq \frac{\pi}{2} \quad (8.10)$$

$$u_1 = T_{OL} \quad (8.11)$$

8.3.2 Control law for $r_{\text{cvt},d}$

To generate the desired CVT ratio $r_{\text{cvt},d}$ it is decided to implement a simplified version of control law (7.38). The control law for $r_{\text{cvt},d}$ is equal for both the CVT and the ZI powertrain and will be derived in this section.

motivation

The simplification of the control synthesis in the experimental environment is beneficial in the implementation overhead and robustness of the closed loop. Moreover, it has transparent tuning and easy validation capabilities. Most importantly, the stability of the experimental control could be demonstrated in closed form. For control law (7.38) this is not done yet. Altogether, these aspects are indispensable during first testing of both *new hardware and software* in a human driven vehicle.

The main goal of the experiments in this report is to measure the expected decrease of fuel consumption by E-line tracking and the qualitative driveability improvement due to the assisting ZI flywheel rather than to optimize the control performance. Using identical control for the CVT and ZI powertrain has the potential to transparently demonstrate the differences in intrinsic dynamics and the associated driveability. Alleviating the intrinsically larger driveability problems of the CVT powertrain, can thus not be guaranteed to the same extent as is demonstrated by using control laws (7.33) and (7.32). The implementation and testing of control laws (7.33) and (7.32) for the CVT powertrain and (7.40), (7.38) for the ZI powertrain are left for future research. The experimental control law is able to track the OOL in quasi-stationary situations as opposed to (7.40) and (7.38) which could only guarantee tracking of the OOL in stationary situations.

simplified control model

The experimental CVT ratio control law is based on a simplified version of the powertrain model (7.23):

$$\dot{x} = \frac{u_1 - T_d r_d r_{\text{cvt}}}{J_1^*(r_{\text{cvt}})}; \quad (8.12)$$

$$r_{\text{cvt}} = \frac{\omega_w}{r_d x}, \quad (8.13)$$

where x is the primary pulley speed $\omega_p (= \omega_e$ for locked torque converter) and ω_w is the wheel speed. The control model in fact is the equivalent primary inertia J_1^* loaded with the torques u_1 and $T_d r_d r_{\text{cvt}}$, see Figure 8.13.

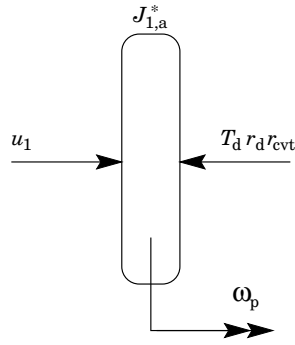


Figure 8.13: Simplified control model

design of $r_{cvt,d}$

The control objectives are equal to those given by y in (7.20), but now they apply for the simplified model (8.12). The setpoint for the CVT ratio is then given by:

$$r_{cvt,d} = \frac{\omega_w}{r_d x_d}, \quad (8.14)$$

$$\dot{x}_d = \frac{u_1 - \frac{T_{d,d}}{x_d} \omega_w}{J_{1,a}^*(r_{cvt,d})} \quad (8.15)$$

subject to

$$r_{ud} \leq r_{cvt,d} \leq r_{od} \quad \text{and} \quad \omega_{e,\min} \leq x_d \leq \omega_{e,\max} \quad (8.16)$$

$J_{1,a}^*$ is the same approximation of J_1^* suggested by equation (7.42). Laws (8.10) and (8.14) obviously simplify the coordinated control at the cost of accuracy. Through discarding all (equivalent) inertias downstream from the primary pulley in the model (8.12), they are not compensated for by the control law (8.14). This will be shown by a simulation in Section 8.3.1. First, the stability of the experimental control is demonstrated.

8.3.3 Stability of the experimental control

Assuming $\eta_{cvt} = 1$, the equations (7.12) and (7.11) lead to $T_{d,d}\omega_w = T_{OL}\omega_{OL}$, thus equation (8.15) can also be written as

$$\dot{x}_d = \frac{T_{OL}(x_d - \omega_{OL})}{x_d J_{1,a}^*}. \quad (8.17)$$

Define the difference $\xi = x_d - \omega_{OL}$ and the Lyapunov function V :

$$V = \xi^2. \quad (8.18)$$

Furthermore assume that ω_{OL} is constant and using equation (8.17) the time derivative of V yields

$$\dot{V} = 2\xi\dot{\xi} = 2\xi^2 \frac{T_{OL}}{x_d J_{1,a}^*}. \quad (8.19)$$

For x_d , $T_{OL} > 0$ and $\xi \neq 0$ there holds $\dot{V} < 0$ as $J_{1,a}^* < 0$, see equation (7.42). Hence, $x_d = \omega_{OL}$ is a globally asymptotically stable equilibrium point. In the implementation a lower bound $x_d = \omega_{e,\min}$ is set, hence the restriction $x_d > 0$ is not violated. The restriction $T_{OL} > 0$ is violated for pedal back-out, *i.e.*, $\delta \leq \varepsilon$. In that case T_{OL} becomes negative according to equations (7.17) and (7.12), see also Figure 7.8(a). To circumvent instability, $J_{1,a}^*$ in the shifting law (8.15)→(8.14) is changed into $|J_{1,a}^*|$ for $\delta \leq \varepsilon$.

8.3.4 Simulation with model (7.23)

In Figure 8.14 the responses of the ZI and CVT with the experimental control is presented and compared with ZI using control laws (7.40) and (7.38). The sequence of the pedal tip-in and back-out $\delta(t)$ is the same as used in Sections 7.4.2 and 7.4.3. In the plots 'ZI' stands for the ZI powertrain with shifting law (7.38). The other indications are self-explanatory. A number of conclusions can be drawn from these figures:

- the offset in wheel torque (Figure 8.14(b)) for the ZI powertrain with experimental control is caused naturally because the secondary inertias are not taken into account. In the actual powertrain these secondary inertias subtract a part of the torque $T_{d,d}$ leaving less for the drive shafts;
- alternatively, ratio shifting law (7.38) clearly shifts more down (Figure 8.14(c)) to enlarge the engine speed (Figure 8.14(b)). The engine thus delivers more power to compensate for the secondary inertias, hence $T_d = T_{d,d}$;
- the offset in wheel torque may be hardly noticed by the driver. In effect the driver would probably press the drive pedal a little more if he or she desires to have more wheel torque;
- the wheel torque response (Figure 8.14(b)) of the CVT powertrain with the experimental control performs surprisingly well especially for pedal tip-in. For pedal back-out the wheel torque decreases rather slowly. The consequence of that can also be seen in the wheel speed response (Figure 8.14(d)). The wheel speed, or vehicle speed, continues to increase slightly even though the pedal is (partly) released;
- as the course of the CVT ratio $r_{cvt}(t)$ (Figure 8.14(c)) and engine torque (Figure 8.14(a)) are almost identical for CVT and ZI with experimental control the differences in wheel torque response and wheel speed can be attributed to the different intrinsic dynamics of both powertrains;
- the course of $r_{cvt}(t)$ for the CVT powertrain is not exactly identical to that of the ZI powertrain with experimental control because the different course of $\omega_w(t)$ for either powertrains is reflected in equation (8.14).

8.4 Model validation: drive shaft resonance

The frequency of the first eigenmode (drive shaft resonance) in the linearized powertrain model (6.66) is validated by examining those seen in the test vehicle. Through (near) step-wise throttle actuations with stationary CVT ratios, the frequencies of wheel torque responses of the CVT and ZI powertrain are examined. The results are presented in Figure 8.15 and Table 8.3 for three CVT ratios. The responses are scaled for clarity, all the more since their frequency is of interest only. The first eigenmode clearly dominates the responses and the first eigenfrequency corresponds fairly well with the model frequencies. The somewhat larger discrepancies between model and measurement for the ZI powertrain can be explained by

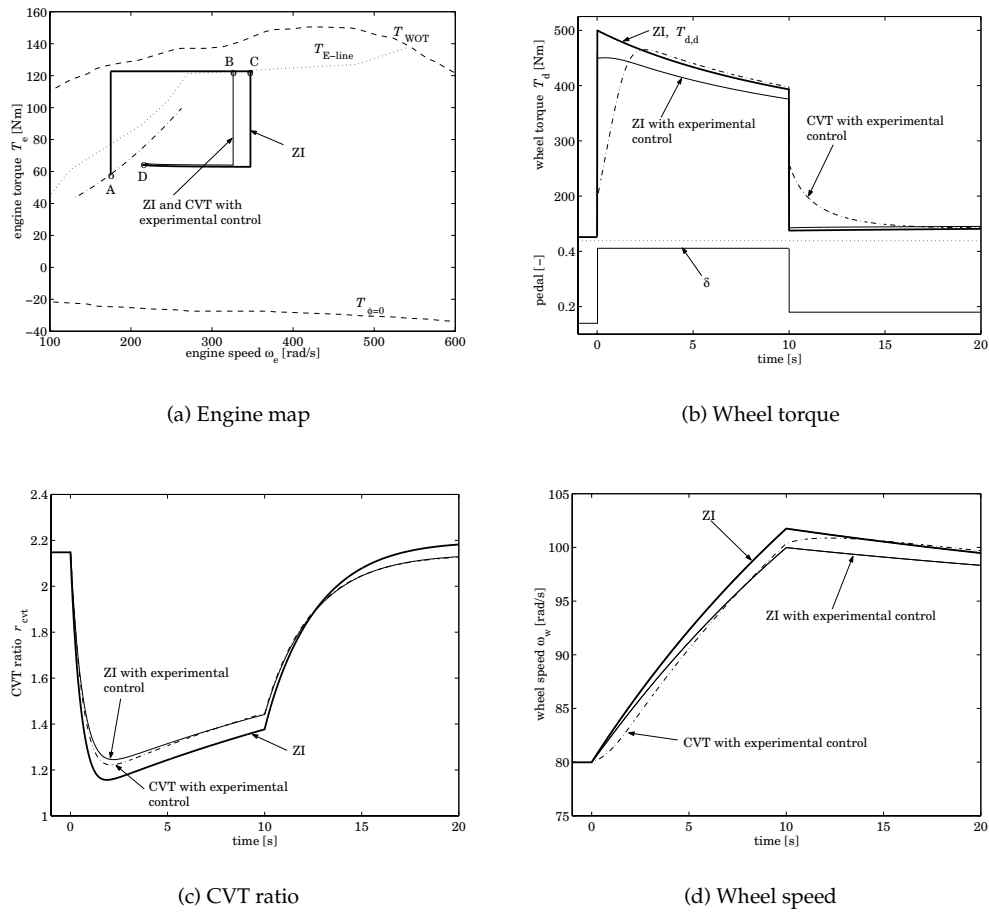


Figure 8.14: Comparison ZI control according to equations (7.40) and (7.38) with experimental control laws (8.10) and (8.14)

the measurement technique that had to be adopted. Since the CVT and its control reacts noticeably on varying torques, it is generally hard to keep the ratio stationary. Due to external disturbances from the engine, hydraulics, road/tires, etc. the useful observation time window appeared to be very limited, at least not long enough to use frequency response analysis techniques such as FFT. Therefore, the frequencies are determined by simply measuring the period time of the periodical responses. This introduces apparent inaccuracies especially for the low resonance frequencies observed within the entire CVT ratio coverage in the case of the ZI powertrain.

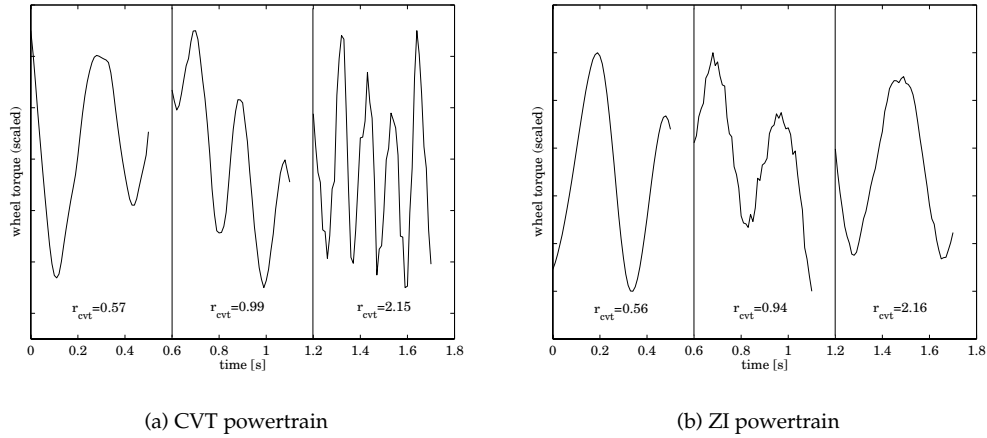


Figure 8.15: Drive shaft resonances (scaled wheel torques) at different CVT ratios

	CVT		ZI		CVT		ZI	
	$r_{cvt} = 0.57$	$r_{cvt} = 0.56$	$r_{cvt} = 0.99$	$r_{cvt} = 0.94$	$r_{cvt} = 2.15$	$r_{cvt} = 2.16$		
estimated	3.1	3.4	5.3	3.4	9	2.4		
model (6.66)	3.14	3.09	4.97	3.89	8.84	1.77		

Table 8.3: Frequencies (in [Hz]) of the estimated drive shaft resonance compared with the linearized model (6.66)

8.5 Driveability

In this section the qualitative driveability—defined in Section 7.2.2—is assessed. For that purpose the measurements of T_d , ϕ , δ , ω_w , ω_e , ω_p and ω_s are streamed into the host PC during a number of test sequences on an oval test track. While driving the test vehicle, the driveability is also judged subjectively by the author and co-workers. To quantify this subjective judgment, a large panel of test drivers should ride the vehicle with and without the flywheel and rate their findings through questionnaires. Elaborating this is thought to lie outside the scope of the current project and is left for future research. For that, also more accurate controllers, *e.g.*, those proposed in Chapter 7, could be implemented in order to maximize the driveability potentials of the CVT and ZI powertrain.

Three types of experiments are shown in this section. First the responses of both powertrains upon a semi kick-down of the drive pedal are shown and explained. Then, the responses of ‘pedal jogging’, *i.e.*, pushing the pedal in and out in a (near) periodical manner are given. Finally, the responses of a full kickdown for the CVT, ZI and 4AT (4 gear automatic transmission) powertrains are shown. As explained in Chapter 7, kickdowns are not a part of the driveability objective but rather show the maximal performance of the powertrain. However, it is decided to investigate up to what extent the powertrains at issue are able to fulfill the driveability objective in a performance test.

8.5.1 Semi kick-down

In Chapter 7 it is argued that driveability is related to the response of the wheel torque T_d upon changes in the pedal deflection not more than 50% of the total pedal travel (semi-kick down).

CVT powertrain

Figure 8.16 shows the response of the CVT powertrain on a semi-kick down for the CVT powertrain, whereas Figure 8.17 presents the results of a similar experiment with the ZI powertrain. The WOT torque and E-line of the test vehicle's engine differ from the ones used

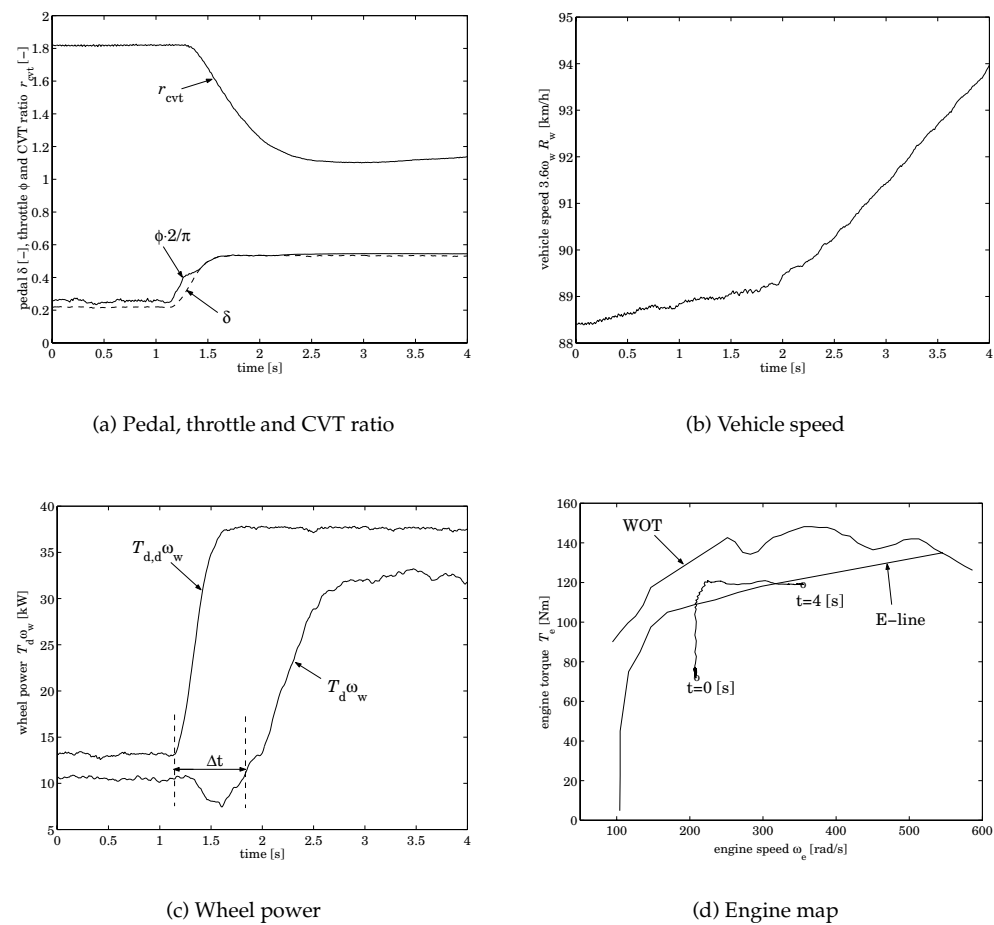


Figure 8.16: Responses for semi-kickdown experiment with the CVT powertrain

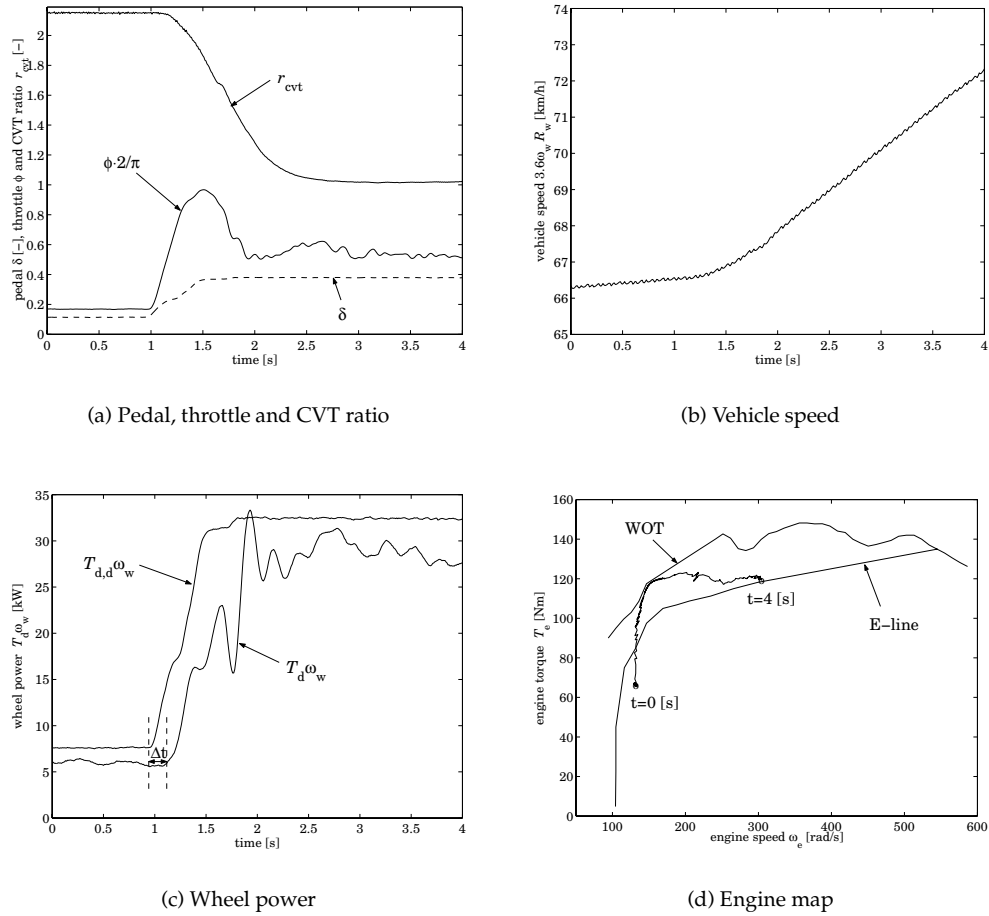


Figure 8.17: Responses for semi-kickdown experiment with the ZI powertrain

in the previous chapters. First, the experiment with the CVT powertrain is discussed. The initial conditions of this experiment are such that $r_{cvt} < r_{od}$. Clearly, the vehicle is already accelerating lightly, see Figure 8.17(b) before the pedal is pushed at $t \approx 1.2$ [sec] further from $\delta = 0.21 \rightarrow 0.55$, Figure 8.16(a). The throttle valve opening ϕ slightly draws ahead of δ during the transient. This is required to raise the engine torque quickly up to the final level on the E-line. From the wheel power response, Figure 8.16(c) a slight inverse response can be seen with a time delay Δt of about 0.7 [sec]. In this case it does not lead to a short deceleration of the vehicle because the minimal power reached in the transient is obviously still high enough to overcome the road load power. The permanent offset between $T_{d,d}\omega_w$ and $T_d\omega_w$ is caused by the mechanical and hydraulic losses, moreover the engine torque T_e is not accurately con-

trollable according to equation (8.10) because the throttle map of the installed engine is known with limited accuracy only. Therefore, the transient plotted in the engine map, Figure 8.16(d), most likely does not represent the actual course of the engine torque. In this experiment the engine speed is shifted from 210 to 350 [rad/s].

ZI powertrain

A comparable experiment for the ZI powertrain in Figure 8.17 shows a quite different response. Here, the pedal is deflected from $\delta = 0.10 \rightarrow 0.4$, which is slightly less than for the CVT experiment. The engine speed leap, however, is larger in this experiment, *i.e.*, $\omega_e = 125 \rightarrow 300$ [rad/s]. The throttle opening shortly reaches WOT—see Figure 8.17(a) where $\phi = \pi/2$ at $t = 1.5$ —to facilitate the instant torque response up to the final level on the E-line. In Figure 8.17(d) it can be seen that the engine torque tips the WOT line.

In the wheel power response, a shuffle lasting for one period is observed. Not much of it is noticeable in the vehicle's interior though. The shuffle is probably caused by the slight hitch in the CVT ratio at $t = 1.6$ [sec]. It could also be assigned to the engine torque transient. Anyhow, it is phased out relatively fast, mostly attributed to the damping capabilities of the flywheel. Although not really annoying in this case, occasional shuffles can be actively damped by determining the throttle setpoint ϕ_d with more refinement, for instance see [Mo *et al.*, 1996], [Karlsson and Jacobsson, 2000], and references therein. This is left for future research.

Altogether, the trend of the wheel power transient shows a persistent rise. Furthermore, the time delay between pedal deflection and the initial rise in $T_d\omega_w$ is a mere 0.16 [sec], and is hardly noticeable by the driver.

conclusion

In the demonstrated semi-kickdowns the ZI powertrain generates an increasing wheel torque about 0.5 [sec] faster than the CVT powertrain does.

8.5.2 Pedal jogging

In Figures 8.18 and 8.19 the (scaled) torque responses upon a jogging pedal are shown. The pedal frequently changes more than 50% of the total pedal travel and should therefore not be related to driveability as such. On the other hand, the wheel torque response should at least show some significant driveability potential. Besides the engine speed in both graphs, Figure 8.19 also shows the absolute flywheel speed ω_f ⁴.

The experiments for both powertrains were conducted with about the same jogging 'frequency', but the induced pedal deflections larger than zero have shorter time intervals in case of the CVT powertrain. This can obviously be attributed to impreciseness of the driver. It could, on the other hand, also be related to the specific behaviour of either of the powertrains that reflects differently on the actions of the driver through sound, vibration, acceleration feel, *etc.* In a qualitative sense the experiments are comparable though. Pedal jogging results in up and down shifting of the CVT ratio to increase and decrease the engine speed according to the translated wheel torque demand.

Regarding the experimental results for pedal jogging, the following observations are made:

⁴In the definition (6.29) ω_f is negative for $r_{cvt} > r_{gn}$.

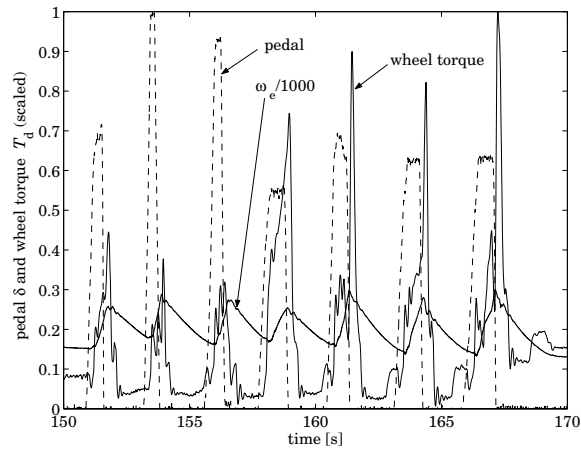


Figure 8.18: CVT powertrain wheel torque response for pedal jogging

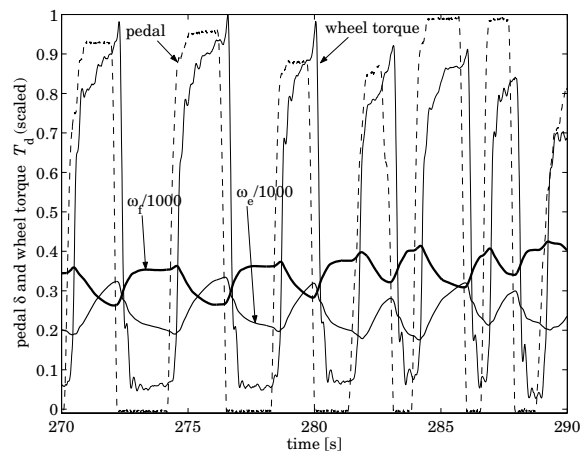


Figure 8.19: ZI powertrain wheel torque response for pedal jogging

- accompanied by slight inverse response the torque responses on positive pedal deflections of the CVT powertrain seems to have the same time delay though is far less persistent than the response of the ZI powertrain;
- contrary to the CVT powertrain, the wheel torque for the ZI powertrain decreases steadily after a pedal back-out;
- the CVT powertrain even shows a relatively high increase of wheel torque after pedal back out, which is caused by the torque stemming from the decelerating primary inertias ($\dot{\omega}_p < 0$). In the ZI powertrain clearly this torque is used to accelerate the flywheel;

- the vehicle speed (or equivalently the secondary pulley speed ω_s) increases upon this sequence of pedal deflections and according to equation (6.31) this will also increase the average (absolute) flywheel speed at equal average engine speed. This can indeed be observed in Figure 8.19.

conclusion

These observations lead to the following conclusions:

- the driveability penalty on *pedal back-out* is remarkably high for the CVT powertrain. This is predicted, although to a lesser extent in the simulations of Figure 8.14;
- the ZI powertrain fulfills the driveability objective equally well for both pedal tip-in and back-out, see again Figure 8.14;
- the response of the ZI powertrain shows a more or less repeatable response, whereas for the CVT powertrain this is less predictable. Most likely this is caused by a combination of lack of responsiveness and a multitude of drive shaft oscillations induced after every pedal tip-in and back-out. The ZI powertrain has the tendency to phase out such oscillations more than the CVT powertrain, see Section 6.5.1.

8.5.3 Kick-down

The response after a full pedal kick down is said to be related to the *performance* instead of *driveability*. However, it is interesting to investigate to what extent the driveability objective is met for such a performance demand. Therefore, kick down experiments are undertaken for the vehicle with 4AT and later with the CVT and ZI powertrains. The wheel torque responses are shown in Figure 8.20. All powertrains started at their respective overdrive ratios which is $r_{od} = 2.15$ for CVT and ZI and $r_{od} = 1.25$ (4th gear) for the 4AT. For the present case, the kick down starts with $\omega_e = 270$ [rad/s] for the 4AT and at $\omega_e = 157$ [rad/s] for the other two powertrains. This difference of initial operating point, results in a power reserve for the 4AT of 27 [kW], whereas for the CVT and ZI this is about 9 [kW], at least if the 80 [km/h] is driven stationary.

The initial values of the wheel torques, however, differ somewhat. This is reflected in slightly different engine torques for CVT and ZI although the engine speeds are equal. In practice it is difficult to have equal initial torques because they have to be controlled by the driver who is focused on approximately maintaining a stationary vehicle speed instead of torque. Apparently, the vehicle speed does not deviate from 80 [km/h] in a way the driver would adapt the drive pedal position, hence the different initial wheel torques.

The transients of the three powertrains differ remarkably. The AT4 initially has a more prompt response due to the much higher power reserve. However, when the 4AT starts to shift from the fourth gear towards the third at $t = 1.2$ [sec], the wheel torque shows a severe transient that lasts until the shift is finished at $t = 1.8$ [sec]. Shortly thereafter, at $t = 2.1$ [sec], the automatic gearbox shifts further down to the second gear ratio. Again accompanied by an even more severe transient, the wheel torque finally becomes (quasi-) stationary at $t = 2.8$ [sec], *i.e.*, more than two seconds after the pedal is fully pressed down.

The CVT transient shows the expected jet start behaviour, but nevertheless reaches the final torque level about 0.8 [sec] earlier than the 4AT. Finally, the ZI powertrain shows a prompt and persistent increase of the wheel torque for the entire observation interval. There is however, a slightly longer time interval between the pedal kick-down and the response than for the 4AT. Moreover, the initial response of the 4AT is steeper. This initial torque increase is

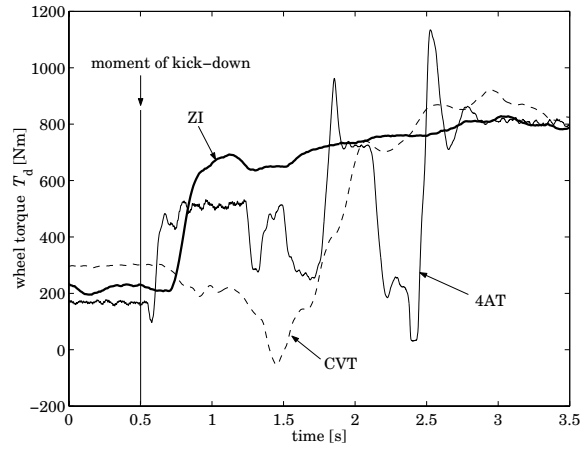


Figure 8.20: Kickdowns from 80 [km/h] for 4AT, CVT and ZI powertrains

inflicted by the substantially higher power reserve for the 4AT powertrain that is approximately 27 [kW], whereas for the ZI powertrain this is about 9 [kW]. For the ZI powertrain, the increase is inflicted merely by the torque emerging from the (decelerating) flywheel, *i.e.*, by down shifting the CVT. According to equation (7.21) the wheel torque then changes with the input \dot{r}_{cvt} . The dynamic response of the hydraulically controlled CVT is significantly slower than the engine torque response and explains that the ZI powertrain initially has a less steep response.

conclusion

In conclusion, the ZI powertrain—contrary to the CVT and 4AT powertrains—shows a response that fulfills the *qualitative driveability objective* fairly close even though a *performance manoeuvre* is demanded.

8.6 Fuel economy

The fuel economy of the 4AT, CVT and ZI powertrains is measured at the emission testing facilities of TNO Automotive, Delft, The Netherlands. The CVT is tested in two modes: an economy mode 'E' and a driveability mode 'D'. The E-mode resembles the control strategy described by equations (8.10) and (8.14). The E-line of the engine in the test vehicle could not be measured with the same accuracy as is possible with the engine displayed in Figure 7.3. The driveability mode resembles the same, but here, the minimal engine speed is set at $\omega_{\text{e,min}} = 157$ [rad/s], instead of 94 [rad/s] for E. Moreover, the overdrive ratio is fixed to $r_{\text{od}} = 1.2$ instead of 2.15. For E the torque converter lockup is closed and opened (using the appropriate hysteresis in the lockup control logic) at 15 [km/h]. For D this is 35 [km/h].

The fuel economy of the ZI powertrain—termed 'Z' in the following—is measured only for constant vehicle speeds up to 80 [km/h]. The reason for this is the not yet verified safety of the flywheel unit: the maximum flywheel speed is restricted to 420 [rad/s]. This implies

that above 80 [km/h] stationary vehicle speeds have to be driven with CVT ratios lower than $r_{od} = 2.15$, cf. equation (6.31). This clearly does not push the fuel economy to the lowest possible, hence driving vehicle speeds higher than 80 [km/h] is not considered useful at the moment. The fuel economy results of the 4AT powertrain are indicated by 'A'. The results of the emission tests are listed in Table 8.5. Before interpreting these results, first a brief discussion about estimating the OOL of the test vehicle's engine is given.

8.6.1 Estimation of the OOL

The E-line (to be used in the OOL) of the test vehicle's engine is estimated in the following way. The vehicle is put on a dynamometer roller bench. The drive clutch is closed and the torque converter lockup is kept open, hence $\omega_e \neq \omega_p$. Furthermore, through adapting the load at the wheels by the dynamometer the wheel speed is kept constant. For 14 different valve positions between $\phi = 0.1$ and $\phi = 1$ (WOT), the primary speed is gradually increased with the CVT between 100 and 350 [rad/s] at a wheel speed of 36 [rad/s] and between 300 and 550 [rad/s] at a wheel speed of 63 [rad/s]. The torque T_e stemming from the engine is then estimated using the torque converter characteristic described by equation (6.10) and taking the pump torque T_{pump} into account, *i.e.*,

$$T_e = b_{tc}(r_{tc})\omega_e^2 + T_{pump}(p_s, \omega_e), \quad r_{tc} = \frac{\omega_p}{\omega_e}, \quad (8.20)$$

where p_s is the pressure on the secondary pulley (equal to pump pressure). Along with the primary speed trajectories the injection time intervals at one of the four injectors is estimated. It is assumed that the injection time interval τ_{inj} at every engine speed and torque provides a direct measure for the fuel consumption (in [g/s]). With the results of the injection time intervals a measure for the BSFC b_e is known according to

$$\frac{\tau_{inj}(\omega_e, T_e)}{\pi T_e(\omega_e, \phi)} = B \cdot b_e(\omega_e, T_e). \quad (8.21)$$

The constant B is unknown but is unimportant as estimating the E-line comprises finding combinations (ω_e, T_e) with minimal b_e and if $B \cdot b_e$ is minimal then also b_e is minimal.

This measurement setup appeared to have some drawbacks. First the engine speed could not be suppressed to extremely low values. Clearly, the slip $r_{tc} < 1$ in the torque converter establishes transmitting of torque to the turbine, see equation (6.11), where $\omega_t = \omega_p$. Thus $\omega_e > \omega_p$ at all times and in the experiments it appeared that the engine speed is at least 157 [rad/s]. In other words, a large part of the E-line could not be estimated. This part of the E-line is particularly encountered when driving a NEDC.

Extrapolations are used instead to generate virtual measurements and the missing part of the E-line with apparent inaccuracies.

In the fuel economy measurements the stationary engine speeds ω_{OL} are chosen as:

$$\omega_{OL} = \max\left(\frac{\omega_w}{r_d r_{od}}, \omega_{e,min}\right). \quad (8.22)$$

For instationary (also quasi-stationary) situations the inaccurately estimated E-line is used.

8.6.2 Constant vehicle speeds

The fuel economy for constant vehicle speeds is illustrated in Figures 8.21(a) and (b). In Figure

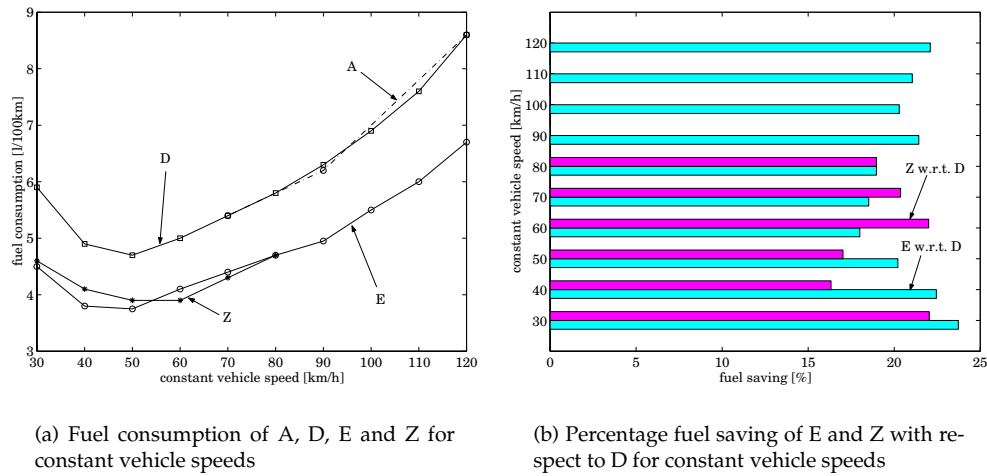


Figure 8.21: Fuel consumption and savings for constant vehicle speeds

8.21(a) the fuel consumption for constant vehicle speeds between 30 [km/h] and 120 [km/h] are shown for A, E, D and Z. Vehicle speeds lower than 30 [km/h] are not considered useful in practice as a *constant speed*. Vehicle speeds higher than 120 [km/h] lie outside the legal speed range. In Figure 8.21(b) the fuel savings for constant vehicle speeds of E and Z with respect to D are shown. From these figures it can be seen that the fuel savings of E and Z vary between 15% and 24% which is remarkably high. Clearly the extremely low engine speeds, see Figure 8.22, that apply for E and Z during constant speed driving bring the engine operating points to regions with much lower BSFC. In Figure 8.22 also the flywheel speed ω_f in the case of Z is shown. The horizontal parts in Figure 8.22 refer to $\omega_e = \omega_{e,\min}$, whereas the linearly increasing parts refer to $\omega_e = \omega_w / (r_d r_{od})^5$. For Z a slightly higher $\omega_{e,\min}$ is chosen for no particular reason. However, it explains the slightly higher fuel consumption seen for Z with respect to E between 30 and 50 [km/h]. Between 60 and 80 [km/h], the engine speed of Z and E are equal. The slightly lower fuel consumption of Z with respect to E seen in this region can not be explained clearly. A plausible explanation might be the different testing conditions (measurements of E and Z are conducted at 16-05-2001 and 4-10-2001, respectively). For instance, front wheel misalignments have been removed in between the indicated dates, supposedly leading to less rolling resistance. The reproducibility and accuracy of the test bench dynamometer and emission measurement is questioned although mismatches are extremely unlikely. Nonetheless, the flywheel speed ω_f that amounts up to 413 [rad/s] at 80 [km/h] does not introduce significant reduction of transmission efficiency. According to [van Druten, 2001] the power loss due to the flywheel unit at $\omega_f = 413$ [rad/s] is projected to be a mere 80 [W].

⁵The relationship between the vehicle speed v in [km/h] and the wheel speed in [rad/s] is $v = 3.6 R_w \omega_w$ [km/h].

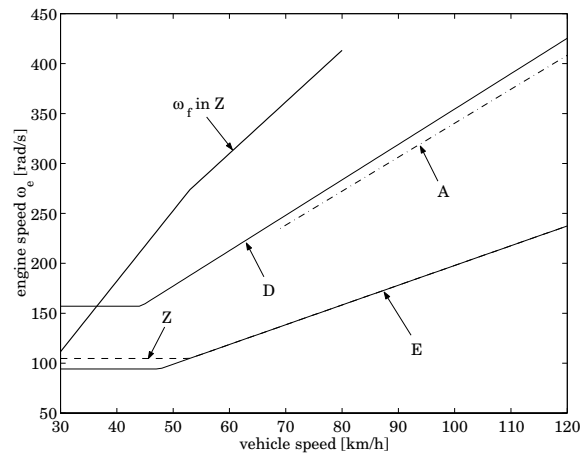


Figure 8.22: Engine speeds at constant vehicle speeds for A, D, E and Z

8.6.3 Drive cycles

Figure 8.23(a) shows the fuel savings of E with respect to D and A for five different drive cycles. For the most important drive cycle, the NEDC, the CVT powertrain in E mode shows a fuel saving with respect to A and D of 9% and 11% respectively. These results match surprisingly well with the projected fuel saving in Table 3.1 for the NEDC being 11.4%.

Assuming an average transmission efficiency $\eta_{\text{cvt}} = 0.85$ (see [Serrarens, 2001]) the stationary operating points for $r_{\text{od}} = 1.2$ lie quite near to the $\text{OL}_{15\%}$ as can be seen in Figure 8.23(b). The fact that the operating lines coincide well might be considered to be no more than an indication for the good match between the computed fuel saving in Table 3.1 and the measured fuel saving. Nevertheless, the engines used in the computation and in the measurements are different. The $\text{OL}_{15\%}$ of the engine used in the measurements might therefore be located elsewhere. Also the location of the OOL (E-line) is different for both engines. Finally, the transmission efficiency can not be considered as a constant value as is done in Figure 8.23(b). Instead, the fuel economy is computed with the simulation model in Figure 6.15 and the BSFC map displayed in Figure 2.3. Furthermore a driver model is adopted from [Mitschke and Zhenfu, 1991]. The results are plotted in Figure 8.24.

From these figures it can be concluded that the simulation model and the virtual driver are well able to track the UDC cycle and demonstrate the fuel consumption as a function of time. Even though different engines are used in the experiment and the simulation, the fuel consumption trajectories show remarkable resemblance. The trajectory for D is slightly less accurate. Nevertheless, the simulation model is judged as an instrumental tool to estimate the fuel consumption of Z on the NEDC. This is discussed next.

8.6.4 Fuel consumption of ZI on the NEDC

Using the simulation model with virtual driver the fuel consumption on the NEDC is computed to be 1.5% higher than E. This increase is caused by the additional kinetic flywheel energy that has to be generated by the engine. This energy is not regenerated in any sense,

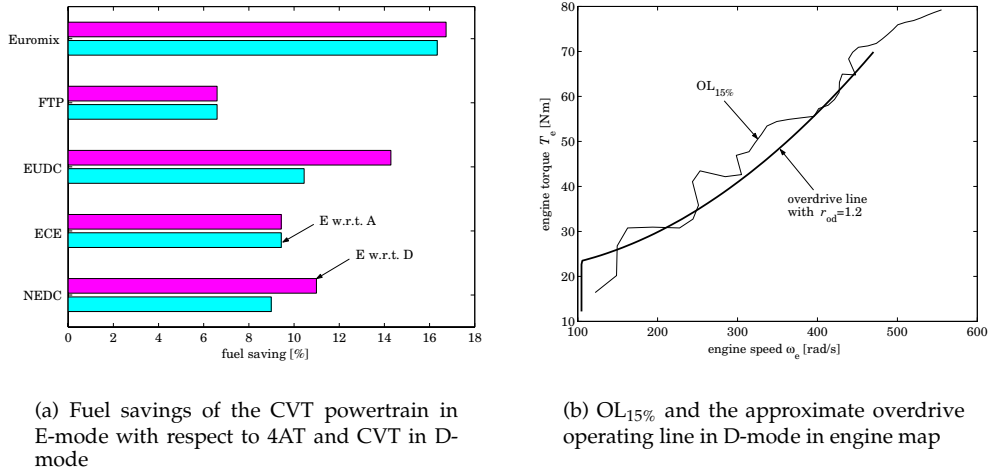


Figure 8.23: Fuel savings and resemblance between $OL_{15\%}$ with D-mode

and is basically wasted at the brakes during every full vehicle stop. In the case of Stop-Go the accumulated flywheel energy is reused for launching the vehicle and starting the engine. Hence, the fuel saving with respect to A and D would become 7.6% and 9.9% respectively. On the other hand, it is the opinion of the author that the fuel consumption of E, D and Z can be reduced be at least 2%. This can be established by the following measures:

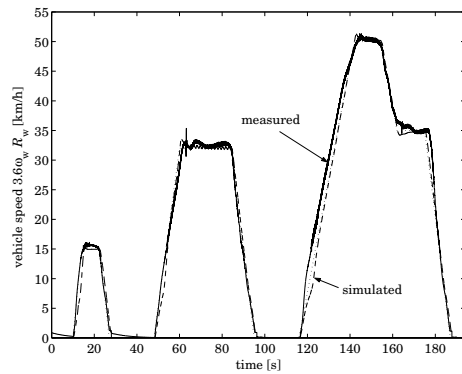
- accurately estimating the engine torque and BSFC characteristics as a function of ϕ and ω_e , the OOL (E-line, $\omega_{e,min}$) and thus the setpoint ϕ_d can be more accurately determined;
- more refinement of the lockup strategy can combine a proper driving behaviour with reduced time intervals where torque converter slip applies;
- the latter can also be combined with some fuel optimizing strategy when the torque converter is still open, see also Section 7.2.1.

Adopting these measures, the fuel economy of the ZI is estimated with respect to the 4AT as presented in Table 8.4. The projection of the additional fuel economy due to Stop-Go is

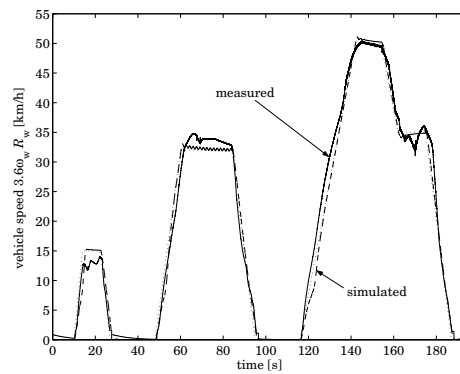
	4AT	E-MODE	ZI	ZI+STOP-GO
theoretical minimum [l/100km]	–	6.0	6.0	5.2
estimated consumption [l/100 km]	8.9	7.9	8.0	7.3
fuel saving	–	11%	10%	18%

Table 8.4: Estimated fuel savings of E-mode (E), ZI (Z) and ZI+Stop-Go with respect to 4AT (A). The theoretical minima according to Section 3.2.3 are also given

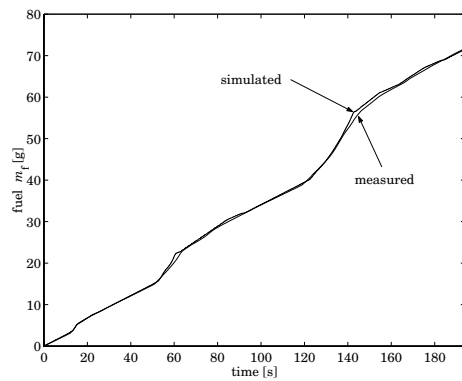
estimated by subtracting the consumption of the NEDC where the engine would normally idle, that is during decelerations at low engine speed and vehicle halts. Hence, the *accumulated*



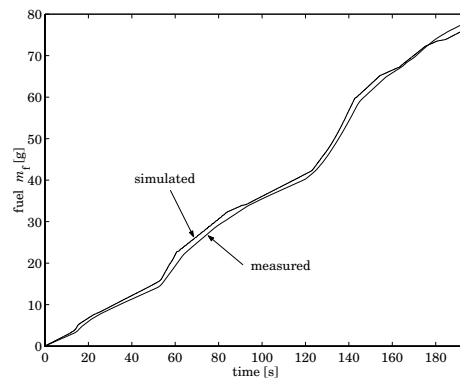
(a) UDC cycle for E



(b) UDC cycle for D



(c) Accumulated fuel for E



(d) Accumulated fuel for D

Figure 8.24: Measured and simulation results on the UDC drive cycle

idle fuel consumption given in Table 8.5 by 'Idle-D', *i.e.*, fuel consumption with closed drive clutch, is subtracted from the ZI consumption.

8.7 Concluding remarks

For the experiments a simple coordinated powertrain control is proposed and implemented. This stable controller proved to be robust, easy to implement and applicable for both powertrains. The performance of the controller is not assessed but rather the driveability and fuel economy realized with the powertrains are investigated. Considering the results presented in

this chapter, the following conclusions and recommendations for future research are given

8.7.1 Conclusions

The conclusions scattered over this chapter are summarized next.

- in a qualitative sense, the wheel torque responses for CVT and ZI seen in the simulations of Figure 8.14 are not seen in the semi-kickdown experiments of Figure 8.16 and Figure 8.17. The experiments showed more reluctance in the wheel power (at the hardly increasing wheel speed equivalent with wheel torque) than the simulations. Clearly, the limited bandwidth of the engine and the CVT actuators—which were assumed infinite in the simulations—influence the responses importantly;
- for pedal jogging, the responsiveness of the ZI powertrain is superior to that of the CVT powertrain. Slightly hampered by the actuator bandwidth the wheel torque response of the ZI powertrain is consistent with the pedal tip-ins and back-outs. This is not true for the CVT powertrain, the responsiveness of which is also not repeatable. Pedal back-outs are penalized most for the CVT powertrain;
- a kickdown manoeuvre showed that the ZI powertrain is able to establish an immediate and persistent wheel power response. Contrary to the 4AT and CVT powertrain, the ZI powertrain realizes the driveability objective also for performance demands, *i.e.*, a kickdown.
- through a combination of measurements and simulations the ZI powertrain is estimated to show a fuel consumption benefit with respect to the 4AT of 10% on the NEDC cycle. The extension with Stop-Go is projected to gain an additional 8% of fuel saving arriving at 18% fuel saving on the NEDC. This is 7% below the project target which is quite a lot. Apparently other fuel saving techniques should be adopted to gain the projected fuel saving, *viz.* Chapter 3. On the other hand, 18% fuel economy improvement by itself is judged as a respectable result;
- from Table 8.5 it can be seen that the emissions CO, NO_x and HC are penalized for E with respect to A. The emissions of D with respect to A are less penalized. The fuel economic strategy applied to the engine apparently brings the engine to operating points where the specific emissions are higher.

8.7.2 Recommendations

Based on the results of this chapter and open problems encountered, the following suggestions for future research are suggested.

- the engine torque and BSFC characteristics should be estimated accurately and for the entire engine operating range;
- with this information more refined control of the engine throttle setpoint but also for the CVT pulley clamping can be designed;
- a fuel optimizing strategy during vehicle launch, *i.e.*, an open torque converter lockup should be investigated, implemented, tested and assessed on fuel economy benefits;
- driveability is judged qualitatively in this chapter. Extensive research could focus on quantitative assessment of the driveability. Furthermore, attempting to translate subjective driveability rating by test drivers into objective figures can be utilized instrumentally in defining constraints for coordinated control strategies. Also new constraints for

the design of powertrains in general and possibly in any conceivable redesign of the ZI powertrain in particular can be defined what that;

- bringing the coordinated control more in concert with the component controllers for the CVT and throttle could enlarge the performance of the powertrain and comfort of the vehicle. Coordinated controllers more tailored to the actual powertrains, *e.g.*, those presented in Chapter 7, could enlarge this potential even more;
- as far as fuel economy of the ZI powertrain is concerned still extensive work should be undertaken to further optimize the operation of the torque converter lockup, CVT ratio and the engine torque. Furthermore, the Stop-Go transmission and its control should be further researched up to a level where it can be successfully implemented and tested in the test vehicle. Adaptations in engine management should focus on restricting emissions during first ignition at every engine startup. Most likely profound temperature management of the catalytic converter must be elaborated on;
- finally, the engine management controlling the fuel metering and spark advance should be adapted to find a new optimum between fuel economy and emissions for the specific application.

CYCLE w_i [km/h]	FUEL [l/100km]			CO [g/km]			CO ₂ [g/km]			HC [g/km]			NO _x [g/km]		
	A	E	D	A	E	D	A	E	D	A	E	D	A	E	D
NEDC	8.9	8.1	9.1	0.65	2.29	1.70	212	190	215	0.12	0.26	0.16	0.05	0.09	0.05
UDC	10.6	9.6	10.6	0.21	0.79	0.57	254	230	253	0.01	0.04	0.02	0.09	0.00	0.00
EUDC	6.7	6.0	7.0	0.11	0.14	0.27	161	144	167	0.01	0.01	0.01	0.00	0.00	0.00
FTP	9.1	8.5	9.1	0.71	3.11	2.02	213	195	210	0.09	0.22	0.16	0.11	0.10	0.10
30		4.5	5.9		0.11	0.11		107	141		0.17	0.01		0.00	0.00
40		3.8	4.9		0.12	0.08		91	116		0.15	0.01		0.00	0.00
50		3.8	4.7		0.08	0.07		90	113		0.01	0.01		0.00	0.00
60		4.1	5.0		0.07	0.10		97	119		0.00	0.00		0.00	0.00
70	5.4	4.4	5.4	0.07	0.04	0.16	130	105	129	0.01	0.00	0.00	0.00	0.00	0.00
80		4.7	5.8		0.08	0.23		113	138		0.00	0.01		0.00	0.00
90	6.2	5.0	6.3	0.28	0.17	0.57	148	118	150	0.04	0.00	0.06	0.01	0.00	0.00
100		5.5	6.9		0.16	0.84		132	165		0.00	0.10		0.00	0.01
110		6.0	7.6		0.23	0.78		144	180		0.04	0.08		0.00	0.00
120	8.6	6.7	8.6	0.16	0.29	1.00	205	161	205	0.03	0.07	0.11	0.01	0.01	0.01
IDLE		0.19	[g/s]		0.63	[mg/s]		0.61	[g/s]		0.03	[mg/s]		0.00	[mg/s]
IDLE-D		0.23	[g/s]		0.10	[mg/s]		0.73	[g/s]		0.20	[mg/s]		0.00	[mg/s]

Table 8.5: Results of the fuel economy and emission tests

Part III
Closure

Chapter 9

Conclusions and Outlook

In this chapter the conclusions based on the results of the research covered in this thesis are drawn. Moreover, an outlook for future research is conveyed. The chapter is organized as follows. In Section 9.1 a brief overview of this research is given. Then, in Section 9.2, the overall conclusions with respect to the EcoDrive project target and the outcome of part I are given. In Section 9.3, the conclusions with respect to part II are presented. Finally, in Section 9.4 an outlook to future research topics is presented.

9.1 Overview

A novel automotive transmission concept, designated the *Zero Inertia (ZI)* powertrain, has been proposed. This powertrain combines a Continuously Variable Transmission (CVT), a low-speed flywheel and a planetary gear stage, enabling a substantial reduction of fuel consumption while maintaining a high level of *driveability*, *i.e.*, longitudinal vehicle response and comfort. The latter is due to the flywheel which acts as a power-dense mechanical power assist source. Augmenting the ZI concept with two clutches created the *ZI Stop-Go* powertrain which enables shutdown of the engine during vehicle standstill, and hence save an additional amount of fuel. The challenge in that was to guarantee a simultaneous restart of vehicle and engine without a noticeable delay. To show the potential of the ZI and ZI Stop-Go concepts as means to save fuel, an overview of fuel saving principles and associated (development, costs, packaging, etc) has been presented in part I. The fuel savings on the NEDC driving cycle were predicted to amount up to 21% for ZI Stop-Go. Furthermore it was argued that a purely mechanical power assist system to facilitate both E-line tracking and Stop-Go yields a promising fuel saving potential especially when regarding the modest research efforts that have to be undertaken for it. Considering the outcome of the fuel economy experiments undertaken, conclusions with respect to the project goals are listed in Section 9.2.

One of the research efforts is the development of a coordinated powertrain control system both in software as in hardware. The control system and ZI powertrain are implemented in a test vehicle. Experiments have been undertaken to demonstrate the fuel economy and driveability improvements. This was covered in Chapter 8. In Chapter 6 and 7 respectively, modeling and control of the CVT and ZI powertrains were the main topics. The conclusions especially with respect to these two chapters, but also parts of Chapter 8 are listed in Section 9.3.

9.2 EcoDrive

The target of the EcoDrive ZI project was set at saving 25% fuel consumption on the NEDC driving cycle, with respect to a 4-speed automatic transmission (4AT) vehicle, and without loss of driveability. As predicted in Part I, achieving this target was deemed nearly possible, *i.e.*, a fuel saving of 21% was projected. The actually obtained fuel savings on the NEDC using only ZI are estimated at 10.0% with respect to 4AT. Stop-Go is estimated to add another 8%, thus

ZI + Stop-Go is estimated to save 18% of fuel on the NEDC cycle with respect to a 4-speed automatic transmission powertrain.

This value is actually quite close to the theoretically predicted fuel saving of 21%, but obviously even more below the project target. In the overview of fuel saving principles of Chapter 3, other methods were shown to have more fuel saving potential, but also be far more complex. It is therefore believed that the chosen solution offers a fair trade-off between achieving the initially set targets and actually realizing the ZI and ZI Stop-Go powertrains, respectively in a test vehicle and on a testrig, within a timeframe of less than four years.

The driveability of the ZI powertrain appeared to be superior with respect to that of a CVT and 4AT powertrain. The response to pedal deflections inflicted by the driver in terms of wheel torque appeared to have a nearly a slight hesitation (< 0.2 [sec]) and it persistently increased to a maximum in case of pedal tip-in and with the same persistence to a minimum for pedal back-out. Apart from an occasional highly damped drive shaft oscillation this occurs without sag, stumble, shuffle or stretchiness, see Section 7.2.2. For the CVT powertrain this favourable behaviour was not seen and especially for ‘pedal-jogging’ rather unpredictable torque responses often hampered by moderately damped drive shaft oscillations were observed. In effect, the

jet start behaviour—often penalizing the driveability of CVT powertrains—is shown to be solved by the ZI principle.

Apart from the research outcome described in this thesis, the EcoDrive project yielded an extensive amount of knowledge on mechanical and hydraulic properties of the CVT. This knowledge is applied instrumentally in proposing new insights in modeling of power losses in the CVT. Furthermore, alternative hydraulic actuation is suggested leading to increased performance and robustness of the CVT. These aspects are covered in [Vroemen, 2001], where also control development for and experimental testing of the hydraulically actuated CVT is shown. Furthermore, the development, modeling and testing of the Stop-Go extension upon ZI is illustrated there.

In [van Druten, 2001] insights regarding the use and specification of flywheel energy exchange systems in passenger cars, an intuitive design tool for analyzing power-split transmissions, and obviously the realization of two transmissions used to prove the concepts are the main topics.

The generation of this knowledge, naturally raises proposals for new research assignments. A non-exhaustive list of these proposals is presented in the last section of this thesis. First, detailed conclusions regarding Chapter 6, 7 and 8 are drawn in the next section.

9.3 Coordinated powertrain control

The covered topics concerning the powertrain modeling, control and testing are briefly discussed and conclusions are given along. Here and there also suggestions for future research are given. The most important directions in this respect are given in Section 9.4 though. The conclusions regarding modeling and control of the ZI powertrain in this thesis are:

- powertrain modeling on various levels of complexity suited for the specific purpose is suggested. Descriptions of the operation and modeling of the relevant components in the powertrain are shown. These components together compile a model termed ‘dissipative compliance powertrain model’, see Figure 6.15. This model describes engine dynamics, torque converter dynamics, torque losses, CVT dynamics and kinematics, flywheel unit kinematics and dynamics, drive shaft flexibility, tire-road slip, rolling resistance and the longitudinal vehicle dynamics including hill climbing/descending. Furthermore, the continuity of the model is alternated by discrete events;
- a practical cross-section of all possible continuous model modes is made and the non-linear compliance model is linearized for a large amount of stationary states within the operation envelope. With this linearized model, two torsional eigenmodes are identified, one of them related to longitudinal vehicle comfort. This eigenmode is also identified in the experiments. The differences between the longitudinal comfort level of the CVT and ZI powertrain are stipulated. The conclusion is that the flywheel is instrumental in applying additional damping to the first eigenmode (drive shaft resonance). The obtained level of comfort is theoretically somewhat disappointing since, human drivers are more sensitive to lower frequencies (but not too low) which appeared for the ZI powertrain. In practice however, this appeared to yield diverging opinions by the drivers, clearly showing that comfort levels are largely subjective. These opinions are not validated stochastically or what so ever, and is left for future research;
- a second model level described the exchange of kinetic energy between the several inertias within the powertrain. This approach was shown to be instrumental in deciding what optimal design parameters for the flywheel unit can be used. The results coincide with those found in [van Druten, 2001], who used an alternative approach, although also related to kinetic energy;
- the third model level is in fact the model used for powertrain control synthesis. It describes the most pregnant non-linear phenomena seen in the powertrains. The most important observation is that non-linearities are introduced because a time dependent coordinate transformation (by the continuously variable CVT ratio $r_{cvt}(t)$) is applied to inertias. These nonlinearities get more ‘severe’ though in a beneficial way in the case of the ZI powertrain. The reason for that is found to lie in the location of the single zero of the linearized transfer function from CVT ratio shift speed to wheel speed. For the CVT powertrain this zero is positive real for the entire ratio coverage, whereas this zero is negative real for about half of the ratio coverage. A negative zero shows minimal phase behaviour which is a favourable property for the majority of dynamic systems seen in practice. The appreciable negative zero applies between overdrive and around medium being exactly the problem area for basic CVT powertrains in practice;
- the non-linear model addressed in the previous bullet is used as a control model. In the case of the CVT powertrain observations made with the model are used to synthesize an appropriate shifting law for the CVT as well as trajectory generation for the engine torque. The non-linear model of the ZI powertrain could be used almost literally to write down a shifting law for the CVT ratio. In regions where the beneficial features of

the flywheel unit are reduced to zero and less, an approximation of the control model appeared to be practically sufficient for obtaining satisfactory driveability results. The approximation implied that the structure of the controller could be maintained, which yields apparent implementation and tuning benefits. Nevertheless, a search for alternative approximations or perhaps a complete novel approach might improve the closed loop performance even more;

- an experimental setup is designed and built in a test vehicle. It comprises the original 1.6 l petrol engine, a CVT transmission augmented by the ZI extension, *i.e.*, the flywheel unit (see [van Druten, 2001]), sensors, actuators, signal conditioning, driver stages and a flexible software development platform. The test vehicle appeared to provide a flexible and robust platform for the assessment of driveability and fuel economy;
- special attention is given to a component controller for the electronic air throttle. This throttle chokes the air flow to the engine cylinders. The throttle opening serves as a setpoint for the fuel injection system. The latter is not altered in this thesis, since it is already implemented (as an off-the-shelf device) by the vehicle manufacturer. The controller forms a high bandwidth (10 Hz) closed loop system with the electronic throttle. Accuracy is slightly penalized because integral control was thought to impair the closed loop bandwidth too much. It is interesting to investigate the sensitivity of this in terms of wheel torque response and fuel economy. The author has the opinion that at least for the wheel torque sensitivity the impact is rather low in practice as the driver would compensate for possible offsets. Also for fuel economy it is thought that the impact is low since there is a relatively large area around the fuel optimal operating points for which fuel economy remains within 1% deviation from the fuel optimal operating points, see Figure 7.3;
- the experiments covered a number of aspects, such as closing of clutches, model validation, driveability and fuel economy tests;
- to facilitate the ease of tuning and the graduality with which (human) driver-in-the-loop experiments are conducted a simpler control strategy for the CVT ratio shift speed is proposed. This controller was validated in other publications of the author through simulation and test rig experiments and showed the ability to unveil the beneficial properties of the ZI powertrain upon those of basic CVT powertrains. Furthermore it is able to control optimal fuel economy with global asymptotic stability. The controller was also used for the CVT, consequently not fully exploiting the feasibility of the CVT shown in Chapter 7. Tuning of the controller can be performed with one variable only. The tuning has given rather low attention all the more since a very brief iteration already gave satisfactory results in practice. Sustained research has to be undertaken to investigate the closed loop performance when applying the controllers presented in Chapter 7;
- driveability was investigated through three types of experiments: semi-kick down, pedal jogging and a full kick-down. These experiments showed that driveability improved tremendously in all situations. Torque responses for both pedal tip-in and back-out of the ZI powertrain are prompt, persistent and apart from an occasional drive shaft oscillation rather smooth. Contrary to those seen for the CVT powertrain, the ZI powertrain in practice is able to fulfill the driveability objective defined in Section 7.2.2. Even in the case of performance demands, *i.e.*, a full pedal kick-down, the ZI powertrain appears to be able to comply with the driveability objective;
- through a combination of measurements and simulations the ZI powertrain is estimated to show a fuel consumption benefit with respect to the 4AT of 10% on the NEDC cycle. The extension with Stop-Go is projected to gain an additional 8% of fuel saving, arriving

at 18% fuel saving on the NEDC. This is 7% below the project target which is quite a lot. Apparently other fuel saving techniques should be adopted to gain the projected fuel saving, *viz.* Chapter 3. On the other hand, 18% fuel economy improvement by itself is judged as a respectable result;

- the emissions CO, NO_x and HC are penalized substantially when driving along the OOL (E-line).

9.4 Outlook

In this section directions and recommendations for future research are given. The section is divided in two paragraphs. Section 9.4.1 presents research directions regarding coordinated powertrain control whereas Section 9.4.2 gives those resulting from this thesis, [van Druten, 2001] and [Vroemen, 2001] jointly.

9.4.1 Powertrain modeling and control

In this thesis an outline of the problems concerning coordinated control of CVT powertrains is given. The main difficulty appeared to be the fact that a CVT powertrain can realize a high fuel economy and driveability, but hardly at the same time. In the case of the ZI powertrain this contrast can largely be countervailed by the modified dynamic properties imposed by the flywheel unit. In Chapter 7 it was shown that through carefully choosing the engine and CVT setpoints (control laws (7.33) and (7.32) respectively) during transients in engine power the contrast between driveability and fuel economy can also be neutralized for a plain CVT powertrain, though only up to a limited extent. Adopting this control strategy, the wheel torque increase will always be slower than seen in the ZI powertrain, basically due to the imposed physical limitations of the CVT powertrain. In the experiments discussed in Chapter 8, these differences could not be examined to a full extent as the plain CVT powertrain control strategy was not implemented. There, a simplified powertrain control strategy tailored for the ZI powertrain was used for both the CVT and ZI powertrains. This control strategy (given by equations (8.10) and (8.14)) did not even exploit the potentials of the ZI powertrain to a full extent, even though satisfactory results were obtained with it in practice. By using the *same* control strategy for both the CVT and ZI powertrain, primarily the *physical* differences of both powertrains could be investigated. Although this was done qualitatively only, the differences are considered to be convincing enough. This conclusion is confirmed by the subjective assessment of the driveability by a number of test drivers. Future research could focus on finding more quantitative models for the assessment of the driveability. Therefore, also models of drivers need to be developed focusing on their behaviour in traffic situations. This is not straightforward, as drivers appear to be quite whimsical when exposed to real traffic situations. The interaction between the driveability features of a particular powertrain and the dynamic behaviour of the driver may be quite complex. The current research did not focus on this interaction, also known as *driver in the loop*. In order to make the follow-up research regarding driver-in-the-loop as transparent as possible, the performance of the powertrains should be as optimal as possible. Thereto the implementation and tuning of the control strategies proposed in Chapter 7 could be adopted. Nonetheless, it is interesting also to research and implement alternative control strategies.

Concerning powertrain modeling and control more directions for improvements and extensions can be thought of. The powertrain model schematically depicted in Figure 6.15 has

been validated only on a few aspects, that is the eigenfrequency in various points of operation, fuel consumption and the wheel torque response during full kick-down launching. On the other hand, the black box model of the hydraulically controlled CVT variator was based on actual measurements. Even so, a model of the electronic throttle was based on estimated parameters and experiments. The torque response of the test vehicle's engine upon changes in the throttle opening in every operating condition should still be validated. A more thorough investigation of the interaction between engine and powertrain dynamics—in fact determining the vehicle's level of comfort—form an open field for further research. Investigating these aspects could result in proposals for active control of vehicle *comfort* using the electronic air throttle, see [Mo *et al.*, 1996], [Karlsson and Jacobsson, 2000].

Furthermore using the throttle, traction control to prevent wheel skid on slippery surfaces is suggested an interesting field of research. Both areas implicate some sort of refined control of the torque in the drive shafts. Since torque measurements within the powertrain are generally expensive and uncommon in automotive engineering, the suggested extensions of controlling the drive shaft torque should utilize a more dedicated powertrain model. The powertrain model in Figure 6.15 may serve as a useful starting point for that matter.

Also related to comfort are the engagement of the drive and lockup clutch. In the field experiments it was observed that closing of the drive clutch still appears with some uncomfortable torque jerks. In some cases this is also true for the engagement of the torque converter lockup clutch. In conjunction with the extended research necessary on the ZI Stop-Go powertrain (see below) improvements for more gradual control of these clutches can be undertaken.

9.4.2 Powertrain design

In Chapter 1, the EcoDrive project organization was outlined, see Figure 1.1. EcoDrive existed in two parts, the results of which can in principle be combined to some extent. The part of EcoDrive not described in this thesis, termed EcoDrive SI, resulted in a number of modifications and controls aiming at improvement of the (CVT) transmission and engine efficiency, [Veenhuizen and van Spijk, 2000]. The most important improvement in fuel economy was due to the integration of a so-called *torque fuse* in the CVT. This torque fuse allows a very small slip speed in the (secondarily positioned) drive clutch and as such safeguards the pushbelt of the CVT during torque shocks. Hence, the pulley clamping force can be substantially reduced and thus improving the CVT efficiency in part load especially. Given the layout of the ZI Stop-Go transmission, see Figure 4.6, the 'secondary pulley clutch' can be utilized as a torque fuse. Furthermore, in EcoDrive SI a CVT having a much larger ratio coverage (RC) is designed. The CVT in this thesis embodied a RC of 5.2, whereas the one in EcoDrive SI constitutes a RC of 6.5. Adopting such a large RC within the ZI configuration can reduce the engine speed even more, leading to apparent fuel economy benefits. Altogether, integrating these transmission modifications in the ZI design can be expected to improve the fuel economy by about 5%.

The ZI Stop-Go requires further control implementation and testing in order to validate its functionality and performance on the testrig. From this point on ZI Stop-Go can be implemented in a test vehicle to demonstrate the driveability and fuel economy. Therefore, extensive modifications to the engine management must be undertaken in order to automate fuel injection, and ignition without increasing the amount of emissions (especially HC and CO). The emission control for normal ZI operation should be optimized for the specific use (E-line tracking).

Further improvement of the overall control and powertrain performance might involve a reconsideration of the CVT and engine setpoints more tailored to their specific dynamics. In fact, coordinated and component control respectively described in this thesis and [Vroemen,

2001], become more intertwined then.

Finally, a number of research topics are proposed, involving more rigorous adaptations to the current ZI and ZI Stop-Go powertrains. The increasing popularity of the diesel engine in Europe, combined with its appreciable fuel economy, argues for investigating the combination of this engine with the ZI (and ZI Stop-Go) concept. Because the diesel engine has different torque and speed characteristics than the petrol engine, this would involve a modification of transmission parameters. The torque converter in the ZI transmission is primarily installed to facilitate vehicle launch. In ZI Stop-Go the torque converter might be omitted when the fly-wheel can be shown to enable an acceptable vehicle launch. Probably the most rigorous future research topic is to conceive and develop a mechanical full hybrid powertrain. From Chapter 3, it was concluded that such a hybrid powertrain has a large fuel saving potential combined with relatively low manufacturing costs, even though research efforts are challenging. In fact, a few solutions in this direction were already developed, see [Kok, 1999] and [Dietrich *et al.*, 1999]. Searching for a combination of such concepts and the ZI functionality such that fuel economy and driveability are maximized at minimal weight, volume, costs and complexity seems well worth the effort.

Bibliography

- Adcock, I. "Stop-go systems get the green light". *European Automotive Design*, pp. 24–26, 1998.
- Allen, R. R. "Multiport representations of inertia properties of kinematic mechanisms". *Journal of the Franklin Institute*, vol. 308, no. 3, 1979.
- An, F. and Ross, M. "Model of fuel economy with applications to driving cycles and traffic management". *Transportation Research Record*, no. 1416, pp. 105–114, 1993.
- Baumann, B., Rizzoni, G., and Washington, G. "Intelligent control of the Ohio State University hybrid-electric vehicle". In: Proc. of the 2nd IFAC Workshop on Advances in Automotive Control, pp. 123–128. Mohican State Park (OH), 1998.
- Becker, H. J. "Mechanik des Van-Doorne-Schubgliederbandes". *Antriebstechnik*, vol. 26, no. 8, pp. 47–52, 1987.
- Bergman, W. "Measurement and subjective evaluation of vehicle handling". *SAE Technical Paper Series*, no. 730492, 1973.
- Brace, C. J., Vaughan, N. D., Burrows, C. R., and Deacon, M. "Integrated control strategies for a direct-injection diesel engine and CVT". In: Proc. EAEC European Automotive Congress, pp. 249–260. Barcelona, Spain, 1999.
- Bürger, K. G., Gröter, H. P., Lutz, H. J., Meyer, F., and Schleuter, W. "Alternators in automotive applications—state of the art and development trends (translation from German text)". In: Proc. Symposium Nebenaggregate im Fahrzeug. Haus der Technik Essen, 1994.
- CEC. "CEC Cold weather driveability test procedure". Coordinating European Council, 1983.
- Chan, C., Yang, D., Volz, T., Breitweiser, D., Jamzadeh, F. S., and Frank, A. "System design and control considerations of automotive continuously variable transmissions". *SAE Technical Paper Series*, no. 840048, 1984.
- Cho, D. and Hedrick, J. K. "Automotive powertrain modeling for control". *Trans. of ASME, Journal of Dynamics Systems, Measurement, and Control*, vol. 111, pp. 568–576, 1989.
- Chockalingam, F. and Singh, S. N. "Dorsal fin control of a non-minimum phase undersea vehicle under surface waves". In: Proc. American Control Conference, pp. 482–486. Chicago, IL, 2000.

Bibliography

- Deacon, M. and Brace, C. J. "Impact of alternative controller strategies on emissions from diesel CVT powertrain—preliminary results". In: Proc. IMechE Conf. on Appl. of Powertrain and Fuel Techn. to meet Emission Standards. London, 1996.
- Delsey, J. "How to reduce the fuel consumption of a road vehicle". In: Proc. OECD/IEA Informal Expert Panel on Low Consumption Low Emission Automobile. Rome, 1991.
- Dietrich, P., Eberle, M. K., and Hörler, H. U. "Results of the ETH-hybrid III-vehicle project and outlook". *SAE Technical Paper Series*, no. 1999-01-0920, 1999.
- Dietrich, Th. "Ultracapacitors—power for innovative automotive applications (in German)". *VDI Berichte*, vol. 1565, pp. 731–735, 2000.
- DOE and EPA. "Energy technology and fuel economy". <http://www.fueleconomy.gov/feg/atv.shtml>, U. S. Department of Energy, U. S. Environmental Protection Agency, 2001.
- Dorey, R. E., Maclay, D., Shenton, A. T., and Shafiei, Z. "Advanced powertrain control strategies". In: Proc. 1st IFAC workshop on Advances in Automotive Control. Ascona, Switzerland, 1995.
- Dorisen, H. T. and Höver, N. "Antriebschlupfregelung (ASR)—ein Beitrag zur aktiven fahrsicherheit". *Automobiltechnische Zeitschrift (ATZ)*, vol. 95-4, pp. 194–201, 1995.
- DoT. "Transport statistics Great Britain 1994". Department of Transport, HMSO, London, 1994.
- van Druten, R. M. "Transmission design of the zero inertia powertrain". Ph.D. thesis, Technische Universiteit Eindhoven, 2001.
- van Druten, R. M. and Kok, D. B. "Design optimization of a compact flywheel system for passenger cars". *VDI Berichte*, vol. 1459, 1998.
- van Druten, R. M., Mussaeus, M. A., Vroemen, B. G., Serrarens, A. F. A., and Veenhuizen, P. A. "Transmission system, especially for a motor vehicle (patent WO9956039A2)". World Intellectual Property Organization, 2000a.
- van Druten, R. M., Mussaeus, M. A., Vroemen, B. G., Serrarens, A. F. A., and Veenhuizen, P. A. "Vehicle drive assembly (patent WO995549A1)". World Intellectual Property Organization, 2000b.
- van Druten, R. M., Serrarens, A. F. A., Vroemen, B. G., van den Tillaart, E., and de Haas, J. "Mild hybrids with CVT: comparison of electrical and mechanical torque assist". *VDI Berichte*, vol. 1610, pp. 331–345, 2001.
- van Druten, R. M., van Tilborg, P. G., Rosielle, P. C. J. N., and Schouten, M. J. W. "Design and construction aspects of a zero inertia CVT for passenger cars". In: Proc. FISITA World Automotive Congress (CD-ROM), CDROM A058. Seoul, Korea, 2000c.
- Evans, L. "Driver behavior effects on fuel consumption in urban driving". *Human Factors*, vol. 21, no. 4, pp. 389–398, 1979.
- Everett, R. L. "Measuring vehicle driveability". *SAE Technical Paper Series*, no. 710137, 1971.

- Fukuba, H. and Morita, S. "Optimization control of the fuel consumption ratio for an engine-CVT-load system using decoupling control theory". *JSME International Journal, Series II*, vol. 35, no. 3, pp. 442–447, 1992.
- Graham, J. P., Leard, A. T., and Valade, C. T. "Coordinating research council high and intermediate temperature driveability program". *SAE Technical Paper Series*, no. 881671, 1988.
- Greve, P. and Liesner, W. P. "Der neue VW Golf Ecomatic". *Automobiltechnische Zeitschrift (ATZ)*, vol. 95, no. 9, pp. 438–446, 1993.
- Guo, Z. Y., Yang, X. C., Yang, D., and Frank, A. A. "On obtaining the best fuel economy and performance for vehicles with engine-CVT transmissions". *SAE Technical Paper Series*, no. 881735, 1988.
- Guzzella, L. and Schmid, A. "Control of SI-Engines with CVTs—a feedback linearization approach". In: Proc. of the Third IEEE Conference on Control Applications, vol. 1, pp. 633–638. 1994.
- Guzzella, L. and Schmid, A. M. "Feedback linearization of spark-ignition engines with continuously variable transmissions". *IEEE Transactions on Control Systems Technology*, vol. 3, no. 1, pp. 54–60, 1995.
- Ha, I-J., Tugcu, A. K., and Boustany, N. M. "Feedback linearizing control of vehicle longitudinal acceleration". *IEEE Transactions on Automatic Control*, vol. 34, no. 7, pp. 689–698, 1989.
- Harms, K. "Perspectives in automotive control". In: Proc. 3rd IFAC workshop Advances in Automotive Control, pp. 1–12. Karlsruhe, Germany, 2001.
- Hauser, J., Sastry, S., and Kokotovic, P. "Nonlinear control via approximate input-output linearization: the ball and beam example". *IEEE Transactions on Automatic Control*, vol. 37, no. 3, pp. 392–398, 1992.
- Healey, J. R. "VW Lupo: rough road to fuel economy". *USA Today*, 1999.
- Heavenrich, R. M., Murrell, J. D., and Hellman, K. H. "Light-duty automotive technology and fuel economy trends through 1991". Tech. Rep. EPA/AA/CTAB/91-02, Control Technology and Applications Branch, Ann Arbor, MI: U. S. Environmental Protection Agency, 1991.
- Heemels, W. P. M. H. "Linear Complementarity Systems: A Study in Hybrid Dynamics". Ph.D. thesis, Technische Universiteit Eindhoven, 1999.
- Hendricks, E. and Sorensen, S. C. "Mean value modelling of spark ignition engines". *SAE Transactions*, vol. 99-3, no. 900616, 1990.
- Hirschlieb, G. C., Schiller, G., and Stottler, S. "Engine control". In: Ronald K. Jurgen (editor), *Automotive Electronics Handbook*, chap. 12. McGraw-Hill, 1999.
- Hitzert, R. "The modular electromotive system—modelling and control (in Dutch)". Tech. Rep. DCT 2001.29, Technische Universiteit Eindhoven, 2001.
- Hochgraf, C. G., Ryan, M. J., and Wiegmann, H. L. "Engine control strategy for a series hybrid electric vehicle incorporating load-leveling and computer energy management". *SAE Technical Paper Series*, no. 960230, 1996.

- Hofmann, L., Petersen, R., Adamis, P., and Brunner, H. "Optimierungspotential von CVT-getrieben für sparkonzepte verbrauchseinsparung kontra fahrspass-ein lösbarer konflikt?" *VDI Berichte*, vol. 1418, pp. 549–567, 1998.
- Höhn, B.-R. "Konzepte weit gespreitzter stufenloser getriebe". *Konstruktion*, vol. 46, pp. 359–364, 1994.
- Höhn, B.-R. "Alternative getriebesysteme". *VDI Berichte*, vol. 1610, 2001.
- Ironside, J. M. and Stubbs, P. W. R. "Continuously variable transmission control". *IEEE Vehicular Technology Society*, 1980.
- ISO. "International standard ISO 2631-1: mechanical vibration and shock—evaluation of human exposure to whole-body vibrations—Part I: general requirements". International Organisation for Standardisation, 1997.
- Jacobson, B. "Gear shifting with retained power transfer". Ph.D. thesis, Chalmers University of Technology Göteborg, Sweden, 1993.
- James, I. B. and Vaughan, N. D. "Design and component matching of a pressure control circuit". *SAE Technical Paper Series*, no. 96854, 1996.
- Jamzadeh, F. S. and Frank, A. A. "Optimal control for maximum mileage of a flywheel energy-storage vehicle". *SAE Technical Paper Series*, no. 820747, 1982.
- Jo, H. S., Park, Y. I., Lee, J. M., Lee, H. D., and Sul, S. K. "A development of an advanced shift control algorithm for a hybrid vehicle with automated manual transmission". *Heavy Vehicle Systems*, vol. 7, no. 4, pp. 281–298, 2000.
- Junio, M., Roesgen, A., and Corvasce, F. "Rolling resistance of tires". *VDI Berichte*, vol. 1505, pp. 255–298, 1999.
- Karlsson, J. and Fredriksson, J. "Cylinder-by-cylinder engine models vs mean value engine models for use in powertrain control applications". *SAE Technical Paper Series*, no. 1999-01-0906, 1999.
- Karlsson, J. and Jacobsson, B. "Optimal control of an automotive powertrain system for increased driveability". In: Proc. 5th Int. Symposium Advanced Vehicle Control, pp. 335–342. Ann Arbor, MI, USA, 2000.
- Karnopp, D. "Computer simulation of stick-slip friction in mechanical dynamic systems". *Trans. of ASME, Journal of Dynamics Systems, Measurement, and Control*, vol. 107, pp. 100–103, 1985.
- Kim, T. and Kim, H. "Development of a stepping motor drive CVT ratio control system and engine-CVT consolidated control". In: Proc. Int. Congress on Continuously Variable Power Transmission CVT'99, pp. 218–224. Eindhoven, The Netherlands, 1999.
- Kluger, M. A. and Long, D. M. "An overview of current automatic, manual and continuously variable transmission efficiencies and their projected future improvements". *SAE Technical Paper Series*, no. 1999-01-1259, 1999.
- Kok, D. B. "Design optimisation of a flywheel hybrid vehicle". Ph.D. thesis, Technische Universiteit Eindhoven, 1999.

- Kolmanovsky, I., Sun, J., and Wang, L. "Coordinated control of lean burn gasoline engines with continuously variable transmissions". In: Proc. of the American Control Conference, pp. 2673–2677. San Diego, CA, 1999.
- Lechner, G. and Naunheimer, H. "Automotive transmissions". Springer-Verlag, 1999.
- Lehna, M. "Audi Duo, ein hybridfahrzeug für die city-logistik". *VDI Berichte*, vol. 1378, pp. 119–128, 1998.
- List, O. H., , and Schoeggel, P. "Objective evaluation of vehicle driveability". *SAE Technical Paper Series*, no. 980204, 1998.
- Liu, S. and Paden, B. "A Survey of today's CVT controls". In: Proc. 36th IEEE Conf. Decision & Control, pp. 4738–4743. San Diego, CA, USA, 1997.
- Liu, S., Stefanopoulou, A. G., and Paden, B. E. "Effects of control structure on performance for an automotive powertrain with a continuously variable transmission". In: Proc. 5th Int. Symposium Advanced Vehicle Control, pp. 461–468. Ann Arbor, MI, USA, 2000.
- Machida, H. "Traction drive CVT up to date". In: Proc. Int. Congress on Continuously Variable Power Transmission, CVT'99, pp. 71–769. Eindhoven, The Netherlands, 1999.
- Matsuo, I., Nakazawa, S., Maeda, H., and Inada, E. "Entwicklung eines hybridantriebsystems mit CVT". In: Proc. Aachener Kolloquium Fahrzeug- und Motorentechnik, VDI, pp. 1299–1312. Aachen, Germany, 1999.
- Mayer, T. and Schröder, D. "Operating modes and control aspects for a special hybrid drivetrain". In: Proc. 1st IFAC workshop on Advances in Automotive Control, pp. 127–132. Ascona, Switzerland, 1995.
- Mayer, T. and Schröder, D. "Robust control of a parallel hybrid drivetrain with a CVT". *SAE Technical Paper Series*, no. 960233, 1996.
- Mayer, T. and Schröder, D. "Nonlinear adaptive control of a CVT based parallel hybrid passenger car". In: Proc. 2nd IFAC Workshop Advances in Automotive Control, pp. 115–121. 1998.
- MITI. "Changes in fuel efficiency of Japanese passenger cars (10 mode fuel efficiency)". <http://www.eccj.or.jp/databook/1998e/p95.html>, source: Ministry of International Trade and Industry, Japan, 1996.
- Mitschke, M. "Dynamik der kraftfahrzeuge—band B: schwingungen". Springer, 1997.
- Mitschke, M. and Zhenfu, C. "Der fahrer als adaptiver regler". *FAT Schriftenreihe, Frankfurt am Main*, no. 91, 1991.
- Mo, C. Y., Beaumont, A. J., and Powell, N. N. "Active control of driveability". *SAE Technical Paper Series*, no. 960046, 1996.
- Müller, F. and Köhle, S. "Hybrid electric vehicles—discussion of different configurations". In: Proc. of the 2000 Global Powertrain Congress, pp. 54–63. Detroit (MI), 2000.
- Mussaëus, M. A. "Steering of a CVT based drive line for a passenger car". Master's thesis, Eindhoven University of Technology, 1998.

Bibliography

- Mussaëus, M. A., Serrarens, A. F. A., and Veldpaus, F. E. "CVT Ratio Optimization For Minimal System Losses in Passenger Cars". In: Proc. 2nd IFAC Workshop Advances in Automotive Control, pp. 129–134. Mohican State Park, OH, 1998.
- Mussaëus, M. A. and Veenhuizen, B. A. "personal communication". Van Doorne's Transmissie, 1998.
- Narumi, N., Suzuki, H., and Sakakiyama, R. "Trends of powertrain control". *SAE Technical Paper Series*, no. 901154, 1990.
- Ohyama, Y., Ohsuga, M., Nogi, T., and Minowa, T. "A totally integrated electronic control system for the engine and transmission". In: Proc. 8th International Conference on Automotive Electronics, pp. 39–42. IEE, London, England, 1991.
- Oppenheim, A. K., Maxson, J. A., and Shahed, S. M. "Can the maximization of fuel economy be compatible with the minimization of pollutant emissions". *SAE Technical Paper Series*, no. 940479, 1994.
- OTA. "Advanced automotive technology: visions of a super-efficient family car". Tech. Rep. OTA-ETI-638, Office of Technology Assessment (DOE), 1995.
- Paefgen, F.-J. and Lehna, M. "Der Audi Duo—das erste serienmässige hybridfahrzeug". *Automobiltechnische Zeitschrift (ATZ)*, vol. 99, pp. 316–320, 1997.
- Paganelli, G., Guerra, T. M., Delprat, S., Santin, J.-J., Delhom, M., and Combes, E. "Simulation and assessment of power control strategies for a parallel hybrid car". *Journal of Automotive Engineering*, vol. 214, no. D7, pp. 705–717, 2000.
- Park, J. H. and Kim, C. Y. "Wheel slip control in traction control system for vehicle stability". *Vehicle System Dynamics*, vol. 31, no. 1, pp. 263–278, 1999.
- Pesgens, M. F. M. "Driveability issues of the zero-inertia powertrain". Tech. Rep. DCT 2001.23, Faculteit Werktuigbouwkunde, Technische Universiteit Eindhoven, 2001.
- Pfiffner, R. "Steuerstrategien von CVT-getrieben: Übersicht und Ausblick". *VDI Berichte*, vol. 1467, pp. 313–331, 1999.
- Pfiffner, R. "Optimal operation of CVT-based powertrains". Ph.D. thesis, Swiss Federal Institute of Technology (ETH), Zürich, 2001.
- Polder, J. W. "A network theory for variable epicyclic gear trains". Ph.D. thesis, Eindhoven University of Technology, 1969.
- Rabeih, E. M. A. and Crolla, D. A. "Intelligent control of clutch judder and shunt phenomena in vehicle drivelines". *Int. J. of Vehicle Design*, vol. 17, no. 3, pp. 318–332, 1996.
- Reik, W. "Startergenerator im antriebsstrang". In: LuK Fachtagung: E-Maschine im Antriebsstrang, pp. 37–64. 1999.
- Riezenman, M. J. "Engineering the EV future". *IEEE Spectrum*, vol. 35, no. 11, pp. 18–20, 1998.
- van Rooij, J. and Schaerlaeckens, W. "Kräfte und wirkungsgrad beim schubgliederband—teil I: allgemeine kräftebetrachtungen, teil II: im band auftretende kräfte, teil III: leistungsverluste im schubgliederband und CVT-getriebe". *Antriebstechnik*, vol. 32, no. 8, pp. 55–86, 1993.

- Sackmann, M. and Krebs, V. "Nonlinear control of a continuously variable transmission using hyperstability theory". In: Proc. of the European Control Conference. Karlsruhe, Germany, 1999.
- Sakaguchi, S., Kimura, E., and Yamamoto, K. "Development of an engine-CVT integrated control system". *SAE Technical Paper Series*, no. 1999-01-0754, 1999.
- van der Schaft, A. J. and Schumacher, J. M. "An introduction to hybrid dynamical systems". In: *Lecture Notes in Control and Information Sciences*, vol. 251. Springer, London, 1999.
- Schlüter, F. and Wälterman, P. "Hierarchical control structures for hybrid vehicles – modelling, simulation, and optimization". In: Proc. 1st IFAC workshop on Advances in Automotive Control. Ascona, Switzerland, 1995.
- Schmid, A., Dietrich, P., Ginsburg, S., and Geering, H. P. "Controlling a CVT-equipped hybrid car". *SAE Technical Paper Series*, no. 950492, 1995.
- Schwab, M. "Electronically-controlled transmission systems—current position and future developments". *SAE Technical Paper Series*, no. 901158, 1990.
- Seiffert, U. and Walzer, P. "Automobiltechnik der zukunft". VDI Verlag, 1989.
- Serrarens, A., Vroemen, B., and Veldpaus, F. "A new CVT powertrain without jet start behaviour: analysis of design, dynamics and control". *Vehicle System Dynamics*, in press, 2001.
- Serrarens, A. F. A. "Driveability control of the ZI powertrain", pp. 19–30. *Integrated Powertrains and their Control*. IMechE, 2001.
- Serrarens, A. F. A. and Veldpaus, F. E. "A Management system for a flywheel hybrid driveline". In: Proc. of the 4th International Symposium on Advanced Vehicle Control, pp. 159–164. Nagoya, Japan, 1998.
- Serrarens, A. F. A. and Veldpaus, F. E. "New concepts for control of power transients in flywheel assisted drivelines with CVT". In: Proc. FISITA World Automotive Congress, CDROM A129. Seoul, Korea, 2000.
- Shafai, E. and Geering, H. P. "Control issues in a fuel-optimal hybrid car". In: Proc. IFAC 13th Triennial World Congress, pp. 231–236. 1996.
- Slotine, J.-J. and Li, W. "Applied nonlinear control". Prentice-Hall, 1991.
- Spijker, E. "Steering and control of a CVT based hybrid transmission for a passenger car". Ph.D. thesis, Technische Universiteit Eindhoven, 1994.
- Streib, H.-M. and Leonhard, R. "Hierarchical control strategy for powertrain functions". In: Proc. of 24th FISITA Congress, 925052, pp. 95–99. IMechE, London, England, 1992.
- Takiyama, T. and Morita, S. "Engine-CVT consolidated control using LQI control theory". *JSAE Review*, vol. 20, no. 2, pp. 251–258, 1999.
- Tenberge, P. "E-Automat: automatikgetriebe mit esprit". *VDI Berichte*, vol. 1610, pp. 455–479, 2001.

Bibliography

- Thoolen, F. J. M. "Development of an advanced high speed flywheel energy storage system". Ph.D. thesis, Technische Universiteit Eindhoven, 1993.
- van Tilborg, P. "Development of a concept electromechanical clamping system for a Van Doorne pushbelt variator". Master's thesis, Technische Universiteit Eindhoven, Eindhoven, The Netherlands, 2001.
- Vahabzadeh, H. and Linzell, S. M. "Modeling, simulation, and control implementation for a split-torque, geared neutral, infinitely variable transmission". *SAE Technical Paper Series*, no. 910409, 1991.
- Vanvuchelen, P. "Virtual engineering for design and control of continuously variable transmissions". Ph.D. thesis, Katholieke Universiteit Leuven, 1997.
- Vaughan, N. D., Guebeli, M., and Burrows, C. R. "Fuel economy benefits with effective powertrain control". In: Proc. Conf. Automotive Electronics, C481/023, pp. 1–13. IMechE, London, 1994.
- Veenhuizen, P. A. and van Spijk, G. "General background of the application of the CVT by example of the VDT EcoDrive transmission". In: Proc. CVT-Tagung 2000. Haus der Technik, Essen, 2000.
- van der Voort, M. C., Dougherty, M. S., and van Maarseveen, M. "A new generation fuel-efficiency support tool". *Transportation Research Part C*, vol. 9, no. 4, pp. 279–296, 2001.
- Vroemen, B. "Component control for the zero inertia powertrain". Ph.D. thesis, Technische Universiteit Eindhoven, 2001.
- Vroemen, B. G., Serrarens, A. F. A., and Veldpaus, Frans E. "CVT Control: A Hierarchical Approach". In: Proc. 5th Int. Symposium Advanced Vehicle Control, pp. 619–627. Ann Arbor, MI, USA, 2000.
- Vroemen, B. G. and Veldpaus, F. E. "Alternative concepts for hydraulic CVT control". In: Proc. of the 4th International Symposium on Advanced Vehicle Control, pp. 153–158. Nagoya, Japan, 1998.
- Wallentowitz, H. and Ludes, R. "System control application for hybrid vehicles". In: IEEE Conference on Control Applications, vol. 1, pp. 639–650. 1994.
- Wang, D. F., Olatunbosun, O. A., Zheng, L. Z., and Jia, J. Z. "Stability analysis for self-excited torsional oscillation of vehicle driveline". *Int. J. Vehicle Design*, vol. 24, no. 2/3, pp. 211–223, 2000.
- Waters, M. H. L and Laker, I. B. "Research on fuel conservation for cars". Tech. Rep. 921, Transport and Road Research Laboratory, Crownthorpe, England, 1980.
- Wright, K., Stasik, A., Sayce-Jones, R., Griffith, S., and Cross, R. "Advanced integrated driveline control". In: Proc. of 24th FISITA Congress, 925053. IMechE, London, England, 1992.
- Yamamoto, K. and Aoki, T. "Analysis of the influence on fuel economy by transmission type and the estimation of fuel economy". In: Proc. of FISITA'00, CDROM A148. 2000.
- Yasuoka, M., Ushida, M., Katakura, S., and Yoshino, T. "An integrated control algorithm for an SI engine and CVT". *SAE Technical Papers*, no. 1999-01-0752, 1999.

Zeyen, K.-P. and Pels, Th. "ISAD—A computer controlled integrated starter-alternator-damper-system". *SAE Technical Paper Series*, no. 972660, 1997.

Bibliography

Appendix A

Nomenclature, Acronyms, Symbols

A.1 Abbreviations, Acronyms

A/F	Air Fuel mixture
BSFC	Brake Specific Fuel Consumption
CVT	Continuously Variable Transmission
DBW	Drive By Wire
DNR	Drive Neutral Reverse gear set
ECU	Electronic Control Unit
E-	Economy-
IVS	Inertial Variable Shunt
MPI	Multi Point Injection
NVH	Noise Vibration Harshness
OOL	Optimal Operating Line
RC	Ratio Coverage
SA	Starter Alternator
SG	Stop-Go
SI	Spark Ignition
TC	Torque Converter
TSFC	Time Specific Fuel Consumption
WOT	Wide Open Throttle
ZI	Zero Inertia

A.2 Symbols

greek	description	unit
Γ	objective function	[-]
α	torque ratio	[-]
β	normalized brake pedal force	[N]
γ	dimensionless inertia	[-]
δ	drive pedal position	0..1
κ	tunable control gain	[-]
ϕ	air throttle angle	$0..\frac{\pi}{2}$
ω	angular speed	[rad/s]

roman	description	unit
A	area	[m ²]
E	energy content	[J]
F	force	[N]
J	inertia	[kgm ²]
P	power	[kW]
R	radius	[m]
T	torque	[Nm]
W	weigh factor	[-]
b	dissipative coefficient	varying
c	model parameter	varying
d	difference	varying
e	dimensionless energy	[-]
g	gravity acceleration	[m/s ²]
k	stiffness	[Nm/rad]
p	pressure	[bar]
r	speed ratio	[-]
t	time	[s]
u	input	varying
v	translational speed	[m/s]
w	noise, unknown inputs	varying
x	state	varying
y	output	varying
z	epicyclic gear ratio	[-]

A.3 Subscripts

1	equivalent primary (sided)
1,a	approximate equivalent primary (sided)

2	equivalent secondary (sided)
B	Boost
E-line	Economy Line
L	Launch
OL	Optimal (operating) Line
a	annulus
b	belt
c	carrier
cl	lockup clutch
cd	drive clutch
cvt	continuously variable transmission
d	drive shaft
,d	desired
dc	direct current
e	engine
f	flywheel
gn	geared neutral
i	impeller
j	row index
k	column index
ℓ	lockup
n	net
od	overdrive
p	primary (sided)
r	rolling (resistance)
s	secondary (sided)
t	turbine
tc	torque converter
ud	underdrive (low)
v	vehicle
w	wheel
zi	zero inertia

Appendix B

Inertial Variable Shunt: Kinematics and Dynamics

This appendix discusses the dynamic properties of the flywheel and planetary gear set, integrated into a unit also including the CVT. The kinematics of this unit shows analogies with the *variable shunt* circuit from electric network theory, see also [Polder, 1969]. Since the involved inertias significantly affect the dynamic properties of the contemplated unit it is also termed 'Inertial Variable Shunt' (IVS).

In this appendix, the kinematics and dynamics of the IVS are discussed. Definitions derived from this analysis are used throughout the thesis.

B.1 Layout and definitions

Figure B.1 shows the IVS from the underlying project. At the left side the primary pulley is connected with the engine (via the torque converter and DNR set). At the right side it is connected with the annulus gear wheel that decreases and reverses the speed of the annulus wheel with a factor r_a . The secondary pulley is connected downstream with the final reduction gear. At the other side this pulley is connected with the carrier gear decreasing and reversing the speed of the carrier by a factor r_c . Finally, the sun gear wheel placed in the center of the set is integrated with the flywheel shaft. Table B.1 explains all symbols indicated in Figure B.1.

B.2 Powersplit planetary gear set

The planetary gear set consists of a sun wheel, three planet wheels borne on a carrier frame, and an annulus wheel, see Figure B.2. These three members of the planetary gear set are respectively connected with the flywheel, the differential cage and the engine. In this section the kinematics and dynamics of the planetary gear set are derived.

In Figure B.2 the circumferential speed vectors v_a at the interface of the planet and the annulus, v_c at the axis of the planet wheels on the carrier, and v_f at the interface of the planet wheels and the sun are drawn. Moreover, the radius of the sun gear R_s and the radius of the annulus gear R_a are defined. Since the planet is assumed rigid these circumferential speeds

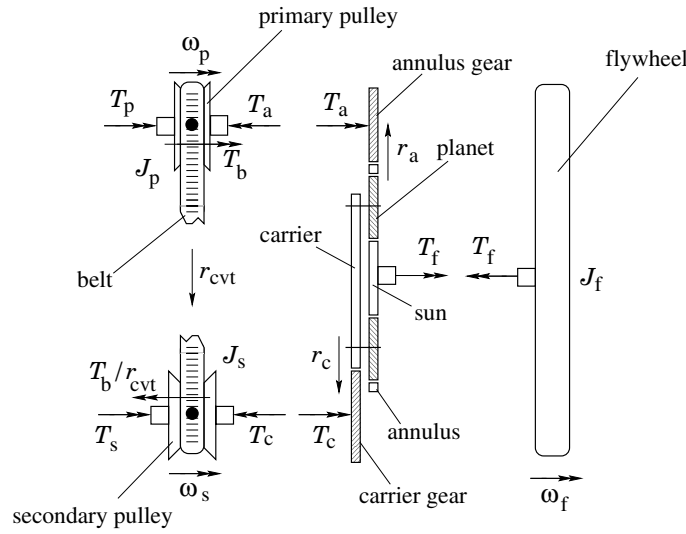


Figure B.1: Variable Shunt: topology, nomenclature and definitions

VARIABLE	DESCRIPTION	REMARK
T_a	torque at the annulus gear	reduced with $1/r_a$ from annulus
T_b	gross belt torque at primary pulley	multiplied by $1/r_{cvt}$ at sec. pulley
T_c	torque at the carrier gear	reduced with $1/r_c$ from carrier
T_f	flywheel torque	induced by flywheel acc./dec.
T_p	external drive/load torque at pri. pulley	
T_s	external load/drive torque at sec. pulley	
J_p	primary pulley inertia	including DNR, annulus and ann. gear
J_s	secondary pulley inertia	including carrier and carrier gear
J_f	flywheel inertia	including sun gear and shaft
r_{cvt}	CVT speed ratio	$r_{cvt} := \omega_s/\omega_p$
r_a	ratio of annulus gear speed over ann. speed	
r_c	ratio of carrier gear speed over car. speed	
z	ratio of annulus radius over sun radius	characteristic ratio for planetary sets
ω_a	annulus speed	$\omega_a = \omega_p/r_a$
ω_c	carrier speed	$\omega_c = \omega_s/r_c$
ω_f	flywheel speed	equals the sun speed
ω_p	primary pulley speed	
ω_s	secondary pulley speed	

Table B.1: Glossary of symbols used in the IVS model

relate linearly. The carrier speed v_c is the mean of the annulus speed v_a and sun speed v_f , *i.e.*,

$$v_c = \frac{1}{2}(v_f + v_a). \quad (\text{B.1})$$

Using the radii R_a and R_s this relation can be rewritten as:

$$\frac{\omega_c}{2}(R_s + R_a) = \frac{1}{2}(\omega_f R_s + \omega_a R_a). \quad (\text{B.2})$$

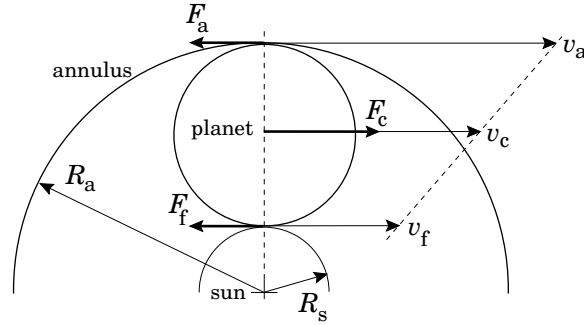


Figure B.2: Planetary gearset with forces, geometries and circumferential speed vectors

Rearranging (B.2) and using the definition of the characteristic planetary gear set number $z := \frac{R_a}{R_s}$ yields for the sun (=flywheel) speed:

$$\omega_f = (z + 1)\omega_c - z\omega_a. \quad (\text{B.3})$$

Finally, expressed in terms of primary and secondary pulley speed (B.3) becomes

$$\omega_f = \frac{z}{r_a}\omega_p - \frac{z+1}{r_c}\omega_s, \quad (\text{B.4})$$

or using the definitions

$$\alpha_p := \frac{z}{r_a}; \quad \alpha_s = \frac{z+1}{r_c}, \quad (\text{B.5})$$

the flywheel speed may also be written as

$$\omega_f = \alpha_p\omega_p - \alpha_s\omega_s. \quad (\text{B.6})$$

Assuming all planetary set members to be inertialess and the energy dissipation to be zero emerges the typical torque splitting functionality of the planetary gear set. In that case the law of power conservation can be used yielding:

$$T_a\omega_p + T_c\omega_s + T_f\omega_f = 0. \quad (\text{B.7})$$

For all ω_p and ω_s and ω_f according to (B.6) this results in

$$T_a = -\alpha_p T_f \quad (\text{B.8})$$

$$T_c = \alpha_s T_f \quad (\text{B.9})$$

From these equations the torque splitting functionality of the planetary gear set is apparant. The torque stemming from the flywheel acceleration $\dot{\omega}_f$, *i.e.*,

$$T_f = J_f \dot{\omega}_f, \quad (\text{B.10})$$

is split up (and amplified) into the torques at the annulus and the carrier. Using (B.10) equations (B.8) and (B.9) may also be written as:

$$T_a = -\alpha_p J_f \dot{\omega}_f; \quad (\text{B.11})$$

$$T_c = \alpha_s J_f \dot{\omega}_f. \quad (\text{B.12})$$

If one of the members is unloaded (no external torque), the two other torques within the planetary set will also become zero. Two speeds within the planetary set are already determined by the vehicle speed and the annulus speed, which is manipulated by the CVT. According to equation (B.4) the flywheel speed is also determined. The reaction torques necessary to restrain the speeds of the associated planetary set members is then provided by the CVT. The variator transmits a blind torque such that the reaction torques at the carrier and annulus are provided by the variable shunt internally. In [Vroemen, 2001], it is shown that the direction of the blind torque is profitable in terms of variator shifting dynamics.

Summarizing, the CVT is capable to manipulate the power balance (B.7) of the planetary gearset. This enables the possibility to let the flywheel torque T_f provide boost torque at the secondary pulley and absorb power whenever necessary. This is the subject of the next section.

B.3 Inertial variable shunt

Substitution of $\omega_s = r_{cvt}\omega_p$ in equation (B.6) yields

$$\omega_f = \left(\frac{\alpha_p}{r_{cvt}} - \alpha_s \right) \omega_s. \quad (\text{B.13})$$

Figure B.3, the speeds of the primary and secondary pulley and the flywheel are drawn as a function of the CVT ratio. For convenience the signals are normalized with the secondary

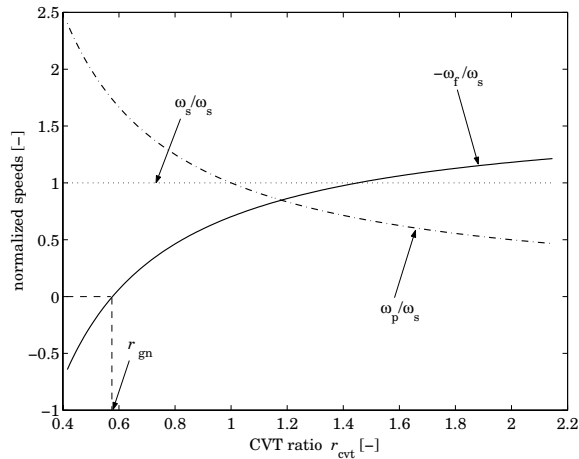


Figure B.3: Normalized speeds of the variable shunt

pulley speed. Note that the flywheel speed is actually negative for the larger part of the ratio coverage. Clearly, the kinematic design of the shunt including the reversing gears r_c and r_a make the flywheel rotate in the opposite direction of the primary and secondary pulley, at least from the maximum ratio r_{od} until the so called *gared neutral* ratio r_{gn} . This particular CVT ratio puts the flywheel to a complete standstill. From equation (B.13) it is readily seen

that this geared neutral CVT ratio equals

$$r_{\text{gn}} := \frac{\alpha_p}{\alpha_s}. \quad (\text{B.14})$$

Another interesting point is the opposite response of the primary speed and the flywheel speed to changes in the CVT ratio. For increasing ratio, the primary speed decreases whilst the (absolute) flywheel speed increases, and vice versa. In fact this mechanism constitutes the key idea of the Zero Inertia Powertrain. Obviously, for positive accelerations of the primary pulley with all its associated inertias, the flywheel inertia will decelerate, assuming that the secondary pulley speed does not change significantly. In practice, this assumption makes sense since the total inertia downstream from the secondary pulley (final drive, wheels and vehicle) is much larger than that of the primary sided components and the flywheel.

The mutually opposite acceleration of the primary and flywheel inertia enables a very favourable exchange of kinetic energy within the powertrain. For basic CVT powertrains (but also for any other conventional powertrain), this exchange of kinetic energy occurs between the vehicle and the primary inertias. At least for rapid changes of the primary speed to fastly increase the engine output power, the required increase of kinetic energy can only partly be delivered by the engine, and the temporary deficit of kinetic energy is withdrawn from the vehicle's kinetic energy. This results in a short term, but annoying deceleration of the vehicle. The mechanism within the variable shunt provides the opportunity to withdraw the short term energy deficit from the flywheel's kinetic energy.

To further understand the variable shunt mechanism more elaboration on the torques within the IVS is required. A torque balance at the secondary pulley learns

$$T_s - J_s \dot{\omega}_s = T_n - \frac{T_p - J_p \dot{\omega}_p}{r_{\text{cvt}}} \quad (\text{B.15})$$

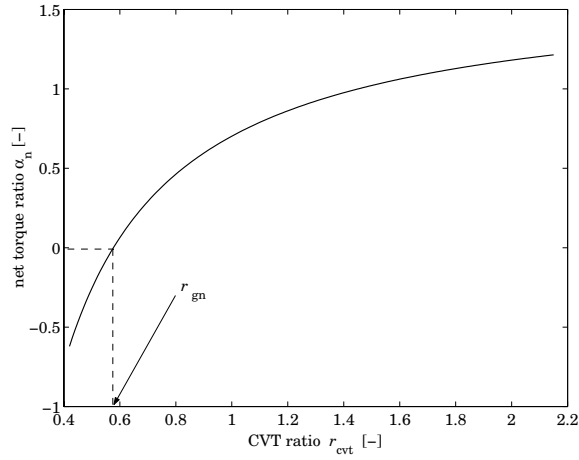
$$T_n = \frac{T_a}{r_{\text{cvt}}} + T_c = \alpha_s \left(1 - \frac{r_{\text{gn}}}{r_{\text{cvt}}} \right) J_f \dot{\omega}_f, \quad (\text{B.16})$$

where T_n can be interpreted as the net assist torque exerting at the secondary pulley. Whenever the flywheel is absent, thus $J_f = 0$, the torque balance is equal to that of a basic CVT powertrain. For convenience the net torque (B.16) is written as

$$T_n = r_n J_f \dot{\omega}_f \quad (\text{B.17})$$

$$\alpha_n = \alpha_s \left(1 - \frac{r_{\text{gn}}}{r_{\text{cvt}}} \right) \quad (\text{B.18})$$

The net torque ratio α_n is drawn in Figure B.4. In terms of torque dynamics the assisting mechanism of the IVS roughly works as follows. If a large acceleration of ω_p is desired, for instance to substantially and rapidly increase the engine power, the CVT ratio r_{cvt} is shifted quickly to a lower value. The primary torque then is amplified by a factor $1/r_{\text{cvt}}$, which is basically the purpose of the downshift. On the other hand T_p is lowered by the accelerating primary inertia, leaving less or even negative torque for the vehicle propulsion. Now, with the flywheel unit, the downshifting CVT emerges a deceleration of the flywheel, inducing a positive net IVS torque T_n . This 'boost torque' fills the torque gap otherwise present during the acceleration of the primary inertias. The opposite mechanism occurs whenever decreasing primary speeds are induced by an upshifting CVT. In that case the primary inertias boost the secondary pulley whereas the IVS torque T_n in turn subtracts secondary pulley torque.

Figure B.4: Net torque ratio α_n as a function of the CVT ratio

B.4 Equivalent inertias: IVS becomes a CVT again

As the flywheel speed can be expressed in terms of primary and secondary pulley speed according to equation (B.4), the torque balance at the secondary pulley (B.15) may also be expressed in terms of primary and secondary pulley kinetics. However, the resulting *equivalent primary and secondary inertias* turn out to be nonlinear functions of the CVT ratio. Quite remarkable, the primary equivalent inertia is *negative* for about half of the CVT ratio coverage. According to equation (B.4) the expression for the flywheel acceleration straightforwardly becomes:

$$\dot{\omega}_f = \alpha_p \dot{\omega}_p - \alpha_s \dot{\omega}_s \quad (\text{B.19})$$

Substituting this in equation (B.15) and reworking yields

$$T_s - J_2 \dot{\omega}_s = -\frac{T_p - J_1 \dot{\omega}_p}{r_{\text{cvt}}}, \quad (\text{B.20})$$

where

$$J_1 = J_p + \alpha_p(\alpha_p - \alpha_s r_{\text{cvt}}) J_f \quad (\text{B.21})$$

$$J_2 = J_s + \alpha_s \left(\alpha_s - \frac{\alpha_p}{r_{\text{cvt}}} \right) J_f \quad (\text{B.22})$$

The zero inertia CVT ratio r_{zi} can be found by equating J_1 to zero, *i.e.*,

$$r_{\text{zi}} := \frac{J_p}{\alpha_p \alpha_s J_f} + \frac{\alpha_p}{\alpha_s}. \quad (\text{B.23})$$

This zero inertia ratio differs from the one in equation (6.41) in that the primary inertia J_p is increased with the other engine sided inertias J_e and J_i . The structure of equation (B.20)

is essentially the same as for a basic CVT powertrain, however the inertias J_1 and J_2 are not constant. They boil down to the constants J_p and J_s if $J_f = 0$.

Figure B.5 the equivalent inertias are drawn. Here J_1^* is equal to J_1 though raised with the remaining primary sided inertias J_e and J_t :

$$J_1^* = J_e + J_p + J_t + \alpha_s(\alpha_p - \alpha_s r_{\text{cvt}}) J_f \quad (\text{B.24})$$

is used since it gives more insight in the balance between all primary sided inertias vs. the flywheel inertia.

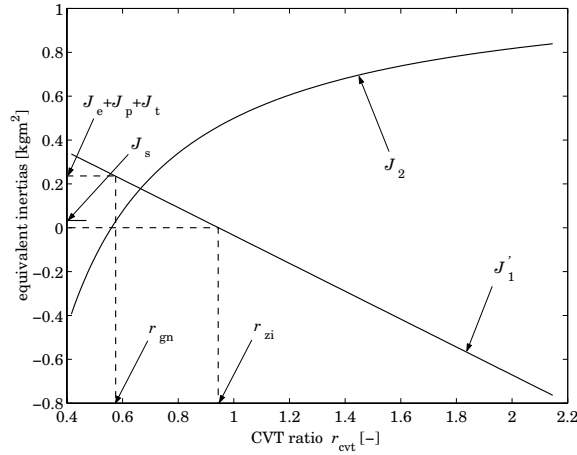


Figure B.5: Equivalent primary and secondary inertias as a function of the CVT ratio

From this figure it can be seen that the equivalent primary inertia J_1 is negative for $r_{\text{cvt}} \leq r_{\text{od}}$. Again the boost phenomenon of the IVS can be understood from this. Clearly, if $r_{\text{cvt}} > r_{\text{zi}}$ and $\dot{\omega}_p > 0$, that is if the engine output power is increased, the accelerating equivalent primary inertia will add up to the primary torque T_p , viz. equation (B.20). On the other hand, the equivalent secondary inertia is increased remarkably. Also this inertia is negative for some limited CVT ratio span, but for the remaining ratios it is substantially higher than the original secondary inertia J_s . However, when compared to the equivalent vehicle inertia seen at the secondary pulley (5.82 [kgm²]), J_2 is still relatively low. Especially high vehicle accelerations (high $\dot{\omega}_s$) are generally induced with a CVT ratio considerably lower than r_{od} , where J_2 approaches the original value.

Appendix C

Model Equations

C.1 Non-linear simulation model

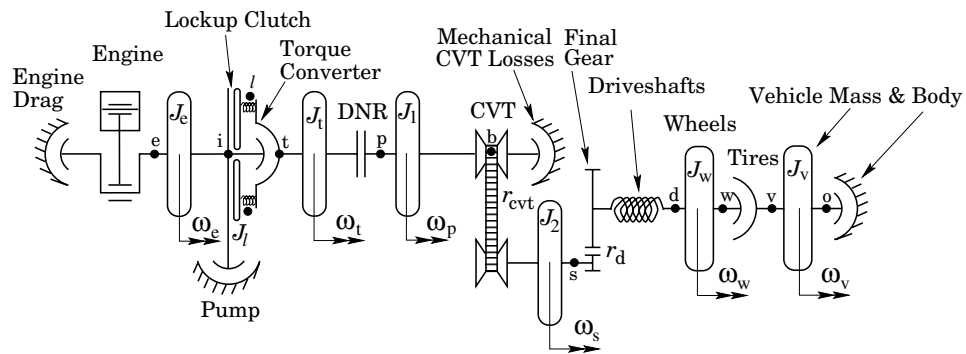


Figure C.1: Dissipative torsional compliance powertrain model

The total powertrain model displayed in Figure 6.15 as the graphical representation of a hybrid dynamical system with varying order:

$$\dot{x}_q(t) = f_q(x_q(t)) \quad (C.1)$$

$$y_q = g_q(x_q(t)) \quad (C.2)$$

$$q \in Q: \text{ a finite set of modes} \quad (C.3)$$

The system is hybrid in the sense that it contains both continuous and discrete states due to variable-structures, input and state constraints, binary inputs (on/off) and several switching models. The particular sub-system the continuous state x_q may be in, is determined by the particular mode q at that moment. Generally the transition from one mode q to another is governed by a collection of *jump sets*, i.e., all particular (state) conditions from which a mode transition takes place. The mode transitions themselves are known via the *jump transition*

maps, describing which new continuous state must be jumped to from the current state x_q , [Heemels, 1999].

In the case of the powertrain model, the hybridization is caused by the following discrete events, states and inputs:

1. the engine speed is constrained between 70 [rad/s] and 600 [rad/s].
2. the engine torque is constrained between the drag torque and the torque at wide open throttle (WOT)
3. the pump mode may be either single sided (SS) or double sided (DS), changing the model for the torque take-off at the engine
4. the torque converter may be either unlocked, locking or locked.
5. the flexibility in the torque converter itself has two stiffness parameters, switching between one another at a certain absolute value of the relative angle of rotation between impeller and turbine.
6. the 'D' clutch of the DNR set may be either disengaged, engaging or engaged. The latter reduces the number of degrees of freedom by 1 as the turbine and equivalent primary inertia become rigidly connected.
7. the CVT ratio is mechanically constrained between r_{ud} and r_{od} .
8. the CVT ratio dynamics are described by a switching model, one for up and one for downshifting
9. the tire-road interaction is described by a threefold switching model, one for vehicle standstill, one for driving tires and one for driven (also braking) tires

The discrete events leading to mode transitions are described by 4, 6, 8 and 9 from the list above, except for the (practical) exclusions:

- the disengaged 'D' is essentially the same as an engaging 'D' except the applied control input is zero
- an engaging 'D' never occurs when the vehicle is moving
- an engaging 'D' never occurs if the torque converter clutch is locked or locking
- the unlocked mode is essentially the same as a locking torque converter except the applied control input is zero
- a locking or locked torque converter clutch never occurs during vehicle standstill

The equations of motion seen from left to right in Figure 6.15 become

engine & pump

$$J_e \dot{\omega}_e = T_e - T_{\text{pump}} - T_i \quad (\text{C.4})$$

$$\dot{T}_e = -c_1 (T_e - \bar{T}_e(\phi, \omega_e)) \omega_e^2 - c_2 \omega_e \dot{T}_e \quad (\text{C.5})$$

$$T_{\text{pump}} = \begin{cases} T_{\text{SS}} & \text{if pump in SS - mode} \\ T_{\text{DS}} & \text{if pump in DS - mode} \end{cases} \quad (\text{C.6})$$

impeller & lockup

$$T_i = \begin{cases} b_{\text{tc}} \omega_e^2 + c_l p_l \text{sign}(\omega_e - \omega_l) & \text{if TC unlocked} \\ \frac{T_e J_l + T_l J_e}{J_l + J_e} - T_{\text{pump}} & \text{if TC locked} \end{cases} \quad (\text{C.7})$$

$$J_l \dot{\omega}_l = c_l p_l \text{sign}(\omega_e - \omega_l) - T_l \quad (\text{C.8})$$

$$\dot{T}_l = k_l (\omega_l - \omega_t) \quad (\text{C.9})$$

turbine & primary, D slipping

$$(J_t + J_1 + r_{\text{cvt}}^2 J_2) \dot{\omega}_p = T_p - T_{\text{mech}} - T_s r_{\text{cvt}} - J_2 \omega_s \dot{r}_{\text{cvt}} \quad (\text{C.10})$$

$$T_p = \begin{cases} c_{\text{cd}} p_{\text{cd}} \text{sign}(\omega_t - \omega_p) & \text{if D engages} \\ \frac{(J_1 + J_2 r_{\text{cvt}}^2) T_t + J_t T_s r_{\text{cvt}}}{J_t + J_1 + J_2 r_{\text{cvt}}^2} & \text{if D engaged} \end{cases} \quad (\text{C.11})$$

$$J_t \dot{\omega}_t = T_t - T_p \quad (\text{C.12})$$

$$T_t = \alpha_{\text{tc}} b_{\text{tc}} \omega_e^2 + T_l \quad (\text{C.13})$$

turbine & primary, D locked

$$(J_t + J_1 + r_{\text{cvt}}^2 J_2) \dot{\omega}_p = T_t - T_{\text{mech}} - T_s r_{\text{cvt}} - J_2 \omega_s \dot{r}_{\text{cvt}} \quad (\text{C.14})$$

$$T_t = \alpha_{\text{tc}} b_{\text{tc}} \omega_e^2 + T_l \quad (\text{C.15})$$

CVT & belt

for upshifting :

$$\dot{r}_{\text{cvt}} = -c_3 \left(\dot{r}_{\text{cvt}} - \frac{r_{\text{cvt}} \dot{r}_{\text{cvt,d}}}{r_{\text{cvt,d}}} \right) - c_4 r_{\text{cvt}} \ln(r_{\text{cvt}} - r_{\text{cvt,d}}) + \frac{\dot{r}_{\text{cvt}}^2}{r_{\text{cvt}}} \quad (\text{C.16})$$

for downshifting :

$$\dot{r}_{\text{cvt}} = -c_5 r_{\text{cvt}} \ln(r_{\text{cvt}} - r_{\text{cvt,d}}) \quad (\text{C.17})$$

$$T_b = \frac{J_1 r_{\text{cvt}} T_s + J_2 r_{\text{cvt}}^2 T_p}{J_1 + J_2 r_{\text{cvt}}^2} - T_{\text{mech}} \quad (\text{C.18})$$

final & shafts

$$T_s = r_d T_d \quad (\text{C.19})$$

$$\dot{T}_d = k_d(r_d \omega_s - \omega_w) \quad (\text{C.20})$$

wheels

$$J_w \dot{\omega}_w = T_d - T_w \quad (\text{C.21})$$

$$T_w = R_w F_w + T_r + T_{\text{brake}} \quad (\text{C.22})$$

$$F_w = \begin{cases} b_w \left(1 - \frac{v_v}{R_w \omega_w}\right) & \text{for driving wheels} \\ b_w \left(1 - \frac{R_w \omega_w}{v_v}\right) & \text{for driven wheels} \end{cases} \quad (\text{C.23})$$

vehicle

$$(m_v + J_w/R_w^2) \dot{v}_v = F_w - c_v v_v^2 \quad (\text{C.24})$$

C.2 Linearized model

For small vibration analysis, pole-zero maps and frequency diagnostics, the system equations are linearized around stationary states of interest. Here, the linear equations are given in the case of engaged 'D' and locked torque converter. Moreover, the dynamics of the actuation inputs T_e and \dot{r}_{cvt} are left out, the wheels are driving the vehicle, and finally, the pump and mechanical losses are omitted. Regarding these assumptions the nonlinear system equations are given first:

$$\dot{x}(t) = f(x(t)) + g(x(t))u(t), \quad (\text{C.25})$$

where $x = [\omega_e \ T_t \ \omega_p \ r_{\text{cvt}} \ \omega_w \ T_d \ v_v]^T$, $T_e = u_1$, $\dot{r}_{\text{cvt}} = u_2$, and

$$\dot{\omega}_e = \frac{u_1 - T_t}{J_e + J_i} \quad (\text{C.26})$$

$$\dot{T}_t = k_t(\omega_e - \omega_p) \quad (\text{C.27})$$

$$\dot{\omega}_p = \frac{T_t - r_d r_{\text{cvt}} T_d - J_2(r_{\text{cvt}}) \omega_p r_{\text{cvt}} u_2}{J_t + J_1(r_{\text{cvt}}) + r_{\text{cvt}}^2 J_2(r_{\text{cvt}})} \quad (\text{C.28})$$

$$\dot{r}_{\text{cvt}} = u_2 \quad (\text{C.29})$$

$$\dot{\omega}_w = \frac{T_d - R_w F_w(\omega_w, v_v) - T_r}{J_w} \quad (\text{C.30})$$

$$\dot{T}_d = k_d(r_d r_{\text{cvt}} \omega_p - \omega_w) \quad (\text{C.31})$$

$$\dot{v}_v = \frac{F_w - c_v v_v^2}{m_v + J_w/R_w^2} \quad (\text{C.32})$$

Linearizing (C.25) around a stationary operating point (x_0, u_0) gives:

$$\delta \dot{x} = \left(\left. \frac{\partial f(x)}{\partial x} \right|_{x_0} + u_0 \left. \frac{\partial g(x)}{\partial x} \right|_{x_0} \right) \delta x + g(x_0) \delta u \quad (\text{C.33})$$

For convenience (C.33) is written in standard linear form as

$$\dot{\tilde{x}} = A\tilde{x} + B\tilde{u}, \quad (\text{C.34})$$

where $A(j, k)$ and $B(j, m)$ with $j = 1..7$, $k = 1..7$ and $m = 1, 2$, and $\tilde{x} = \delta x$, $\tilde{u} = \delta u$

$$\begin{aligned} A(1, 1) &= 0 & A(5, 7) &= \frac{b_w}{J_w \omega_{w_0}} \\ A(1, 2) &= \frac{-1}{J_e + J_i} & A(6, 1..2) &= 0 \\ A(1, 3..7) &= 0 & A(6, 3) &= k_d r_d r_{cv_{t_0}} \\ A(2, 1) &= k_l & A(6, 4) &= k_d r_d \omega_{p_0} \\ A(2, 2) &= 0 & A(6, 5) &= -k_d \\ A(2, 3) &= -k_l & A(6, 6..7) &= 0 \\ A(2, 4..7) &= 0 & A(7, 1..4) &= 0 \\ A(3, 1) &= 0 & A(7, 5) &= \frac{R_w b_w v_{v_0}}{(m_v R_w^2 + J_w) \omega_{w_0}^2} \\ A(3, 2) &= \frac{1}{J_t + J_1(r_{cv_{t_0}}) + r_{cv_{t_0}}^2 J_2(r_{cv_{t_0}})} & A(7, 6) &= 0 \\ A(3, 3) &= 0 & A(7, 7) &= -\frac{b_w R_w + 2c_v R_w^2 v_{v_0} \omega_{w_0}}{(m_v R_w^2 + J_w) \omega_{w_0}} \\ A(3, 4) &= \frac{-T_{d_0} r_d}{J_t + J_1(r_{cv_{t_0}}) + r_{cv_{t_0}}^2 J_2(r_{cv_{t_0}})} & B(1, 1) &= \frac{1}{J_e + J_i} \\ A(3, 5) &= 0 & B(1, 2) &= 0 \\ A(3, 6) &= \frac{-r_d r_{cv_{t_0}}}{J_t + J_1(r_{cv_{t_0}}) + r_{cv_{t_0}}^2 J_2(r_{cv_{t_0}})} & B(2, 1..2) &= 0 \\ A(3, 7) &= 0 & B(3, 1) &= 0 \\ A(4, 1..7) &= 0 & B(3, 2) &= \frac{-J_2(r_{cv_{t_0}}) \omega_{p_0} r_{cv_{t_0}}}{J_t + J_1(r_{cv_{t_0}}) + r_{cv_{t_0}}^2 J_2(r_{cv_{t_0}})} \\ A(5, 1..4) &= 0 & B(4, 1) &= 0 \\ A(5, 5) &= \frac{-b_w v_{v_0}}{J_w \omega_{w_0}^2} & B(4, 2) &= 1 \\ A(5, 6) &= \frac{1}{J_w} & B(5..7, 1..2) &= 0 \end{aligned}$$

C.3 Parameters

VARIABLE	DESCRIPTION	VALUE	UNIT
α_s	torque amplification flywheel to secondary pulley	1.66	[-]
α_p	torque amplification flywheel to primary pulley	0.96	[-]
b_w	tire-road friction coefficient	8.8	[-]
c_1	engine model coefficient	0.24	[-]
c_2	engine model coefficient	0.882	[s]
c_3	CVT model coefficient	2.06	[1/s]
c_4	CVT model coefficient	1.77	[1/s ²]
c_5	CVT model coefficient	2.88	[1/s]
c_v	air drag coefficient	0.39	[m/kg]
k_l	torsional stiffness lockup clutch springs	1182	[Nm/rad]
k_d	torsional stiffness drive shaft	6200	[Nm/rad]
m_v	vehicle mass	1364	[kg]
r_d	final reduction gear ratio	0.2127	[-]
r_{gn}	(flywheel) geared neutral CVT ratio	0.577	[-]
r_{od}	highest CVT gear ratio	2.15	[-]
r_{ud}	lowest CVT gear ratio	0.42	[-]
r_{zi}	zero (primary) inertia CVT ratio	0.95	[-]
J_e	engine+pump+impeller inertia	0.156	[kgm ²]
J_f	flywheel inertia	0.393	[kgm ²]
J_l	lockup inertia	1e-5	[kgm ²]
J_p	primary pulley+DNR sun gear inertia	0.042	[kgm ²]
J_s	secondary+final+differential inertia	0.033	[kgm ²]
J_t	turbine+DNR carrier,planets and annulus inertia	0.036	[kgm ²]
J_w	two wheels inertia	1.7	[kgm ²]
R_w	wheel radius	0.307	[m]
T_r	rolling resistance torque	55	[Nm]

Table C.1: Numerical values of the parameters used in the nonlinear and linearized models

Samenvatting

Aandrijfsystemen voor personenauto's hebben de laatste jaren een aanzienlijke ontwikkeling doorgemaakt. Op het gebied van motoren, luchtweerstand en banden is en wordt succesvol werk verricht om het brandstofverbruik te verlagen. Gewichtsbesparing heeft de meeste invloed op de verbruiksvermindering maar blijkt met de toegenomen veiligheids- en comfort eisen moeilijk of helemaal niet realiseerbaar te zijn. Veel vernieuwingen en innovaties op dit gebied worden aangezet en vaak ook financieel gestimuleerd door de overheden. De reden hiervoor is het dringende verzoek vanuit de samenleving emissies en energieverbruik te verminderen vaak vanuit kosten overwegingen maar meer nog vanuit de algemene wens voor een schoner milieu.

Sinds een jaar of tien wordt ingezien dat ook met de transmissie een aanzienlijk verbruiksverbetering kan worden bereikt. Het gaat dan in de eerste plaats niet om het verbeteren van de transmissie zelf als wel een alternatief samenspel van de motor en de transmissie te realiseren. Dit samenspel kan worden geïntensiveerd door het toepassen van een *continu variabele transmissie* (CVT). Een dergelijke transmissie is in staat het koppel van de motor continu door te leiden terwijl het motortoerental naar wens continu variabel kan worden versteld. Naast deze functionele voordelen ten opzichte van getrapte transmissies is het belangrijkste voordeel van de CVT de relatief hoge *overdrive* overbrengingsverhouding bij een relatief geringe inbouwruimte. Deze hoge overdrive is in staat het motortoerental extreem laag te houden bij normaal gebruik van het voertuig. Ter vergelijking: in de huidige toepassing kan de motor bij 80 [km/h] op 1500 toeren per minuut worden gehouden terwijl dat voor de meeste voertuigen nu minimaal zo'n 1900 à 2200 bedraagt. Dergelijke lage toerentallen hebben een enorme invloed op het verbruik. In het voorbeeld kan al zo'n 10 to 15% brandstof worden bespaard. Het grootste nadeel van de lage toerentallen is een tegenvallende initiële responsie van het voertuig indien het gaspedaal verder wordt ingetrapt, bijvoorbeeld bij een inhaalmanoeuvre. Precies dit nadeel wordt maatschappelijk gezien alleen al vanwege de veiligheid nauwelijks geaccepteerd en het zoeken naar oplossingen voor de *paradox* tussen de *rijdbaarheid* en *zuinigheid* is dus noodzakelijk.

In het kader van het *EcoDrive project* werd op de Technische Universiteit Eindhoven een innovatief idee uitgewerkt dat afrekenet met deze paradox. Een deel van het onderhavige werk staat beschreven in dit proefschrift. Twee andere werken voortkomend uit het EcoDrive project zijn 'Component Control for the Zero Inertia Powertrain' geschreven door Bas Vroomen en 'Transmission Design of the Zero Inertia Powertrain' door Roëll van Druten.

De vernoemde innovatie wordt gerealiseerd door het slim inzetten van een vliegwiel in een bestaande CVT waardoor het mogelijk is de motor te assisteren bij de vereiste initiële responsie. Fysiek wordt een planetair tandwielstelsel parallel over de CVT geplaatst en het vliegwiel wordt hiermee verbonden. Het vliegwiel draait op hoog toerental bij een laag motortoerental en wordt afgetoerd als de motor moet worden opgetoerd met de CVT, bijvoorbeeld

bij een inhaalmanoeuvre. Het koppel dat zodoende van het vliegwiel vrijkomt wordt rechtstreeks naar de aandrijfassen geleid totdat de motor is opgetoerd en de vermogensafgifte kan overnemen. In dit proefschrift wordt aangetoond dat er een unieke situatie optreedt waarbij de massastraagheidskrachten aan de motorzijde exact worden gecompenseerd door de massastraagheidskrachten van het vliegwiel. Deze situatie wordt 'zero inertia', oftewel nul massastraagheid genoemd. De nieuwe CVT-gebaseerde aandrijving is daarom *Zero Inertia Powertrain* (ZI) gedoopt.

Een goede coördinatie tussen motorkoppel en het schakelen van de CVT is tijdens maar ook na zo'n transitie heel belangrijk. Door continu in de tijd de juiste setpoints aan de elektronische motor gasklep en de hydraulische CVT regeling te geven kan de rijdbaarheid (driveability) en zuinigheid (fuel economy) worden geoptimaliseerd. Het ontwerp van een coördinerende regeling (coordinated control) en het demonstreren van de zuinigheid in combinatie met een goede rijdbaarheid van een testvoertuig zijn de hoofdonderwerpen van dit proefschrift. Voor het ontwerp van de coördinerende regeling zijn modellen van het aandrijfsysteem noodzakelijk. De modellen, ontwerp van coördinerende regelingen voor zowel de CVT- als de ZI aandrijflijn en tenslotte de implementatie in en experimenten met een testvoertuig zijn beschreven in deel II van dit proefschrift. Deel I betreft een samenwerking met Bas Vroemen en Roëll van Druten en laat zien dat brandstofbesparing moet worden afgewogen tegen de inspanning (kosten, inbouwruimte, gewicht, etc.) die er voor moet worden geleverd. De ZI aandrijving blijkt een goede middenweg te zijn.

Dankwoord

Middels dit nawoord wil ik een aantal mensen bedanken die direct of indirect hebben bijgedragen hebben aan dit proefschrift en het onderliggende werk.

Ten eerste wil ik de partners en de subsidiegever bedanken voor het mogelijk maken en ondersteunen van het EcoDrive project. EcoDrive was een samenwerking van Van Doorne's Transmissie (VDT) te Tilburg, TNO Automotive te Delft en de Technische Universiteit Eindhoven (TU/e). Het project werd gesubsidieerd door EET (Ecologie, Economie en Technologie), een programma van de ministeries van EZ en OC&W.

De afgelopen vier en half jaar heb ik dagelijks met groot plezier samengewerkt met een heleboel mensen die dit project tot een succes hebben helpen maken. Op de TU/e zijn dat in de eerste plaats mijn co-promotor Frans Veldpaus en directe collega's Bas Vroemen en Roëll van Druten. Frans bleef altijd achter ons en onze standpunten staan. Discussieren met hem is een waar genoegen en hij is zelden slecht gemutst. Ik bewonder ook je volhardendheid in het bekritisieren van onze proefschriften onder de toch wat grote tijdsdruk. Je vakantie verhalen over de huttentochten zullen me bij blijven Frans. Ik weet weliswaar niet zeker of ik er zelf ooit een zal maken. Bas en Roëll en ik zijn eerder dit jaar een bedrijf begonnen: Drive Train Innovations (DTI). Het behoeft denk ik weinig betoog dat dit bedrijf ontstaan is uit een goede sfeer die onderlinge kritiek toelaat, de wederzijdse waardering en het naadloos aanvullen van elkaars capaciteiten. Bovenal heb ik de afgelopen jaren veel plezier gehad met jullie als collega's en vrienden. Bas en Roëll bedankt dat we zover zijn mogen komen!

Dan is er Erwin Meiders, een verhaal apart. Boeken vol kun je schrijven over hem maar ik moet het kort houden. Erwin doet alles wat bijna niemand anders doet. We hebben geleerd dat die dingen onontbeerlijk zijn voor de voortgang van het project. Daarnaast is het altijd lachen met Erwin, hij heeft een heel eigen benaderingswijze van de belangrijke en minder belangrijke dingen in het leven. Zelf noemt hij het hoofd- en bijzaken, beide moeten behandeld worden door te *blijven praten*. Erwin bedankt!

De testauto, eigenlijk een lastig kind, is omgebouwd tot een compleet rijdend laboratorium. De inzet van Toon van Gils en Karel Koekkoek zijn van onschatbare waarde gebleken. Na ontelbare problemen te hebben opgelost paste uiteindelijk alles in elkaar en het werkte! Gouden handjes en een pientere geest zijn de beste combinatie dat hebben jullie laten zien. Boven alles zijn jullie fijne lui en ik denk met veel plezier terug aan onze samenwerking.

Een verademing waren de bijna wekelijkse meetings op de kamer van Dick Landheer. Er stond altijd een kan koffie klaar en feilloos wist Dick de meetings luchtig doch helder te houden. De notulen werden echt gelezen temeer omdat het taalgebruik zo bloemrijk was. Ook tijdens de voorbereidingen van het Maxima evenement kwamen jouw talenten goed van pas. Bedankt Dick voor je oprechte inzet!

Maarten Steinbuch wil ik graag bedanken voor zijn 'prik-acties' die ons snel weer op het juiste spoor brachten. Maarten ik denk dat jij efficiency hebt heruitgevonden. Je bent een

prettig en open persoon, niet voor niets willen alle studenten bij jou afstuderen. Jan Kok bedankt dat je in de beginperiode mee hebt willen denken over mens-machine interactie. Jij bent bovendien toonaangevend als het gaat om de moderne (digitale) fotografie. Bedankt ook dat je zitting wilt nemen in de promotiecommissie.

Uiteraard wil ik de stagiaires en afstudeerders bedanken voor het werk binnen het project: Rob Karmiggelt, Roel Verhoeven, Tinka Verhagen, Rob Hitzert, Michiel Pesgens en Peter de Bruijn.

Er bleef naast alle werkzaamheden weinig tijd over voor een gezellige bak koffie bij mijn collega AiO's. De borrels op vrijdag konden hier en daar wat inhalen. In die spaarzame momenten heb ik wel genoten, vooral tijdens het lustrumfeest is er een hoogtepunt bereikt (<http://www.wfw.wtb.tue.nl/horaest/movies/movies.html>). De voorbereidingen waren ook erg komisch. Eric, Francois, Leonie, Roel en onze manager Rene jullie waren enig! Ook wil ik het Hora Est bestuur van 1998-1999: Liesbeth, Roel, Eric, Dave bedanken voor de prettige samenwerking. De Symposiumcommissie 2000: Arnim, Harold, Liesbeth, Arjen, Roel en Wilco, hartelijk dank. Ons thema "De Stuurloze Wetenschap ?/!" liet inderdaad zien hoe stuurloos sommige sprekers kunnen zijn.

Verder wil ik bedanken Bram Veenhuizen en Marc Mussaerus van VDT. Bram, je hebt ons geleerd dat het niet erg is planningen te overschrijden zolang er maar een plausibele verklaring voor te geven valt. Marc, ik ben je zeer erkentelijk voor het meedenken in de beginperiode van het project. Al heel snel heb je mij en mijn collega's op een juist denkspoor gezet. Uiteraard wordt iedereen van VDT, en met name afdeling EWG3, bedankt voor de ondersteunende werkzaamheden. De jaarlijkse hike met EWG3 in de onherbergzame gebieden van Europa was altijd een uitstekende gelegenheid om weer eens bij te praten over EcoDrive, althans als er niet gezongen werd.

In de beginperiode heb ik prettig samengewerkt met Jos van de Venne van TNO Automotive. Samen hebben we ingezien hoe moeilijk het is een simulatie van een stadsritje tot een goed einde te brengen. Gelukkig was het maar de simulatie die ergens crashte of vast kwam te zitten. De andere betrokkenen van TNO Automotive Joeri de Haas, Erik van den Tillaart, bedankt voor jullie inzet.

Verder wil ik PD&E te Helmond, de testbaan van DAF Trucks N.V. te Sint Oedenrode en het Motoren Emissie Laboratorium van TNO Automotive te Delft hartelijk danken voor het gebruik van de testfaciliteiten.

Gemeente Eindhoven, Máxima en Prins-Willem Alexander bedankt voor de onvergetelijke 4 september 2001!

Tenslotte wil ik mijn ouders, zus en al mijn vrienden bedanken voor hun enthousiasme en interesse die ze tonen in alles wat ik doe. Mijn speciale dank gaat uit naar de 'vrienden van de Catharina'. Ik heb ontzettend genoten van de vele avondjes uit en de vakanties. De laatste vakantie naar Mexico was wat dat betreft een echte topper!

Alex Serrarens,
Eindhoven, 10 oktober 2001

Curriculum Vitae

- 6 September 1973** Born in Hulst, The Netherlands
- 1985-1991** Atheneum-B, Jansenius Lyceum, Hulst
- 1991-1997** He has been working towards MSc. in Mechanical Engineering at the Technische Universiteit Eindhoven (TU/e).
– Practical assignments: 1) Preview observer for a tractor-semitrailer active suspension (at TU/e). 2) Ethernet control of 6-DOF manipulator (at Mech. Eng. Lab., Tsukuba, Japan).
– Graduation project: \mathcal{H}_∞ Control as Applied to Torsional Drill-string Dynamics (at Shell International Exploration & Production Laboratory B.V., Rijswijk, The Netherlands).
- 1997-2001** He has been working towards his PhD degree at the Technische Universiteit Eindhoven, in the EcoDrive project. This project was a co-operation of the Technische Universiteit Eindhoven, Van Doorne's Transmissie (VDT) in Tilburg and TNO Automotive in Delft.
- 3 November 1998** He received the annual KIVI Control Technology Award for best national graduation project related to control.
- 17 November 1999** The ZI powertrain received the Novem Energy Conversion Award for the most promising idea related to energy conversion.
- 21 April 2000** World patent granted: "Vehicle drive assembly" (pat. WO9955549A1) R. M. van Druten, M. A. Mussaeus, B. G. Vroemen, A. F. A. Serrarens and P. A. Veenhuizen.
- 24 April 2000** World patent granted: "Transmission system, especially for a motor vehicle" (pat. WO9956039A2) R. M. van Druten, M. A. Mussaeus, B. G. Vroemen, A. F. A. Serrarens and P. A. Veenhuizen.